UNIVERSIDADE DE SÃO PAULO

FACULDADE DE ZOOTECNIA E ENGENHARIA DE ALIMENTOS

LARISSA TESSARO

Filmes nanocompósitos a base de gelatina ativados com extrato de folha de pitangueira (*Eugenia uniflora* L.) encapsulado em emulsão dupla: permeabilidade a gases e digestão *in vitro*

Pirassununga

2024

LARISSA TESSARO

Filmes nanocompósitos a base de gelatina ativados com extrato de folha de pitangueira encapsulado em emulsão dupla: permeabilidade a gases e digestão *in vitro*

Versão Corrigida

Tese apresentada à Faculdade de Zootecnia e Engenharia de Alimentos da Universidade de São Paulo, como parte dos requisitos para a obtenção do título de Doutor em Ciências do Programa de Pós-graduação em Engenharia de Alimentos.

Área de Concentração: Ciências da Engenharia de alimentos

Orientador: Prof. Dr. Paulo José do Amaral Sobral

Pirassununga

2024

Esta tese é dedicada à minha mãe, Antônia, que partiu durante o meu doutorado, mas continua sendo meu maior exemplo de força e resiliência, e ao meu querido pai, Paulo.

AGRADECIMENTOS

Agradeço a Deus, por tudo.

Aos meus pais, Antônia E. Damasceno Tessaro (*in memoriam*) e Paulo Roberto Tessaro, que sempre abraçaram esse sonho comigo e foram meus maiores incentivadores, apoiadores e exemplos de dedicação, comprometimento, honestidade e perseverança. Agradeço por serem os melhores pais do mundo e por todo amor.

À Universidade de São Paulo (USP), instituição que eu tanto amo e onde eu tive o privilégio de ser aluna de graduação, mestrado e doutorado. Em especial, agradeço à Faculdade de Zootecnia e Engenharia de Alimentos (FZEA) e ao Departamento de Engenharia de Alimentos, pela oportunidade de desenvolver minha tese de doutorado.

Ao meu orientador, Prof. Dr. Paulo José do Amaral Sobral, que me deu a oportunidade de ser sua aluna há 6 anos, e desde então, é o meu maior exemplo e inspiração na vida acadêmica. Agradeço pela orientação irrepreensível, pela confiança no meu trabalho, pelo comprometimento e todo conhecimento compartilhado. Agradeço, principalmente, pela compreensão e por todo suporte que meu deu nos momentos difíceis.

Aos meus colegas e amigos do Laboratório de Tecnologia de Alimentos (LTA), Carla Luciano, Alessandra, Lía, David, Palmer, Paula, Camily, Kamila, Beatriz e Daniel, por toda ajuda, troca, aprendizado, apoio e momentos de descontração. Agradeço à aluna de iniciação científica, Ana Gabrielle, pela dedicação no desenvolvimento de parte desta tese.

À Paula Benoso, pela parceria e pelos dados obtidos durante seu intercâmbio na Itália (Universidade de Bologna), que originaram o capítulo 3 desta tese.

Aos especialistas de laboratório e amigos, Ana Mônica Quinta Barbosa Bittante e Rodrigo Vinícius Lourenço, por toda ajuda no desenvolvimento desta tese, pelas dicas, ensinamentos, conhecimentos compartilhados, companhia diária e, principalmente, pela amizade e apoio nos momentos difíceis.

À Universidade do Minho, Campus Gualtar (Braga, Portugal), em especial, ao Centro de Engenharia Biológica, onde eu tive o privilégio de desenvolver parte da minha pesquisa na modalidade Doutorado Sanduíche no Exterior.

Ao meu orientador na Universidade do Minho, Prof. Dr. António Augusto Vicente, por toda a excelência com que desempenha os papéis de orientador,

pesquisador, gestor e amigo, o que contribuiu grandiosamente para o meu desenvolvimento pessoal e profissional.

A todos os colegas que conheci no Laboratório de Indústria e Processos (LIP, Universidade do Minho) e que me ensinaram tanto sobre pesquisa, parceria, responsabilidade, companheirismo e empatia.

Aos coautores dos artigos resultantes desta tese, pela colaboração e conhecimentos compartilhados: Profa. Milena Martelli-Tosi, Rodrigo V. Lourenço, Ana Gabrielle R. Pereira, Paula Benoso, Profa. Valentina Siracusa, Prof. Marco Dalla Rosa, Raquel F.S. Gonçalves, Joana T. Martins e Ana C. Pinheiro.

Ao meu namorado, Maike Braz Pinto, por todo apoio, compreensão, incentivo, amor e companheirismo. Aos meus sogros, Rosemeire Braz Pinto e Luís Roberto Braz Pinto, que são minha segunda família e que me apoiaram e incentivaram de inúmeras formas durante todo o processo.

Aos amigos que fiz durante o meu intercâmbio, Fernanda, Isabela, Kétura, Leandro, Leandro Lins, Luíz e Kamilla, por terem sido meus amigos, companheiros e família em Portugal.

"Se eu vi mais longe, foi por estar sobre ombros de gigantes."

Sir Isaac Newton (1675)

RESUMO

TESSARO, L. **Filmes nanocompósitos a base de gelatina ativados com extrato de folha de pitangueira encapsulado em emulsão dupla: permeabilidade a gases e digestão *in vitro*.** 2024. 205 f. Tese (doutorado) – Faculdade de Zootecnia e Engenharia de Alimentos, Universidade de São Paulo, Pirassununga, 2024.

Filmes ativos são materiais finos e flexíveis incorporando compostos ativos (CA) e que por isso, podem apresentam, por exemplo, atividades antimicrobiana e/ou antioxidante. Eles podem ser produzidos a partir de biopolímeros, como a gelatina, que possui excelente propriedade formadora de filmes. O extrato hidroetanólico de folhas de pitangueira (PLE) é rico em CA e pode ser utilizado para ativar esses materiais, na forma livre ou encapsulado. Além disso, a incorporação de cargas de reforço, como a nanocelulose cristalina (CN), pode ser conveniente para aprimorar algumas propriedades físico-químicas dos filmes ativos. Esses filmes ativos podem, ainda, apresentar propriedades comestíveis e atuarem como liberadores de CA em condições gastrointestinais. Assim, o objetivo geral desta tese foi estudar as propriedades de barreira a gases e a digestão *in vitro* de filmes e filmes nanocompósitos a base de gelatina, sem e com carga de CN, e ativados com PLE encapsulado em emulsão dupla A/O/A (DE) e não encapsulado. Na primeira parte deste trabalho, as propriedades físico-químicas, funcionais, microestruturais e ativas de filmes e filmes nanocompósitos a base de gelatina, quitosana e blenda gelatina/quitosana, ativados pela incorporação de DE, foram estudadas. A incorporação de CN e DE melhorou consideravelmente as propriedades mecânicas, de barreira à luz UV/Vis e de sensibilidade à água. Com base neste estudo, a gelatina foi escolhida como o biopolímero mais conveniente para a produção dos filmes e filmes nanocompósito, considerando-se que apresentou melhor atividade antioxidante e tem menor custo. Em seguida, filmes e filmes nanocompósitos a base de gelatina ativados com PLE não encapsulado foram estudados para um melhor entendimento da ação do PLE na matriz biopolimérica e do efeito da sua encapsulação na DE. Assim como para os filmes produzidos na primeira parte deste trabalho, o PLE não encapsulado e a CN aprimoraram as propriedades mecânicas, de barreira à luz UV/Vis e a atividade antioxidante, embora em menor intensidade. O efeito da umidade

relativa (UR) na taxa de transmissão dos gases O_2 e CO_2 (GTR) através de filmes e filmes nanocompósitos ativados com DE ou PLE também foi estudado. A CN e o PLE e/ou DE modificaram a morfologia e cristalinidade dos filmes e filmes nanocompósitos, o que afetou a GTR em diferentes URs (0, 34, 59 e 76%). Os filmes nanocompósitos apresentaram, no geral, as melhores propriedades de barreira aos gases estudados. Por fim, realizou-se um estudo de digestão *in vitro* dos filmes e filmes nanocompósitos ativados com PLE ou DE, a fim de se determinar a biodisponibilidade do PLE após a digestão *in vitro* e a citotoxicidade dos filmes digeridos. Como controle de todo o processo, o PLE, a emulsão água-em-óleo (SE), e a DE, também foram submetidas à digestão *in vitro*. O filme nanocompósito ativado com DE apresentou a maior biodisponibilidade e estabilidade do PLE. Todos os filmes digeridos foram não citotóxicos nas condições estudadas. No geral, os estudos conduzidos nesta tese demonstraram que os filmes e filmes nanocompósitos produzidos podem, eventualmente, ser comestíveis e seguros para a saúde humana. Estes materiais podem ser valorizados e aprimorados pela adição de CN e PLE encapsulado em DE, e atuar como liberadores do PLE em condições gastrointestinais e como materiais de barreira a gases em diferentes umidades relativas. Alguns resultados obtidos nesta tese permitem sugerir que esses filmes e filmes nanocompósitos podem ser aplicados com segurança como embalagens ativas de alimentos.

Palavras-chave: biopolímeros; filmes comestíveis; compostos fenólicos; encapsulação; propriedade de barreira; biodisponibilidade.

ABSTRACT

TESSARO, L. **Gelatin-based nanocomposite films activated with "Pitanga" leaf extract encapsulated in double emulsion: gas permeability and *in vitro* digestion** 2024. 205 p. PhD thesis – Faculdade de Zootecnia e Engenharia de Alimentos, Universidade de São Paulo, Pirassununga, 2024.

Active films are thin and flexible materials incorporating active compounds (AC) and therefore may have, for example, antimicrobial and/or antioxidant activities. They can be produced from biopolymers such as gelatin, which has an excellent film-forming property. The hydroethanolic extract of "pitangueira" leaves (PLE) is rich in CA and can be used to activate these materials, in free or encapsulated form. Furthermore, the incorporation of reinforcing fillers, such as crystalline nanocellulose (CN), may be convenient to improve some physicochemical properties of active films. These active films may also have edible properties and act as CA delivers in gastrointestinal conditions. Thus, the general objective of this thesis was to study the gas barrier properties and in vitro digestion of gelatin-based films and nanocomposite films, without and with CN loading, and activated with PLE encapsulated in a W/O/W emulsion (DE) and not encapsulated. In the first part of this work, the physicochemical, functional, microstructural and active properties of nanocomposite films and films based on gelatin, chitosan and gelatin/chitosan blend, activated by the incorporation of DE, were studied. The incorporation of CN and DE considerably improved the mechanical properties, UV/Vis light barrier and water sensitivity. Based on this study, gelatin was chosen as the most convenient biopolymer for the production of films and nanocomposite films, considering that it presented better antioxidant activity and has a lower cost. Next, gelatin-based films and nanocomposite films activated with non-encapsulated PLE were studied to better understand the action of PLE on the biopolymeric matrix and the effect of its encapsulation on DE. As for the films produced in the first part of this work, the non-encapsulated PLE and CN improved the mechanical properties, barrier to UV/Vis light and antioxidant activity, although to a lesser extent. The effect of relative humidity (RH) on the transmission rate of O_2 and CO_2 gases (GTR) through DE or PLE activated films and nanocomposite films was also studied. CN and PLE and/or DE modified the morphology and crystallinity of films and nanocomposite films, which affected the GTR at different RHs (0, 34, 59 and 76%).

The nanocomposite films showed, in general, the best gas barrier properties studied. Finally, an in vitro digestion study of films and nanocomposite films activated with PLE or DE was carried out to determine the bioavailability of PLE after in vitro digestion and the cytotoxicity of the digested films. As a control for the entire process, the PLE, the water-in-oil (SE) emulsion and the DE were also subjected to in vitro digestion. The DE-activated nanocomposite film showed the highest bioavailability and stability of PLE. All digested films were non-cytotoxic under the conditions studied. Overall, the studies conducted in this thesis demonstrated that the nanocomposite films and films produced can eventually be edible and safe for human health. These materials can be valorized and enhanced by the addition of CN and PLE encapsulated in DE, and act as PLE releasers in gastrointestinal conditions and as gas barrier materials at different relative humidities. Some results obtained in this thesis suggest that these films and nanocomposite films can be safely applied as active food packaging.

Sumário

1 INTRODUÇÃO GERAL

As embalagens de alimentos desempenham, entre outras funções, um papel fundamental na proteção do alimento embalado contra fatores externos biológicos, químicos e físicos, que podem comprometer a integridade do alimento (Liu et al., 2024). A maioria das embalagens flexíveis de alimentos são produzidas a base de polímeros derivados do petróleo, oferecendo algumas vantagens, como barreira aos gases, vapores, umidade e odores, boas propriedades mecânicas e ópticas, durabilidade e custo relativamente baixo. Apesar da versatilidade, esses materiais causam uma série de danos ambientais consideráveis, incluindo a sua decomposição em microplásticos que causam um desequilíbrio na segurança dos alimentos (Vargas-Torrico et al., 2023). Motivados pelos problemas ecológicos e alimentares causados pelo uso indiscriminado das embalagens convencionais, muitos pesquisadores têm focado seus estudos no desenvolvimento de embalagens a base de biopolímeros, por serem biodegradáveis, contribuindo assim, para a redução dos problemas ambientais provocados pelas embalagens sintéticas (Zhao et al., 2022).

As embalagens biopoliméricas normalmente são produzidas com filmes produzidos a partir de biopolímeros. Filmes são materiais finos e flexíveis produzidos por via seca, como por exemplo, termocompressão ou extrusão, ou por via úmida, como com o "casting", em que o biopolímero é disperso em um solvente, normalmente a água, na presença de um plastificante, aplicado num suporte e desidratado convenientemente (Sobral et al., 2001). Entre os diversos biopolímeros estudados, a gelatina é um dos mais promissores na produção de filmes biopoliméricos.

A gelatina é uma proteína de origem animal, produzida pela hidrólise parcial do colágeno de peles, ossos, tecidos conjuntivos e tendões de animais vertebrados e invertebrados (Shamsallah; Rashid, 2024). A gelatina apresenta excelentes propriedades formadoras de filmes, versatilidade, biodegradabilidade, biocompatibilidade, capacidade de incorporar diferentes componentes e de formar blendas com outros biopolímeros, além de ser produzida em todo o mundo (Acharya et al., 2024; Li et al., 2024).

Os filmes a base de gelatina são sensíveis à água, o que pode afetar negativamente as propriedades mecânicas e de barreira a gases e a vapores e, consequentemente, limitar a aplicação como embalagens de alimentos. Uma

alternativa para reduzir esse problema é o emprego de cargas de reforço, como nanopartículas ou nanofibras, visando melhorar as propriedades físicas (Acharya et al., 2024; Nikoukheslat et al., 2022).

Dentre as nanopartículas de interesse, as nanoceluloses são extraídas de resíduos celulósicos, na forma nanocristalina ou nanofibrilada, podendo atuar como excelentes cargas de reforço em filmes biopoliméricos (Martelli-Tosi et al., 2018). A celulose é um biopolímero estrutural, da classe dos polissacarídeos, que ocorre naturalmente nas paredes celulares de plantas (Omran et al., 2021). Por causa da expressiva atividade agrícola no Brasil, muitos subprodutos celulósicos gerados podem ser utilizados como fonte de celulose, como é o caso do bagaço de cana-de-açúcar e da palhada de soja (Billato et al., 2020; Martelli-Tosi et al., 2018). As nanoceluloses compartilham algumas características com seu material de origem, como biodegradabilidade, biocompatibilidade e atoxicidade, além de apresentarem baixa densidade e excelente desempenho mecânico (Dufresne, 2013).

Os filmes biopoliméricos incorporados com nanoceluloses, ou quaisquer outras nanoestruturas, podem ser chamados de filmes nanocompósitos. Filmes nanocompósitos a base de gelatina podem ter, por exemplo, a resistência e rigidez consideravelmente aumentadas (Kwak et al., 2020), e ainda apresentarem melhoraria das propriedades de barreira à gases e vapores, pois as nanoceluloses são rígidas, impermeáveis e criam um caminho "tortuoso" na matriz biopolimérica (Fukuzumi et al., 2009; Ilyas et al., 2022).

A adição de compostos ativos com atividades antioxidante e antimicrobiana, por exemplo, em filmes a base de gelatina tem sido explorada para a valorização e aumento da funcionalidade desses materiais, produzindo os chamados filmes ativos (Bonilla; Sobral, 2016; Vargas-Torrico et al., 2023; Yan et al., 2021). Os filmes ativos, então, podem interagir com o alimento embalado e estender a vida de prateleira, pela redução das taxas das reações de oxidação dos alimentos e do crescimento de microrganismos, dentre outras atividades (Almeida et al., 2023; Luciano et al., 2022; Zhao et al., 2022). Os compostos ativos podem ser incorporados puros, no caso de produtos comerciais (Almeida et al., 2023), ou na forma de extratos vegetais (Vargas-Torrico et al., 2023).

Os extratos vegetais (caules, sementes e/ou folhas) são ricos em compostos fenólicos com atividades antioxidante e/ou antimicrobiana, e por isso, tem sido bastante empregados em estudos sobre o desenvolvimento de filmes biopolméricos

ativos. Esses extratos podem ser produzidos por diversas técnicas e empregando-se diversos solventes, como o metanol (que por ser tóxico, não é usado em estudos sobre alimentos), etanol, água e soluções hidroetanólicas, dentre outros (Ahmad et al., 2024; Bonilla; Sobral, 2016; Schumacher et al., 2015).

Um vegetal que tem ganho interesse em estudos sobre a produção de extratos vegetais é a pitangueira, que é uma árvore frutífera nativa do Brasil, cujas folhas são utilizadas há décadas para a produção de chá com propriedades anti-inflamatórias, que auxilia no tratamento dos sintomas de algumas doenças (Araujo et al., 2021; Fidelis et al., 2022). Os compostos fenólicos presentes no extrato de folhas de pitangueira são os responsáveis pelas suas excelentes propriedades biológicas (Lorenzo et al., 2018). O extrato hidroetanólico de folhas de pitangueiras (PLE), quando incorporado em filmes a base de gelatina, produz filmes ativos com excelentes atividades antioxidantes e antimicrobianas (Chakravaertula et al., 2020), e potencialmente aplicáveis como embalagens ativas de alimentos (Luciano et al., 2022).

Uma inovação interessante relacionada ao uso do PLE como fonte de compostos ativos para a produção de filmes ativos é a sua prévia encapsulação em emulsões do tipo água-em-óleo-em-água (A/O/A) (Tessaro et al., 2021). As emulsões A/O/A são sistemas coloidais multicompartimentados que podem encapsular o PLE na fase A interna, a fim de prevenir a degradação pelo oxigênio atmosférico e, consequentemente, a perda da sua atividade biológica (Rakshit; Srivastav; 2022).

As emulsões A/O/A são, basicamente, "emulsões de emulsões" (Dickinson, 2011). Elas são formadas, geralmente, pela dispersão de uma emulsão do tipo água-em-óleo (A/O) previamente preparada, cuja fase aquosa interna (A) está dispersa em uma fase lipídica dispersante (O), em uma fase aquosa externa dispersante (A) (Dima; Dima, 2020). A principal vantagem de se produzir emulsões A/O/A é a capacidade de encapsular compostos ativos aquosos na sua fase aquosa interna, como é o caso do PLE, e posteriormente poder ser dispersa em alimentos ou produtos alimentícios aquosos (He et al., 2023), como é o caso de filmes ativos a base de gelatina (Tessaro et al., 2021). A presença da emulsão A/O/A em filmes ativos pode, ainda, ocasionar melhorias de propriedades mecânicas e de barreira aos gases, vapores e luz, por exemplo (Yuan et al., 2022).

A produção de filmes ativos pela incorporação de emulsão A/O/A encapsulando um composto ativo aquoso é uma tecnologia bastante recente, e pouco explorada

(Tessaro et al., 2021; Yuan et al., 2022). Algumas propriedades desses filmes ainda não têm sido estudadas, nem o efeito do PLE sobre elas, como é o caso da permeabilidade aos gases. A permeabilidade aos gases (O_2 e CO_2) dos filmes ativos é um parâmetro fundamental a ser estudado, já que avalia a quantidade desses gases que permeiam através desses materiais e, consequentemente, a adequabilidade para aplicação em certos nichos de alimentos (Li et al., 2024). Por outro lado, esses filmes ativos podem atuar como liberadores de compostos ativos e desempenhar funções comestíveis quando produzidos com ingredientes no nível geralmente reconhecido como seguro (GRAS) (Liu et al., 2024; Vargas-Torrico et al., 2023). Além disso, considerando-se que na produção desses materiais foram utilizados produtos considerados GRAS, eles podem ser considerados como comestíveis. Assim, estudos sobre a digestão *in vitro* desses materiais podem elucidar se esses filmes ativos atuam, de fato, liberando o composto ativo encapsulado, e permitir estudar características como a biodisponibilidade e citotoxicidade (Giménez et al., 2013).

2 OBJETIVO GERAL E HIPÓTESE

2.1 OBJETIVO GERAL

O objetivo geral desta pesquisa foi estudar as propriedades de barreira a gases e a digestão *in vitro* de filmes e filmes nanocompósitos a base de gelatina, ou seja, sem e com carga de nanocelulose cristalina de palhada de soja (CN), respectivamente, e ativados com extrato de folha de pitangueira (*Eugenia uniflora* L.) (PLE) encapsulado em emulsão A/O/A e não encapsulado. Pretendeu-se continuar com as pesquisas conduzidas na dissertação de mestrado desta doutoranda, de forma que as formulações da emulsão A/O, A/O/A e dos filmes e filmes nanocompósitos corresponderam àquelas que foram escolhidas como as melhores, na referida dissertação. Pretendeu-se, ainda, complementar as pesquisas da dissertação, realizando-se experimentos necessários para se explicar alguns resultados obtidos.

Assim, os objetivos específicos desta tese foram:

I) Produzir filmes nanocompósitos a base de gelatina, quitosana ou blenda gelatina/quitosana ativados com a emulsão A/O/A encapsulando o PLE, e avaliar o efeito da CN e da emulsão A/O/A nas propriedades físico-químicas, funcionais, microestruturais e ativas, para melhor compreensão dos resultados obtidos previamente.

II) Produzir e caracterizar filmes e filmes nanocompósitos a base de gelatina com o PLE não encapsulado, e estudar as propriedades físico-químicas, funcionais, microestruturais e ativas. A gelatina foi escolhida como o biopolímero para dar continuidade nos estudos, com base nos resultados obtidos na pesquisa do Objetivo I. Este estudo foi importante para se verificar o efeito do PLE nas propriedades dos filmes e filmes nanocompósitos.

III) Estudar o efeito dos diferentes componentes nas propriedades de barreira aos gases O_2 e CO_2 dos filmes e filmes nanocompósitos a base de gelatina ativados com o PLE encapsulado na DE e não encapsulado.

IV) Estudar a digestão *in vitro* do PLE não encapsulado, das emulsões A/O e A/O/A encapsulando PLE e de filmes e filmes nanocompóstos ativados, a fim de se observar o efeito da encapsulação do PLE na sua bioacessibilidade e citotoxicidade.

2.2 HIPÓTESES

A hipótese desta tese é que filmes e filmes nanocompósitos a base de gelatina e quitosana, incorporados com nanoceluloses extraídas de palhada de soja e contendo extrato hidroetanólico de folha de pitangueira encapsulado em emulsão dupla podem apresentar boas propriedades de barreira ao O_2 e CO_2 e podem ser comestíveis.

3 DESCRIÇÃO DOS CAPÍTULOS

Esta tese é composta por cinco capítulos, sendo o Capítulo 1 escrito em português, e o restante em inglês, por terem sido publicados ou em processo de submissão, em revistas internacionais. Por estar neste formato, a tese contém ainda uma Introdução geral e uma Conclusão geral, ambas escritas em português.

Os cinco capítulos, acima referidos, são os seguintes:

Capítulo 1: Revisão bibliográfica.

Neste capítulo, se contextualizou os estudos realizados nesta tese sobre compostos ativos naturais, em particular os extratos vegetais, como é o caso do PLE, e o interesse de se fazer a encapsulação destes compostos ativos em emulsões A/O/A para a aplicação na área de alimentos, incluindo a produção de filmes ativos para eventuais aplicações como embalagens comestíveis de alimentos. Neste capítulo, os conceitos, produção e aplicações de compostos ativos, incluindo extratos vegetais, emulsões A/O e A/O/A, filmes biopoliméricos a base de gelatina sem e com carga de reforço, e de filmes ativos, foram abordados, incluindo as motivações para a realização deste estudo e considerações sobre a temática. Por fim, a importância de estudos sobre as propriedades de barreira a gases e de digestão *in vitro* de filmes ativos foi apresentada.

Uma revisão sobre filmes a base de gelatina, quitosana e blenda gelatina/quitosana foi realizada nesta tese por ter sido previamente realizada na dissertação de mestrado desta doutoranda.

Capítulo 2: Gelatin/chitosan-based films loaded with nanocellulose from soybean straw and activated with "Pitanga" (*Eugenia uniflora* L.) leaf hydroethanolic extract in W/O/W emulsion.

Este capítulo corresponde ao artigo publicado "Tessaro, L.; Lourenço, V.R.; Martelli-Tosi, M.; Sobral, P.J.A. Gelatin/chitosan based films loaded with nanocellulose from soybean straw and activated with "Pitanga" (*Eugenia uniflora* L.) leaf hydroethanolic extract in W/O/W emulsion. **International Journal of Biological Macromolecules**, v. 186, p. 328-340, 2021".

Neste capítulo, filmes nanocompósitos a base de gelatina, quitosana e blenda de gelatina/quitosana foram desenvolvidos com a adição de nanocelulose cristalina

extraída da palhada de soja, como carga de reforço, e ativados pela incorporação de emulsão A/O/A encapsulando o PLE. As propriedades físicas e funcionais dos filmes nanocompósitos, como sensibilidade à água, permeabilidade ao vapor de água, microestrutura, brilho, cor e opacidade, de barreira à luz UV/Vis, mecânicas, térmicas e biológicas (antioxidante e antimicrobiana), foram estudadas. Além disso, a nanocelulose cristalina foi caracterizada em relação à morfologia, potencial-ζ e rendimento. As propriedades das emulsões A/O e A/O/A foram previamente estudadas (Tessaro; Martelli-Tosi; Sobral, 2021; Tessaro et al., 2022), bem como as propriedades dos filmes a base de gelatina, quitosana e blenda gelatina/quitosana ativados pela incorporação da emulsão A/O/A encapsulando o PLE sem a incorporação de nanocelulose cristalina (Tessaro et al., 2021). Com base nos resultados apresentados neste capítulo, os filmes e filmes nanocompósitos a base de gelatina foram os escolhidos para dar continuidade à pesquisa.

Capítulo 3: Improving the properties of gelatin-based nanocomposite films by incorporation of "Pitanga" leaf extract and crystalline nanocellulose.

Este capítulo corresponde a um artigo recém submetido: Tessaro, L.; Pereira, A.G.R.; Martelli-Tosi, M.; Sobral, P.J.A. Improving the properties of gelatin-based nanocomposite films by incorporation of "Pitanga" leaf extract and crystalline nanocellulose. **Foods**, 2024.

Neste capítulo, as propriedades físicas e funcionais (sensibilidade à água, permeabilidade ao vapor de água, microestrutura, brilho, cor e opacidade, de barreira à luz UV/Vis, mecânicas, térmicas e antioxidante) dos filmes e filmes nanocompósitos a base de gelatina ativados pela incorporação PLE não encapsulado, foram estudadas. O PLE foi adicionado nos filmes e filmes nanocompósitos na mesma concentração do PLE na emulsão A/O/A. Esses filmes e filmes nanocompósitos foram desenvolvidos para se compreender melhor o efeito da encapsulação do PLE em emulsão A/O/A nas suas propriedades. Desta forma, foi avaliado como o PLE não encapsulado interage com a matriz biopolimérica de gelatina com e sem nanocelulose cristalina, e quais os efeitos resultantes destas interações.

Capítulo 4: Gas permeability of gelatin nanocomposite films and incorporated with "Pitanga" leaf extract encapsulated into double emulsion.

Capítulo correspondendo a um artigo submetido recentemente: Tessaro, L.; Benoso, P.; Lourenço, V.R.; Siracusa, V.; Dalla Rosa, M.; Sobral, P.J.A. Gas permeability of gelatin nanocomposite films and incorporated with "Pitanga" leaf extract encapsulated into double emulsion. **Food Packaging and Shelf Life**, 2024. Ele contém dados obtidos na Universidade de Bolonha, Cesena.

Sabendo que as embalagens de alimentos precisam, necessariamente, controlar de forma desejada a concentração de gases como o O_2 e o CO_2 em contato com o alimento embalado, as propriedades de barreira a gases dos filmes e filmes nanocompósitos a base de gelatina foram estudadas neste capítulo. Estudou-se o efeito de diferentes umidades relativas (0, 34, 59 e 76%) na taxa de transmissão dos gases O_2 e CO_2 através dos filmes e filmes nanocompósitos a base de gelatina incorporados com o PLE não encapsulado e encapsulado na emulsão A/O/A. As propriedades como microestrutura, cristalinidade, umidade e espessura também foram analisadas.

Capítulo 5: Gelatin-based nanocomposite films activated by double emulsion loaded with "Pitanga" leaf extract: bioaccessibility and cytotoxicity of emulsions and films after *in vitro* digestion.

Este capítulo corresponde ao artigo aceito para publicação, Tessaro, L.; Gonçalves, R.F.S.; Martins, J.T.; Pinheiro, A.C.; Vicente, A.A.; Sobral, P.J.A. Gelatin-based nanocomposite films activated by double emulsion loaded with "Pitanga" leaf extract: bioaccessibility and cytotoxicity of emulsions and films after *in vitro* digestion. **Food Hydrocolloids**, 2024. Ele apresenta dados obtidos durante o estágio sanduiche realizado na Universidade do Minho, de fevereiro a julho de 2023, sob a supervisão do Prof. Dr. António Vicente.

Um estudo sobre a digestão *in vitro* desses materiais foi realizado considerando-se que os filmes e filmes nanocompósitos a base de gelatina ativados com PLE não encapsulado e encapsulado na emulsão A/O/A foram produzidos com materiais GRAS provenientes de fontes renováveis e podem desempenhar funções comestíveis. Neste estudo, o efeito da encapsulação do PLE e adição das nanoceluloses cristalinas sobre a biodisponibilidade do PLE e citotoxicidade dos filmes após a digestão *in vitro* foi estudado. Como controle, o PLE não encapsulado, e as emulsões A/O e A/O/A também foram digeridos *in vitro*, e propriedades como tamanho

de partícula, potencial-ζ, morfologia e liberação de ácidos graxos livres foram estudadas.

4 CAPÍTULO 1: REVISÃO BIBLIOGRÁFICA

4.1 COMPOSTOS ATIVOS

Chamam-se compostos ativos, as substâncias que apresentam alguma atividade biológica, como atividade anti-inflamatória, antioxidante e antimicrobiana, dentre outras, sendo essas duas últimas, as mais interessantes na tecnologia de alimentos. Os compostos ativos naturais (CA) são produzidos naturalmente por animais e vegetais, podendo fazer parte da cadeia alimentar e ter algum efeito positivo na saúde humana (Biesalski et al., 2009). Além disso, os CA podem ser adicionados em produtos alimentícios, a fim de estender sua vida útil, como aditivos naturais (Ahmad et al., 2024; Parafati et al., 2023), ou podem ser utilizados para o desenvolvimento de alimentos funcionais e de maior valor nutricional (Biesalski et al., 2009; Moura et al., 2019).

Os CA são metabólitos secundários produzidos pelas plantas, como os compostos fenólicos (ex: terpenos fenólicos, ácidos hidroxinâmicos e derivados, flavonoides, entre outros) (Rubió; Motilva; Romero, 2013). Em particular, os compostos fenólicos estão abundantemente presentes nas plantas porque protegem as células vegetais da ação prejudicial da luz ultravioleta e da ação de microrganismos e pestes, facilitam a polinização por insetos (Ligor et al., 2018), e geralmente são os responsáveis pelas atividades antioxidante e antimicrobiana dos CA. Diversas partes das plantas são fontes de compostos fenólicos: polpa de frutas, sementes, folhas, caules, raízes, e cascas podem ser ricos em CA de alto valor (Ligor et al., 2018).

Quando incorporados em produtos alimentícios, os compostos fenólicos podem desempenhar ação antioxidante e antimicrobiana, atuando como conservantes naturais (Lorenzo et al., 2018; Vargas et al., 2019). Essa tecnologia é bastante interessante por atender às demandas dos novos hábitos alimentares que os consumidores têm criado. A preocupação destes para com a segurança dos alimentos e, ao mesmo tempo, a busca por alimentos considerados naturais e saudáveis tem aumentado (Kowalczyk et al., 2023). O uso de conservantes alimentícios sintéticos (ex: BHA, BHT, PG) têm perdido espaço na indústria de alimentos, pois a suspeita de toxicidade e riscos ocasionados à saúde está gerando uma pressão por parte dos

consumidores pela substituição destes aditivos por compostos naturais (Yuan et al., 2022).

A ação antioxidante dos compostos fenólicos está relacionada com a sua estrutura: eles são compostos orgânicos com um ou mais grupos hidroxilas (OH) ligados a um anel fenil (Papuc et al., 2017), atuando assim, principalmente, como redutores e eliminadores de espécies reativas ao oxigênio (Santos et al., 2023). Geralmente, as espécies reativas ao oxigênio são radicais livres (ex: HO$^{\bullet}$, O2$^{\bullet-}$, ROO$^{\bullet}$, RO$^{\bullet}$ e NO$^{\bullet}$), não radicais (H_2O_2, HOCl, O_3) e íons de metais de transição (ex: Fe^{2+}, Cu^+), que são formados, principalmente, em alimentos ricos em lipídios contendo ácidos graxos insaturados, durante o armazenamento e exposição à luz. Os radicais livres atuam danificando os lipídeos, vitaminas e proteínas, diminuindo o valor nutricional, aceitabilidade sensorial e segurança desses alimentos (Papuc et al., 2017; Stoll et al., 2019). Os compostos fenólicos podem agir eliminando o radical livre (R$^{\bullet}$) por transferência do átomo de hidrogênio (H) do seu grupo OH(s) ativo para o R$^{\bullet}$ (Figura 4.1) (Di Meo et al., 2013).

Figura 4.1 - Mecanismo de eliminação de radicais livres por transferência de átomo de H

Transferência de átomo de H e elétrons acoplados a prótons

Ar – O$\bullet\bullet$H → Ar – O$\bullet$ + H$\bullet$
R$\bullet$ + H$\bullet$ → R + H

Transferência de elétron – transferência de próton

Ar – OH + R$\bullet$ → Ar – OH$^{\bullet+}$ + R$^-$
Ar – OH$^{\bullet+}$ + R$^-$ → Ar – O$\bullet$ + RH

Eliminação do R$\bullet$ pela transferência de átomo de H

Perda de próton seguida por transferência de elétron (condições alcalinas)

Ar – OH → Ar – O$\bullet$ + H$^+$
Ar – O$^-$ + R$\bullet$ → Ar – O$\bullet$ + R$^-$
R$^-$ + H$^+$ → RH

Formação de aduto (Soluções radiolíticas)

Ar – OH + R$\bullet$ → [Ar – OH + R]$\bullet$
[Ar – OH + R]$\bullet$ → Ar – O$\bullet$ + R-H
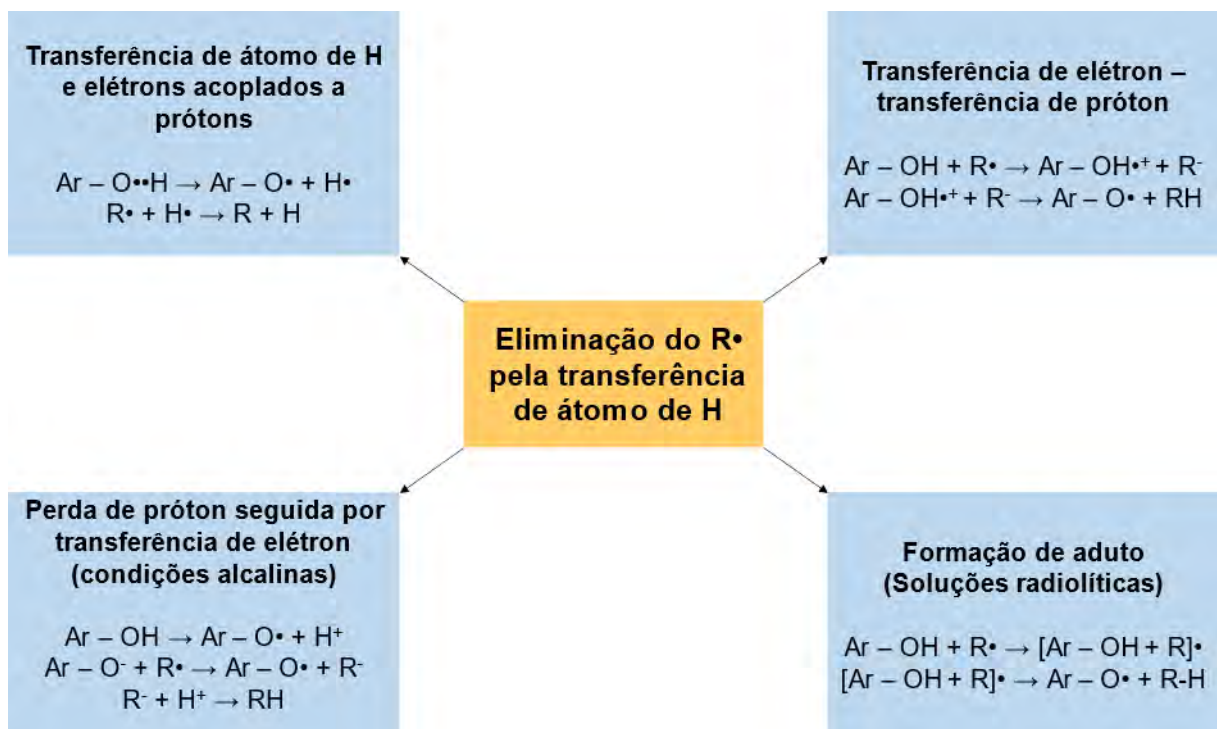
*Ar – OH: polifenol

Fonte: Modificado de Di Meo et al. (2013) e Papuc et al. (2017).

Já em relação à atividade antimicrobiana dos compostos fenólicos, considera-se que os grupos OH dos polifenóis são capazes de interagir com a parede celular dos microrganismos por interações de hidrogênio (Chibane et al., 2019; Efenberger-Zsmechtyk; Nowak; Czyzowska, 2021). Essa interação rompe a parede celular do microrganismo e libera o conteúdo celular, ou promove a deslocalização de elétrons, resultando na despolarização da parede celular (que atua como trocadores de prótons), que afeta a força motora do próton e reduz o gradiente de pH através da parede celular (Chibane et al., 2019), podendo ocasionar a morte celular.

Os CAs podem ser encontrados purificados, ou seja, produzidos industrialmente, e que normalmente, são de alto valor agregado. Mas, eles podem ser produzidos como extratos vegetais utilizando-se diversas técnicas. As mais comuns incluem o uso de solventes extratores, como metanol e acetona (Schumacher et al., 2015), água (Prommachart et al., 2020; Vargas et al., 2016), etanol (Bonilla; Sobral, 2016), soluções hidroetanólicas (Ahmad et al., 2024; Lorenzo et al., 2018; Vargas et al., 2019). Entretanto, o uso de solventes nocivos, como o metanol, não é recomendado para a aplicação em produtos alimentícios. Estudos recentes têm demonstrado que extratos de plantas ricos em compostos fenólicos podem aumentar a estabilidade química e microbiológica de diversos tipos de alimentos (Tabela 4.1).

Apesar de apresentarem resultados promissores na conservação de diversos alimentos, a aplicação direta de extratos de plantas em alimentos tem algumas limitações. Os compostos fenólicos, por exemplo, são altamente instáveis e podem perder sua atividade biológica devido às mudanças nas condições ambientais e gastrointestinais (Rakshit e Srivastav, 2022). A aplicação direta em alimentos pode, ainda, alterar os atributos sensoriais, o que pode afetar negativamente a aceitação pelos consumidores. A encapsulação dos CA por meio de emulsificação, por exemplo, pode ser utilizada para contornar essas limitações e garantir a preservação das atividades biológicas e eventuais alterações no sabor dos alimentos (Pimentel-Moral et al., 2018).

Tabela 4.1 – Exemplos de estudos sobre a aplicação de extratos de plantas como antioxidantes e conservantes naturais de alimentos

Fonte vegetal	Método de extração	Compostos ativos	Aplicação	Ação	Resultados	Referências
Arroz negro	Aquoso	Polifenóis e antocianinas	Hamburgueres de carne	Antioxidante e antimicrobiana	Reduziu a oxidação lipídica e crescimento de bactérias mesófilas	Prommachart et al. (2020)
Folhas de Arônia (*Aronia melanocarpa*)	Aquoso	Ácidos fenólicos, quercetina e flavonóides	Hamburgueres de carne	Antioxidante	Retardou a oxidação lipídica e preservou a textura	Kowalczyk et al. (2023)
Folhas de *Barringtonia acutangula*	Hidroetanólico 40, 60 e 80%	Ácidos fenólicos, flavonoides e taninos	Camarão branco do Pacífico	Antioxidante e antimicrobiana	Retardou a oxidação lipídica e diminuiu a contagem de *Pseudomonas* e Enterobactérias	Ahmad et al. (2024)
Folhas de pitangueira (*Eugenia uniflora* L.)	Hidroetanólico 60%	Ácidos hidroxicinâmicos e tirosois	Hamburgueres suínos	Antioxidante e antimicrobiana	Controlou o crescimento de bactérias viáveis totais e de bactérias láticas, e reduziu a oxidação lipídica e proteica	Lorenzo et al. (2018)
Folhas de pitangueira *Eugenia uniflora* L.)	Hidroetanólico 60%	Miricitrina, quercetina e ácido quínico	Óleo de canola	Antioxidante	Diminuição da oxidação lipídica, em proporções comparáveis à ação do BHT	Vargas et al. (2019)
Folhas jovens de manga (*Mangifera indica* L.)	Aquoso	Benzofenonas e xantona mangiferina	Queijo mussarela	Antioxidante e antimicrobiana	Diminuiu a contagem de *Staphylococcus* ssp.	Parafati et al. (2023)
Polpa de pitaia vermelha (*Hylocereus monacanthus*)	Aquoso	Polifenóis e betacianina	Risoles suínos	Antioxidante	Inibiu a oxidação lipídica e proteica, e melhorou as propriedades sensoriais	Bellucci et al. (2021)

Fonte: Própria autoria.

4.1.1 Extrato de folhas de pitangueira (*Eugenia uniflora* L.)

A pitangueira (*Eugenia uniflora* L.) é uma árvore frutífera (Figura 4.2a), pertencente à família Myrtaceae, nativa da mata atlântica, e largamente cultivada nos países da América do Sul, como o Brasil (Meira et al., 2020; Sobeh et al., 2019), além de já ser cultivada praticamente em todo o mundo (Sobeh et al., 2019). Os frutos comestíveis da pitangueira, conhecidos como pitangas, possuem o tamanho de uma cereja, sabor agridoce, e coloração que varia entre amarela, laranja, vermelha e roxa (Figura 4.2b) (Tambara et al., 2018). As pitangas possuem valor econômico no Brasil, sendo utilizadas para a produção de sucos, polpas, compotas, sorvetes, geleias, vinhos e licores (Costa et al., 2013; Ramalho et al., 2019). A pitanga possui elevador teor de compostos fenólicos e carotenoides (Ramalho et al., 2019), o que torna o seu consumo altamente recomendado para auxílio na prevenção de vários tipos de doenças.

Figura 4.2 – Fotografias a) de parte da pitangueira e b) dos diferentes estágios de maturação das pitangas
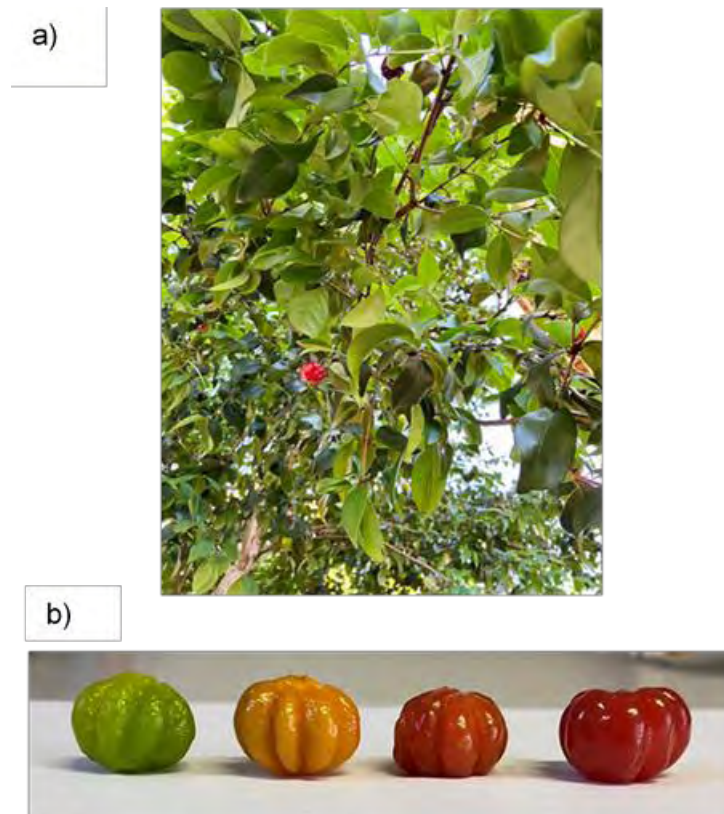
Fonte: Própria autoria.

Embora a pitanga seja a parte da pitangueira de maior interesse, devido ao seu valor econômico, as folhas de pitangueira também são uma excelente fonte de CA (Cunha et al., 2016; Bezerra et al., 2020; Lorenzo et al., 2018; Meira et al., 2020; Sobeh et al., 2019). Certamente por isso, o chá de folhas de pitangueira é usado na medicina popular no auxílio de tratamento de diversas doenças e sintomas, como hipertensão, diabetes, febre, gota, artrite reumatoide, entre outras (Arai et al., 1999; Consolini; Sarubbio, 2002; Sobeh et al., 2019). Além disso, os extratos das folhas de pitangueira apresentam atividades biológicas, como as atividades antioxidante, antibacteriana, antifúngica e/ou anti-inflamatória, e até mesmo ação antiofídica, dependendo do solvente ou método de extração utilizado (Daniele-Silva et al., 2024; Lorenzo et al., 2018; Santos et al., 2023; Tessaro et al., 2021). Quando utilizados como compostos anti-inflamatórios, os extratos de folhas de pitangueira podem auxiliar na prevenção de doenças, como as renais (Meira et al., 2020), e não têm apresentado efeito citotóxico ou genotóxico sobre as células sanguíneas humanas (Cunha et al., 2016). A maioria dos compostos fenólicos encontrados nesse CA são flavonoides (ex: miricetina, flavonas, catequina), ácidos hidroxibenzoicos (ex: ácido gálico e tirosol) e ácidos hidroxicinâmicos (ex: ácido ferúlico) (Bezerra et al., 2018; Lorenzo et al., 2018).

Em particular, o PLE (Lorenzo et al., 2018; Tessaro et al., 2021; Vargas et al., 2019) tem apresentado atividade antioxidante e teor de polifenóis semelhantes (Martinez-Correa et al., 2011) ou superiores (Canabarro et al., 2019) a de extratos de folhas de pitangueira extraídos com fluídos supercríticos, e superiores à de extratos de folhas de pitangueira produzidos com água, etanol puro ou metanol/acetona (Schumacher et al., 2015). Lorenzo et al. (2018) analisaram um PLE produzido com solução hidroetanólica a 60%, por cromatografia acoplada a espectrometria de massas (UHPLC-ESI-QTOF-MS), e identificaram cerca de 160 tipos de polifenóis, sendo os ácidos hidroxicinâmicos e flavonoides, os mais abundantes.

O PLE já foi aplicado como antioxidante e antimicrobiano em hamburgueres suínos (Lorenzo et al., 2018; Rocchetti et al., 2020) e de carneiro (Carvalho et al., 2019), como antioxidante em óleo de canola (Vargas et al., 2019), como CA aquoso encapsulado em emulsões água-em-óleo (A/O) (Tessaro; Martelli-Tosi; Sobral, 2021b) e água-em-óleo-em-água (A/O/A) (Tessaro et al., 2022), e como aditivo para a produção de filmes ativos (Luciano et al., 2021; Chakravartula et al., 2020; Tessaro et al., 2021) e embalagens ativas de copa curada (Luciano et al., 2022), apresentando resultados promissores.

4.2 EMULSÕES

As emulsões são sistemas coloidais formados por dois líquidos imiscíveis, geralmente água e óleo, e podem ser classificadas de acordo com a distribuição espacial da fase aquosa e da fase lipídica (McClements, 2004). Dependendo dos constituintes e da distribuição relativa das fases dispersa e dispersante, as emulsões podem ser denominadas como simples (bifásicas) ou duplas (múltiplas).

Como as emulsões são sistemas coloidais termodinamicamente instáveis, nas quais podem ocorrer processos físicos de desestabilização, como coalescência, cremeação, sedimentação, floculação, separação ou inversão de fases (Han et al., 2022) (Figura 4.3), o uso de emulsificantes é indispensável para a estabilização desses sistemas. Além disso, os emulsificantes afetam a formação das gotas da fase dispersa e as características do produto final (McClements, 2004).

Figura 4.3 - Exemplos de processos físicos de desestabilização de emulsões
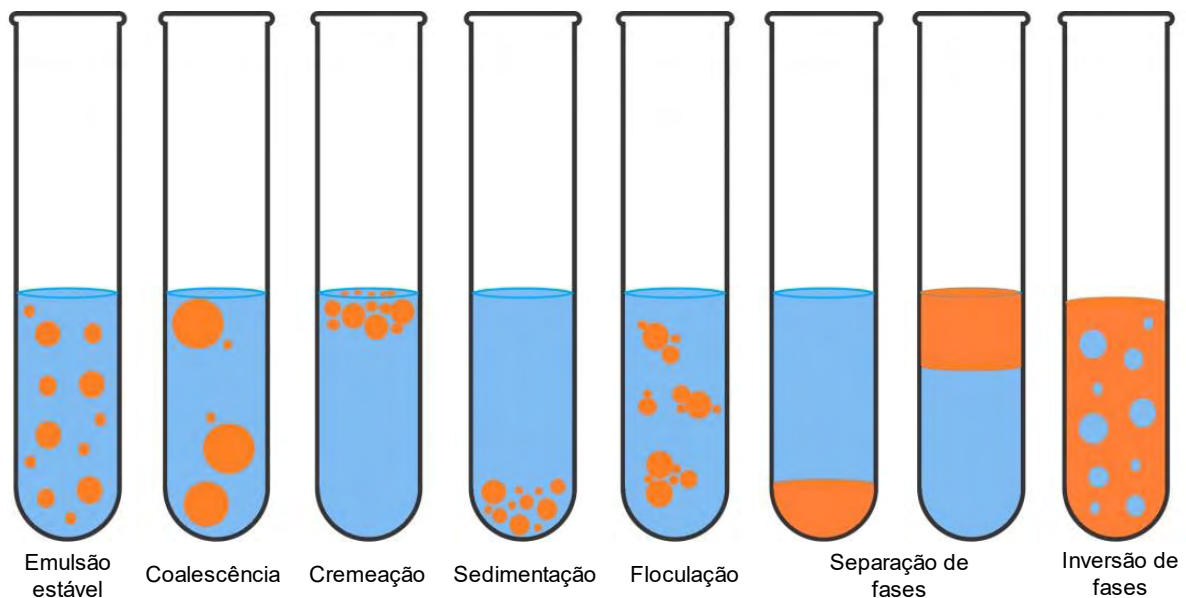
Fonte: Própria autoria.

Os emulsificantes, como os tensoativos de baixo peso molecular (ex: Tweens e Spans), e até mesmo biopolímeros (ex: proteínas e polissacarídeos), são moléculas de caráter anfifílico, que interagem com ambas as fases, dispersa e dispersante, de uma emulsão, promovendo a redução da tensão interfacial entre elas e, consequentemente, aumentando a estabilidade do sistema (Dima; Dima, 2020).

Os emulsificantes podem ter caráter lipofílicos ou hidrofílicos. Os emulsificantes lipofílicos são predominantemente hidrofóbicos, possuem valores baixos de balanço hidrofílico-lipofílico (HBL, 1 a 9) e, portanto, são incorporados na fase lipídica da emulsão (Muschiolik; Dickinson, 2017). Já os emulsificantes hidrofílicos possuem elevado valor de HBL (11 a 20), e são incorporados na fase aquosa das emulsões (Muschiolik; Dickinson, 2017).

Diversos alimentos são constituídos parcialmente ou totalmente de emulsões, como o leite, bebidas de frutas, sopas, massas de bolo, molhos para salada, maionese, margarina, sorvete, entre outros (McClements, 2004). Emulsões bastante estáveis têm sido desenvolvidas para promoverem uma proteção para CA (naturais ou sintetizados) e controlar a liberação de drogas, por exemplo (Kitaoka, Nguyen e Goto, 2021; Han et al., 2022). Desta forma, as emulsões podem desempenhar um papel importante em diversos setores da indústria, principalmente nas indústrias de alimentos, cosmética e farmacêutica.

4.2.1 Emulsões água-em-óleo (A/O)

Uma emulsão simples, na qual pequenas gotas de água estão dispersas em uma fase lipídica dispersante, é chamada de emulsão água-em-óleo (A/O) (Figura 4.4) (McClements, 2004). Os emulsificantes utilizados nestes sistemas são, geralmente, incorporados na fase lipídica dispersante, mas também podem ser adicionados em ambas as fases (Ye et al., 2020).

A emulsificação de emulsões A/O, portanto, consiste na dissolução prévia de um emulsificante lipofílico na fase lipídica dispersa, seguida da incorporação gradual da fase aquosa com a ajuda de algum processo de homogeneização com intensidade moderada (Tessaro, Martelli-Tosi; Sobral, 2021). Tensoativos lipofílicos de baixo peso molecular, como ésteres de sorbitano (Spans), derivados de silicone (ex: cetil dimeticona), lecitina (Ye et al., 2020; Rivas; Schneider; Rohm, 2016), e polirricinoleato de poliglicerol (PGPR), por exemplo, podem ser utilizados como emulsificantes na produção das emulsões A/O. O PGPR é um dos mais utilizados na produção de emulsões A/O, sendo considerado como um emulsificante de elevada eficiência na estabilização (Iqbal et al., 2022; Moura et al., 2019; Tessaro; Martelli-Tosi; Sobral, 2021; Zhang et al., 2022).

Figura 4.4 – Esquema da estrutura de uma emulsão A/O

Composto hidrofílico

Fase aquosa

Emulsificante lipofílico

Fase lipídica

Fonte: Modificado de Salvia-Trujillo et al. (2018)

O PGPR é um emulsificante oligomérico e não iônico (Figura 4.5a), produzido pela esterificação do ácido graxo do óleo de rícino (Figura 4.5b) com o poliglicerol (Ushikubo; Cunha, 2014). Ele é um emulsificante bastante conhecido por ser utilizado na produção de chocolate (Fraj et al., 2017), e é insolúvel em água, mas solúvel em óleos minerais e vegetais (Ushikubo; Cunha, 2014). Mesmo em baixas concentrações (~ 3% m/m), é capaz de auxiliar na formação de emulsões A/O altamente estáveis (Tessaro; Martelli-Tosi; Sobral, 2021).

Figura 4.5 – a) Estrutura química do PGPR, sendo R um hidrogênio, ácido ricinoleico ou ácido poliricinoleico e b) estrutura química do ácido ricinoleico

Fonte: Própria autoria.

No caso de emulsões A/O encapsulando CA, é possível que alguns compostos fenólicos permaneçam na interface das fases aquosa e lipídica, contribuindo para a diminuição da tensão interfacial (Tessaro; Martelli-Tosi; Sobral, 2021; Velderrain-Rodríguez et al., 2019). Isto ocorre, possivelmente, porque os grupos hidroxilas dos polifenóis podem interagir tanto com a cabeça apolar do emulsificante lipofílico presente na fase lipídica, quanto com as moléculas polares da fase aquosa (Figura

4.6) (Shishikura; Khokhar; Murray, 2006). Desta forma, os CA podem contribuir para o aumento da estabilidade física desses sistemas.

Figura 4.6 - Micrografia da interface água-óleo da gota de uma emulsão A/O contendo EHFP e corante rodamina B na fase aquosa interna

Fonte: Tessaro, Martelli-Tosi e Sobral (2021)

Por outro lado, os processos de homogeneização envolvem, por exemplo, homogeneizadores de ultra agitação, homogeneizadores de alta pressão, homogeneizadores ultrassônicos, agitadores mecânicos, ou uma combinação de dois ou mais processos de homogeneização, como, por exemplo, a utilização de um homogeneizador de ultra agitação, seguido de um homogeneizador ultrassônico (Iqbal et al., 2022; Mohammad et al. (2018); Tessaro; Martelli-Tosi; Sobral, 2021; Ye et al., 2022). Além de promoverem a emulsificação, esses homogeneizadores, principalmente os de alta pressão e ultrassônicos, são utilizados para reduzir substancialmente o tamanho das gotas formadas na emulsão (Muschiolik; Dickinson, 2017). A homogeneização de baixa intensidade, como a emulsificação por membrana, também pode ser utilizada na produção de emulsões A/O (Wang et al., 2022).

Na indústria de alimentos, as emulsões A/O são utilizadas para o desenvolvimento de produtos sólidos ou pastosos, como margarina e manteiga

(Ushukubo; Cunha, 2014). Entretanto, outras aplicações de emulsões A/O fluídas têm sido estudadas (Tabela 4.2). Especificamente no caso de emulsões A/O desenvolvidas para encapsular CA aquosos, ou substâncias aquosas ricas em CA, a estabilidade pode ser um fator eminente.

4.2.2 Emulsões água-em-óleo-em-água (A/O/A)

Quando uma emulsão dupla é formada pela dispersão de uma emulsão A/O, previamente formada, em uma fase aquosa externa dispersante, ela é chamada de emulsão água-em-óleo-em-água (A/O/A) (Figura 4.7) (Dickinson, 2011). Como esses sistemas são multi-compartimentados, sua formação e estabilização são mais difíceis em comparação às emulsões simples. Emulsões A/O/A, portanto, necessitam de dois tipos de emulsificantes para sua estabilização: lipofílicos e hidrofílicos (Dickinson, 2011).

Figura 4.7 - Esquema da estrutura de uma emulsão A/O/A
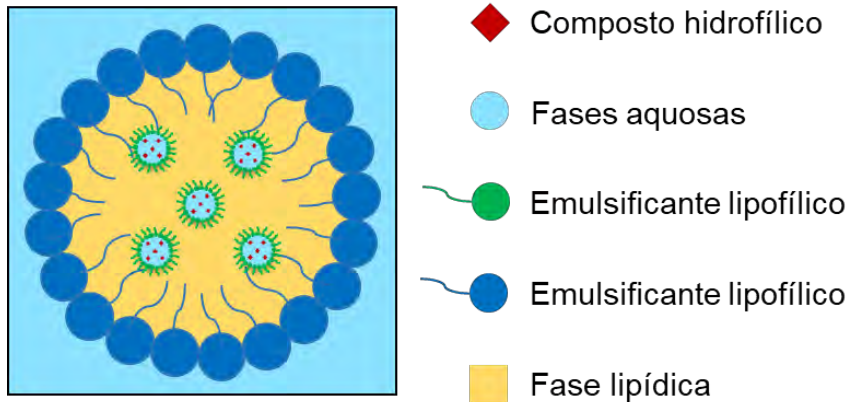
Fonte: Modificado de Salvia-Trujillo et al. (2018)

Tabela 4.2 – Exemplos de estudos sobre a aplicação de emulsões A/O

Fase aquosa (A)	Fase lipídica (O)	Emulsificante na interface A/O	Objetivo	Referência
Água destilada e epigalocatequina-3-galato	Óleo de soja	Ácido oleanólico	Produzir emulsões Pickering A/O com liberação controlada e proteção do composto ativo encapsulado	Liu et al. (2024)
Água destilada e nicotinamida	Esqualano	Monoleína na fase	Formulação para entrega transdérmica de nicotinamida	Kitaoka, Nguyen e Goto (2021)
Água destilada, glicerol, Tween 80 e polifenóis de chá	Óleo de uva	Zeína e Span 80	Produzir emulsões A/O com baixa toxicidade e potencial aplicação na indústria farmacêutica e de alimentos	Ye et al. (2020)
Água ou solução aquosa de sacarose	Manteiga de cacau	PGPR* e lecitina	Criar emulsões A/O estáveis para substituir a gordura de bebidas de chocolate	Mazo Rivas, Schneider e Rohm (2016)
Extrato aquoso de casca de *Prosopis cineraria* (EAPC)	Óleo de parafina	ABIL® EM 90** e cera de abelha	Produzir um creme estável contendo EAPC que pode ser utilizado como coméstico	Mohammad et al. (2018)
Extrato hidroetanólico de folha de pitangueira (EHFP)	Óleo de soja	PGPR*	Encapsular e proteger do EHFP rico em compostos ativos	Tessaro, Martelli-Tosi e Sobral (2021)
Solução aquosa de NaCl e éteres de celulose	Óleo de soja	PGPR*	Produzir emulsões A/O com digestibilidade lipídica reduzida	Iqbal et al. (2022)
Solução salina ou leite desnatado com *Bifidobacterium*	Cera de abelha e óleo de milho	PGPR*	Criar um sistema de encapsulação e proteção de probióticos para aplicação em alimentos com baixo teor de gordura	Zhang et al., (2022)

*PGPR: polirricinoleato de poliglicerol. **ABIL® EM 90: Cetil PEG/PPG-10/1 Dimeticona.

Fonte: Própria autoria.

Geralmente, as emulsões A/O/A são preparadas em dois estágios de emulsificação: no primeiro estágio, a emulsificação da emulsão A/O é realizada, conforme descrito na seção 4.3.1, utilizando-se um emulsificante lipofílico na fase lipídica dispersante. O segundo estágio consiste, então, na incorporação gradual da emulsão A/O previamente formada em uma fase aquosa externa dispersante contendo emulsificante(s) hidrofílico(s), com a ajuda de algum processo de homogeneização de menor intensidade em comparação à intensidade do processo de produção da emulsão A/O (Dima; Dima, 2020; Huang; Zhou, 2019; Tessaro et al., 2022). Assim, como para as emulsões A/O, os homogeneizadores empregados no processo de homogeneização das emulsões A/O/A podem ser homogeneizadores de alta pressão, ultrassônicos, ultra agitação, agitação mecânica (Han et al., 2022; He et al., 2023; Huang; Zhou, 2019; Pimentel-Moral et al., 2018), ou a combinação de dois ou mais processos de homogeneização, como agitação mecânica e homogeneizador ultrassônico (Tessaro et al., 2022), ou homogeneização de baixa intensidade (Berendsen; Güell; Ferrando, 2015).

Especificamente para o caso das emulsões A/O/A produzidas em dois estágios, a escolha dos emulsificantes é um fator determinante para garantir a estabilidade de cada emulsão independente. Para estabilizar as gotas formadas na segunda emulsificação, são utilizados emulsificantes hidrofílicos na fase aquosa externa. Esses emulsificantes são, geralmente, tensoativos de baixo peso molecular, como os polisorbatos (Tweens) e a lecitina (Han et al., 2022; Šipailiene et al., 2022; Velderrain-Rodríguez et al., 2019), os biopolímeros, como a quitosana, a pectina e a goma arábica (Huang; Zhou, 2019; Moura et al., 2019), a mistura de biopolímeros, como a goma arábica, o alginato de sódio e a quitosana (Dima; Dima, 2020); o amido modificado e a k-carragena (He et al., 2022), e a proteína isolada de soro de leite e o glucomanano (Zhuang et al., 2023).

A mistura de tensoativos de baixo peso molecular e biopolímeros na fase aquosa externa de uma emulsão A/O/A também pode ser utilizada para a estabilização desse tipo de emulsão, como misturas de Tween 80 e caseinato de sódio (Tessaro et al., 2022), Tween 20 e caseinato de sódio, e Tween 80 e alginato de sódio (Šipailiene et al., 2022), entre outras. Especificamente no caso de misturas de Tweens e caseinato de sódio, Su e Zhong (2016) demonstraram que emulsões O/A estabilizadas com uma mistura de Tween 20 ou Tween 80 e caseinato de sódio na

fase aquosa dispersa, foram mais estáveis do que emulsões O/A estabilizadas somente com Tween 20, Tween 80 ou caseinato de sódio, individualmente.

Os tensoativos de baixo peso molecular podem se ligar aos biopolímeros por meio de ligações eletrostáticas e/ou hidrofóbicas, e aumentar a atividade de superfície desse complexo (McClements; Jafari, 2018), aumentando, assim, a estabilidade de emulsões do tipo O/A ou A/O/A. Além disso, os tensoativos de baixo peso molecular possuem a capacidade de se adsorver rapidamente na interface água-óleo, mas não causam repulsões eletrostáticas entre duas camadas interfaciais, ao passo que os biopolímeros causam essas repulsões, mas se adsorvem lentamente na camada interfacial. As interações repulsivas formadas entre uma camada interfacial de uma gota e outra (Figura 4.8) evitam a agregação das gotas, e a rápida adsorção do emulsificante na camada interfacial diminui o tamanho das gotas (McClements; Jafari, 2018). Assim, mistura de tensoativos de baixo peso molecular e biopolímeros pode ser interessante na estabilização de emulsões A/O/A.

Figura 4.8 – Esquema da interação
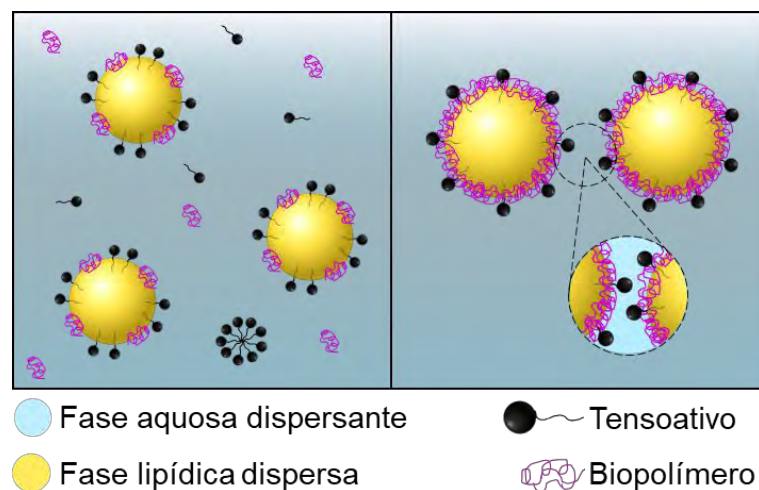
Fonte: Modificado de McClements e Jafari (2018)

Em particular, o Tween 80 é um tensoativo de baixo peso molecular semi-sintético, não iônico, solúvel em água (Figura 4.9a), e que pode ser utilizado em produtos alimentícios dentro dos níveis aprovados, geralmente de até 1% (Huang et al., 2024). E, o caseinato de sódio (Figura 4.9b), proteína obtida pela acidificação da caseína e posterior neutralização com hidróxido de sódio, é composta por frações conhecidas como α_{s1}, α_{s2}, β e κ-caseínas (Ma; Chatterton, 2021). A atividade de

superfície do caseinato de sódio origina-se da elevada quantidade de aminoácidos hidrofóbicos (ex: prolina, tirosina e triptofano), que tornam as caseínas copolímeros de blocos anfifílicos (Su; Zhong, 2016). A estrutura do caseinato de sódio, adsorvido nas gotículas de óleo, assume conformações que fornecem repulsão estérica, juntamente com a repulsão eletrostática, evitando a aglomeração entre as gotículas de óleo (Surk; Decker; McClements, 2006).

Figura 4.9 – Estrutura química a) do Tween 80 e b) do caseinato de sódio
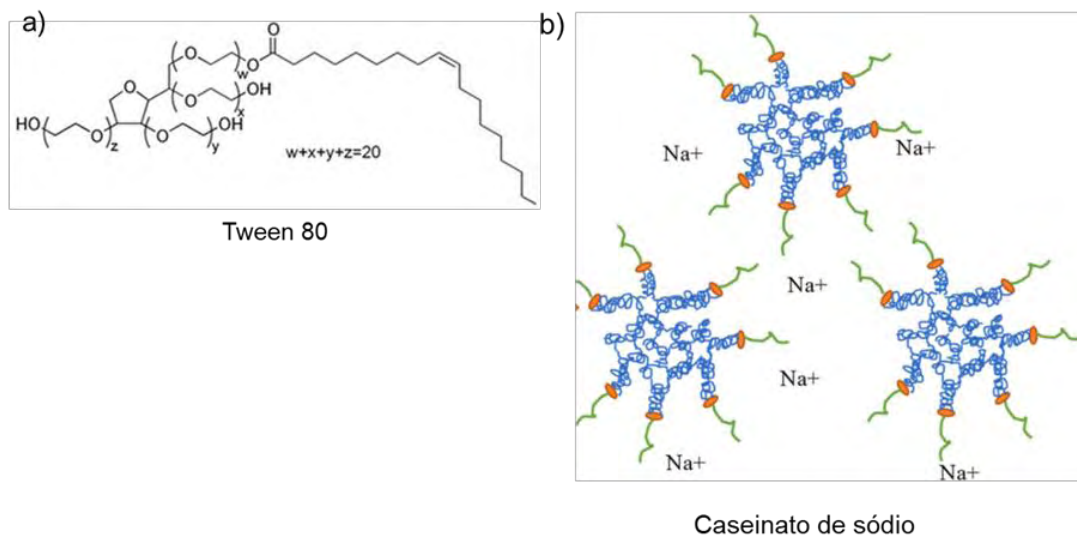
Fonte: Modificado de Ma e Chatterton (2021)

Emulsões A/O/A estáveis possuem algumas vantagens de aplicação em relação às emulsões simples O/A, pois a fase aquosa interna pode ser utilizada como um carregador e/ou protetor de componentes aquosos, como CA aquosos (McClements; Jafari, 2018), e reduzirem eventuais gostos e aromas indesejáveis desses compostos. Por possuírem duas interfaces, A/O e (A/O)/A, comparadas à uma única interface de emulsões simples O/A (Huang; Zhou, 2019), elas podem encapsular compostos hidrofílicos na fase aquosa interna, e controlar a liberação em condições gastrointestinais (Han et al., 2022; He et al., 2023). Podem, ainda, ser mais facilmente incorporadas em matrizes aquosas. Desta forma, as emulsões A/O/A podem ser aplicadas em indústria de alimentos, cosmética e farmacêutica (Tabela 4.3). As emulsões A/O/A podem ser utilizadas para o desenvolvimento de alimentos funcionais e enriquecidos (Dima; Dima, 2020), ou produção de filmes ativos (Tessaro et al., 2021; Yuan et al., 2022), sendo o último, uma tecnologia recente e pouco explorada.

Tabela 4.3 – Exemplos de estudos sobre a aplicação de emulsões A/O/A

Emulsificante da interface A/O	Emulsificante da interface (A/O)/A	Componente encapsulado na fase aquosa interna	Objetivo	Referência
Span 80, lecitina e alginato de sódio	Goma arábica, alginato de sódio e quitosana	Cálcio (e vitamina D_3 na fase lipídica)	Aumentar a biodisponibilidade de cálcio e vitamina D_3 para aplicação em alimentos funcionais e novas drogas	Dima e Dima (2020)
PGPR e pectina	Amido modificado e k-carragena	Capsaicina	Encapsular e aumentar a bioacessibilidade da capsaicina, diminuindo o efeito irritativo gastrointestinal	He et al. (2023)
PGPR	Pectina	Extrato aquoso de hibisco (EAH)	Encapsular o EAH e produzir um iogurte funcional	Moura et al. (2019)
PGPR*	Tween 80 e caseinato de sódio	Extrato hidroetanólico de folha de pitangueira	Produzir filmes ativos a base de gelatina e/ou quitosana para aplicação como embalagens ativas	Tessaro et al. (2021b, 2021c)
ViscOptima™ SE	ViscOptima™ SE	Extratos de folha de alecrim, grãos de aveia e mucilagem de linhaça	Produzir produtos cosméticos ou farmacêuticos seguros e de alta qualidade final	Zlabiene et al., (2021)
Dioleato de Poligliceril-6 (PGD)	laurato de poligliceril-10 (PGL)	Nisina (e carvacrol como fase lipídica)	Aumentar a estabilidade dos compostos ativos encapsulados e produzir embalagens ativas a base de quitosana para carne de peixe fresco	Yuan et al. (2022)
Lecitina, Tween 80 e goma arábica	Tween 80 e alginato	Probiótico, manitol ou trealose (e extrato de bagaço de espinheiro na fase lipídica)	Proteger os probióticos e controlar a liberação dos mesmos	Šipailiene et al. (2022)
PGPR	Proteína de feijão preto, Tween 80, lecitina ou pectina	Solução de insulina bovina (e quercetina na fase lipídica)	Produzir um sistema de liberação eficiente de insulina e quercetina em condições gastrointestinais	Han et al. (2022)

*PGPR: polirricinoleato de poliglicerol.

Fonte: Própria autoria.

4.3 FILMES BIOPOLIMÉRICOS

Os filmes biopoliméricos são materiais finos e flexíveis produzidos por via seca ou por via úmida, que consiste na secagem de uma dispersão de biopolímero contendo plastificante (Sobral et al., 2001). Os filmes biopoliméricos podem ser uma alternativa para a redução ou a substituição do uso de filmes a base de polímeros sintéticos, que são derivados do petróleo, não são biodegradáveis e causam um impacto ambiental considerável (Li et al., 2024; Vargas-Torrico et al., 2024). Por isso, eles possuem potencial aplicação na indústria de alimentos, na forma de embalagens e coberturas biopoliméricas (Almeida et al., 2023; Luciano et al., 2022), e até mesmo na área biomédica, na forma de curativos tópicos (Voss et al., 2020).

Especificamente para a aplicação na indústria de alimentos, filmes biopoliméricos a base de proteínas, como a gelatina (Luciano et al., 2021), o caseinato de sódio (Yoplac; Hidalgo; Vargas, 2022), a proteína de soja (Martelli-Tosi et al., 2018), entre outros, e a base de polissacarídeos, como a quitosana (Esposto et al., 2024; Iaccheri et al., 2023), o amido (Iaccheri et al., 2023), e a pectina (Lin et al., 2023), entre outros, têm sido desenvolvidos e caracterizados. Além disso, as blendas biopoliméricas também podem ser empregadas, como blendas a base de gelatina/quitosana (Tessaro et al., 2021), gelatina/amido (Malherbi et al., 2019), quitosana/amido (Iaccheri et al., 2023), pectina/quitosana (Lin et al., 2023), entre outras. Vários biopolímeros extraídos de diversas fontes naturais (ex: plantas, animais ou microrganismos), podem ser utilizados para a produção de filmes biopoliméricos (Figura 4.10).

Para a produção dos filmes biopoliméricos por via úmida, são necessários, basicamente, três componentes: biopolímero, capaz de formar uma estrutura coesiva; solvente, para dispersar o biopolímero sendo, geralmente, a água; e um plastificante, para evitar a formação de uma matriz rígida e, portanto, quebradiça (Otoni et al., 2017). Em alguns casos, o solvente pode ser uma solução ácida, de metabissulfito de sódio ou hidroetanólica. A quitosana, por exemplo, é normalmente solubilizada em uma solução de ácido acético 1% (v/v) (Tessaro et al., 2021). O plastificante permite a formação de material flexível, pela redução da temperatura de transição vítrea do biopolímero (Otoni et al., 2017).

Figura 4.10 – Classificação e exemplos de biopolímeros naturais
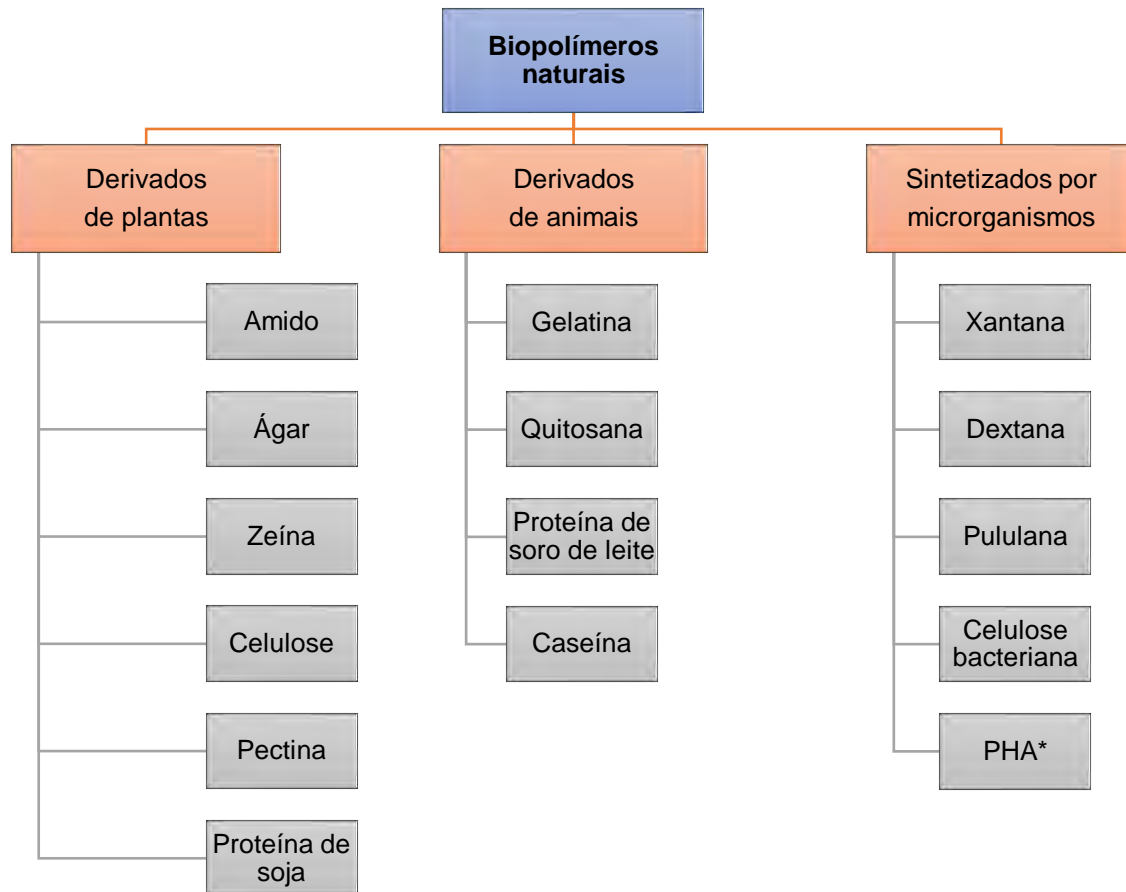
*PHA: polihidroxialcanoato.

Fonte: Modificado de Basumatary et al. (2020)

O método *casting*, que é um exemplo de processo de produção de filmes biopoliméricos por via úmida, é bastante simples e amplamente utilizado em escala laboratorial, por não exigir equipamentos específicos. Neste método (Figura 4.11), a solução filmogênica previamente formada, como descrito acima, é aplicada em placas/moldes adequados e submetida à desidratação.

Esses materiais podem atuar como veículos de diversos tipos de agentes ativos e CA para a produção de filmes ativos. Entretanto, o baixo desempenho em termos de propriedades mecânicas e de barreira dos filmes biopoliméricos, e a elevada sensibilidade à água, podem limitar sua aplicação como embalagens (Li et al., 2024). A incorporação de alguma carga de reforço, particularmente de nanopartículas, pode ser conveniente e, neste caso, o material produzido pode ser chamado de filme nanocompósito (Ilyas et al., 2022).

Figura 4.11 – Esquema representativo do método *casting* para a formação de filmes biopoliméricos

| Solução filmogênica | Desidratação da solução filmogênica | Deposição do filme biopolimérico | Remoção do filme biopolimérico |
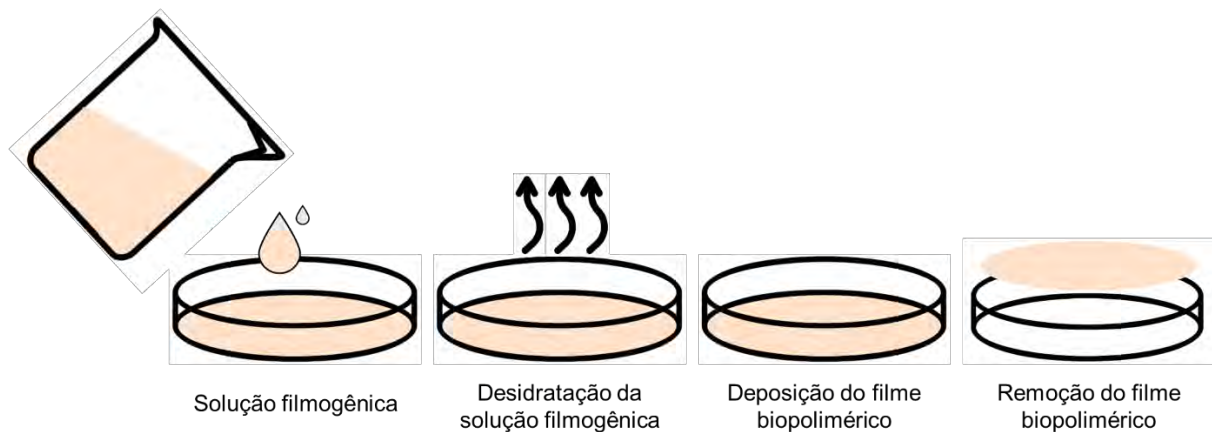
Fonte: Própria autoria.

4.3.1 Filmes a base de gelatina

A gelatina é uma proteína obtida por hidrólise parcial do colágeno, que é uma proteína fibrosa que ocorre naturalmente em tecidos de animais vertebrados e invertebrados, como pele, ossos, tecidos conjuntivos e tendões (Shamsallah; Rashid, 2024), e que possui uma estrutura de cadeias-α: três longas cadeias polipeptídicas que formam uma estrutura de tripla-hélice, que é estabilizada por ligações de hidrogênio intra e inter-cadeias (Hanani; Roos; Kerry, 2014). Assim como o colágeno, a gelatina tem peptídeos que possuem repetições contínuas de sequências de aminoácidos Gly-X-Y, sendo X, principalmente, a prolina, e Y, principalmente, a hidroxiprolina (Duconseille et al., 2015). Ela possui uma estrutura formada por cadeias polipeptídicas α (cadeia simples), β (duas cadeias-α unidas por ligações covalentes) e γ (três cadeias-α unidas por ligações covalentes), uma composição de aminoácidos tipicamente Ala-Gly-Pro-Arg-Gy-Glu-4Hyp-Gly-Pro (Figura 4.12), e composição elementar de 50,5% de carbono, 25,2% de oxigênio, 17% de nitrogênio e 6% de hidrogênio (Hanani; Roos; Kerry, 2014). É essa estrutura da gelatina lhe confere excelentes propriedades formadoras de filmes, biodegradabilidade e biocompatibilidade (Li et al., 2024), e, aos filmes, multifuncionalidade, incluindo a capacidade de incorporar diferentes CA, sistemas de encapsulação, cargas de reforço e formar blendas com outros biopolímeros (Acharya et al., 2024; Al-Maqtari et al., 2022).

Figura 4.12 – Estrutura química representativa da gelatina
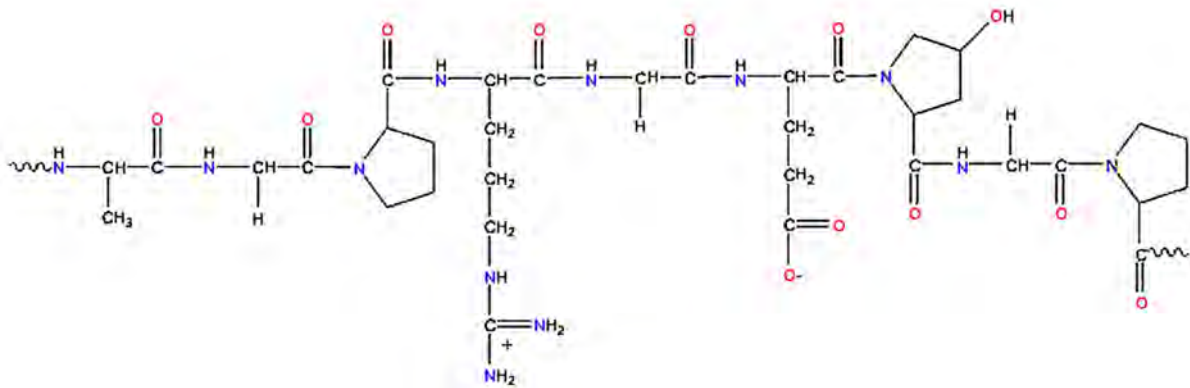
Fonte: Modificado de Hanani, Ross e Kerry (2014).

A gelatina pode ser de dois tipos, dependendo do tipo hidrólise utilizada para a sua extração: gelatina do tipo A (ponto isoelétrico 6 - 9), e do tipo B (ponto isoelétrico ~5), derivadas do colágeno com pré-tratamento ácido e alcalino, respectivamente (Benjakul; Nagarajan; Prodpran, 2016). A gelatina pode ser solubilizada em água a partir de 40 °C, formando géis termorreversíveis durante o resfriamento, propriedade esta que permite a produção de filmes e coberturas (Sobral; Habitante, 2001). Os filmes a base de gelatina são, geralmente, transparentes, levemente coloridos, flexíveis, homogêneos, uniformes e facilmente manuseáveis. Além disso, são considerados biodegradáveis em condições de compostagem ambiental (Bonilla et al., 2021; Bonilla; Sobral, 2020).

A higroscopicidade da gelatina, entretanto, limita algumas aplicações dos seus filmes, devido à elevada sensibilidade à água, com consequências negativas sobre a solubilidade em água, e propriedades mecânicas, térmicas e de barreira (Li et al., 2024). Os filmes de gelatina possuem propriedades de barreira e mecânicas não necessariamente adequadas ao emprego como embalagens. Dentre as alternativas para contornar estas limitações, a adição de cargas de reforço (ex: nanocelulose), tem sido estudadas, dentre outras (Ilyas et al., 2022). Além disso, filmes de gelatina ativados pela adição de CA podem apresentar melhoria de algumas de suas propriedades (Luciano et al., 2021; Yan et al., 2021).

Os CA, como os compostos fenólicos presentes nos extratos vegetais, podem interagir com grupos funcionais de alguns aminoácido das proteínas, como a gelatina, e formar estruturas mais estáveis em filmes biopoliméricos. As interações que ocorrem entre os CA e as proteínas dos filmes biopoliméricos podem ser covalentes ou não

covalentes (ligação de hidrogênio, interações hidrofóbicas ou iônicas), sendo as não covalentes as mais comuns (Li et al., 2024).

As interações não covalentes ocorrem entre os hidrogênios ou grupos hidroxilas dos CA com os grupos carbonila, hidroxila e amino da proteína (interações de hidrogênio), entre os anéis aromáticos apolares dos compostos fenólicos e os resíduos de aminoácidos hidrofóbicos da proteína (interações hidrofóbicas), e/ou entre os grupos hidroxilas dos compostos fenólicos e os grupos carregados positivamente das proteínas (interações iônicas) (Quan et al., 2019). Há, portanto, a formação de conjugados de proteína-polifenóis, que em filmes biopoliméricos, podem aumentar a resistência e a rigidez, e diminuir a sensibilidade à água, por exemplo (Yan et al., 2021). Isto indica que uma estrutura mais coesa, e com melhor interação entre as próprias cadeias de proteína, pode ser formada pela presença de compostos fenólicos, valorizando ainda mais estes materiais (Prodpran; Benjakul; Phatcharat, 2012).

4.3.2 Nanocelulose como carga de reforço de filmes a base de gelatina

As nanoceluloses, ou nanopartículas de celulose, são materiais isolados a partir da fibra de celulose, e que possuem pelo menos uma dimensão em escala nanométrica (Martelli-Tosi et al., 2018). A celulose, um polissacarídeo natural, é o biopolímero estrutural mais abundantemente encontrado na natureza, sendo o principal componente estrutural das paredes celulares de plantas e madeiras (Omran et al., 2021), responsável pelas propriedades mecânicas destes materiais. A celulose é renovável, biodegradável, biocompatível e não-tóxica, o que lhe confere diversas aplicações (Dufresne, 2013). Atualmente, há um grande interesse na extração e isolamento de novas formas de celulose, como as nanoceluloses (Ilyas et al., 2022), pois, além de compartilharem as propriedades da celulose, podem apresentar baixa densidade, excelente desempenho mecânico, elevada área de superfície e capacidade de atuarem como cargas de reforço de outros materiais poliméricos e biopoliméricos (Omran et al., 2021).

Dependendo do tipo de extração utilizada, as propriedades das nanoceluloses, como dimensão e composição, podem ser alteradas (Martelli-Tosi et al., 2018). As nanoceluloses podem ser divididas, então, em dois principais grupos: (i) nanocelulose cristalina (nanocristais de celulose), extraídas por hidrólise ácida, e (ii)

micro/nanocelulose fibrilada (micro/nanofibrilas de celulose), extraídas por hidrólise enzimática e/ou tratamento mecânico (Nechyporchuk; Belgagem; Bras, 2016). Em particular, a nanocelulose cristalina (CN) é normalmente extraída com ácido sulfúrico concentrado, que hidrolisa as regiões amorfas da celulose (Martelli-Tosi et al., 2018). Esses materiais frequentemente possuem estrutura de nanopartículas cilíndricas, alongadas, menos flexíveis e em forma de bastão, com diâmetros que variam de 2 a 100 nm, comprimento entre 500 nm e 2 µm, e índice de cristalinidade entre 65 e 88% (Ilyas et al., 2022). Além disso, as suspensões de CN obtidas a partir da hidrólise ácida são suspensões coloidais bastante estáveis (Klemm et al., 2011).

As propriedades únicas das CNs as tornam candidatas promissoras para a aplicação em diversos ramos da indústria de alimentos, incluindo a aplicação como estabilizadores de emulsões (Iqbal et al., 2022), e cargas de reforço para filmes biopoliméricos (Almeida et al., 2023; Martelli-Tosi et al., 2018), como de filmes a base de gelatina (Acharya et al., 2024; Li et al., 2024;). Kwak et al. (2020) observaram aumento de até 300% na tensão na ruptura, e 170% no módulo elástico, e redução de até 70% na elongação na ruptura de filmes a base de gelatina incorporados com 0 a 20% de CN. As CNs podem, ainda, melhorar as propriedades de barreira à gases e vapores desses filmes, por serem rígidas, impermeáveis e criarem um caminho "tortuoso" na matriz biopolimérica (Fukuzumi et al., 2009; Ilyas et al., 2022).

Esses resultados evidenciam o potencial efeito de reforço das CN em filmes biopoliméricos, tornando os filmes mais resistentes e rígidos, e menos flexíveis, e com melhores propriedades de barreira. Esse aprimoramento das propriedades dos filmes a base de gelatina pela incorporação de CN pode contribuir para o aumento potencial de aplicação desses materiais como embalagens de alimentos, por exemplo.

Sugere-se que este comportamento nos filmes a base de gelatina acontece devido à interação entre a gelatina e as CNs, formando uma matriz biopolimérica estabilizada por ligações de hidrogênio entre ambos os componentes (Alzate-Arbeláez et al., 2019). As ligações cruzadas formadas dificultam, então, a mobilidade das moléculas das cadeias de gelatina, tornando mais difícil a deformação dos filmes sob estresse externo (Taheri et al., 2020).

O reforço da matriz biopolimérica pela adição de CN também pode acontecer pelas propriedades excepcionais, já citadas, que estes materiais apresentam, e que são diferentes das propriedades dos biopolímeros, como resistência, inflexibilidade, elevada superfície específica e dimensões reduzidas (Garavand et al., 2020). As

dimensões reduzidas e a elevada superfície específica, por exemplo, permitem que as CN sejam mais facilmente dispersas e acabem fazendo autoassociações, por conta dos grupos hidroxilas presentes em toda a superfície de interação (Fukuzumi et al., 2009; Dufresne, 2013). A autoassociação entre as partículas de CN é a base da propriedade de carga de reforço, pois ocorre percolação dentro da matriz biopolimérica (Dufresne, 2013). A formação dessa rede tridimensional ajuda a distribuir as tensões ao longo do filme biopolimérico e, consequentemente, melhora a as propriedades mecânicas (Garavand et al., 2020).

4.4 FILMES ATIVOS

Os filmes biopoliméricos ativos, ou simplesmente filmes ativos, são uma geração de filmes biopoliméricos mais recente, desenvolvidos pela incorporação de substâncias com atividade biológicas (ex: antioxidante e antimicrobiana), enzimas, ou ingredientes funcionais (Benbettaïeb; Debeaufort; Karbowiak, 2019). Substâncias ricas em CA, como extratos de plantas ou parte delas, óleos essenciais, ou CA isolados (Almeida et al., 2023), podem ser utilizados como agentes para a produção de filmes ativos (Tabela 4.4).

Essas substâncias podem ser incorporadas diretamente nas matrizes filmogênicas, ou encapsuladas, como por exemplo, em emulsões O/A e A/O/A (Tabela 4.4). A vantagem de se encapsular as substâncias ricas em CA é promover a proteção e prolongação de suas atividades biológicas. A tecnologia de produção de filmes ativos incorporados de emulsões O/A ou A/O/A ricas em CA é recente e inovadora, e ainda pode ser muito explorada (Dammak; Sobral, 2019; Tessaro et al., 2021; Yuan et al., 2022).

Especificamente no caso de incorporação de emulsão A/O/A em filmes ativos, nenhum estudo, até então, havia sido relatado na literatura especializada, além do estudo realizado por Tessaro et al. (2021a). Posteriormente, alguns estudos nesta área foram publicados (Al-Maqtari et al., 2022; Yuan et al., 2022). As emulsões O/A e A/O/A, além de encapsularem e protegerem a ação biológica de substâncias ricas em CA, podem ainda interagir com a matriz do filme ativo e promover o aprimoramento de algumas propriedades físicas e funcionais (Al-Maqtari et al., 2022; Benbettaïeb; Debeaufort; Karbowiak, 2019; Tessaro et al., 2021).

Tabela 4.4 – Exemplos de estudos sobre o desenvolvimento de filmes ativos

Matriz do filme	Substância/composto ativo	Atividade biológica	Referência
Amido de mandioca/quitosana	Extrato hidroetanólico de folha de pitangueira	Antioxidante e antimicrobiana	Chakravartula et al. (2020)
Amido de milho/gelatina	Polpa da fruta guabiroba	Antioxidante	Malherbi et al. (2019)
Carragena	Extrato de folha de oliveira	Antioxidante e antimicrobiana	Martiny et al. (2020)
Caseinato de sódio/goma de guar/ Cera de abelha	Erva doce e húmico de café	Antioxidante e antimicrobiana	Verrillo et al. (2023)
Gelatina	Extrato hidroetanólico de folha de pitangueira	Antioxidante e antimicrobiana	Luciano et al. (2021a)
Gelatina	Extrato etanólico de própolis vermelho e óleos essenciais de cravo e manjericão	Antioxidante e antimicrobiana	Reyes, Landgraf e Sobral (2021)
Gelatina	Eugenol encapsulado em emulsão O/A	Antioxidante	Dammak e Sobral (2019)
Gelatina e/ou quitosana	Extrato hidroetanólico de folha de pitangueira encapsulado em emulsão A/O/A	Antioxidante e antimicrobiana	Tessaro et al., (2021a)
Gelatina/inulina/nanocelulose	Extrato de *Malva sylvestris*	Antibacteriana	Nikoukheslat et al. (2022)
Gelatina/quitosana/nanocelulose	Extrato da fruta de espinheiro	Antioxidante e indicador de pH	Yan et al. (2021)
Pectina e/ou quitosana	Extrato de fruta noni	Antioxidante e antimicrobiana	Lin et al. (2023)
Quitosana	Fitoquímicos extraídos do subproduto da cenoura	Antioxidante	Esposto et al. (2024)
Quitosana	Óleos essenciais de canela, Thymus satureioides Cosson e cravo-da-índia	Antibacteriana e antifúngica	Mouhoub et al. (2024)

Fonte: Própria autoria.

4.5 PERMEABILIDADE AOS GASES

Uma das principais funções de uma embalagem de alimentos é criar uma barreira entre o alimento e o ambiente externo para preservar as propriedades do alimento embalado e, assim, estender sua validade (Baschetti; Minelli, 2020). As embalagens plásticas e biopoliméricas de alimentos são permeáveis, em diferentes graus, a pequenas moléculas, como gases e vapores, e a compostos de baixo peso molecular, como aromas e sabores (Siracusa, 2012). Como consequência dessas propriedades de barreira, a permeação das moléculas para o interior, ou para fora, da embalagem varia de baixa a alta, e afeta diretamente a qualidade do alimento embalado (Ilyas et al., 2022).

Dentre essas propriedades de barreira, o conhecimento da permeabilidade aos gases (O_2 e CO_2), por exemplo, é de extrema importância no projeto de embalagens para alguns tipos de alimentos, como produtos cárneos, para se evitar a migração do oxigênio atmosférico para o interior que pode oxidar os lipídeos presentes no produto, ou produtos vegetais frescos, onde a modulação da respiração desses vegetais é de suma importância (Xue et al., 2023).

O O_2 induz as principais reações de degradação de alguns alimentos, como a oxidação lipídica, escurecimento enzimático e perda de vitaminas, e cria um ambiente favorável para o crescimento de microrganismos aeróbios, resultando na formação de odores, sabores ou alteração de cor, e diminuindo o valor nutricional dos alimentos (Baschetti; Minelli, 2020; Gontard et al., 1996). O CO_2 também afeta a conservação de alimentos embalados, pois sua presença pode limitar ou suprimir o crescimento de microrganismos em alimentos frescos, queijos ou alimentos assados, bem como reduzir a taxa de respiração de alguns alimentos (Baschetti; Minelli, 2020). Controlar as concentrações de oxigênio e gás carbônico em torno do alimento embalado significa, portanto, estender sua vida de prateleira.

Em filmes biopoliméricos, normalmente utilizados para produzir embalagens biopoliméricas, a permeação de gases e vapores pode ser explicada pela Teoria da Permeação, descrita pelo modelo de dissolução-difusão utilizando as leis de Fick e Henry (Figura 4.13) (Xu et al., 2023). Neste modelo, a permeação das moléculas de gases e vapores nesses materiais depende, inicialmente, da absorção dessas moléculas, seguida pela difusão através do filme e, por fim, a dessorção. A absorção

e difusão dependem da "solubilidade" desses penetrantes na matriz biopolimérica (Trinh; Chang; Mekonnen, 2023), que pode ser afetada por fatores externos e pelas características intrínsecas dos materiais biopoliméricos. Mais especificamente, a solubilidade pode ser afetada pelas condições ambientais, como temperatura, umidade relativa, diferença de pressão e concentração, pela estrutura dos filmes biopoliméricos, como grau de cristalinidade, morfologia, polaridade, espessura, e pelas características dos gases e vapores, como peso molecular e polaridade (Siracusa, 2012).

Figura 4.13 – Esquema representativo do modelo de dissolução-difusão através de um filme biopolimérico
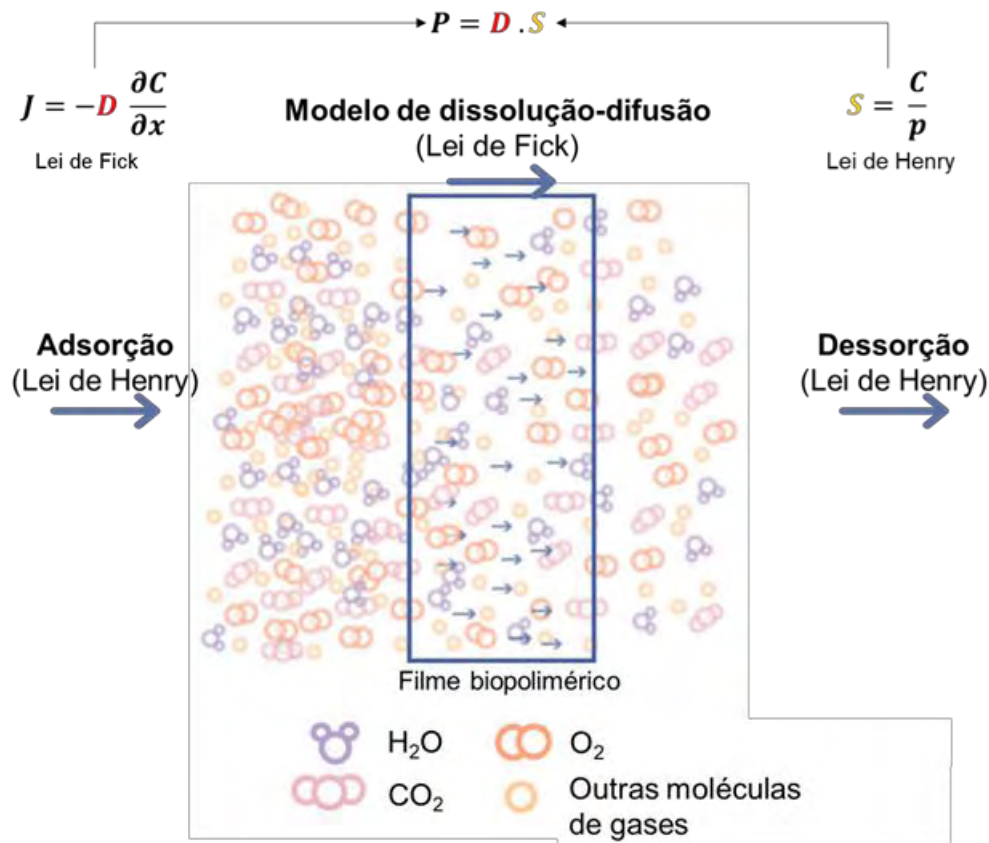
*P: permeabilidade. D: coeficiente de difusividade. S: coeficiente de solubilidade. J: fluxo do gás ou vapor. C: concentração do gás ou vapor. x: direção unidimensional do gradiente de concentração. p: pressão parcial do gás ou vapor.

Fonte: Modificado de Xu et al. (2023).

A permeabilidade (P) pode ser calculada como o produto do coeficiente de difusividade (D) pela solubilidade (S), (eq. 4.1) (Trinh, Chang e Mekonnen, 2023).

$$P = D \cdot S \tag{4.1}$$

Em termos práticos, a permeabilidade ao vapor de água (PVA), quando determinada gravimetricamente, pode ser calculada com a eq. (4.2), sendo Q/t, a taxa de migração do vapor de água que atravessa o filme biopolimérico no tempo, L, a espessura média do filme biopolimérico, A, a área de permeação, e ΔP, a diferença de pressão entre os dois lados do filme biopolimérico.

$$PVA = \frac{Q \cdot L}{A \cdot t \cdot \Delta P} \tag{4.2}$$

No caso de gases não condensáveis, os resultados de P podem ser expressos em termos de diferentes parâmetros (taxa de transmissão, permeância, permeabilidade, coeficiente de transferência, gradiente de concentração, entre outros), e podem ser obtidos por vários métodos, como métodos padronizados pelas *American Society for Testing and Materials* (ASTM) e *International Organization for Standardization* (ISO) (Xu et al., 2023). Em particular, a taxa de transmissão a gases (GTR) indica a quantidade do gás (Q) que atravessa um filme biopolimérico com uma determinada área superficial (A) durante o tempo (t), em estado estacionário, sob uma diferença de pressão parcial (P) do gás entre as duas superfícies do filme biopolimérico (eq. 4.3) (Feldman, 2013).

$$GTR = \frac{Q}{A \cdot t \cdot \Delta P} \tag{4.3}$$

A GTR, ou P, de diferentes gases, como O_2 e CO_2 de plásticos produzidos com polímeros sintéticos já são bastante estabelecidas (Schmid et al., 2015; Wang et al., 2018). Para os filmes biopoliméricos, o estabelecimento dessas propriedades está em constante evolução, já que os biopolímeros são extraídos de fontes renováveis e podem apresentar alguma variabilidade na composição. Vários estudos têm sido conduzidos para investigar, caracterizar e otimizar a GTR ou P dos filmes biopoliméricos, incluindo diferentes formulações de biopolímeros, adição de cargas de reforço e CA, por exemplo (Biscarat et al., 2015; Iaccheri et al., 2023; Kurek et al., 2014; Schmid et al., 2015; Xue et al., 2023), já que esses materiais geralmente apresentam propriedades de barreira insuficientes em condições de elevadas umidades relativas (Kurek et al., 2014).

Além disso, determinar as quantidades de gases que permeiam através dos filmes biopoliméricos permite estabelecer para quais nichos de alimentos esses materiais podem ser adequadamente empregados como embalagens. Para filmes e filmes nanocompósitos ativados com emulsão A/O/A encapsulando CA, nenhum estudo sobre o efeito da incorporação de emulsão AO/A e nanoceluloses na GTR foi encontrado na literatura especializada.

4.6 DIGESTÃO *IN VITRO*

Os processos de digestão que ocorrem no sistema gastrointestinal humano podem ser simulados *in vitro* e, geralmente, os modelos empregados são bastante eficientes em simular a digestão, e uma boa alternativa aos modelos *in vivo* (Brodkorb et al., 2019). A digestão *in vitro* pode ser utilizada para prever como os novos produtos alimentícios serão digeridos, e se estes serão atóxicos e adequados para o consumo humano (Prichapan; McClements; Klinkesorn, 2021). A digestão *in vitro* pode, ainda, prever a biodisponibilidade, taxa e extensão da digestão de ingredientes funcionais presentes em produtos alimentícios, bem como a mudança estrutural destes produtos ao longo da digestão.

Estudos sobre a digestão de CAs encapsulados em diferentes tipos de emulsões, como emulsão A/O (He et al., 2023; Iqbal et al., 2022; Zhang et al., 2022), emulsão O/A (Gonçalves et al., 2021; Pinheiro et al., 2013), e emulsão A/O/A (Chaudhary; Sabikhi; Hussain, 2020; Han et al., 2022; Huang; Zhou, 2019) têm sido realizados com especial interesse na biodisponibilidade do CA encapsulado, bem como na mudança estrutural e composição das emulsões. A digestão *in vitro* pode ser realizada, ainda, em alimentos fortificados com essas emulsões encapsulando CAs (Gonçalves et al., 2024). Embora mais escassos, estudos sobre a digestão *in vitro* de filmes ativos também têm sido realizados (Karkar et al., 2023; López de Lacey et al., 2012).

A biodisponibilidade pode ser definida como a porção de ingredientes ativos que é liberada da sua localização original nos alimentos para o trato gastrointestinal para a absorção luminal, na sua forma original (Boostani; Jafari, 2021). A biodisponibilidade de um CA é o resultado de vários processos, tais como: liberação do CA da matriz do alimento ou do sistema de entrega coloidal, solubilização do CA nos fluídos gastrointestinais, interação ativa com as enzimas digestivas e outros

componentes, transporte através de membranas celulares, entre outros (Dima; Dima, 2020).

Particularmente no caso de CAs encapsulados, é importante prever a sua biodisponibilidade para avaliar possíveis transformações químicas e bioquímicas que podem ocorrer no processo de encapsulação, ou seja, avaliar a estabilidade química e bioquímica (Kaimainen et al., 2015), a potencial absorção desses compostos pelas células epiteliais do intestino delgado (Prichapan; McClements; Klinkesorn, 2021), e se existe alguma evidência de citotoxicidade desses sistemas.

No caso de filmes ativos, também pode ser interessante fazer essas avaliações. Os filmes ativos produzidos com ingredientes GRAS podem ser comestíveis (Vargas-Torrico et al., 2024), como é o caso de um filme de gelatina ativado com vermelho monascus, ficocianina e amarelo cártamo, e aplicado como embalagem ativa para cozinhar juntamente com os ingredientes de mingau de aveia e arroz embalados (Liu et al., 2024). Nesses casos, os CAs presentes na matriz do filme podem ser liberados e se tornarem potencialmente disponíveis para a absorção pelo sistema gastrointestinal (López de Lacey et al., 2012). Não foram encontrados estudos na literatura especializada sobre a digestão *in vitro* de filmes ou filmes nanocompósitos ativados com CA encapsulados em emulsões A/O/A, o que constitui uma das originalidades desta tese.

Existem diversos modelos de digestão *in vitro* disponíveis e que fornecem uma boa correlação *in vitro - in vivo* (Prichapan; McClements; Klinkesorn, 2021), e eles podem ser divididos em modelos estáticos e dinâmicos (Li et al., 2020). Apesar de os modelos dinâmicos demonstrarem boa eficiência para simular a digestão *in vitro* de diversos alimentos e produtos farmacêuticos (Gonçalves et al., 2024), eles são relativamente complexos, caros para serem configurados e mantidos, e consomem uma grande quantidade de amostra, o que pode não ser adequado para a maioria das pesquisas de alimentos (Brodkorb et al., 2019). Os modelos estáticos, por outro lado, são normalmente utilizados para realizar a digestão *in vitro* de alimentos e produtos farmacêuticos devido à sua simplicidade, baixo custo, e boa correlação de resultados com aqueles da digestão *in vivo* (Brodkorb et al., 2019; Gonçalves et al., 2021).

Diversos modelos e protocolos de digestão *in vitro* estática foram desenvolvidos e, certamente por isto, surgiu a necessidade de padronizar o protocolo para se realizar este processo. O INFOGEST, rede internacional de institutos de pesquisas multidisciplinares, desenvolveu um método padronizado e harmonioso (protocolo

INFOGEST 2.0) para se realizar e avaliar a digestão estática *in vitro* de alimentos adequados para a alimentação humana adulta (Brodkorb et al., 2019). Apesar deste modelo apresentar algumas limitações (incapacidade de simular as interações fisiológicas com o sistema gastrointestinal humano, condições experimentais constantes, e não adição gradual dos fluídos gastrointestinais, ausência de esvaziamento gástrico, ausência de análise cinética, entre outras), suas vantagens, como robustez, reprodutibilidade, boa correlação com os modelos *in vivo*, simplicidade, custo relativamente baixo, e fácil manuseio e avaliação da amostra durante cada etapa da digestão, os tornam adequado para avaliar, principalmente, os produtos finais da digestão (Brodkorb et al., 2019).

Com base no protocolo INFOGEST 2.0, a digestão *in vitro* em modo estático pode ser dividida em três fases (Figura 4.14): preparo da amostra, processo de digestão, e tratamento e análise de resultados, de acordo com as respostas pretendidas (Brodkorb et al., 2019). O processo de digestão acontece, ainda, em três etapas, simulando a digestão oral, que ocorre na boca, a digestão gástrica, que ocorre no estômago, e a digestão intestinal, que ocorre no intestino (Figura 4.14).

Inicialmente, na fase de preparação, os fluídos digestivos simulados são preparados para simular as condições encontradas no sistema gastrointestinal, e são formados por uma mistura de ácidos, bases e sais (Brodkorb et al., 2019). Além disso, a atividade enzimática das lipases e pepsina, bem como a atividade da bile, são previamente determinadas por métodos analíticos. O teste de ajuste de pH é realizado para se determinar a quantidade de ácido clorídrico ou hidróxido de sódio que devem ser adicionados em cada fase da digestão *in vitro*, a fim de se obter uma condição experimental com o pH ideal em cada uma delas.

A digestão *in vitro* é realizada, então, mantendo-se as condições experimentais de cada fase constantes, e basicamente, ocorre da seguinte maneira (Brodkorb et al., 2019): (i) na fase oral, a amostra de alimento é diluída no fluído salivar simulado (SSF) após o processo de mastigação simulada (se necessário), com ou sem a adição de amilase salivar, e, em seguida, é feita a incubação com agitação por 2 min a 37 °C, em pH 7,0; (ii) na fase gástrica, o bolo alimentar formado na fase oral é diluído no fluído gástrico simulado (SGF) e misturado com enzimas gástricas (pepsina e lipase gástrica), e em seguida, incubado sob agitação por 2 h a 37 °C, em pH 3,0; (iii) na fase intestinal, o quimo gástrico é diluído no fluído intestinal simulado (SIF) e misturado

com os sais biliares e com a pancreatina (enzima intestinal), e, por fim, incubado sob agitação por 2 h a 37 °C, em pH 7,0.

Figura 4.14 – Esquema representativo do processo de digestão *in vitro* em modo estático do protocolo INFOGEST 2.0

Preparação
- Determinar a atividade enzimática e da bile;
- Preparar as soluções-estoque de SSF, SGF e SIF;
- Realizar o experimento de ajuste do pH.

Fase oral
- Amostra
- SSF
- CaCl₂
2 min/37 °C pH 7,0

Fase gástrica
- Bolo
- SGF
- Pepsina
- lipase
- CaCl₂
2 h/37 °C pH 3,0

Fase intestinal
- Quimo
- SIF
- Bile
- Pancreatina
- CaCl₂
2 h/37 °C pH 7,0

Tratamento
- Bioacessibilidade;
- Estrutura da amostra;
- Hidrólises (lipídica, proteica, de amido);
- Citotoxicidade

*SSF: fluído salivar simulado. SGF: fluído gástrico simulado. SIF: fluído intestinal simulado.

Fonte: Própria autoria.

Os produtos hidrofílicos e lipofílicos de cada fase da digestão são, então, analisados de acordo com as respostas pretendidas. A biodisponibilidade dos CAs e liberação de ácidos graxos livres podem ser determinadas por métodos simples, como espectrofotometria e titulometria, respectivamente (Pinheiro; Coimbra; Vicente, 2016). No caso das emulsões, análises como tamanho de partícula, potencial zeta e morfologia podem ser interessantes para se avaliar a estabilidade dessas emulsões durante e/ou após a digestão.

Referências

ACHARYA, D. R. et al. Nanoemulsion-integrated gelatin/bacterial cellulose nanofibril-based multifunctional film: Fabrication, characterization, and application. **International Journal of Biological Macromolecules**, v. 257, p. 128341, 2024.

AHMAD, A. S. et al. Antioxidant and antimicrobial activities of Ethanolic Jik (*Barringtonia acutangula*) leaf extract and its application for shelf-life extension of Pacific white shrimp meat during refrigerated storage. **Food Control**, v. 155, p. 110037, 2024.

AL-MAQTARI, Q. A. et al. Fabrication and characterization of chitosan/gelatin films loaded with microcapsules of *Pulicaria jaubertii* extract. **Food Hydrocolloids**, v. 129, p. 107624, 2022.

ALMEIDA, T. et al. Biobased ternary films of thermoplastic starch, bacterial nanocellulose and gallic acid for active food packaging. **Food Hydrocolloids**, v. 114, p. 108934, 2023.

ALZATE-ARBELÁEZ, A. F. et al. Immobilization of Andean berry (*Vaccinium meridionale*) polyphenols on nanocellulose isolated from banana residues: A natural food additive with antioxidant properties. **Food Chemistry**, v. 294, p. 503–517, 2019.

ARAI, I. et al. Improving effects of the extracts from *Eugenia uniflora* on hyperglycemia and hypertriglyceridemia in mice. **Journal of Ethnopharmacology**, v. 68, n. 1–3, p. 307–314, 1999.

ARAUJO, N. M. P. et al. Plants from the genus Eugenia as promising therapeutic agents for the management of diabetes mellitus: A review. **Food Research International**, v. 142, p. 110182, 2021.

BASCHETTI, M G.; MINELLI, M. Test methods for the characterization of gas and vapor permeability in polymers for food packaging application: A review. **Polymer Testing**, v. 89, p. 106606, 2020.

BELLUCCI, E. R. B. et al. Red pitaya extract as natural antioxidant in pork patties with total replacement of animal fat. **Meat Science**, v. 171, p. 108284, 2021.

BENBETTAÏEB, N.; DEBEAUFORT, F.; KARBOWIAK, T. Bioactive edible films for food applications: mechanisms of antimicrobial and antioxidant activity. **Critical Reviews in Food Science and Nutrition**, v. 59, n. 21, p. 3431–3455, 2019.

BENJAKUL, S.; NAGARAJAN, M.; PRODPRAN, T. Films and Coatings from Collagen and Gelatin. *In*: **Edible Films and Coatings**. CRC Press, p. 121-142, 2016.

BERENDSEN, R.; GÜELL, C.; FERRANDO, M. Spray dried double emulsions containing procyanidin-rich extracts produced by premix membrane emulsification: Effect of interfacial composition. **Food Chemistry**, v. 178, p. 251-258, 2015.

BEZERRA, I. C. F. et al. Optimization strategy for extraction of active polyphenols from leaves of *Eugenia uniflora* Linn. **Food Analytical Methods**, v. 13, p. 735-750, 2020.

BIESALSKI, H.-K. et al. Bioactive compounds: Definition and assessment of activity. **Nutrition**, v. 25, n. 11–12, p. 1202–1205, 2009.

BILATTO, S. et al. Lignocellulose nanocrystals from sugarcane straw. **Industrial Crops and Products**, v. 151, p. 112938, 2020.

BISCARAT, J. et al. Development of a new family of food packaging bioplastics from cross-linked gelatin bases films. **The Canadian Journal of Chemical Engineering**, v. 93, n. 2, p. 176-182, 2015.

BONILLA, J. et al. Biodegradation of films bed on natural and synthetic biopolymers using an aquatic system from active Sludge. **Journal of Polymers and the Environment**, v. 29, p. 1380-1395, 2021.

BONILLA, J.; SOBRAL, P. J. A. Disintegrability under composting conditions of films based on gelatin, chitosan and/or sodium caseinate containing boldo-of-Chile leafes extract. **International Journal of Biological Macromolecules**, v. 151, p. 178-185, 2020.

BONILLA, J.; SOBRAL, P. J. A. Disintegrability under composting conditions of films based on gelatin, chitosan and/or sodium caseinate containing boldo-of-Chile leafs extract. **International Journal of Biological Macromolecules**, v. 151, p. 178–185, 2020.

BONILLA, J.; SOBRAL, P. J. A. Investigation of the physicochemical, antimicrobial and antioxidant properties of gelatin-chitosan edible film mixed with plant ethanolic extracts. **Food Bioscience**, v. 16, p. 17–25, 2016.

BOOSTANI, S.; JAFARI, S. M. A comprehensive review on the controlled release of encapsulated food ingredients; fundamental concepts to design and applications. **Trends in Food Science & Technology**, v. 109, p. 303–321, 2021.

BRODKORB, A. et al. INFOGEST static *in vitro* simulation of gastrointestinal food digestion. **Nature Protocols**, v. 14, p. 991-1014, 2019.

CANABARRO, N. I. et al. Conveyor-belt drying of *Eugenia uniflora* L. leaves: Influence of drying conditions on the yield, composition, antioxidant activity and total phenolic content of supercritical CO_2 extracts. **Food and Bioproducts Processing**, v. 116, p. 140–149, 2019.

CARVALHO, F. A. L. et al. Effect of guarana (*Paullinia cupana*) seed and pitanga (*Eugenia uniflora* L.) leaf extracts on lamb burgers with fat replacement by chia oil emulsion during shelf life storage at 2 °C. **Food Research International**, v. 125, p. 108554, 2019.

CHAKRAVARTULA, S. S. N. et al. Influence of pitanga (*Eugenia uniflora* L.) leaf extract and/or natamycin on properties of cassava starch/chitosan active films. **Food Packaging and Shelf Life**, v. 24, p. 100498, 2020.

CHAUDHARY, N.; SABIKHI, L.; HUSSAIN, S. A. Emblicanin rich *Emblica officinalis* extract encapsulated double emulsion: controlled release of bioactive during phagocytosis and *in vitro* digestion. **Journal of Food Science and Technology**, v. 57, n. 4, p. 1371-1381, 2020.

CHIBANE, L. et al. Plant antimicrobial polyphenols as potential natural food preservatives. **Journal of the Science of Food and Agriculture**, v. 99, n. 4, p. 1457–1474, 2019.

CONSOLINI, A. E.; SARUBBIO, M. G. Pharmacological effects of *Eugenia uniflora* (Myrtaceae) aqueous crude extract on rat's heart. **Journal of Ethnopharmacology**, v. 81, n. 1, p. 57–63, 2002.

COSTA, A. G. V. et al. Bioactive compounds and health benefits of exotic tropical red–black berries. **Journal of Functional Foods**, v. 5, n. 2, p. 539–549, 2013.

CUNHA, F. A. B. et al. Cytotoxic and antioxidative potentials of ethanolic extract of *Eugenia uniflora* L. (Myrtaceae) leaves on human blood cells. **Biomedicine & Pharmacotherapy**, v. 84, p. 614-621, 2016.

DAMMAK, I.; SOBRAL, P. J. A. Active gelatin films incorporated with eugenol nanoemulsions: effect of emulsifier type on films properties. **International Journal of Food Science & Technology**, v. 54, n. 9, p. 2725–2735, 2019.

DANIELE-SILVA, A. et al. *In vitro* and *in vivo* anti-inflammatory and antiophidic effects of the extract and fraction of *Eugenia uniflora*. **Journal of Ethnopharmacology**, v. 319, p. 117223, 2024.

DI MEO, F. et al. Understanding antioxidant properties of natural compounds at the atomic scale. **Journal of the Serbian Society for Computational Mechanics**, v. 7, n. 1, p. 58–70, 2013.

DICKINSON, E. Double Emulsions Stabilized by Food Biopolymers. **Food Biophysics**, v. 6, n. 1, p. 1–11, 2011.

DIMA, C.; DIMA, S. Bioaccessibility study of calcium and vitamin D_3 co-microencapsulated in water-in-oil-in-water double emulsions. **Food Chemistry**, v. 303, p. 125416, 2020.

DUCONSEILLE, A. et al. Gelatin structure and composition linked to hard capsule dissolution: A review. **Food Hydrocolloids**, v. 43, p. 360–376, 2015.

DUFRESNE, A. Nanocellulose: a new ageless bionanomaterial. **Materials Today**, v. 16, n. 6, p. 220–227, 2013.

EFENBERGER-SZMECHTYK, M.; NOWAK, A.; CZYZOWSKA, A. Plant extracts rich in polyphenols: antibacterial agents and natural preservatives for meat and meat products. **Critical Reviews in Food Science and Nutrition**, v. 61, n. 1, p. 149–178, 2021.

ESPOSTO, B. S. et al. Chitosan films activated with phytochemicals extracted from carrot by-product encapsulated in TPP chitosomes. **International Journal of Food Science & Technology**, v. 53, n. 3, p. 1384-1393, 2024.

FELDMAN, D. Polymer nanocomposite barriers. **Journal of Macromolecular Science, Part A**, v. 50, n. 4, p. 441-448, 2013.

FIDELIS, E. M. et al. Pitanga (*Eugenia uniflora* L.) as a source of bioactive compounds for health benefits: A review. **Arabian Journal of Chemistry**, v. 15, n. 4, p. 103691, 2022.

FRAJ, J. et al. Properties of water in oil emulsions (W/O) stabilized with mixtures of PGPR and polyglycerol fatty acid esters. **Acta Periodica Technologica**, v. 48, n. 48, p. 95–107, 2017.

FUKUZUMI, H. et al. Transparent and high gas barrier films of celulose nanofibers prepared by TEMPO-Mediated oxidation. **Biomacromolecules**, v. 10, n. 1, p. 162-165, 2009.

GARAVAND, F. et al. A comprehensive review on the nanocomposites loaded with chitosan nanoparticles for food packaging. **Critical Reviews in Food Science and Nutrition**, v. 62, n. 5, p. 1383-1416, 2020.

GIMÉNEZ, B. et al. Antioxidant properties of green tea extract incorporate to fish gelatin films after simulated gastrointestinal enzymatic digestion. **LWT**, v. 53, p. 445-451, 2013.

GONÇALVES, R. F. S. et al. Incorporation of curcumin-loaded solid lipid nanoparticles into yogurt: Tribo-rheological properties and dynamic in vitro digestion. **Food Research International**, v. 181, p. 114112, 2024.

GONÇALVES, R. F. S. et al. Lipid-based nanostructures as a strategy to enhance curcumin bioaccessibility: Behavior under digestion and cytotoxicity assessment. **Food Research International**, v. 143, p. 110278, 2021.

GONTARD, N. et al. Influence of relative humidity and film composition on oxygen and carbon dioxide permeabilities of edible films. **Journal of Agricultural and Food Chemistry**, v. 44, p. 1064-1069, 1996.

HAN, L. et al. Co-delivery of insulin and quercetin in W/O/W double emulsions stabilized by different hydrophilic emulsifiers. **Food Chemistry**, v. 369, p. 130918, 2022.

HANANI, Z. A. N.; ROOS, Y. H.; KERRY, J. P. Use and application of gelatin as potential biodegradable packaging materials for food products. **International Journal of Biological Macromolecules**, v. 71, p. 94–102, 2014.

HE, J. et al. Capsaicin encapsulated in W/O/W double emulsions fabricated via ethanol-induced pectin gelling: Improvement of bioaccessibility and reduction of irritation. **International Journal of Biological Macromolecules**, v. 235, p. 123899, 2023.

HUANG, S. et al. Tween 80-mediated size-controlled self-assembly of resistant starch particle: A green and biodegradable white pigment for food applications. **Food Hydrocolloids**, v. 153, p. 109993, 2024.

HUANG, Y.; ZHOU, W. Microencapsulation of anthocyanins through two-step emulsification and release characteristics during in vitro digestion. **Food Chemistry**, v. 278, p. 357–363, 2019.

IACCHERI, E. et al. Studying physical state of films based on casava starch and/or chitosan by dielectric and thermal properties and effects of pitanga leaf hydroethanolic extract. **Journal of Food Engineering**, v. 339, p. 111280, 2023.

ILYAS, Q.A. et al. Oxygen permeability properties of nanocellulose reinforced biopolymer nanocomposites. **Materials Today: Proceedings**, v. 52, p. 2414-2419, 2022.

IQBAL, S. et al. Modulation of viscosity, microstructure and lipolysis of W/O emulsions by cellulose ethers during *in vitro* digestion in the dynamic and semi-dynamic gastrointestinal models. **Food Hydrocolloids**, v. 128, p. 107584, 2022.

KAIMAINEN, M. et al. Encapsulation of betalain into w/o/w double emulsion and release during in vitro intestinal lipid digestion. **LWT**, v. 60, n. 2, p. 899-904, 2015.

KARKAR, B. et al. Development of an edible active chitosan film loaded with Nigella sativa L. extract to extend the shelf life of grapes. **Biocatalysis and Agricultural Biotechnology**, v. 50, p. 102708, 2023.

KITAOKA, M.; NGUYEN, T. C.; GOTO, M. Water-in-oil microemulsions composed of monoolein enhanced the transdermal delivery of nicotinamide. **International Journal of Cosmetic Science**, v. 43, n. 3, p. 302-310, 2021.

KLEMM, D. et al. Nanocelluloses: A new family of nature-based materials. **Angewandte Chemie International Edition**, v. 50, n. 24, p. 5438–5466, 2011.

KOWALCZYK, M. et al. Effect of the addition of chokeberry leaf extract on the physicochemical and sensory properties of burger from dark cutting veal. **Food Chemistry**, v. 399, p. 133978, 2023.

KUREK, M. et al. Effect of relative humidity on carvacrol release and permeation properties of chitosan based films and coatings. **Food Chemistry**, v. 144, p. 9-17, 2014.

KWAK, H. W. et al. Chemical and physical reinforcement of hydrophilic gelatin film with di-aldehyde nanocellulose. **International Journal of Biological Macromolecules**, v. 146, p. 332–342, 2020.

LI, M. et al. Gelatin films reinforced by tannin-nanocellulose microgel with improved mechanical and barrier properties for sustainable active food packaging. **Food Hydrocolloids**, v. 149, p. 109642, 2024.

LIGOR, M. et al. Extraction approaches used for the determination of biologically active compounds (cyclitols, polyphenols and saponins) isolated from plant material. **Electrophoresis**, v. 39, n. 15, p. 1860–1874, 2018.

LIN, X. et al. Fabrication characterization and biological properties of pectin and/or chitosan-based films incorporated with noni (*Morinda citrifolia*) fruit extract**. Food Hydrocolloids**, v. 134, p. 108025, 2023.

LIU, S. et al. Enhanced barrier and antioxidant properties of gelatin films by structural-colored bioactive materials for food packaging**. Food Hydrocolloids**, v. 150, p. 109744, 2024.

LIU, S. et al. Oleanolic acid nanoparticles-stabilized W/O Pickering emulsions: Fabrication, characterization, and delivery application. **Food Chemistry**, v. 444, p. 138598, 2024.

LÓPEZ DE LACEY, A. M. et al. Bioaccessibility of green tee polyphenols incorporated into an edible agar film during simulated human digestion. **Food Research International**, v. 48, p.462-469, 2012.

LORENZO, J. M. et al. Influence of pitanga leaf extracts on lipid and protein oxidation of pork burger during shelf-life. **Food Research International**, v. 114, p. 47–54, 2018.

LUCIANO, C. G. et al. Application of bi-layers active gelatin films for sliced dried-cured Coppa conservation. **Meat Science**, v. 189, p. 108821, 2022.

LUCIANO, C. G. et al. Bi-layer Gelatin Film: Activating Film by Incorporation of "Pitanga" Leaf Hydroethanolic Extract and/or Nisin in the Second Layer. **Food and Bioprocess Technology**, v. 14, n. 1, p. 106–119, 2021.

MA, X.; CHATTERTON, D. E. W. Strategies to improve the physical stability of sodium caseinate stabilized emulsions: A literature review. **Food Hydrocolloids**, v. 119, p. 106853, 2021.

MALHERBI, N. M. et al. Corn starch and gelatin-based films added with guabiroba pulp for application in food packaging. **Food Packaging and Shelf Life**, v. 19, p. 140-146, 2019.

MARTELLI-TOSI, M. et al. Soybean straw nanocellulose produced by enzymatic or acid treatment as a reinforcing filler in soy protein isolate films. **Carbohydrate Polymers**, v. 198, p. 61–68, 2018.

MARTINEZ-CORREA, H. A. et al. Extracts from pitanga (*Eugenia uniflora* L.) leaves: Influence of extraction process on antioxidant properties and yield of phenolic compounds. **Journal of Supercritical Fluids**, v. 55, n. 3, p. 998–1006, 2011.

MARTINY, T. R. et al. Bio-Based Active Packaging: Carrageenan Film with Olive Leaf Extract for Lamb Meat Preservation. **Foods**, v. 9, n. 12, p. 1759, 2020.

McCLEMENTS, D. J. **Food Emulsions**. 2. ed. Boca Raton: CRC Press, 2004.

McCLEMENTS, D. J.; JAFARI, S. M. Improving emulsion formation, stability and performance using mixed emulsifiers: A review. **Advances in Colloid and Interface Science**, v. 251, p. 55–79, 2018.

MEIRA, E. F. et al. *Eugenia uniflora* (pitanga) leaf extract prevents the progression of experimental acute kidney injury. **Journal of Functional Foods**, v. 66, p. 103818, 2020.

MOHAMMAD, I. S. et al. Phytocosmeceutical formulation development, characterization and its *in-vivo* investigations. **Biomedicine & Pharmacotherapy**, v. 107, p. 806–817, 2018.

MOUHOUB, A. et al. Preparation of bioactive film based on chitosan and essential oils mixture for enhanced preservation of food products. **International Journal of Biological Macromolecules**, v. 259, p. 129396, 2024.

MOURA, S. C. S. R. S. R. et al. Stability of Hibiscus Extract Encapsulated by Ionic Gelation Incorporated in Yogurt. **Food and Bioprocess Technology**, v. 12, n. 9, p. 1500–1515, 2019.

MUSCHIOLIK, G.; DICKINSON, E. Double Emulsions Relevant to Food Systems: Preparation, Stability, and Applications. **Comprehensive Reviews in Food Science and Food Safety**, v. 16, n. 3, p. 532–555, 2017.

NECHYPORCHUK, O.; BELGACEM, M. N.; BRAS, J. Production of cellulose nanofibrils: A review of recent advances. **Industrial Crops and Products**, v. 93, p. 2–25, 2016.

NIKOUKHESLAT, H. D. et al. Characterization of physicochemical and antibacterial properties of gelatin and inulin nanobiocomposite films containing crystalline nanocellulose and *Malva sylvestris* extract. **Journal of Polymers and the Environment**, v. 30, p. 3078–3090, 2022.

OMRAN, A. A. B. et al. Micro-and nanocellulose in polymer composite materials: A review. **Polymers**, v. 13, n. 2, p. 1–30, 2021.

OTONI, C. G. et al. Recent Advances on Edible Films Based on Fruits and Vegetables-A Review. **Comprehensive Reviews in Food Science and Food Safety**, v. 16, n. 5, p. 1151–1169, 2017.

PAPUC, C. et al. Plant Polyphenols as Antioxidant and Antibacterial Agents for Shelf-Life Extension of Meat and Meat Products: Classification, Structures, Sources, and Action Mechanisms. **Comprehensive Reviews in Food Science and Food Safety**, v. 16, n. 6, p. 1243–1268, 2017.

PARAFATI, L. et al. Mango (*Mangifera indica* L.) Young leaf extract as brine additive to improve the functional properties of mozzarella cheese. **Food Chemistry**, v. 425, p. 136474, 2023.

PIMENTEL-MORAL, S. et al. Stabilization of W/O/W multiple emulsion loaded with Hibiscus sabdariffa extract through protein-polysaccharide complexes. **LWT**, v. 90, p. 389–395, 2018.

PINHEIRO, A. C. et al. Unravelling the behaviour of curcumin nanoemulsions during *in vitro* digestion: effect of the surface charge. **Soft Matter**, v. 9, n. 11, p. 3147-3154, 2013.

PINHEIRO, A. C.; COIMBRA, M. A.; VICENTE, A. A. *In vitro* behaviour of curcumin nanoemulsions stabilized by biopolymer emulsifiers – Effect of interfacial composition. **Food Hydrocolloids**, v. 52, p. 460–467, 2016.

PRICHAPAN, N.; MCCLEMENTS, D. J.; KLINKESORN, U. Utilization of multilayer-technology to enhance encapsulation efficiency and osmotic gradient tolerance of iron-loaded $W_1/O/W_2$ emulsions: Saponin-chitosan coatings. **Food Hydrocolloids**, v. 112, p. 106334, 2021.

PRODPRAN, T.; BENJAKUL, S.; PHATCHARAT, S. Effect of phenolic compounds on protein cross-linking and properties of film from fish myofibrillar protein. **International Journal of Biological Macromolecules**, v 51, p. 774-782, 2012.

PROMMACHART, R. et al. The effect of black rice water extract on surface color, lipid oxidation, microbial growth, and antioxidant activity of beef patties during chilled storage. **Meat Science**, v. 164, p. 108091, 2020.

QUAN, et al. Protein-polyphenol conjugates: Antioxidant property, functionalities and their applications. **Trends in Food Science & Technology**, v. 91, p. 507-517, 2019.

RAKSHIT, M.; SRIVASTAV, P. P. Encapsulation of hydrolysable tannin from pomegranate peel in W/O/W double emulsion: *In-vitro* digestion, release kinetics, storage and physical stabilities. **Food Hydrocolloids for Health**, v. 2, p. 100067, 2022.

RAMALHO, R. R. F. et al. Variability of polyphenols and volatiles during fruit development of three pitanga (*Eugenia uniflora* L.) biotypes. **Food Research International**, v. 119, p. 850–858, 2019.

REYES, L. M.; LANDGRAF, M.; SOBRAL, P. J. A. Gelatin-based films activated with red propolis ethanolic extract and essential oils. **Food Packaging and Shelf Life**, v. 27, p. 100607, 2021.

RIVAS, J. C. M.; SCHNEIDER, Y.; ROHM, H. Effect of emulsifier type on physicochemical properties of water-in-oil emulsions for confectionery applications. **International Journal of Food Science & Technology**, v. 51, n. 4, p. 1026–1033, 2016.

ROCCHETTI, G. et al. Impact of a Pitanga leaf extract to prevent lipid oxidation processes during shelf life of packaged pork burgers: An untargeted metabolomic approach**. Foods**, v. 9, n. 11, p. 1668, 2020.

RUBIÓ, L.; MOTILVA, M. -J.; ROMERO, M. -P. Recent advances in biologically active compounds in herbs and spices: A review of the most effective antioxidant and anti-inflammatory active principles. **Critical Reviews in Food Science and Nutrition**, v. 53, n. 9, p. 943–953, 2013.

SALVIA-TRUJILLO, L. et al. Emulsion-based nanostructures for the delivery of active ingredients in foods. **Frontiers in Sustainable Food Systems**, v. 2, p. 79, 2018.

SANTOS, P. N. A. et al. Optimization of energized dispersive guided extraction (EDGE) of antioxidants from *Eugenia uniflora* L. (pitanga) leaves using response surface methodology. **Microchemical Journal**, v. 187, p. 108411, 2023.

SCHMID, M. et al. Permeation of water vapour, nitrogen, oxygen and carbon dioxide through whey protein isolate based films and coatings - Permselectivity and activation energy. **Food Packaging and Shelf Life**, v. 6, p. 21-29, 2015.

SCHUMACHER, N. et al. Identification and Antioxidant Activity of the Extracts of *Eugenia uniflora* Leaves. Characterization of the Anti-Inflammatory Properties of Aqueous Extract on Diabetes Expression in an Experimental Model of Spontaneous Type 1 Diabetes (NOD Mice). **Antioxidants**, v. 4, n. 4, p. 662–680, 2015.

SHAMSALLAH, A. A.; RASHID, S. O. Development in gelatin-matrix composite films: The incorporation of vitamin C adducts enhances the optical behaviors of gelatin films. **Arabian Journal of Chemistry**, v. 17, n. 2, p. 105541, 2024.

SHISHIKURA, Y.; KHOKHAR, S.; MURRAY, B. S. Effects of tea polyphenols on emulsification of olive oil in a small intestine model system. **Journal of Agricultural and Food Chemistry,** v. 54, n. 5, p. 1906–1913, 2006.

ŠIPAILIENĖ, A. et al. W/O/W double emulsion-loaded alginate capsules containing Lactobacillus plantarum and lipophilic sea buckthorn (*Hippophae rhamnoides* L.) pomace extract in different phases. **Food Science and Technology International**, p. 397-407, 2022.

SIRACUSA, V. Food Packaging permeability behaviour: A report. **International Journal of Polymer Science**, v. 2012, 2012.

SOBEH, M. et al. Chemical profiling of secondary metabolites of *Eugenia uniflora* and their antioxidant, anti-inflammatory, pain killing and anti-diabetic activities: A comprehensive approach. **Journal of Ethnopharmacology**, v. 240, p. 111939, 2019.

SOBRAL, P. J. A. et al. Mechanical, water vapor barrier and thermal properties of gelatin based edible films. **Food Hydrocolloids**, v. 15, n. 4–6, p. 423–432, 2001.

SOBRAL, P. J. A.; HABITANTE, A. M. Q. B. Phase transitions of pigskin gelatin. **Food Hydrocolloids**, v. 15, n. 4–6, p. 377–382, 2001.

SU, D.; ZHONG, Q. Lemon oil nanoemulsions fabricated with sodium caseinate and Tween 20 using phase inversion temperature method. **Journal of Food Engineering**, v. 171, p. 214–221, 2016.

SURH, J.; DECKER, E.; McCLEMENTS, D. Influence of pH and pectin type on properties and stability of sodium-caseinate stabilized oil-in-water emulsions. **Food Hydrocolloids**, v. 20, n. 5, p. 607–618, 2006.

TAHERI, P. et al. Physical, mechanical and wound healing properties of chitosan/gelatin blend films containing tannic acid and/or bacterial nanocellulose. **International Journal of Biological Macromolecules**, v. 154, p. 421–432, 2020.

TAMBARA, A. L. et al. Purple pitanga fruit (*Eugenia uniflora* L.) protects against oxidative stress and increase the lifespan in Caenorhabditis elegans via the DAF-16/FOXO pathway. **Food and Chemical Toxicology**, v. 120, p. 639–650, 2018.

TESSARO, L. et al. Gelatin and/or chitosan-based films activated with "Pitanga" (*Eugenia uniflora* L.) leaf hydroethanolic extract encapsulated in double emulsion. **Food Hydrocolloids**, v. 113, p. 106523, 2021.

TESSARO, L. et al. Stable and bioactive W/O/W emulsion loaded with "Pitanga" (*Eugenia uniflora* L.) leaf hydroethanolic extract. **Journal of Dispersion Science and Technology**, v. 43, n. 12, p. 1890-1900, 2022.

TESSARO, L.; MARTELLI-TOSI, M.; SOBRAL, P. J. A. Development of W/O emulsion for encapsulation of "Pitanga" (*Eugenia uniflora* L.) leaf hydroethanolic extract: droplet size, physical stability and rheology. **Food Science and Technology**, v. 42, 2021.

TRINH, B. M.; CHANG, B. P.; MEKONNEN, T. H. The barrier properties of sustainable multiphase and multicomponent packaging materials: A review. **Progress in Materials Science**, v. 133, p. 101071, 2023.

USHIKUBO, F. Y.; CUNHA, R. L. Stability of liquid water-in-oil emulsions. **Food Hydrocolloids**, v. 34, p. 145-153, 2014.

VARGAS, F. C. et al. Assessment of the Suitability of Pitanga Leaf Extract as a Natural Antioxidant for Enhancing Canola Oil Stability: Monitoring Lipid Oxidation Parameters. **European Journal of Lipid Science and Technology**, v. 121, n. 5, p. 1800447, 2019.

VARGAS, F. C. et al. Rosemary and Pitanga Aqueous Leaf Extracts On Beef Patties Stability under Cold Storage. **Brazilian Archives of Biology and Technology**, v. 59, 2016.

VARGAS-TORRICO, M. F. et al. Preparation and characterization of gelatin-carboxymethylcellulose active film incorporated with pomegranate (*Punica granatum* L.) peel extract for the preservation of raspberry fruit. **Food Hydrocolloids**, v. 150, p. 109677, 2023.

VELDERRAIN-RODRÍGUEZ, G. R. et al. Encapsulation and stability of a phenolic-rich extract from mango peel within water-in-oil-in-water emulsions. **Journal of Functional Foods**, v. 56, p. 65–73, 2019.

VERRILLO, M. et al. Valorization of organic biomass through the production of active biopolymer film based on sodium caseinate, guar gum, and beeswax. **Food Bioscience**, v. 53, p. 102757, 2023.

VOSS, G. T. et al. Biopolymeric films as delivery vehicles for controlled release of hydrocortisone: Promising devices to treat chronic skin diseases. **Materials Science & Engineering C**, v. 114, p. 111074, 2020.

WANG, J. et al. Moisture and oxygen barrier properties of cellulose nanomaterial-based films. **ACS Sustainable Chemistry & Engineering**, v. 6, n. 1, p. 49-70, 2018.

WANG, Y. et al. Pore structure and surface property design of silicon carbide membrane for water-in-oil emulsification. **Journal of Membrane Science**, v. 648, p. 120347, 2022.

XUE, W. et al. Permeability of biodegradable film comprising biopolymers derived from marine origin for food packaging application: A review. **Trends in Food Science & Technology**, v. 136, p. 2945-307, 2023.

YAN, J. et al. Development of pH-sensitive films based on gelatin/chitosan/nanocellulose and anthocyanins from hawthorn (*Crataegus scabrifolia*) fruit. **Journal of Food Measurement and Characterization**, v. 15, p. 3901-3911, 2021.

YE, Q. et al. Development and evaluation of tea polyphenols loaded water in oil emulsion with zein as stabilizer. **Journal of Drug Delivery Science and Technology**, v. 56, p. 101528, 2020.

YOPLAC, I.; HIDALGO, A.; VARGAS, L. Antimicrobial biofilms with microencapsulation citral and sodium caseinate to extend the shelf life of fresh cheese. **Food packaging and Shel Life**, v. 34, p. 100932, 2022.

YUAN, D. et al. A novel composite edible film fabricated by incorporating W/O/W emulsion into a chitosan film to improve the protection of fresh meat. **Food Chemistry**, v. 385, p. 132647, 2022.

ZHANG, Y. et al. Probiotic encapsulation in water-in-oil high internal phase emulsions: Enhancement of viability under food and gastrointestinal conditions. **LWT**, v. 163, p. 113499, 2022.

ZHAO, R. et al. Fabrication of multifunctional materials based on chitosan/gelatin incorporating curcumin-clove oil emulsion for meat freshness monitoring and shelf-life extension. **International Journal of Biological Macromolecules**, v. 223, p. 837-850, 2022.

ZHUANG, H. et al. Fabrication of grape seed proanthocyanidin-loaded W/O/W emulsion gel stabilized by polyglycerol polyricinoleate and whey protein isolate with konjac glucomannan: Structure, stability, and *in vitro* digestion. **Food Chemistry**, v. 30, p. 135975, 2023.

ZLABIENE, U. et al. *In Vitro* and Clinical Safety Assessment of the Multiple W/O/W Emulsion Based on the Active Ingredients from *Rosmarinus officinalis* L., *Avena sativa* L. and *Linum usitatissimum* L. **Pharmaceutics**, v. 13, n. 5, p. 732, 2021.

5 CAPÍTULO 2: Gelatin/chitosan based films loaded with nanocellulose from soybean straw and activated with "pitanga" (*Eugenia uniflora* L.) leaf hydroethanolic extract in w/o/w emulsion

Larissa Tessaro [a], Rodrigo Vinícius Lourenço [a], Milena Martelli-Tosi [a], Paulo José do Amaral Sobral [a b]

[a] *Department of Food Engineering, Faculty of Animal Science and Food Engineering, University of São Paulo, Av Duque de Caxias Norte, 225, 13635-900 Pirassununga, SP, Brazil.*

[b] *Food Research Center (FoRC), University of São Paulo, Rua do Lago, 250, Semi-industrial building, block C, 05508-080 São Paulo, SP, Brazil.*

Abstract

Mechanical properties of biopolymer films can be a limitation for their application as packaging. Soybean straw crystalline nanocelluloses (NC) can act as reinforcement load to improve these material properties, and W/O/W double emulsion (DE) as encapsulating bioactive agents can contribute to produce active packaging. DE droplets were loaded with pitanga leaf (*Eugenia uniflora* L.) hydroethanolic extract. The mechanical, physicochemical, and barrier properties, and the microstructure of gelatin and/or chitosan films incorporated with NC or NC/DE were determined by classical methods. Film antioxidant activities were determined by ABTS and DPPH methods. The incorporation of NC/DE in gelatin and/or chitosan films (NC/DE films) changed the morphology of these films, which presented more heterogeneous air-side surfaces and cross-sections. They presented rougher topographies, notably greater resistance and stiffness, higher barrier properties to UV/Vis light and higher antioxidant activity than the NC films. Moisture content, solubility in water and water vapor permeability decreased due to the presence of DE. Overall, the NC/DE films improved all properties, when compared to the properties of NC films or those of films with only DE, from a previously published study. In spite of not having antimicrobial activity against the studied bacteria, NC/DE films did display a great antioxidant activity.

Keywords: Active films; nanocomposites; antioxidant activity; antimicrobial activity; mechanical property; biopolymers blends.

5.1 INTRODUCTION

Biopolymers from natural and renewable sources, such as polysaccharides (i.e, chitosan, starch, galactomannans and pectin) (Chakravartula et al., 2020; Dutta; Ravikumar; Dutta, 2002; Kaya et al., 2018; Khan et al., 2012; Pelissari et al., 2017) and proteins (i.e., gelatin, whey protein, sodium caseinate and soy protein isolate) (Bonilla et al., 2018; Dammak et al., 2017; Hosseini; Gómez-Guillén, 2018; Martelli-Tosi et al., 2018; Pereda et al., 2011; Pérez Córdoba; Sobral, 2017; Ranjbaryan; Pourfathi; Almasi, 2019) have been widely studied for the production of edible films, alone or in blends, such as for gelatin and chitosan (Bonilla; Sobral, 2016; Jridi et al., 2014; Hosseini et al., 2016; Pérez Córdoba et al., 2018; Pérez Córdoba; Sobral, 2017; Tessaro et al., 2021a). Edible films can act as a vehicle for active compounds and therefore are interesting for the production of active films for application as food packaging (Hosseini; Gómez-Guillén, 2018; Pérez Córdoba et al., 2018).

Active films are an important alternative to the conventional packaging because they inhibit the growth of microorganisms and lipid oxidation of food with a reduced amount of additives (Lorenzo et al., 2018). Active films can be produced by addition of such additives into a film's matrix. As an example, plant extracts, usually rich in antioxidant and antimicrobial compounds, can be used as sources of natural agents for the production of active films (Bonilla; Poloni; Sobral, 2018; Chakravartula et al., 2020; Kaya et al., 2018). In particular, pitanga (*Eugenia uniflora* L.) leaf hydroethanolic extract (PLHE) has shown promising results for its application as a source of natural antioxidant and antimicrobial components in the production of these materials (Chakravartula et al., 2020).

Eugenia L. is a genus of plants in the family Myrtaceae, which has 400 native Brazilian species. *Eugenia uniflora* L., popularly known as "pitanga" or "pitangueira", is one of these species, and its fruits are known as the Brazilian cherry (Arai et al., 1999; Schumacher et al., 2015). Several studies have shown that different extracts from the leaves of pitanga demonstrated an important antioxidant and/or antimicrobial action (Vargas et al., 2016; Vargas et al., 2019), and the phenolic compounds are primarily responsible for the biological action of pitanga leaf extracts (Lorenzo et al., 2018).

The PLHE can be added directly into a film-forming solution to produce active films (Chakravartula et al., 2020; Luciano et al., 2021); nevertheless, some bioactive

compounds presented into PLHE can be negatively affected by environmental conditions (i.e., temperature, pH, exposure to light and oxygen) (Pimentel-Moral et al., 2018). An alternative to protect, improve and control the release of these active compounds is to encapsulate them in W/O (Tessaro; Martelli-Tosi; Sobral, 2021) or in W/O/W emulsions (Pérez Córdoba et al., 2018; Tessaro et al., 2021), allowing their applications in aqueous systems, in the latter case.

Water-in-oil-in-water (W/O/W) emulsions, also known as double emulsions, are widely used to encapsulate aqueous active compounds in the internal aqueous phase (Muschiolik; Dickinson, 2017). Some aqueous active compounds, such as anthocyanins (Huang; Zhou, 2019), resveratrol (Matos et al., 2018), and even PLHE (Tessaro et al., 2021a), among others, have been encapsulated in W/O/W double emulsions. These complex systems are nothing more than an "emulsion of emulsions" (Muschiolik; Dickinson, 2017), where a previously prepared water-in-oil (W/O) single emulsion is dispersed in an external aqueous phase (W/O)/W. The incorporation of W/O/W double emulsions loaded with active compounds in active films is little studied, but feasible, as reported in a previous study (Muschiolik; Dickinson, 2017).

Another characteristic that can limit the application of active films based on biopolymers, as compared to conventional packaging, is the inferior performance of some physical and mainly mechanical properties. An approach to improve these film properties is the use of nanoparticles as reinforcement (Alexandre et al., 2016; Hosseini; Gómez-Guillén, 2018), which produce a new material of so called nanocomposite films. Specifically, the use of cellulose nanofibers (also called nanocelluloses) as reinforcing elements in biopolymers matrices can improve their thermomechanical properties and decrease the sensitivity of biopolymers to water, thereby preserving biodegradability (Pelissari et al., 2017). Nanocelluloses are nanofibers extracted mainly from vegetable cellulose fibers, which are linear, fibrous, resistant, and water-insoluble homopolysaccharides found mainly in wood, cotton, natural fibers and lignocellulosic materials (Gómez et al., 2016; Hosseini; Gómez-Guillén, 2018).

These nanocelluloses can be extracted by chemical or enzymatic hydrolysis and mechanical treatment of lignocellulosic materials (Martelli-Tosi et al., 2018; Pelissari et al., 2017). Depending on the extraction method, the dimensions and compositions and properties of the nanocelluloses can vary, resulting in two types of materials: crystalline nanocelluloses (obtained by acid hydrolysis) or fibrillated nanocelluloses (resulting

from enzymatic hydrolysis and/or mechanical treatment) (Martelli-Tosi et al., 2018; Nechyporchuk; Belgacem; Bras, 2016). Thus, due to their nano/micro scale, crystalline nanocelluloses incorporated into biopolymeric films can produce nanocomposite films (Martelli-Tosi et al., 2018; Nechyporchuk; Belgacem; Bras, 2016).

Although there are many studies involving the production of active films, no previous study has led to the application of nanocelluloses and W/O/W double emulsion for the production of active nanocomposite films. This study is therefore a continuation of one previously published (Tessaro et al., 2021), in which only the effect of W/O/W emulsion on the properties of the gelatin and/or chitosan-based films has been evaluated. The objective here was to develop active nanocomposite films based on gelatin and/or chitosan. The film's activation was facilitated by the incorporation of W/O/W double emulsion loaded with PLHE, and the nanocomposite character was made possible by charging these materials with soybean straw crystalline nanocelluloses. Thus, the effects of these treatments on the physicochemical, barriers, mechanical and active properties of films were studied.

5.2 MATERIAL AND METHODS

5.2.1 Material

A bovine gelatin type B (225 bloom, medium molecular weight 4-5 x 10^4 Da) and chitosan (medium molecular weight, ~190 kDa; density: 0.15 – 0.3 g/cm³; degree of deacetylation 75-85%; viscosity 200-800 cps) were used as biopolymers and purchased from Gelnex (Santa Catarina, Brazil) and Sigma-Aldrich Chemie GMBH (Steinhelm, Germany), respectively. Glycerol with 95% purity (Synth, São Paulo, Brazil) was used as a plasticizer as necessary for the production of the films matrix.

PLHE was produced from pitanga leaves collected in the city of Pirassununga (21°59'46" S, 47°25'36" W), São Paulo, Brazil. The emulsifiers Grinsted PGPR® (Polyglycerol Polyricinoleate) (DuPont, São Paulo, Brazil) and Tween® 80 (Polysorbate 80) (Sigma-Aldrich, St Louis, Missouri, USA), sodium caseinate with > 90% purity (Fonterra, Auckland, New Zeland) and food grade soybean oil (Cargill, Minas Gerais, Brazil) were used for the production of the W/O/W double emulsion (DE).

Acetone (PA), ethanol (PA), hydrogen peroxide, sodium hydroxide and acetone (PA), ethanol (PA), hydrogen peroxide, sodium hydroxide and magnesium sulfate heptahydrate (Dinâmica Química Contemporânea LTDA, São Paulo, Brazil) were used for the extraction of the soybean nanocelluloses from soybean straw that was donated by Embrapa Soja, Londrina, Paraná (Brazil).

The 2,2'-azino-bis (3-ethylbenzothiazoline-6-sulphonic acid) (ABTS), gallic acid, 6-hydrox-2,5,7,8-tetramethylchroman-2-carboxylic acid (Trolox), iron (III) chloride hexahydrate and 2,4,6-Tri(2-pyridyl)-1,2,3-triazine (TPTZ) (Sigma-Aldrich, St Louis, Missouri, USA), and the Folin-Ciocalteu reagent, potassium persulfate, sodium acetate trihydrate and sodium carbonate (Merck, Darmstadt, Germany) were used for the antioxidant analysis. Brain heart infusion (BHI) and trypic soy broth (TSB) (Acumedia®, São Paulo Brazil), the Mueller-Hinton medium (Dfico^{TM}, São Paulo, Brazil), and *Pseudomonas aeruginosa* (ATCC 15442), *Salmonella ssp* (ATCC 13076) and *Staphylococcus aureus* (ATCC 25923) strains were used for the antimicrobial analysis.

5.2.2 Production of pitanga leaf hydroethanolic extract (PLHE)

The pitanga leaves were selected according to their color (uniform and dark green), washed with distilled water, and submitted to drying at 42 °C/72 h in an air circulating oven (MA035/5, Marconi, Brazil). The dried leaves were ground (commercial blender) and sieved (48-mesh sieve). The PLHE was extracted from these powdered pitanga leaves using hydroethanolic solvent, according to Tessaro et al. (2021).

5.2.3 Production of the W/O/W double emulsion (DE)

The W/O/W (DE) was produced in two steps. In the first step, a W/O primary emulsion was prepared using the aqueous dispersion of PLHE (1 g of freeze-dried PLHE/10 g of water) as internal aqueous phase (20% w/w) and soybean oil containing the polyglycerol polyricinoleate (PGPR), a hydrophobic emulsifier (3 g PGPR/100 g oil) as the dispersant oil phase (80% w/w) (Tessaro; Martelli-Tosi; Sobral, 2021). In the second step, the DE was prepared by dispersing the previously prepared W/O emulsion (40% w/w) in the external aqueous phase (60% w/w) containing a hydrophilic

emulsifier (3 g Tween 80/100 g water) and sodium caseinate (0.5 g/100 g water), which acted as emulsion stabilizer and yielded a DE containing 0.73 g of freeze-dried PLHE/100 of emulsion (Tessaro et al., 2021). The produced DE was immediately used for the production of films. This DE has been characterized in a previous work.

5.2.4 Extraction of soybean straw crystalline nanocelluloses

First, the soybean straw was sanitized with distilled water and dried at 50 °C for 72 h in an air circulating oven (MA035/5, Marconi, Brazil). The dried soybean straw samples were ground (Knife mill SL31, Solab, Brazil) and sieved (100-mesh sieve). Uniform samples of the dried straw were then subjected to chemical treatments (alkali and bleaching) for the extraction of the soybean straw crystalline nanocelluloses (NC), as described by Martelli-Tosi et al. (2018).

5.2.5 Characterization of soybean straw crystalline nanocelluloses

The NCs were analyzed for morphology, Zeta-potential and yield. The morphology of the NC was studied using an atomic force microscopy (AFM, NT-MDT, Russia) operating in semi-contact mode with 240 kHz of resonant frequency, 11.8 N/m of contact force and 0.6 Hz of scan speed. For these analyzes, the NC suspensions were diluted to a concentration of 0.01 g NC in dry matter/100 ml, dried, and the analyzed area was 5 x 5 μm^2.

The Zeta-potential value of the NC suspension was determined using a Zetasizer Nano ZS instrument (Malvern Instruments, UK) coupled with a ZEN 1020 dip cell at 25 °C. Zeta-potential values were obtained by equipment software. The yield of the NC was determined gravimetrically by drying (50 °C) the NC suspension to a constant weight and expressed as g NC in dry matter/100 g NC suspension and g NC in dry matter/100 g soybean straw (Martelli-Tosi et al., 2017).

5.2.6 Production of films

Gelatin (4 g/100 g film-forming solution), chitosan (1 g/100 g film-forming solution) and gelatin/chitosan 70/30 blend (2 g/100 g film-forming solution) were

produced by the casting method, which is by the drying of the respective film-forming solutions (FFS). FFS were prepared as described by Tessaro et al. (2021) with just one difference: the addition of NC. Briefly, gelatin (G) was hydrated and solubilized at 55 °C for 10 min., while chitosan (C) was dispersed in 1% (v/v) glacial acetic acid solution at room temperature for 12 h. For the gelatin/chitosan blend (GC), previously prepared solutions were conveniently mixed using a rotor-stator homogenizer (Ultraturrax® IKA T25, Labotechnik, Germany) at 10,000 rpm for 5 min. at room temperature. Then, glycerol (25 g/100 g biopolymer) and 4.5 g NC $_{d.b.}$/100 g biopolymer were added to FFS under agitation at 10,000 rpm for 5 min (Ultraturrax® IKA T25, Labotechnik, Germany) at room temperature.

Finally, the DE was added dropwise under magnetic stirring (1000 rpm, AA-2050, Gehaka, Brazil) to the FFSs to perform a concentration of 0.25 g PLHE/100 g biopolymer. Films without DE were also were produced as a control. The following treatments were then analyzed: passive (without DE) and active nanocomposite films based on gelatin (G- NC, G-NC/DE), chitosan (C-NC, C-NC/DE) and on gelatin/chitosan blend (GC-NC, GC- NC/DE) (respectively).

The FFSs were poured into acrylic plates (12 x 12 cm) then dried at 30 °C for 24 h (MA035/5, Marconi, Brazil). Before characterizations, films were conditioned for 7 days in desiccators with saturated NaBr solution (relative humidity = 58%) at 25 °C, but for microstructure analyses, films were previously conditioned over silica gel for 15 days.

The concentrations of oil, sodium caseinate and PLHE in the film's samples were 11.1 g oil/100 g biopolymers, 0.10 g sodium caseinate/100 g biopolymers and 0.25 g PLHE/100 g biopolymers.

5.2.7 Characterizations of the films

5.2.7.1 Visual aspect and thickness

The aspect, homogeneity, and uniformity of the films were observed visually and described as a visual aspect. Ten random thickness measurements were made on the surface of the films (Sobral et al., 2001) with the aid a digital micrometer (Mitutoyo, Sakado, Japan).

5.2.7.2 Moisture content and solubility in water

The moisture content (MC) was determined gravimetrically (Gontard; Guilbert; Cuq, 1992). Sample films were dried at 105 °C for 24 h, and the MC was expressed as g water/100 g of wet film.

The solubility in water (SW) was determined by shaking (60 rpm) films sample (2 cm diameter and known dry weight) with 50 mL of distilled water at 25 °C for 24 h (Shaker incubator MA-41, Marconi, Brazil) (Gontard; Guilbert; Cuq, 1992). The non-solubilized part of the films was dried at 105 °C for 24 h, and the SW (%) was calculated gravimetrically.

5.2.7.3 Water vapor permeability

Film samples with a diameter of 30 mm were sealed into aluminum cells (permeation area = 31.17 cm²) containing silica gel (RH = 0% and vapor pressure = 0 Pa), which were kept in desiccators containing distillated water (RH = 100% and vapor pressure = 3.2691 kPa), according to the standard ASTM E96-E80 (ASTM, 1989) with slight modifications (Gontard; Guilbert; Cuq, 1992). The weight gain of the aluminum cells was taken every 24 h for 7 days. The WVP was calculated with the eq. (5.1), with $\Delta g/\Delta t$ being the rate of weight change (g/h); x, the film thickness (mm); A, the permeation area (cm²), and ΔP, the partial pressure difference across the films (3.1691 kPa).

$$WVP = \frac{\Delta g}{\Delta t}\left(\frac{x}{A\Delta P}\right)$$
(5.1)

5.2.7.4 Scanning electron microscopy (SEM)

Air-side surface and cryo-fractured cross-section of the films were analyzed by scanning electron microscopy (SEM, TM-3000, Hitachi, Japan) in a random position at an accelerating voltage of 15 kV (Valencia et al., 2016). For air-side surface analysis, sample films were attached to the equipment without any prior preparations, and for the cross-section analysis, sample films were cryo-fractured after quench freezing using liquid nitrogen.

5.2.7.5 Atomic force microscopy (AFM)

The topography and roughness of the air-side surface films (20 x 20 µm) were analyzed by atomic force microscopy (AFM, NT-MDT, Russia) in semi-contact mode, 240 kHz of resonant frequency, 11.8 N/m of contact force and 0.3 Hz of scan speed (Valencia et al., 2016). The roughness (R_a) was calculated as the absolute value of the height deviations by using the equipment software (Nova Px 3.2.5 Rev 1266 software).

5.2.7.6 Fourier-transform infrared spectroscopy (FTIR)

FTIR spectra were obtained with a spectrophotometer (Spectrum-One, Perkin Elmer, USA), equipped with a Universal Attenuator Total Reflectance (UATR) accessory, by performing 20 scans in the spectral range of 4000 - 650 cm^{-1} (Tessaro et al., 2021). Spectra were analyzed using the Spectrum One software (Spectrum One, version 5.3, Perkin Elmer).

5.2.7.7 Gloss

The film's gloss was determined at the angle of 60° using a glossmeter (Rhodopoint NGL 20/60) according to standard ASTM D523 (ASTM, 1999). Ten measurements were made at random places on the film air-side surface, which were expressed as gloss units (GU).

5.2.7.8 Color and opacity

The color parameters (L*, a* and b*) were obtained using a colorimeter (MiniScan EX 4500 L, Hunter Associates Laboratory, USA) in reflectance mode (CIElab scale, illuminant D65, angle 10°) (Valencia et al., 2016). Total color difference (ΔE^*) was calculated with eq. (5.2), being $\Delta L^* = L^*_{sample} - L^*_{standard}$ (93.79), $\Delta a^* = a^*_{sample} - a^*_{standard}$ (-1.00) and $\Delta b^* = b^*_{sample} - b^*_{standard}$ (1.75).

$$\Delta E^* = \sqrt{(\Delta L^*)^2 + (\Delta a^*)^2 + (\Delta b^*)^2} \tag{5.2}$$

5.2.7.9 UV/Vis light barrier

The ultraviolet and visible (UV/Vis) light barrier properties were carried out in a UV-Vis spectrophotometer (Lambda 25 UV/Vis, Perkin-Elmer, USA) in transmittance mode and a wavelength range from 200 to 800 nm (Bonilla; Sobral, 2016). Sample films (10 x 100 mm) were fixed in the cuvette so the light passed over the surface of the films.

5.2.7.10 Thermal properties

The thermal properties of the films were determined using a differential scanning calorimeter (DSC TA2010, TA Instruments, USA). Samples, placed in hermetically sealed aluminum TA pans, were heated from -50 to 120 ºC at 5 ºC/min, twice, in an inert atmosphere (45 mL/min N_2). An empty pan was used as reference. Before both scans, the DSC cell was cooled using liquid nitrogen. Glass (Tg) and melting (Tm) temperatures and melting enthalpy (ΔH) were calculated directly of the thermal curves using the software Universal Analysis V1.7F (TA Instruments, USA) (Gontard; Guilbert; Cuq, 1992; Tessaro et al., 2021).

5.2.7.11 Mechanical properties

Tensile strength (TS), elongation at break (EB) and elastic modulus (EM) were determined by tensile tests using a texturometer (TA. XT2i, TA Instruments, NC, USA), at room temperature (25 ± 2 °C), according to the standard ASTM D88/12 (ASTM, 2001). The sample films were cut in 15 x 100 mm size and fixes on grips distant by 50 mm. The test was performed with speed of separation of the grips of 1 mm/s. TS and EB were determined from the stress versus deformation curves, and the EM was calculated from the slope of the linear region of that curve with the aid of the equipment software (Exponent Lite Express, v4.0.13.0).

5.2.7.12 Antimicrobial activity

The disk diffusion test was used to assess the antimicrobial activity of the films against *P. aeruginosa*, *Salmonella* and *S. aureus* strains and followed the standard

procedure of the National Committee for Clinical Laboratory Standard (NCCLS, 2000). *The P. aeruginosa* culture was regenerated in TSB broth, and *Salmonella* and *S. aureus* cultures were regenerated in BHI broth, at 37 °C for 24 h. The strains of bacterial suspensions were then standardized using a UV-Vis spectrophotometer at 625 nm (0.08 - 0.10 of the absorbance and 1×10^8 UFC/mL). Sample film disks (6 mm diameter) were placed on the Mueller-Hinton agar surface containing the bacterial strains' suspensions and incubated at 37 °C for 24 h. Chloramphenicol antibiotic (2.5 mg/mL) and distilled water were used as positive (C^+) and negative (C^-) control, respectively. The extent of the inhibition areas against growth of the bacteria were considered as the antimicrobial activity.

5.2.7.13 Folin-Ciocalteu reducing capacity (FCRC) and Antioxidant activity (AA)

The Folin-Ciocalteu reducing capacity (FCRC) of the films was determined according to Singleton and Rossi (1965), and their AA was determined by both the ABTS$^{\bullet+}$ free radical scavenging method (ABTS$^{\bullet+}$ method), according to methodology described by Re et al. (1999), and by the Ferric reduction antioxidant power method (FRAP method), according to Benzie and Strain (1996), with some modifications proposed by Pulido et al. (2000). For all these analyzes, films (0.200 ± 0.005 g) were cut in small pieces and added into the hydroethanolic solution (1:1) (0.2 g film/10 mL solution) and shaken at 50 rpm for 12 h (Shaker incubator MA-41, Marconi, Brazil) in the dark (Tessaro et al., 2021). Supernatants were used for these analyzes.

5.2.8 Statistical analysis

All films were produced in triplicate, and analyzes were carried out with at least three measurements from each replicate. The results were submitted to variance analysis to compare the averages using two-way (ANOVA) analysis and Tukey test comparisons ($p < 0.05$) with the aid of the Statistica 7 software.

5.3 RESULTS AND DISCUSSION

5.3.1 Morphology, Zeta-potential and yield of the NC

The NC extracted from soybean straw presented a rod-like structure with nanometric diameter (Figure 5.1a), which varied in length from 3 to 9 nm (Figure A1, Appendix A). Unfortunately, it was not possible to determine the length of the NCs accurately because some agglomeration occurred (Figure 5.1b), which is very common. Similar structures were observed on nanocelluloses produced from banana peels (Pelissari et al., 2017), soybean straw (Martelli-Tosi et al., 2018; Okamoto-Schalch et al., 2020), and from other sources (Nechyporchuk; Belgacem; Bras, 2016), and also on an industrialized NC (unknown botanical origin) (Cao; Elimelech, 2021).

Figure 5.1 – Atomic force micrograph of one soybean straw crystalline nanocellulose (a) and of agglomerates (b)
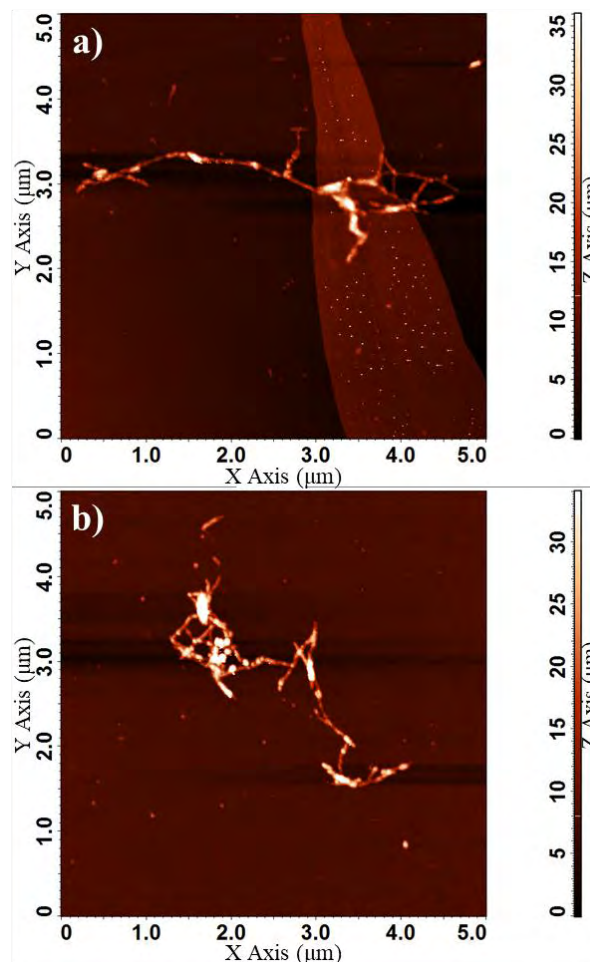
Source: Own authorship.

The Zeta-potential of the NC was -15 ± 3 mV, which is almost similar to that reported by Okamoto-Schalch et al. (2020) for NC extracted from soybean straw (-19 mV) and by Pelissari et al. (2017) for NC extracted from banana peels (-16.1 mV). Nevertheless, in this last case, the Zeta-potential increased to |-44.1| mV when the NC suspension was treated by high-pressure homogenization for 7 cycles (Pelissari et al., 2017). Desirable values of Zeta- potential to avoid agglomeration of nanoparticles are above |±30| mV (Martelli-Tosi et al., 2018), which may avoid the agglomeration of NC, so maintaining well-dispersed NC during the nanocomposite films-forming solution processing is of great importance since aggregation dramatically decreases surface area and hinders successful applications of NC (Cao; Elimelech, 2021).

The extraction yield of the NC from soybean straw was 0.3 ± 0.0 g NC in dry matter/100 g NC suspension, or 13.4 ± 1.4 g NC in dry matter/100 g soybean straw, similar to the yield reported by Martelli-Tosi et al. (2018). The yields are always of these orders because these nanostructures are in low amount in raw materials.

5.3.2 Films properties

5.3.2.1 Visual aspect and thickness

Visually, all films presented a uniform aspect without fractures or bubbles and were easily removed from the acrylic plates without deformation or rupture (Figure A2). NC films were transparent, whereas NC/DE films were translucent. The average film thickness remained ($p > 0.05$) around 82 μm (Table 5.1). This result, similar to that determined by Tessaro et al. (2021), was possible because the mass of FFS deposited on Petri plates was controlled, as observed by Pelissari et al. (2017). This control was necessary to avoid interference of different thicknesses on films properties.

5.3.2.2 Moisture content (MC) and solubility in water (SW)

The incorporation of the DE decreased ($p < 0.05$) the MC of all NC/DE films (Table 5.1) since the soybean oil present in the DE can reduce the hydrophilicity of the films. Regarding the effect of the biopolymer, C films had the highest MC value ($p < 0.05$), whereas G films had the lowest MC value ($p < 0.05$) for both loads. The MC of

G and GC films were lower than some values found in the literature, as for example, for incorporated O/W single emulsions in G and/or C films without NC (15 - 18%) (Dammak et al., 2017; Pérez Córdoba et al., 2018).

Table 5.1 - Physicochemical properties, gloss, color parameters and opacity of gelatin (G), chitosan (C) and gelatin/chitosan (GC) films with soybean straw crystalline nanocelluloses without (NC) or with NC and double emulsion (NC/DE)**

Properties	Treatments	G	C	GC
Thickness (mm)	NC	79 ± 9^{aA}	83 ± 5^{aA}	80 ± 6^{aA}
	NC/DE	82 ± 7^{aA}	85 ± 5^{aA}	82 ± 8^{aA}
Moisture Content (%)	NC	12.7 ± 0.6^{cA}	29.1 ± 1.9^{aA}	16.9 ± 1.5^{bA}
	NC/DE	11.0 ± 0.8^{bB}	25.5 ± 1.1^{aB}	13.3 ± 1.5^{bB}
Solubility in Water (%)	NC	52.9 ± 1.8^{aA}	41.4 ± 2.4^{bA}	41.5 ± 2.1^{bA}
	NC/DE	48.8 ± 1.3^{aB}	36.5 ± 1.4^{bB}	35.9 ± 1.9^{bB}
WVP (g mm/m² h kPa)	NC	0.30 ± 0.03^{aA}	0.22 ± 0.01^{bA}	0.17 ± 0.01^{cA}
	NC/DE	0.23 ± 0.02^{aB}	0.16 ± 0.02^{bB}	0.12 ± 0.02^{bB}
Gloss	NC	106 ± 5^{bA}	91 ± 5^{bA}	110 ± 7^{aA}
	NC/DE	24 ± 2^{bB}	13 ± 2^{bB}	22 ± 3^{aB}
L*	NC	88.6 ± 0.4^{aA}	87.8 ± 0.2^{aA}	88.2 ± 0.4^{aA}
	NC/DE	87.1 ± 0.6^{aB}	82.4 ± 0.8^{bB}	82.8 ± 0.5^{bB}
a*	NC	-0.6 ± 0.0^{cA}	-1.4 ± 0.0^{aA}	-0.9 ± 0.0^{bA}
	NC/DE	-0.6 ± 0.1^{bA}	-0.8 ± 0.0^{aB}	-0.8 ± 0.1^{abA}
b*	NC	7.0 ± 0.8^{bA}	9.7 ± 0.6^{aA}	6.9 ± 0.6^{bB}
	NC/DE	7.1 ± 0.6^{bA}	8.8 ± 0.6^{aA}	8.7 ± 0.5^{aA}
ΔE*	NC	7.8 ± 0.8^{bA}	10.4 ± 0.6^{aB}	7.9 ± 0.6^{bB}
	NC/DE	8.6 ± 0.8^{bA}	13.4 ± 1.0^{aA}	13.1 ± 0.6^{aA}
Opacity (%)	NC	2.2 ± 0.2^{aB}	1.4 ± 0.2^{bB}	1.4 ± 0.1^{bB}
	NC/DE	4.8 ± 0.6^{abA}	4.5 ± 0.5^{bA}	6.2 ± 0.7^{aA}

Different lowercase letters on the same line and uppercase letters in the same column indicate significant differences between averages according to Tukey test ($p < 0.05$). WVP is water vapor permeability, and ΔE* is total difference of color.
**Average ± standard deviation (n = 9).

Source: Own authorship.

The presence of NC decreased the values of MC of the G and GC films when compared to the values of films produced under the same conditions, but without NC (Tessaro et al., 2021). This decrease was rarely observed in C films. These reductions in MC values (about 20% in G films and 15% in GC films) may have occurred due to the rigid structure and high crystallinity of the NC, which reduces water absorption (Ranjbaryan; Pourfathi; Alsami, 2019). Pelissari et al. (2017), working on starch-based films, observed that the incorporation of NC also reduced nanocomposite MC and explained this result by stating that NC have lower affinity for water as compared with starch.

Like the MC, the SW values of NC/DE films were lower ($p < 0.05$) than that of NC films (Table 5.1). Dammak et al. (2017) and Pérez-Córdoba et al. (2018) also observed a reduction in SW for G and/or C films incorporated with emulsified oils, and they attributed these results to the increase in the hydrophobic character of films due to the presence of DE oil droplets. The same behavior was observed in a previous study, without the presence of NC in the films (Tessaro et al., 2021); however, the SW values found in the present study were lower than those reported for films incorporated with O/W emulsions without the presence of NC (43 - 58%) (Dammak et al., 2017; Pérez Córdoba et al., 2018). Regarding the effects of the biopolymer, the G films showed the highest SW values ($p < 0.05$) for both loads; no significant difference ($p > 0.05$) was observed for C and GC films (Table 5.1). This result was due to the higher affinity of gelatin chains for water molecules as compared with the chitosan chains.

The presence of NC had little effect on the SW values of the G films, but provoked a decrease averaging 8.5% in the SW of the C and GC films, as compared with respective films without any load (Tessaro et al., 2021). This can be explained by the greater affinity of the G matrix for water, which could explain its high solubility, and by the probability for better interfacial bonding between the NC and C. This explains the positive effect of NC loading without neglecting some effect due to the formation of NC networks, which hinders water diffusion through the matrix (Pelissari et al., 2017). NC is negatively charged, i.e., it is anionic (Okamoto-Schalch et al., 2020) as noted by its Zeta-potential (Section 5.3.1). This allows strong interactions between the negative groups of the NC and the positively charged functional groups of chitosan. Type-B gelatin, on the other hand, is also a polyelectrolyte whose predominant charge depends on the solution's pH. In addition, gelatin has a greater affinity for water than chitosan, which may not have been affected by the presence of NC.

5.3.2.3 Water vapor permeability (WVP)

The WVP of the NC/DE films was lower ($p < 0.05$) than that of NC films (Table 5.1). The hydrophobicity of soybean oil, present in DE, possibly inhibits the permeation of water vapor in the biopolymeric matrix (Ranjbaryan; Pourfathi; Almasi, 2019). A reduction in WVP in biopolymeric films incorporated with different types of oil, emulsified or not, has also been observed by Dammak and Sobral (2019) and Hosseini et al. (2016) for single films and by Ranjbaryan, Pourfathi and Almasi (2019) for films charged with NC. Nevertheless, this effect is not always evident due to the difficulties to well disperse lipids in the biopolymeric matrix, which may cause disruptions and create void spaces at the biopolymer-lipid interface that negatively affect the film WVP (Bonilla et al., 2018). In relation to biopolymer effect, G films showed the highest ($p < 0.05$) WVP values, possibly due to the greater solubility and affinity of gelatin for water. The same behavior was observed in the study with the same films without NC (Tessaro et al., 2021).

With the incorporation of NC, all films had their WVP values decreased compared to the same films without NC (Tessaro et al., 2021). These reductions in the WVP were 25, 48 and 34% for G-NC, C-NC and GC-NC films, respectively. These reductions can be explained by the effect of NC in the tortuosity of the biopolymeric matrix, which hinders the diffusion of water vapor and, consequently, decreases the WVP (Martelli-Tosi et al., 2018; Pereda et al., 2011a). Khan et al. (2012) also observed a reduction in the WVP values in C films reinforced with NC that were present in different concentrations (1 to 10%). Similar results were also determined by Pelissari et al. (2017), who worked on nanocomposite films based on starch. Nevertheless, for NC it is also possible to observe the negative effect of NC on WVP, as was observed by Pereda et al. (2011a) for nanocomposite films based on sodium caseinate due to the presence of some defects on NC-biopolymer matrix. Nevertheless, in practical terms, all these films cab be considered as very permeable to water vapor, with no effective change for application as a higher water vapor barrier.

5.3.2.4 Microstructure

According to scanning electron micrographs, the air-side (Figure 5.2) and internal surfaces (Figure 5.3) of NC films were smoother and more homogeneous and

continuous than those of NC/DE films. In the NC films, some particles or bubble spaces can be observed randomly dispersed on the air-side surface. This was more visible in GC-NC film than in the C and G-NC films (Figure 5.2). These microstructures probably corresponded to some agglomerated NC particles. In the cross-section of NC films some white spots can be observed, possibly corresponding to clusters of NC particles (Figure 5.3); however, the NC structures were well dispersed in the matrices, and fractures and phase separation were not observed. Similar porous morphology was observed by Martelli-Tosi et al. (2018), working on soy protein films incorporated with NC, and by Khan et al. (2012), working on C nanocomposite films.

In the NC/DE films, the air-side (Figure 5.2) and cross-section (Figure 5.3) were less homogeneous and had some visible porous structures. These results were possibly due to the separation of oil and other components present in the DE, which were dragged by moisture migration to the air-side surface during the drying process (Kaya et al., 2018). DE destabilization processes during drying (i.e., flocculation and coalescence) can favor the grouping of droplets and oil and migration to the surface (Tessaro et al., 2021). Indeed, when DE was added to film-forming solution, the inner W/O droplets were dispersed into water and biopolymer, but some W/O droplets were broken delivering the PLHE to the biopolymer matrix. And, in this case, oil migrated to air side surface during drying.

In the G-NC/DE and GC-NC/DE films, a large number of clear bubbles were visible, including some pores. In the C-CN/DE film, oil drops became more evident and were like dark regions. In the cross-section (Figure 5.3), some dark micropores can be observed suggesting that these volumes were reserved to the oil droplets of the inner phase of DE. Although the morphology of these films was more heterogeneous, the structures observed were well dispersed in the matrix. Similar morphology was observed by Tessaro et al. (2021), for G and/or C films incorporated only with DE. Other authors also observed that G and/or C film microstructures had porous morphology when incorporated with oils, emulsified or not (Bonilla et al., 2018; Kaya et al., 2018; Tessaro et al., 2021).

Figure 5.2 – Electronic scanning micrographs of the air-side surface of gelatin (G), chitosan (C) and gelatin/chitosan (GC) films with soybean straw crystalline nanocelluloses (NC) or films with NC and double emulsion (NC/DE)
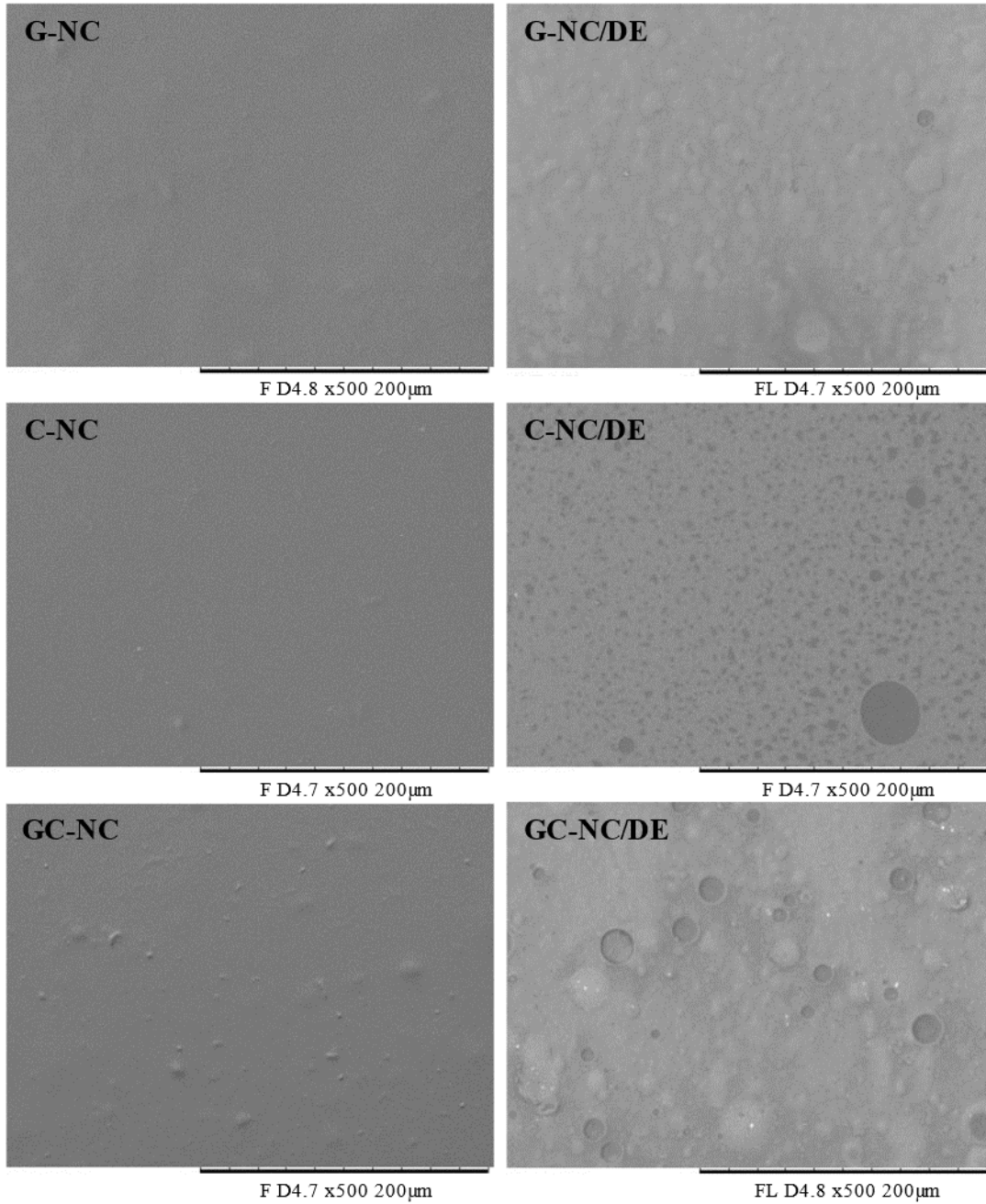
Source: Own authorship.

Figure 5.3 – Electronic scanning micrographs of the cross-section of gelatin (G), chitosan (C) and gelatin/chitosan (GC) films with soybean straw crystalline nanocelluloses (NC) or films with NC and double emulsion (NC/DE)
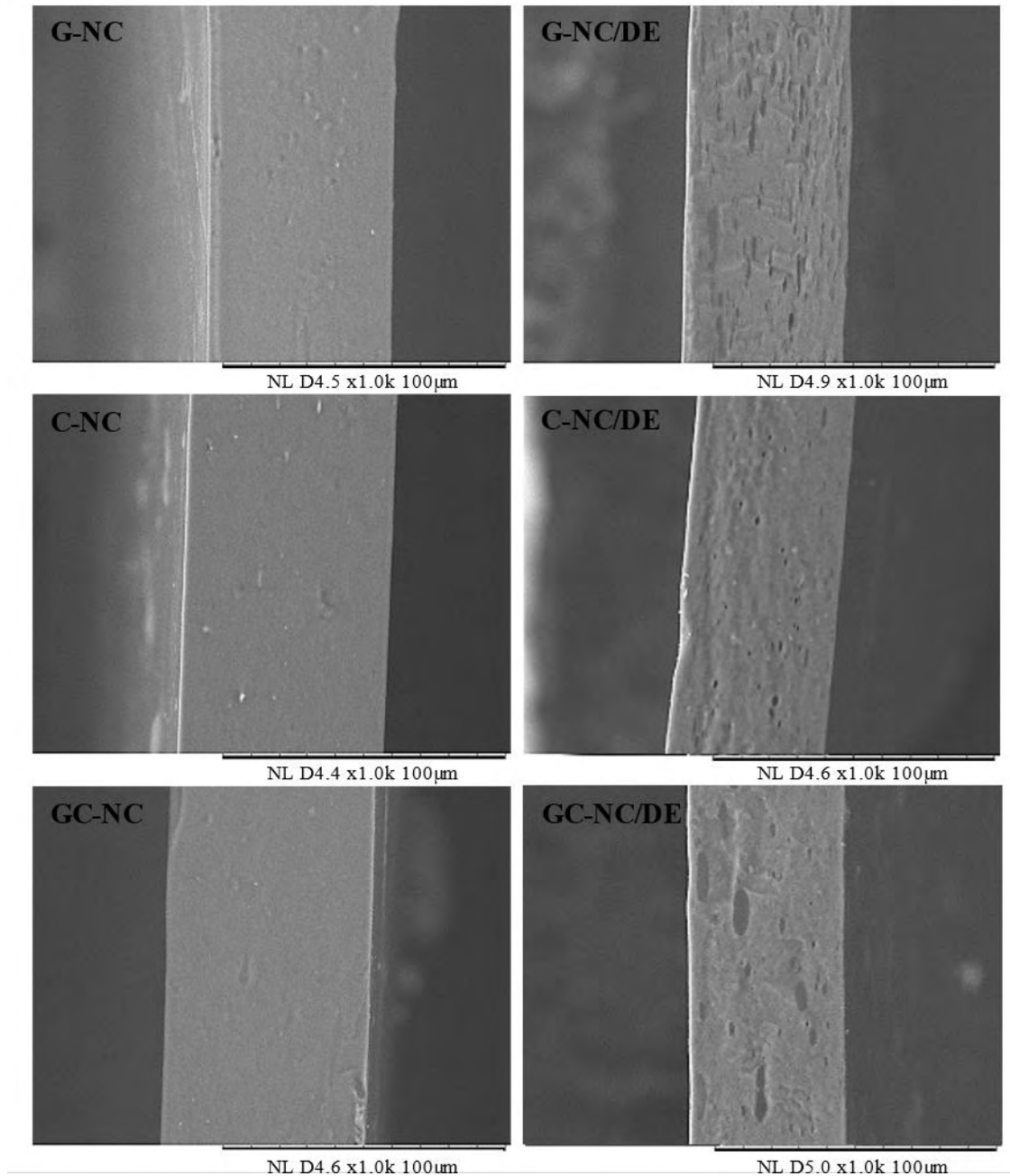
Source: Own authorship.

5.3.2.5 Atomic force microscopy (AFM)

The presence of DE modified the topographies of NC/DE films compared to NC films. The 3D topographies of the NC/DE films (Figure 5.4) presented a very irregular topography with peaks and valleys (~200 - 800nm), which is an effect of the possible

migration of soybean oil from broken DE droplets to the surface of these films (which can be better observed in the 2D AFM micrographs, Figure A3). These results corroborate with those of SEM analyzes (Figure 5.2). The highest number of wide peaks can be observed in the topography of the C-NC/DE film surface. A few peaks (<400nm) and troughs can also be seen in NC films (Figure 5.4), which may be the result of clusters of NC.

Figure 5.4 – 3D atomic force micrographs of gelatin (G), chitosan (C) and gelatin/chitosan (GC) films with soybean straw crystalline nanocelluloses (NC) or films with NC and double emulsion (NC/DE).
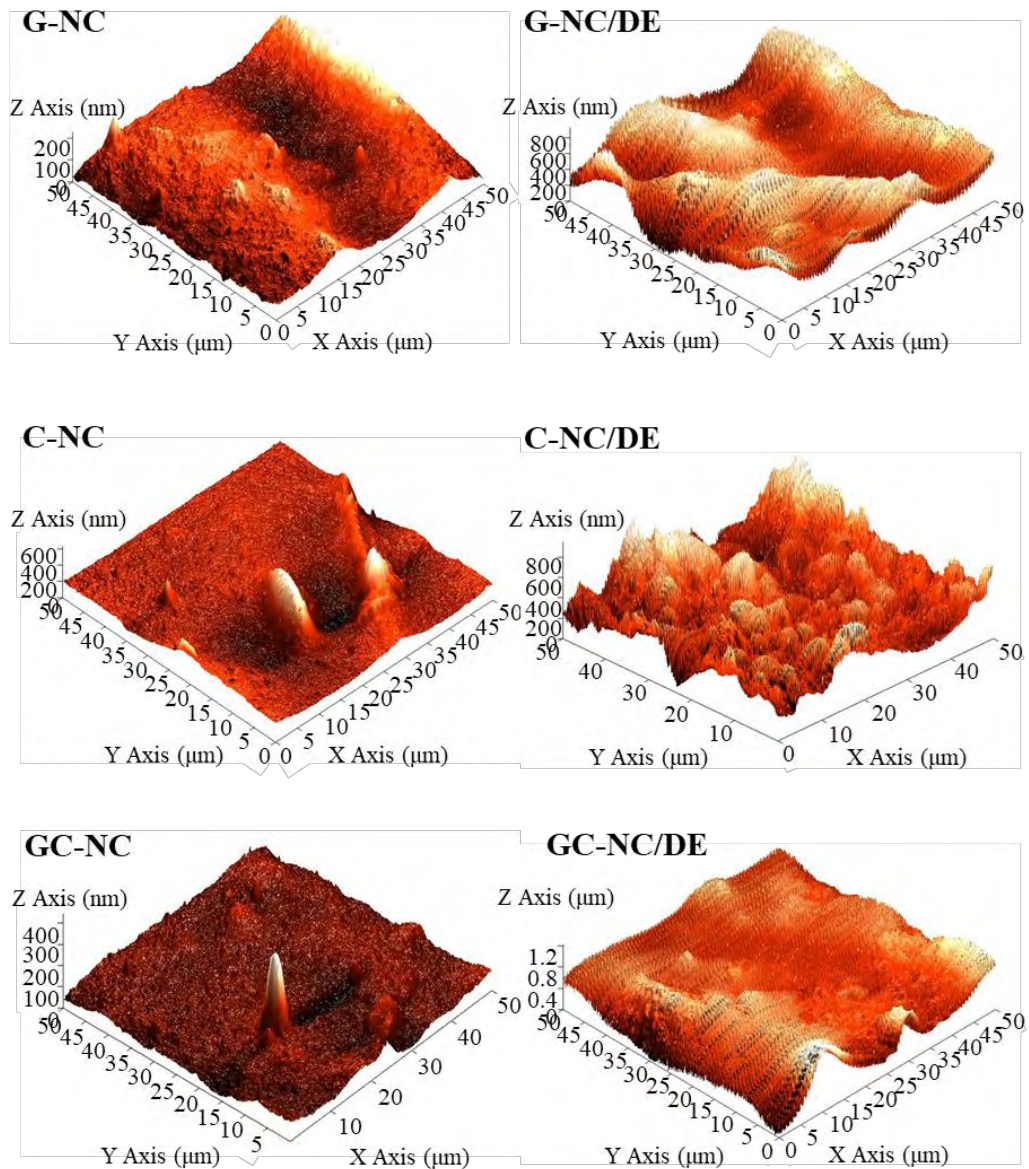

Source: Own authorship.

The calculated roughness of the topographies of all films showed large deviations, especially in NC/DE films. This was due to the observed surface irregularities provoked by nanoparticles and/or DE (Alexandre et al., 2016). The calculated roughness varied between 17 and 49 nm for NC films and between 95 and 2970 nm for NC/DE films (Table A1). These data variations were not observed for all films without NC, meaning that only DE (without DE: 8.4 – 16.3 nm, with DE: 75 – 88 nm) (Tessaro et al., 2021) did not affect the film's surface topography as in the present work. Thus, the observed behavior must be credited to the presence of NC together with DE into films. Bonilla et al. (2018), after AFM analyzes of films based on G and/or C, observed a smooth and continuous surface for films without oils, but the addition essential oils into films increased the roughness of all films. Similar results were observed by Pérez-Córdoba et al. (2018), working on films loaded with nanoemulsions.

5.3.2.6 Fourier-transform infrared spectroscopy (FTIR)

The change in the FTIR spectra for NC/DE films was minimal, compared to the FTIR spectra for NC films (Figure 5.5), possibly due to the low amount of incorporated NC (< 5 g NC/100 g biopolymer). The appearance of a small peak at 1744 cm^{-1} in all films containing DE was a consequence of the stretching of the C=O bond of fatty acid esters of oils, from soybean oil. This same signal has been observed in others studies on films based on gelatin and/or chitosan incorporated with different types of oil, emulsified or not (Kaya et al., 2018; Tessaro et al., 2021). Regarding the presence of NC, no changes in films spectra were observed, similarly to that observed in other studies involving the production of G and/or C-based films without NC (Bonilla; Sobral, 2016; Jridi et al., 2014; Kaya et al., 2018; Qiao et al., 2017; Tessaro et al., 2021), which may be related to the similarity between the cellulose, macromolecule forming NC, and glycerol, used as plasticizer, both formed by a sequence of hydroxyl groups (Pereda et al., 2011). Okamoto-Schalch et al. (2020) studied hybrid systems produced with NC and chitosan nanoparticles and observed a tangle of NCs around the particles, mainly due to electrostatic interactions.

All films spectra showed bands in approximately 3287-3260 cm^{-1} (overlapping of OH and NH-stretching coupled with hydrogen bonding of amide A groups), 2935-2924 cm^{-1} (asymmetric stretching vibration =C−H and −NH^{3+}, of amide B groups), 1636-1630 cm^{-1} (C=O stretching and hydrogen bonding coupled with COO, of amide-

I groups), 1550-1545 cm^{-1} (bending and stretching vibrations of N−H e C−N, respectively, of amide-II groups) and 1238-1229 cm^{-1} (vibrations in plane of C−N e N−H groups, of amide-III groups, or vibrations of CH$_2$ of glycerol) (Bonilla; Sobral, 2016; Jridi et al., 2014; Kaya et al., 2018).

Figure 5.5 – FTIR spectra of gelatin (G), chitosan (C) and gelatin/chitosan (GC) films with soybean straw crystalline nanocelluloses (NC) or films with NC and double emulsion (NC/DE)
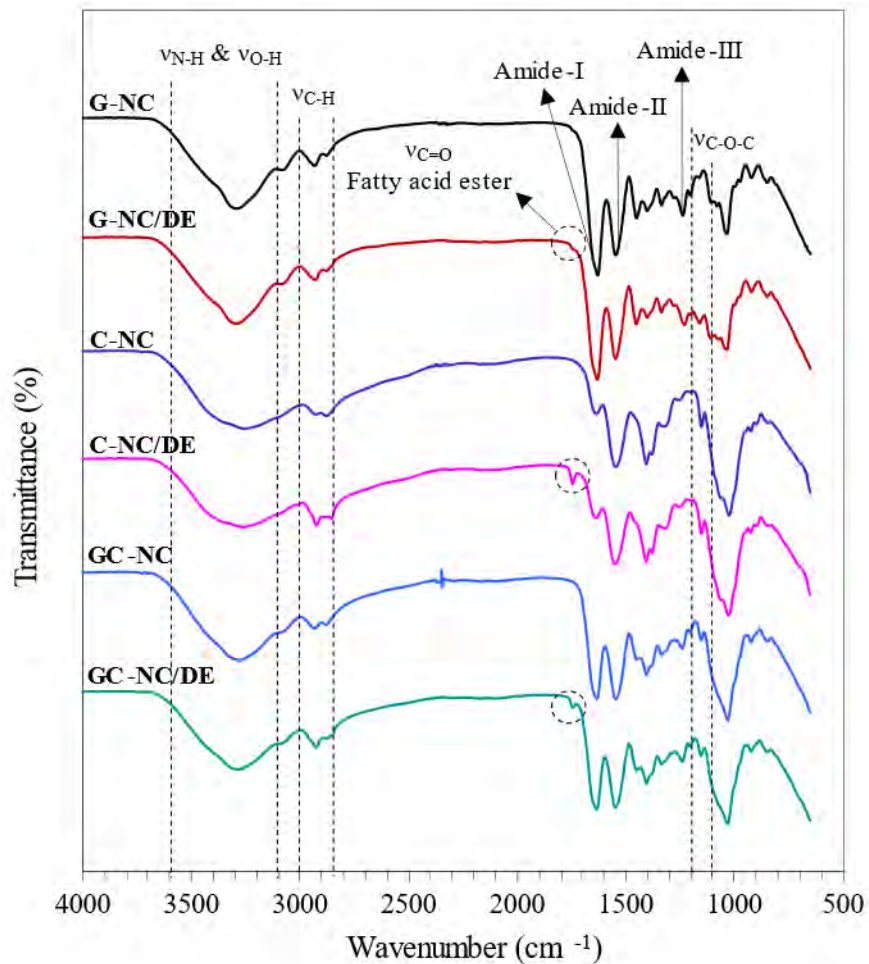
Source: Own authorship.

For G films, the band at 1452 cm^{-1} corresponds to the vibration of -OH groups of the gelatin (Bonilla; Sobral, 2016). For the C films, the vibration of -OH groups of the chitosan was seen in the band around 1407 cm^{-1} (Bonilla; Sobral, 2016). In addition, for C films, the most pronounced band at approximately 1028 cm^{-1} corresponded to the stretching of the C-O-C group bond, typical of saccharine structures (Alves et al.,

2018). The bands around 925 cm^{-1} are also characteristic of saccharide structures (Bonilla; Sobral, 2016; Kaya et al., 2018).

In the GC films, bands characteristics of both biopolymers (gelatin and chitosan) were observed (Figure 6.5). However, the bands referring to amide A, amide-I and amide-II showed less amplitude in GC films compared to G films. This indicates that there was a substitution of gelatin by chitosan and that, probably, the number of α-helices structures of gelatin was reduced by the presence of chitosan (Jridi et al., 2014; Qiao et al., 2017).

5.3.2.7 Gloss

Gloss is a property related to the surface texture, and therefore is related to the degree of polishing of the material (Dammak et al., 2017; Pelissari et al., 2017). The NC/DE films showed lower gloss ($p < 0.05$) as compared to the NC films (Table 5.1). According to Pelissari et al. (2017), the particle size distributions of the components incorporated in the film matrices can influence the gloss property: More uniform particle distributions generate more polished surfaces, and therefore, the greater the gloss. The fact that DE presented trimodal droplet sized distributions with high polydispersity (Tessaro et al., 2022) may explain the great decrease in the gloss of NC/DE films. In addition, the high roughness of NC/DE films may also explain this decrease in gloss. Tessaro et al. (2021) observed a negative linear relationship between Gloss and R$_a$. This relationship cannot be determined in the present work due to high R$_a$ dispersion for NC/DE films.

Regarding the effect of the biopolymer, G and GC films showed higher ($p < 0.05$) gloss than C films (Table 5.1). This may have occurred due to the effect of some insolubilized chitosan particles (Tessaro et al., 2021) that decreased the gloss of the C films. The presence of NC reduced the gloss of the NC and NC/DE films when compared to the same films produced without NC in the previous study (Tessaro et al., 2021). This was expected because roughness of the NC and NC/DE films was higher as compared to the roughness of the films studied previously (Tessaro et al., 2021), and the NC had varying lengths and diameters (Figure 5.1a,b).

5.3.2.8 Color and opacity

The NC/DE films showed lower ($p < 0.05$) L* than NC films; however, all films showed high luminosity (L* > 80), meaning they have a light color (Table 5.1). Despite some significant differences, the values of a* were close to 0 in the limit of green-red colors, and b* varied between 7 and 10 for all films (Table 5.1), meaning they have almost the same yellowish color. The total color difference (ΔE*), which indicates the coloring of the material, was not affected by loads for G films, but C and GC-NC/DE films were more colored than NC films (Table 5.1). Conversely, C films were more colored when having only NC load, but when loaded with NC/DE, both C and GC films were the more colored when compared with other biopolymers-based films (Table 5.1). Overall, all films produced in this work were relatively more colored than films based on these same biopolymers without and with DE (Tessaro et al., 2021). Ranjbaryan, Pourfathi and Alsami (2019) also observed that the addition of cinnamon essential oil nanoemulsion into sodium caseinate films had a significant effect on its color characteristics, but NC alone had no such effect. Differently, Pelissari et al. (2017) observed a slightly increasing in ΔE* as a consequence of addition of NC into starch films.

All NC/DE films were opaquer ($p < 0.05$) than NC films (Table 5.1), probably due to the effect on the gelatin matrix of light dispersion from the oil droplets, as observed by Tessaro et al. (2021). Similar behavior was observed by Bonilla et al. (2018), who observed overall that G and/or C films containing essential oils were more opaque than films without these components. Regarding the effect of bio- polymers, it was observed that G films were more opaque than films containing C in their composition (Table 5.1). The opacity of NC films was almost similar to that of the same films without loading (Tessaro et al., 2021). This differs from observations by Pelissari et al. (2017) and Pereda et al. (2011a), who observed an increasing in the film's opacity due to addition of NC, as could be expected, because the presence of a disperse phase promotes opacity as a function of the differences in the refractive index of both phases, promoting light scattering by the NC distributed in the biopolymer network (Pereda et al., 2011a). Oil droplets and NC can constitute these dispersed phases.

5.3.2.9 UV/Vis light barrier

In the region of UV light (100 to 380 nm), NC films presented a complete barrier to UV until 250 nm (Figure 5.6). Between 250 and 380 nm, the UV transmittance (T) of these films increased sharply attaining T ≈ 55% for G and C films, and T ≈ 70% for GC films (Figure 5.6), i.e., the NC loads alone were not able to prevent the UV transmission across films in this domain. Further, all NC/DE films had a very high UV barrier (*T* < 3%) until 280 nm. After that, the T increased and attained at 380 nm, 15, 20 and 30% for G, G and C films, respectively. Similar results were observed with G and/or C films incorporated with non-encapsulated plant extracts (Bonilla; Sobral, 2016), active essential oils (Bonilla et a., 2018) and O/W active nano- emulsion (Dammak et a., 2017).

Figure 5.6 – UV/Vis spectra of gelatin (G), chitosan (C) and gelatin/chitosan (GC) films with soybean straw crystalline nanocelluloses (NC) or films with NC and double emulsion (NC/DE).
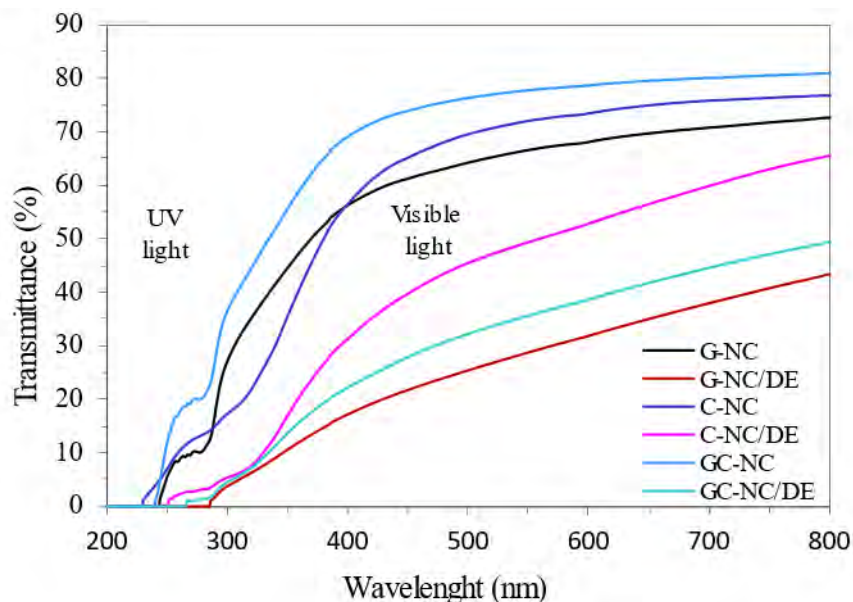
Source: Own authorship.

In the visible light region (380 to 800 nm), NC/DE films showed lower transmission than NC films (Figure 5.6), or in another words, films having NC/DE presented a higher barrier to visible light. Overall, in this domain, the light barrier varied as G-NC/DE > GC-NC/DE > C-NC/DE > G-NC > C-NC > GC-NC (Figure 5.6); therefore, the presence of DE significantly improved the barrier properties of films in

the region of visible light. Bonilla, Poloni and Sobral. (2018), Dammak et al. (2017) and Kaya et al. (2018) have reported the same behavior for films incorporated with plant extracts, O/W emulsions, or essential oils, respectively. The NC particles present in the films can cause light scattering, as explained previously (Pereda et al., 2011). Nevertheless, the bioactive compounds present in PLHE, especially those in phenolic compounds, may have also contributed to the better barrier property of the NC/DE films because phenolic compounds are able to absorb UV/Vis light (Chakravartula et al., 2020; Tessaro et al., 2021). The presence of some unsaturated double bonds conjugated to saturated covalent bonds in some phenolic compounds are responsible for the absorption of UV/visible light radiation (Luciano et al., 2021b; Reyes; Landgraf; Sobral, 2021).
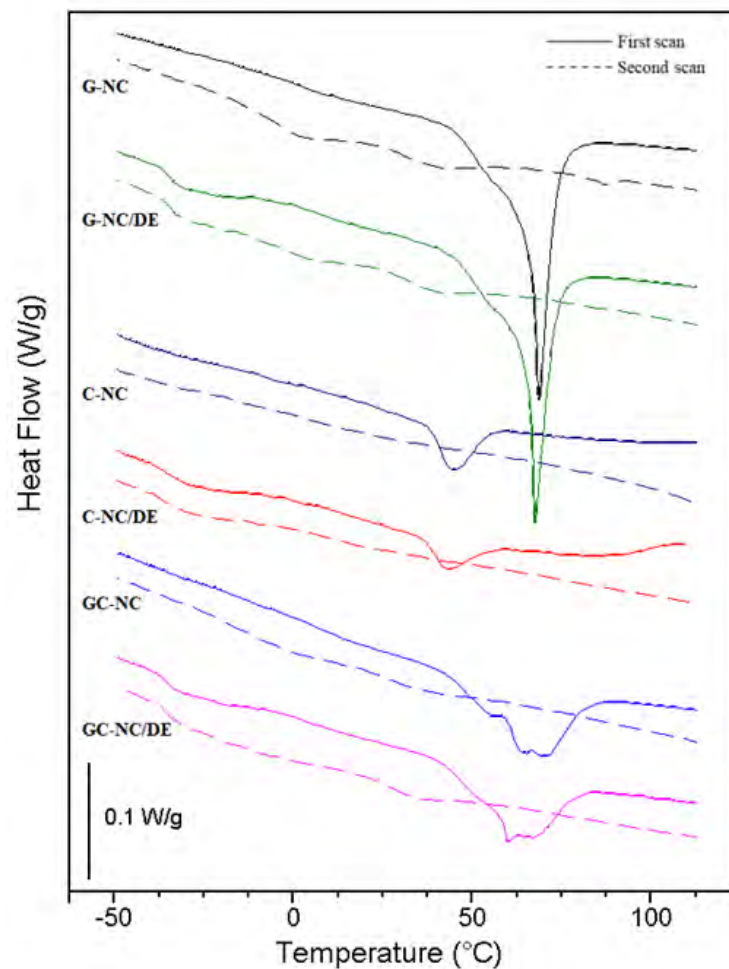
5.3.2.10 Thermal properties

The first scan samples heating in the temperature range of analysis (Figure 5.7) allowed observance of a first melting phenomenon in films containing DE, occurring around 36 °C (Table 5.2). This thermal event was associated to the lipid, without effect of biopolymers, as observed by Tessaro et al. (2021), who worked with similar films. Following the temperature increasing, a glass transition (Tg) can be observed only in films containing gelatin; after that a melting phenomenon associated with biopolymers appeared for all films (Figure 5.7). This glass transition temperature was not affected ($p > 0.05$) by any treatments, staying around 51 °C (Table 5.2), while the melting phenomenon was affected only by biopolymers, which means that the presence of DE did not affect this thermal property. For this melting temperature (Tm), films containing gelatin (G and GC films, ~69 °C) presented higher Tm than film C (~44 °C) (Table 5.2). Similar behavior was observed for melting enthalpy (ΔH), despite the observed significant difference for values of G-N and G-NC/DE films and considering these values very close: ΔH was higher for film G (~22 J/g) and lower for film C (2.8 J/g) (Table 5.2).

These values of Tg, Tm and ΔH for gelatin films were close to those determined by several authors working on this kind of films (Alexandre et al., 2016; Jridi et al., 2014; Pérez-Córdoba et al., 2018; Reyes; Landgraf; Sobral, 2021; Okamoto-Schalch et al., 2020; Valencia et al., 2016). Nevertheless, Bonilla, Bittante and Sobral (2017), analyzed films based on chitosan, conditioned at 53% RH in chambers containing

saturated solutions of Mg(NO$_3$)$_2$, and determined higher values for Tm (70.6 °C) and ΔH (4.2 J/g, corresponding to a crystallinity of 2%). Higher values (≥ 88 °C) were also determined by Madeleine-Perdrillat et al. (2016), studying thermal properties of chitosan films with different hydration degrees. However, it must be observed that none of these authors worked with composite films. On another side, Kaya et al. (2018) working on chitosan films loaded with *B. crataegina* seed oil determined an intermediary value for Tm (~69 °C) explaining this result as a consequence of oil plasticizer effect. Moreover, differences on chitosan characteristics must also affect these results.

Figure 5.7 – DSC thermal curves (Exo up) of gelatin (G), chitosan (C) and gelatin/chitosan (GC) films with soybean straw crystalline nanocelluloses (NC) or films with NC and double emulsion (NC/DE)

Source: Own authorship.

Table 5.2 – Thermal properties (Tg: glass transition temperatures, Tm_1 and Tm_2: melting temperatures of oil and biopolymers matrix, respectively, and ΔHm_2: melting enthalpy of biopolymer matrix) of gelatin (G), chitosan (C) and gelatin/chitosan (GC) films with soybean straw crystalline nanocelluloses without (NC) or with NC and double emulsion (NC/DE)*

Properties	Treatment	G	C	GC
1st scan				
Tm_1 (°C)	NC	nd	Nd	nd
	NC/DE	-38.8 ± 1.2^a	-36.2 ± 1.2^a	-36.5 ± 1.4^a
Tg (°C)	NC	51.4 ± 1.2^{aA}	nd	50.2 ± 0.5^{aA}
	NC/DE	51.4 ± 0.3^{aA}	Nd	49.1 ± 3.2^{aA}
Tm_2 (°C)	NC	69.1 ± 0.9^{aA}	44.0 ± 1.0^{bA}	69.2 ± 1.3^{aA}
	NC/DE	68.3 ± 0.8^{aA}	44.2 ± 0.9^{bA}	68.1 ± 1.2^{aA}
ΔH_2 (J/g)	NC	22.7 ± 0.1^{aA}	2.0 ± 0.2^{cA}	14.6 ± 1.5^{bA}
	NC/DE	21.4 ± 0.3^{aB}	3.5 ± 1.1^{cA}	13.4 ± 1.5^{bA}
2st scan				
Tm_1 (°C)	NC	nd	Nd	nd
	NC/DE	-35.5 ± 0.2^a	-36.2 ± 2.0^a	-36.0 ± 0.5^a
Tg (°C)	NC	30.5 ± 1.5^{aA}	Nd	26.3 ± 3.5^{aA}
	NC/DE	28.4 ± 2.7^{aA}	Nd	30.4 ± 7.4^{aA}

Different uppercase letters in the same column and different lowercase letters on the same line indicate significant differences between averages according to Tukey test ($p < 0.05$).
*Average ± standard deviation (n = 3), nd: not detected.
Source: Own authorship.

During the second scan heating, the first Tm was also observed at the same temperature (Table 5.2). This result allows confirmation that this phenomenon can be associated to lipids from DE, considering that the lipid's Tm is not affected by the cooling rate differently than that of the melting of biopolymers, which was not observed in the second scan (Figure 5.6). This behavior occurred because these materials became completely amorphous from the cryoscopic cooling after the first scan (Gontard; Guilbert; Cuq, 1992). Also because of these characteristics, Tg as

determined in second scan occurred at lower temperatures (around 29 °C) without effect of any treatments (Table 5.2).

The effect of NC in the thermal properties of films can be analyzed by comparing the results of Tg (~51 °C) determined in this work with those determined by Tessaro et al. (2021) for films based on gelatin and/or chitosan without and with DE, whose values varied between 47.2 and 28 °C. This behavior can be explained as being not only a kind of antiplasticization effect due to eventual absorption of water and glycerol by NC, but also as the reinforcement of the biopolymer matrix, which reduces the macromolecular mobility contributing to increase Tg.

5.3.2.11 Mechanical properties

Overall, all NC/DE films showed greater ($p < 0.05$) resistance (higher tensile strength, TS), stiffness (higher elastic modulus, EM) and stretchability (higher elongation at break, EB), as compared to NC films (except for C films), where EB was not influenced ($p > 0.05$) by loads (Table 5.3). In general, these behaviors demonstrated that an improvement of mechanical properties occurred due to DE's incorporation into nanocomposite films. These behaviors can be observed in the stress x strain curves obtained during tensile tests (Figure A4).

Table 5.3 – Mechanical properties of gelatin (G), chitosan (C) and gelatin/chitosan (GC) films with soybean straw crystalline nanocelluloses without (NC) or with NC and double emulsion (NC/DE)*

Properties	Treatments	G	C	GC
Tensile Strength (MPa)	NC	64.9 ± 7.2^{aB}	60.6 ± 6.2^{aB}	59.4 ± 5.4^{aB}
	NC/DE	150.0 ± 22.8^{aA}	161.9 ± 20.6^{aA}	190.3 ± 24.9^{aA}
Elongation at Break (%)	NC	5.9 ± 1.1^{cB}	45.7 ± 5.5^{aA}	15.6 ± 1.8^{bB}
	NC/DE	31.6 ± 4.0^{bA}	44.2 ± 3.8^{aA}	45.2 ± 5.1^{aA}
Elastic Modulus (MPa)	NC	18.3 ± 2.3^{aB}	7.6 ± 0.9^{bB}	11.5 ± 2.0^{bB}
	NC/DE	30.7 ± 4.4^{abA}	21.1 ± 3.6^{bA}	31.5 ± 4.3^{aA}

Different lowercase letters on the same line and uppercase letters in the same column indicate significant differences between averages according to Tukey test ($p < 0.05$).
*Average ± standard deviation (n = 9).
Source: Own authorship

Two contributions to this impressive improvement on film mechanical properties may be hypothesized: i) the emulsifier from broken DE may have contributed to better interfacial interactions between the NC and the biopolymer matrix, improving its load effect; ii) eventual interactions between some reactive bioactive compounds present in PLHE, which was delivered by W/O inner fraction, and functional groups of residue of some amino acids (ex.: lysine), as a kind of crosslinking (Hosseini; Gómez-Guillén, 2018), and with amine groups present in chitosan (Hu; Lu, 2016) occurred, although these interaction have not provoked changes in film FTIR spectra (Figure 5.5). Nevertheless, further studies are necessary to elucidate these results.

Regarding the biopolymers, no effect ($p > 0.05$) was observed in the TS of NC and NC/DE films, which varied between 59 and 65 MPa and 150 and 190 MPa, respectively. Nevertheless, some effects of biopolymers were observed on EM and EB (Table 5.3). For NC films, the G films EM values were higher ($p < 0.05$) than those of C and GC films ($p > 0.05$); while for NC/DE films, G and GC films presented the higher EM value (Table 5.3). This means that the principal effect must be due to the gelatin matrix, which is able to produce a more rigid matrix than chitosan for the same plasticizer (glycerol) concentration. Moreover, the higher value of Tm (Table 5.2) for films with gelatin can suggest that this material had a higher crystallinity, which also can explain these mechanical results.

Among NC films, the C films presented the higher ($p < 0.05$) EB, which is coherent with the results of EM (less rigid more stretchable material) (Table 5.3). Further, when DE was added into films, the GC films also presented a higher EB together with C films ($p > 0.05$), or in another words, G films presented the lower EB value for films with DE. This was probably due to a possible lubricant effect of the soybean oil contained in DE (Tessaro et al., 2021), that is, the presence of oil droplets on the film matrix could reduce the "friction" between macromolecules chains and enable the longitudinal displacement of adjacent macromolecules. This observation was different from the studies carried out by Kaya et al. (2018), which observed a plasticizer effect of *B. crataegina* seed oil on chitosan films increasing its EB and decreasing its TS. The EB value of C-NC film was quite high as compared to other those determined in some studies (Bonilla et al., 2018; Kaya et al., 2018).

Comparing the mechanical properties of nanocomposite films with that of films without NC, as produced in a previous study, it can be observed that NC increased TS of G and C films, from 27 and 40 MPa to 65 and 61 MPa (Table 5.3), respectively, but

reduced it from 68 to 59 MPa for GC films (Tessaro et al., 2021). Regarding EM, an improvement due to NC was observed only for G films, and the EB's were almost similar. An overall improvement on mechanical properties due to NC load must be expected, principally when fillers with a high aspect ratio are used because their high specific surface area provides better reinforcing effects (Khan et al., 2012; Pereda et al., 2011a). This behavior has been observed by Khan et al. (2012), Pelissari et al. (2017) and Pereda et al. (2011a), who also found very high values of TS with their nanocomposite films. Nevertheless, Ranjbaryan, Pourfathi and Almasi (2019), working with sodium caseinate films, observed that NC had a different effect on the nanocomposite mechanical properties depending on its concentration: With 2.5%, NC caused the decrease of the TS and EM, but by increasing it to 5%, these values increased significantly; however, EB decreased due to NC content.

5.3.2.12 Antimicrobial activity

None of the NC and NC/DE films promoted the formation of a halo of inhibition for *P. aeruginosa*, *Salmonella* and *S. aureus* bacteria (Figure 5.8); however, C and GC films showed inhibition of the growth of the bacteria analyzed in the region of contact between the film disks and the agar. Regarding the G films, only the G-NC/DE film showed inhibition against the growth of *S. aureus* in the region of contact between the film and the agar (Figure 5.8). This behavior can be explained by the natural antimicrobial activity of chitosan and the inability of gelatin to inhibit the growth of microorganisms, as already reported by other authors (Bonilla; Sobral, 2016; Pereda et al., 2011b; Pérez-Córdoba et al., 2018). The antimicrobial activity of chitosan can be related to the positively charged groups of the chitosan structures that are able to interact with the microorganism's cell membrane, which are negatively charged (Dutta; Ravikumar; Dutta, 2002). This interaction causes the leakage of proteins and other intracellular components of microorganisms (Dutta; Ravikumar; Dutta, 2002; Bonilla; Sobral, 2016; Pereda et al., 2011b; Pérez-Córdoba et al., 2018).

Figure 5.8 – Inhibition against the growth of *Pseudomonas aeruginosa*, *Salmonella ssp* and *Staphylococcus aureus* bacteria. C⁻: negative control (distilled water), C⁺: positive control (chloramphenicol 2.5 mg/mL), G: gelatin-based film, C: chitosan-based film, GC: chitosan/gelatin-based film, NC: films with soybean straw crystalline nanocelluloses, and NC/DE: films with soybean straw crystalline nanocelluloses and double emulsion.
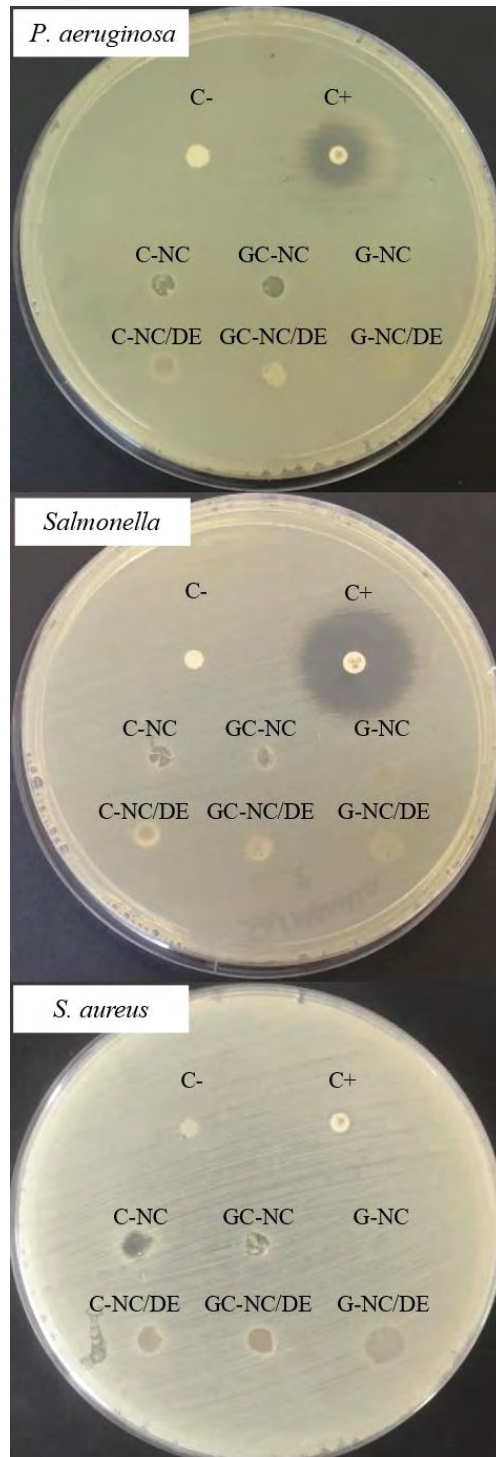
Source: Own authorship.

The absence of a halo of inhibition of the studied bacteria in the NC/DE films can be explained by the difficulty that the active compounds present in the PLHE have to diffuse through the agar, since the PLHE is doubly encapsulated. According to Lorenzo et al. (2018), the PLHE produced in the same conditions of this work have high antimicrobial activity against the same studied bacteria. The presence of NC in the films did not change the results observed in the previously published study (Tessaro et al., 2021).

5.3.2.13 Folin-Ciocalteu reducing capacity (FCRC) and antioxidant activity (AA)

All NC/DE films showed higher ($p < 0.05$) FCRC and AA (ABTS$^{\bullet+}$ and FRAP methods) than NC films (Table 5.4), as would be expected because the PLHE was the only source of bioactive compounds used for film production. Comparing the biopolymer's effect, all NC films FCRC results were null, but for NC/DE film the G films presented the higher ($p < 0.05$) FCRC result followed by GC and C (Table 5.4). This can be explained by the fact that the G films showed greater solubility in water (Table 5.1), which could facilitate the extraction of the active compounds of the PLHE. In addition, it is possible that some lost bioactivity occurred during film processing due to heating and mixing, implying an incorporation of air. It is possible that this occurred in a more important manner on films made with C because the film forming solution based on gelatin was more viscous, protecting the bioactive compounds (Tessaro et al., 2021).

Regarding the film's AA determined using both ABTS$^{\bullet+}$ and FRAP methods, the C-NC film AA was very low, because chitosan has no AA. G films presented some AA because some functional groups of amino acids, such as proline and glycine, can act as donors of electrons (Gómez-Estaca et al., 2009; Reyes; Landgraf; Sobral, 2021. Reyes, Landgraf and Sobral (2021) and Ranjbaryan, Pourfathi and Almasi (2019) also determined some AA working with gelatin and sodium caseinate films, respectively, without bioactive additives, and evidently, both films with PLHE presented very high AA (Table 5.4).

In comparing the evaluations of the effect of NC, slightly lower values of FCRC and AA were observed in NC and NC/NE-films than those published by Tessaro et al. (2021), who worked on these same films but without NC. It's possible that some phenolic compounds can be adsorbed on the NC surfaces, reducing its availability.

This possible phenolic compounds-NC complex may have contributed to the reinforcement of the NC/DE films, which corroborates the high resistance and rigidity as observed in the Table 5.3.

Table 5.4 – The Folin-Ciocalteu reducing capacity (FCRC) and antioxidant activity by ABTS•+ and FRAP methods of gelatin (G), chitosan (C) and gelatin/chitosan (GC) films with soybean straw crystalline nanocelluloses without (NC) or with NC and double emulsion (NC/DE)*

Method	Treatments	G	C	GC
FCRC (mg GAE/g film)	NC	0.02 ± 0.01^{aB}	0.00 ± 0.00^{bB}	0.00 ± 0.00^{bB}
	NC/DE	1.17 ± 0.01^{aA}	0.27 ± 0.01^{cA}	0.56 ± 0.05^{bA}
ABTS•+ (mg TE/g film)	NC	0.50 ± 0.02^{aB}	0.00 ± 0.00^{cB}	0.36 ± 0.02^{bB}
	NC/DE	4.39 ± 0.04^{aA}	2.11 ± 0.09^{cA}	2.97 ± 0.17^{bA}
FRAP (µmol TE/g film)	NC	7.83 ± 0.26^{aB}	6.90 ± 0.00^{cB}	7.02 ± 0.10^{bB}
	NC/DE	12.10 ± 0.62^{aA}	7.71 ± 0.26^{cA}	8.81 ± 0.25^{bA}

Different lowercase letters on the same line and uppercase letters in the same column indicate significant differences between averages according to Tukey test ($p < 0.05$). GAE is gallic acid equivalent, and TE is Trolox equivalent.
*Average ± standard deviation (n = 9).

Source: Own authorship.

5.4 CONCLUSIONS

NC and DE were used to load films based on gelatin and/or chitosan in order to produce active nanocomposite films. These materials presented characteristics of nanocomposite flexible materials such as high mechanical and water vapor barrier properties, low sensitivity to vapor and liquid water, and excellent UV/VIS light barrier properties. Moreover, these films were active materials. Nanocomposite films containing chitosan presented antimicrobial activity against the growth of common pathogenic bacteria in foods, and all nanocomposite films containing DE presented highly antioxidant activity.

References

ALEXANDRE, E. M. C. et al. Gelatin-based films reinforced with montmorillonite and activated with nanoemulsion of ginger essential oil for food packaging applications. **Food Packaging and Shelf Life**, v. 10, p. 87-96, 2016.

ALVES, V. L. C D. et al. Preparation and characterization of a chitosan film with grape seed extract-carvacrol microcapsules and its effect on the shelf-life of refrigerated Salmon (*Salmo salar*). **LWT**, v. 89, p. 525-534, 2018.

AMERICAN SOCIETY FOR TESTING AND MATERIALS (ASTM). Standard test methods for water vapor transmission of materials, E96-E80. **Annual Book of ASTM Standards**, 1989.

AMERICAN SOCIETY FOR TESTING AND MATERIALS (ASTM). Standard test methods for water vapor transmission of materials, D523. **Annual Book of ASTM Standards**, 1999.

AMERICAN SOCIETY FOR TESTING AND MATERIALS (ASTM). Standard test methods for water vapor transmission of materials, D882/12. **Annual Book of ASTM Standards**, 2001.

ARAI, I. et al. Improving effects of the extracts from *Eugenia uniflora* on hyperglycemia and hypertriglyceridemia in mice. **Journal of Ethnopharmacology**, v. 68, p. 307-314, 1999.

BENZIE, L. F. F.; STRAIN, J. J. The ferric reducing ability of plasma (FRAP) as a measure of "Antioxidant Power": the FRAP assay. **Analytical Biochemistry**, v. 239, n. 1, p. 70-76, 1996.

BONILLA, J. et al. Antioxidant potential of eugenol and ginger essential oils with gelatin/chitosan films. **Food Bioscience**, v. 23, p. 107-114, 2018.

BONILLA, J.; BITTANTE, A. M. Q. B.; SOBRAL, P. J. A. Thermal analysis of gelatin-chitosan edible film mixed with plant ethanolic extracts. **Journal of Thermal Analysis and Calorimetry**, v. 130, p. 1221-1227, 2017.

BONILLA, J.; POLONI, T.; SOBRAL, P. J. A. Active edible coatings with boldo extract added and their application on nut products: reducing the oxidative rancidity rate. International **Journal of Food Science & Technology**, v. 53, p. 700-708, 2018.

BONILLA, J.; SOBRAL, P. J. A. Investigation of the physicochemical, antimicrobial and antioxidant properties of gelatin-chitosan edible film mixed with plant ethanolic extracts. **Food Bioscience**, v. 16, p. 17-25, 2016.

CAO, T.; ELIMELECH, M. Colloidal stability of cellulose nanocrystals in aqueous solutions containing monovalent, divalent, and trivalent inorganic salts. **Journal of Colloidal and Interface Salts**, v. 584, p. 456-463, 2021.

CHAKRAVARTULA, S. S. N. et al. Influence of pitanga (*Eugenia uniflora* L.) leaf extract and/or natamycin on properties of cassava starch/chitosan active films. **Food Packaging and Shelf Life**, v. 24, p. 100498, 2020.

DAMMAK, I. et al. Properties of active gelatin films incorporated with rutin-loaded nanoemulsions. **International Journal of Biological Macromolecules**, v. 98, p. 39-49, 2017.

DAMMAK, I.; SOBRAL, P. J. A. Active gelatin films incorporated with eugenol nanoemulsions: effect of emulsifier type on films properties. **International Journal of Food Science & Technology**, v. 54, p. 2725-2735, 2019.

DUTTA, P. K.; RAVIKUMAR, J. D., DUTTA, J. Chitin and chitosan for versatile applications. **Journal of Macromolecular Science, Part C: Polymer Reviews**, v. 42, n. 3, p. 307-354, 2002.

GÓMEZ, C. H. et al. Vegetable nanocellulose in food science: a review. **Food Hydrocolloids,** v. 57, p. 178-186, 2016.

GÓMEZ-ESTACA, J. et al. Physical and chemical properties of tuna-skin and bovine-hide gelatin films with added aqueous oregano and rosemary extracts. **Food Hydrocolloids**, v. 23, p. 1334-1341, 2009.

GONTARD, N.; GUILBERT, S.; CUQ, J. -L. Edible wheat gluten films: influence of the Main process variables on film properties using response surface methodology. **Journal of Food Science**, v. 57, n. 1, p. 190-195, 1992.

HOSSEINI, S. F. et al. Development of bioactive fish gelatin/chitosan nanoparticles composite films with antimicrobial properties. **Food Chemistry**, v. 194, p. 1266-1274, 2016.

HOSSEINI, S. F.; GÓMEZ-GUILLÉN. A state-of-the-art review on the elaboration of fish gelatin as bioactive packaging: special emphasis on nanotechnology-based approaches. **Trends in Food Science & Technology**, v. 79, p. 125-135, 2018.

HU, Q.; LUO, Y. Polyphenol-chitosan conjugates: synthesis, characterization, and applications. **Carbohydrate Polymers**, v. 151, p. 624-639, 2016.

HUANG, Y.; ZHOU, W. Microencapsulation of anthocyanins through two-step emulsification and release characteristics during *in vitro* digestion. **Food Chemistry**, v. 278, p. 357-363, 2019.

JRIDI, M. et al. Physical, structural, antioxidant and antimicrobial properties of gelatin-chitosan composite edible films**. International Journal of Biological Macromolecules**, v. 67, p.373-379, 2014.

KAYA, M. et al. Production and characterization of chitosan based edible films from *berberis crataegina's* fruit extract and seed oil. **Innovative Food Science & Emerging Technologies**, v. 45, p. 287-297, 2018.

KHAN, A. et al. Mechanical and barrier properties of nanocrystalline cellulose reinforced chitosan based nanocomposite films. **Carbohydrate Polymers**, v. 90, n. 4, p. 1601-1608, 2012.

LORENZO, J. M. et al. Influence of pitanga leaf extracts on lipid and protein oxidation of pork burger during shelf-life. **Food Research International**, v. 114, p. 47-54, 2018.

LUCIANO, C. G. et al. Bi-layer gelatin film: activating film by incorporation of "Pitanga" leaf hydroethanolic extract and/or nisin in the second layer. **Food and Bioprocess Technology**, v. 14, p. 106-119, 2021.

LUCIANO, C. G. et al. Effects of nisin concentration on properties of gelatin film-forming solutions and their films. **International Journal of Food Science & Technology**, v. 56, n. 2, p. 587-599, 2021.

MADELEINE-PERDRILLAT, C. et al. Effect of hydration on molecular dynamics and structure in chitosan films. **Food Hydrocolloids**, v. 61, p. 57-65.

MARTELLI-TOSI, M. et al. Chemical treatment and characterization of soybean straw and soybean protein isolate/straw composite films. **Carbohydrate Polymers**, v. 157, p. 512-520, 2017.

MARTELLI-TOSI, M. et al. Soybean straw nanocellulose produced by enzymatic or acid treatments as a reinforcing filler in soy protein isolate films. **Carbohydrate Polymers**, v. 198, p. 61-68, 2018.

MATOS, M. et al. Encapsulation of resveratrol using food-grade concentrated double emulsions: emulsion characterization and rheological behavior. **Journal of Food Engineering**, v. 226, p. 79-81, 2018.

MUSCHIOLIK, G.; DICKINSON, E. Double emulsions relevant to food systems: preparation, stability, and applications. **Comprehensive Reviews in Food Science and Food Safety**, v. 16, p. 532-555, 2017.

NATIONAL COMMITTEE ON CLINICAL LABORATORY STANDARDS. Performance standards for antimicrobial disk susceptibility tests: Approved standard. 7h ed. **Clinical Laboratory Standards Institute: Document M2 – A7**, 2000.

NECHYPORCHUK, O.; BELGACEM, M. N.; BRAS, J. Production of cellulose nanofibrils: a review of recent advances. **Industrial Crops and Products**, v. 93, p. 2-25, 2016.

OKAMOTO-SCHALCH, N. O. et al. Production and characterization of chitosan-TPP/cellulose nanocrystal system for encapsulation: a case study using folic acd as active compound. **Cellulose**, v. 27, p. 5855-5869, 2020.

PELISSARI, F. M. et al. Nanocomposites based on banana starch reinforced with cellulose nanofibers isolated from banana peels. **Journal of Colloid and Interface Science**, v. 505, p. 154-167, 2017.

PEREDA, M. et al. Chitosan-gelatin composites and bi-layer films with potential antimicrobial activity. **Food Hydrocolloids**, v. 25, p. 1372-1381, 2011b.

PEREDA, M. et al. Structure and properties of nanocomposite films based on sodium caseinate and nanocellulose fibers. **Journal of Food Engineering**, v. 103, p. 76-83, 2011a.

PÉREZ-CÓRDOBA, L. J. et al. Physico-chemical, antimicrobial and antioxidant properties of gelatin-chitosan based films loaded with nanoemulsions encapsulating active compounds. **Food Hydrocolloids**, v. 79, p. 544-559, 2018.

PÉREZ-CÓRDOBA, L. J., SOBRAL, P. J. A. Physical and antioxidant properties of films lased on gelatin, gelatin-chitosan or gelatin-sodium caseinate blends loaded with nanoemulsified active compounds. **Journal of Food Engineering**, v. 213, p. 47-53, 2017.

PIMENTEL-MORAL, S. et al. Stabilization of W/O/W multiple emulsion loaded with *Hibiscus sabdariffa* extract through protein-polysaccharide complexes. **LWT**, v. 90, p. 389-395, 2018.

PULIDO, R.; BRAVO, L.; SAURA-CALIXTO, F. Antioxidant activity of dietary polyphenols as determined by a modified ferric Reducing/Antioxidant power assay. **Journal of Agricultural and Food Chemistry**, v. 48, n. 8, p. 3396-3402, 2000.

QIAO, C. et al. Molecular interactions in gelatin/chitosan composite films. **Food Chemistry**, v. 235, p. 45-50, 2017.

RANJBARYAN, S.; POURFATHI, B.; ALMASI, H. Reinforcing and release controlling effect of cellulose nanofiber in sodium caseinate films activated by nanoemulsified cinnamon essential oil. **Food Packaging and Shelf Life**, v. 21, p. 100341, 2019.

RE, R. et al. Antioxidant activity applying an improved ABTS radical cation decolorization assay. Free Radical Biology and Medicine, v. 26, n. 9-10, p. 1231-1237, 1999.

REYES, L. M.; LANDGRAF, M.; SOBRAL, P. J. A. Gelatin-based films activated with red propolis ethanolic extract and essential oils. **Food Packaging and Shelf Life**, v. 27, p. 100607, 2021.

SCHUMACHER, N. et al. Identification and antioxidant activity of the extracts of *Eugenia uniflora* leaves: characterization of the anti-inflammatory properties of aqueous extract on diabetes expression in an experimental model of spontaneous type 1 diabetes (NOD Mice). **Antioxidants**, v. 4, 662-680, 2015.

SINGLETON, V. L.; ROSSI, J. A. Colorimetry of total phenolics with phosphomolybdic-phosphotungstic acid reagens. **American Journal of Enology and Viticulture**, v. 16, n. 3, p. 144-158, 1965.

SOBRAL, P. J. A. et al. Mechanical, water vapor barrier and thermal properties of gelatin based edible films. **Food Hydrocolloids**, v., 15, n. 4-6, p. 423-432, 2001.

TESSARO, L. et al. Gelatin and/or chitosan-based films activated with "Pitanga" (*Eugenia uniflora* L.) leaf hydroethanolic extract encapsulated in double emulsion. **Food Hydrocolloids**, v. 113, p. 106523, 2021.

TESSARO, L., et al. Stable and bioactive W/O/W emulsion loaded with "Pitanga" (*Eugenia uniflora* L.) leaf hydroethanolic extract. **Journal of Dispersion Science and Technology**, v. 43, n. 12, p. 1890-1900, 2022.

TESSARO, L.; MARTELLI-TOSI, M.; SOBRAL, P. J. A. Development of W/O emulsion for encapsulation of "Pitanga" (*Eugenia uniflora* L.) leaf hydroethanolic extract: droplet size, physical stability and viscosity. **Food Science and Technology**, v. 42, 2021.

VALENCIA, G. A. et al. Physical and morphological properties of nanocomposite films based on gelatin and laponite. **Applied Clay Science**, v. 124-125, p. 260-266, 2016.

VARGAS, F. C. et al. Assessment of the suitability of Pitanga leaf extract as a natural antioxidant for enhancing canola oil stability: monitoring lipid oxidation parameters. **European Journal of Lipid Science & Technology**, v. 121, p. 1800447, 2019.

VARGAS, F. C. et al. Rosemary and Pitanga aqueous leaf extracts on beef patties stability under cold storage. **Brazilian Archives of Biology and Technology**, v. 59, 2016.

6 CAPÍTULO 3: Improving the properties of gelatin-based films by incorporation of "pitanga" leaf extract and crystalline nanocellulose

Larissa Tessaro [a], Ana Gabrielle R. Pereira [a], Milena Martelli-Tosi [a], Paulo José do Amaral Sobral [a, b]

[a] Department of Food Engineering, Faculty of Animal Science and Food Engineering, University of São Paulo, Av Duque de Caxias Norte, 225, 13635-900 Pirassununga, SP, Brazil.

[b] Food Research Center (FoRC), University of São Paulo, Rua do Lago, 250, Semi-industrial building, block C, 05508-080 São Paulo, SP, Brazil.

Abstract

Biopolymer-based films can be activated by the incorporation of active compounds into their matrix. Plant extracts are rich in phenolic compounds, which have antimicrobial and/or antioxidant properties. The aim of this study was to produce gelatin-based active films and nanocomposite films incorporated with "pitanga" (*Eugenia uniflora* L.) leaf extract (PLE) and/or crystalline nanocellulose extracted from soybean straw (CN), and to study the physicochemical, functional, microstructural, thermal, UV/Vis light barrier, and antioxidant properties of these materials. PLE enhanced some film properties, such as tensile strength (from 30.2 MPa to 40.6 MPa), elastic modulus (from 9.3 MPa to 11.3 MPa), the UV/Vis light barrier, and antioxidant activity, in addition to affecting the micro-structural, surface, and color properties. These improvements were even more significant in nanocomposites simultaneously containing PLE and CN (59.5 MPa for tensile strength and 15.1 MPa for elastic modulus), and these composites also had lower moisture content (12.2% compared to 13.5–14.4% for other treatments) and solubility in water (from 48.9% to 44.1%). These improvements may be the result of interactions that occur between PLE's polyphenols and gelatin, mainly in the presence of CN, probably due to the formation of a stable PLE–CN–gelatin complex. These results are relevant for the food packaging sector, as the activated nanocomposite films exhibited enhanced active, barrier, and mechanical properties due to the presence of PLE and CN, in addition to being entirely produced with sustainable components from natural and renewable sources.

Keywords: nanocomposite; active films; biopolymer; plant extract; agricultural by-product; physical properties.

6.1 INTRODUCTION

The food and beverage industry is notorious for its extensive use of non-biodegradable packaging materials, such as single-use plastics, which often end up polluting ecosystems and harming wildlife. Additionally, large-scale agricultural practices associated with this industry can contribute to deforestation, soil degradation, and water pollution through the heavy use of pesticides, fertilizers, and irrigation. The disposal of food waste further exacerbates environmental concerns, as organic matter decomposes in landfills, emitting methane, a potent greenhouse gas. Consequently, addressing these issues requires comprehensive strategies to minimize waste generation, promote sustainable packaging alternatives, and encourage responsible production and consumption practices within the industry (Rodríguez-Félix et al., 2022). Specifically, an alternative way to avoid or reduce these problems is to replace plastic packaging with more eco-friendly materials, such as biopolymer-based films (Almeida et al., 2023).

Edible and flexible biopolymer-based films can be used as food packaging, as they offer greater safety and can also extend shelf life. This technology emerged as an alternative to the use of conventional packaging, as it has characteristics such as biodegradability, biocompatibility, and is produced with natural and renewable components (Liu et al., 2024), and therefore can be considered eco-friendly and safe at the generally recognized as safe (GRAS) level (Vargas-Torrico et al., 2023).

Biopolymers such as proteins, such as gelatin and chitosan, and polysaccharides, such as starch, are generally used for the development of biopolymer-based films (Liu et al., 2019; Luciano et al., 2021; Pelissari et al., 20147). Gelatin, a versatile material utilized in the food industry, offers enhanced elasticity, stability, and consistency to food products. Moreover, it boasts exceptional barrier properties, permeability, and is characterized by its biocompatibility, biodegradability, and non-toxicity (Figueroa-Enriquez et al., 2023). These attributes make gelatin an ideal candidate for coatings or films production, effectively prolonging the shelf life of food items. Derived from collagen, gelatin can be obtained through either alkaline or acid processes, resulting in type B or type A gelatin, respectively. Furthermore, gelatin can be sourced from mammals or marine origins, and is produced all over whole world (Yan et al., 2021), adding to its diverse applications within the food sector (Figueroa-Enriquez et al., 2023). Gelatin-based films (or films based on other biopolymers)

incorporated with active components constitute active films. Depending on the active component incorporated, active films, when applied as food packaging, can perform enhanced functions that help preserve food, extending shelf life and allowing the incorporation of lower amounts of preservatives into products.

The antioxidant and antimicrobial activities of plant extracts make them particularly interesting components for biopolymer-film activation, reducing the use of syn-thetic food preservatives (Luciano et al., 2021). Pomegranate peel extract (Vargas-Torrico et al., 2023), *Malva sylvestris* extract (Nikoukheslat et al., 2022), hawthorn fruit extract (Yan et al., 2021), and "pitanga" leaf extract (Luciano et al., 2021; Tessaro et al., 2021a,b), among others, have been used to activate films based on gelatin or gelatin blended with other biopolymers. In addition to providing antioxidant and/or antimicrobial activity to the gelatin films, the plant extracts can also improve some properties of the films by chemical modification of the protein by active compounds.

Plant extracts are substances rich in polyphenols and other active substances. Polyphenols are considered natural antioxidants, antimicrobials, and/or anti-inflammatories, as they have at least one aromatic ring linked to one or more hydroxyl groups, which allows them to prevent or delay oxidative degradation induced by reactive oxygen species (Quan et al., 2019). Because of their structure, polyphenols can interact with gelatin via covalent and non-covalent interactions, with the latter (ionic, hydro-phobic, and hydrogen bonds) (Figure 6.1) being the most common (Quan et al., 2019). In fact, Var-gas-Torrico et al. (2023) and Yan et al. (2021) have reported improvements in the properties of gelatin-based films incorporated with plant extracts, mainly in water sensitivity and mechanical properties, possibly caused by polyphenol–gelatin interactions.

Figure 6.1 - Non-covalent interactions that can occur between gelatin, polyphenols and nanocelluloses
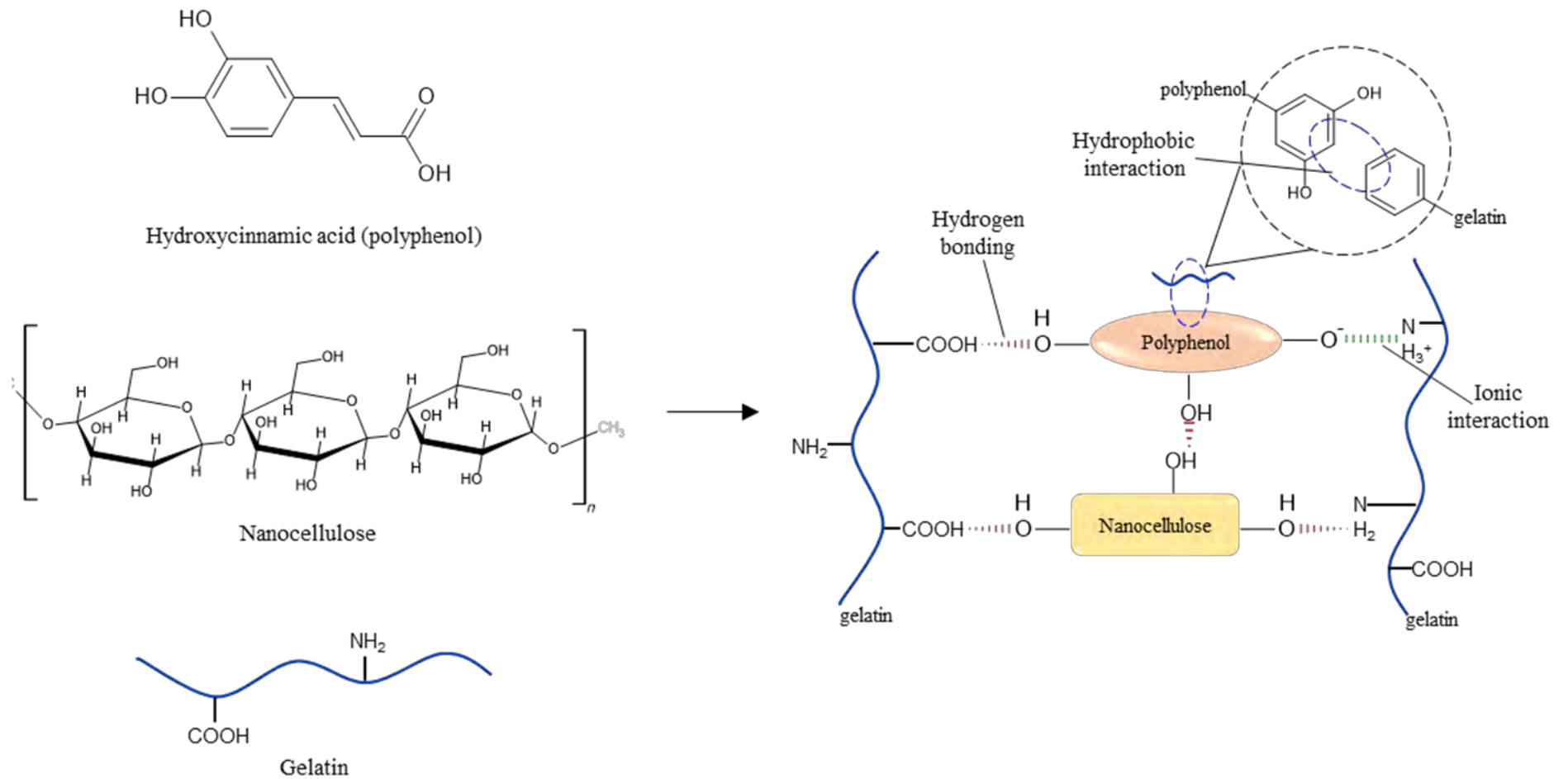
Source: Modified from Quan et al. (2019).

In particular, "pitanga" (*Eugenia uniflora* L.) leaf extract (PLE) has found potential application in active films. "Pitanga" is a native Brazilian tree, which has edible fruits, also called "pitanga" and "Brazilian cherry", and dark green leaves, widely used to produce teas that assist in folk medicine in the treatment of various diseases and symptoms (Fidelis et al., 2022). More than 160 polyphenols were identified in the PLE, with hydroxycinnamic acids being the most abundant, followed by tyrosols, among other classes such as hydroxycoumarins, alkylmethoxyphenols, flavonoids, and flavones (Garmus et al., 2014). This wide variety of polyphenols gives PLE high antioxidant and antimicrobial activities, and it can then enhance active films for better biological activities and, possibly, physicochemical and mechanical properties of films. Gelatin-based packaging activated with PLE has been shown to reduce lipid oxidation and bacterial counts in dried-cured Coppa throughout the storage period (Luciano et al., 2022).

Despite the improvements that plant extracts can provide to gelatin-based active films, they still present poor mechanical and water sensitivity properties, which limits their applications in areas such as food packaging. Just as gelatin is versatile and can incorporate different active compounds, it can also be combined with reinforcing fillers, such as nanocellulose, to form nanocomposite films to overcome these limitations (Nikoukheslat et al., 2022). Nanocellulose is extracted from cellulose in a nanostructured form. Cellulose of vegetable origin can come from different materials, such as waste generated by agricultural production, including that of soybean straw, residue from the threshing of soybeans, which is one of the largest commodities from Brazil (Martelli-Tosi et al., 2018).

Nanocellulose has characteristics such as high crystallinity, biocompatibility, biodegradability, and low toxicity (Alzate-Arbeláez et al., 2019), which makes it an interesting reinforcement material for biopolymer-based films, as it can improve the mechanical and thermal properties and water sensitivity of films (Pelissari et al., 2017). Because of its structure, nanocellulose can interact with biopolymers such as gelatin, and with compounds such as polyphenols, through hydrogen bonding (Figure 6.1). In gelatin-based active nanocomposite films, for example, this means that a more stable gelatin–polyphenol–nanocellulose complex can be formed, improving the performance of these films' properties (Almeida et al., 2023; Nikoukheslat et al., 2022).

In a previous study (Tessaro et al., 2021a), we developed gelatin-based nanocomposite films, activated with PLE and encapsulated in a double emulsion, with improved properties. The effect of PLE together with NC on the properties of these materials was not clear, as it was encapsulated. Based on our knowledge, the effect of the interaction between PLE and nanocellulose on the properties of gelatin-based films and nanocomposite films has not been reported. In this study, we hypothesized that the simultaneous presence of PLE, rich in polyphenols, and crystalline nanocellulose in the gelatin matrix can lead to the formation of complexes and stable interactions that, consequently, improve the performance of nanocomposite films for applications such as food packaging. Hence, the aim of this study was to produce gelatin-based active films and nanocomposite films incorporated with PLE and/or crystalline nanocellulose extracted from soybean straw, and to study the physicochemical, functional, microstructural, thermal, UV/Vis light barrier, and antioxidant properties of these materials.

6.2 MATERIAL AND METHODS

6.2.1 Material

The PLE was produced using "pitanga" leaves collected in the city of Pirassununga-SP, Brazil (21°59′ 46″ S, 47°25′ 36″ W). Embrapa Soja (Londrina-PA, Brazil) supplied soybean straw was used to extract CN. The reagents used in the production of PLE and CN (acetone P.A., sulfuric acid P.A., ethanol P.A., sodium hydroxide P.A., hydrogen peroxide, and magnesium sulfate heptahydrate) were purchased from Química Dinâmica Contemporânea LTDA (São Paulo-SP, Brazil).

To produce the films and nanocomposite films, Gelnex (Itá-SC, Brazil) supplied type B bovine gelatin (bloom 225, average molecular weight $4–5 \times 10^4$ Da), and glycerol (95% purity) was purchased from Labsynth® (São Paulo-SP, Brazil).

For antioxidant analysis, the reagents 2,2′-azino-bis(3-ethylbenzothiazoline-6-sulphonic acid) (ABTS), 6-hydrox-2,5,7,8-tetramethylchorman-2-carbxylic acid (Trolox), (2-pyridyl)-1,3,5- triazine (TPTZ), gallic acid, and iron (III) chloride hexahydrate were purchased from Sig-ma-Aldrich (St Louis-MO, USA). Folin–

Ciocalteu reagent, potassium persulfate, sodium acetate trihydrate, and sodium carbonate were purchased from Merck (Darmstadt, Germany).

6.2.2 Production of the "pitanga" leaf extract

The PLE was produced according to methodology described by Tessaro et al. (2021b). "Pitanga" leaves were collected, selected based on color and integrity (dark green and without damage), sanitized with water with detergent and distilled water, and soaked in sodium hypochlorite (0.1% w/v) for 15 min. Then, the sanitized leaves were dehydrated at 42 °C for 72 h (forced-air circulation drying oven, MA035, Marconi, Piracicaba-SP, Brazil). The dried leaves were ground in a commercial blender and sieved (48 mesh) to make the powder uniform. The powdered leaves were then dispersed in a 60% hydroethanolic solution (1 g powdered leaves/10 mL solution), and the formed dispersion was homogenized and subjected to ultrasonic extraction for 40 min (Ultra-sound, MaxiClean 1400A, Unique, Indaiatuba-SP, Brazil), and then heated until 80 °C for 30 min under stirring (Magnetic stirrer integrated with temperature digital control, AA-2050, Gehaka, São Paulo-SP, Brazil). The formed PLE was filtered through a paper filter (Whatman n°1), rotary evaporated at 42 °C for 5 h (Rotary Evaporator Systems, TE 211, Tecnal, Piracicaba-SP, Brazil), and freeze-dried in a freeze-dryer (FD 1.0-60E, Heto-Holten A/S, Allerod, Denmark). The freeze-dried PLE was sieved (48 mesh) and stored protected from light in a freezer (−18 °C).

6.2.3 Production of the crystalline nanocelluloses

The CNs were extracted from soybean straw (SS), according to the methodology described by Martelli-Tosi et al. (2018) with slight modifications. Initially, the SS (stem and pod) were separated, washed with running water, dried at 50 °C for 24 h in a forced-air circulation drying oven, ground in a knife mill (SL31, Solab, Piracicaba-SP, Brazil) and sieved (35 mesh). The ground SS was subjected to an alkaline pre-treatment with a 17.5% (m/v) sodium chlorite solution (100 g SS/1 L solution) under vigorous agitation at room temperature for 15 h (Mechanical stirrer, TE 039, Tecnal, Piracicaba-SP, Brazil). The pre-treated SS was washed with water and finally distilled water until it reached a neutral pH, using a set of sieves (200 and 400 mesh). Then, the pre-treated SS was bleached with 1 L of bleaching solution (4%

hydrogen peroxide, 0.3% magnesium sulfate heptahydrate, and 2% sodium chlorite, w/v) under vigorous stirring at 90 °C for 3 h using a magnetic stirrer integrated with a digital temperature control.

The bleached SS was washed using a set of sieves (200 and 400 mesh) with water until neutral pH, followed by washings with distilled water, ethanol PA, and acetone PA, consecutively, and then dried at 50 °C for 4 days in a forced-air circulation drying oven. The bleached and dried SS was then ground in a commercial blender, sieved (28 mesh), and submitted to an acid hydrolysis with 64% (w/v) sulfuric acid solution (1 g SS/30 mL solution) under stirring at 65 °C for 40 min in a magnetic stirrer integrated with a digital temperature control. Finally, the acid hydrolysis reaction was stopped by diluting the dispersion with distilled water 10 times, and letting the CN and SS decant for 24 h. The decanted material was dialyzed (cellulose membrane) with tap water until neutral pH, and later homogenized in a rotor stator homogenizer at 14,000 rpm for 5 min (Ultraturrax® IKA T25, Labotechnki, Staufen, Germany), plus 3 min of 550 W probe-type sonication at 50% amplitude (SFX550, Branson Ultrasonics Corp., Danbury, CT, USA). The formed CN suspension was freeze-dried and stored at room temperature.

6.2.4 Production of gelatin-based films

The films (F) and nanocomposite films (N) were developed using the casting method, which consisted of drying the respective film-forming solution (FFS) according to Tessaro et al. (2021a,b). To prepare the film-forming solutions of F, gelatin (4 g/100 g FFS) was hydrated in distilled water for 30 min at room temperature, and solubilized at 55 °C for 10 min, using a thermostatic bath (MA-184/20, Marconi, Piracicaba-SP, Brazil). Then, glycerol (25 g/100 g gelatin) was added to FFSs under moderate magnetic stirring (AA-2050, Gehaka, São Paulo-SP, Brazil). To produce film-forming suspension of N, the freeze-dried CN was added during the hydration of gelatin in water, at a concentration of 4.5 g/100 g gelatin. To produce the F and N film-forming solutions, PLE was subsequently added, at a concentration of 0.25 g PLE/100 g of gelatin, also under moderate magnetic stirring.

All FFSs were deposited on acrylic plates (12 × 12 cm) and dehydrated at 30 °C for 24 h (air-forced circulation drying oven, MA035, Marconi, Piracicaba-SP, Brazil).

Before characterization, F and N were conditioned for 7 days in desiccators containing a saturated NaBr solution, whose relative humidity (RH) was 58%, at 25 °C. For the scanning electron microscopy (SEM), atomic force microscopy (AFM), and Fourier transformed infrared spectroscopy (FTIR) analyses, the F and N had been previously conditioned in silica gel (RH = 0%) for 15 days at 25 °C.

Therefore, four treatments were produced: control and active films (F-C and F-PLE, respectively) and control and active nanocomposite films (N-C and N-PLE, respectively).

6.2.5 Characterization of the gelatin-based films and nanocomposite films

6.2.5.1 Visual aspect and thickness

The appearance, homogeneity, and uniformity of the films were visually observed and described as their visual aspect (Tessaro et al., 2021b).

Ten thickness measurements at random points were carried out on the film surfaces with a digital micrometer (±0.001 mm; Mitutoyo, Tokyo, Japan). The thickness of the films was calculated as the average of these measurements (Tessaro et al., 2021b).

6.2.5.2 Moisture content

Films samples with known weights were dried at 105 °C for 24 h in a forced-air circulation drying oven, and moisture content expressed as g water/100 g wet film (Gontard et al., 1992).

6.2.5.3 Solubility in water

Films samples (2 cm diameter and known weight) were added to 50 mL of distilled water and shaken at 25 rpm and 25 °C for 24 h in an orbital shaker (MA141, Marconi, Piracicaba-SP, Brazil). The non-solubilized part of the films was filtered and dried at 105 °C for 24 h in a forced-air circulation drying oven. Solubility in water (SW)

was calculated as the difference between initial and end films weights, in dry basis (Gontard et al., 1992).

6.2.5.4 Water vapor permeability

Water vapor permeability (WVP) of films was determined using the E-96-E80 standard test (ASTM, 1989) modified by Gontard et al. (1992). Films samples with 30 mm diameter were fixed in aluminum permeation cells containing silica gel inside (RH = 0%) and with permeation area of 31.17 cm^2. These systems were placed in desiccators contain distilled water (RH = 100% and vapor pressure = 3.2691 kPa), and the permeation mass gain were noted at 24 h intervals for 7 days. The WVP (g.mm/m.h.kPa) of films were calculated using eq. (6.1), where Δg/Δt is the rate of weight change (g/h), x is the thickness film (mm), A is the permeation area (cm^2), and ΔP, is the partial pressure difference across the films (kPa).

$$WVP = \frac{\Delta g}{\Delta t}\left(\frac{x}{A\Delta P}\right)$$
(6.1)

6.2.5.5 Water contact angle

The water contact angle (WCA) with the air-side surface of the films was determined using an optical tensiometer (Attension Theta lite, KSV Instruments, Helsinki, Finland) equipped with OneAttension image analysis software (Version 4.1.9.8). Film samples were fixed to the equipment support and a drop of Milli-Q water was deposited on the film's air-side surfaces using a precision syringe. Images were recorded each second for 60 s, and the WCA values were obtained in the chosen time of 15 s (Tessaro et al., 2021b).

6.2.5.6 Scanning electron microscopy (SEM)

The air-side surface and the cryo-fractured cross-section of the films were analyzed in random positions using a Hitachi tabletop microscope-SEM (TM3000, Hitachi Ltd., Tokyo, Japan), operating at a voltage of 15 kV. For the analysis of the drying surface, the film samples (20 × 20 μm) were fixed on stubs without any prior

preparation. For the cryo-fractured internal structure analysis, the film samples were cryo-fractured after freezing with liquid nitrogen (Tessaro et al., 2021b).

6.2.5.7 Atomic Force Microscopy (AFM)

The topography and roughness of the air-side surface of the films (20 × 20 µm) were analyzed using atomic force microscopy (AFM NT-MDT, Moscow, Russian) in semi-contact mode with a resonance frequency of 240 kHz, contact force of 11.8 N/m, and scan speed of 0.3 Hz. The average roughness (Ra) was calculated as the absolute value of height deviations using the Nova Px 3.2.5 Rev 1266 equipment software (Tessaro et al., 2021b).

6.2.5.8 Gloss

The gloss of films was determined using a glossimeter (NGL 20/60, Rhopoint, Bexhill on Sea-West), at the angle of 60°, according to D523 standard test (ASTM, 1999). Ten measurements were made at random points on the films' air-side surface, and the gloss was expressed as a gloss unit (GU).

6.2.5.9 Color and opacity

The color parameters (L*, a*, and b*) were obtained using a MiniScan colorimeter (MSEZ 1049, HunterLab, Reston-VA, USA), in the reflectance mode (CIELab scale, illuminant/angle D65/10°, 30 mm opening), according to Tessaro et al. (2021b). Total color difference (ΔE*) was calculated with eq. (6.2), where $\Delta L^* = L^*_{sample} - L^*_{standard}$ (93.59), $\Delta a^* = a^*_{sample} - a^*_{standard}$ (-1.00), and $\Delta b^* = b^*_{sample} - b^*_{standard}$ (1.75).

$$\Delta E^* = \sqrt{(\Delta L^*)^2 + (\Delta a^*)^2 + (\Delta b^*)^2} \tag{6.2}$$

The opacity (Y) of the films was obtained using the same MiniScan colorimeter with the same parameters. The opacity was calculated using eq. (6.3), where Yb is the opacity of the films under the standard black plate, and Yw is their opacity under the standard white plate.

$$Y = \frac{Y_b}{Y_w} \tag{6.3}$$

6.2.5.10 UV/Vis light barrier

The UV/Vis light barrier properties of films were determined using a UV-Vis spectrophotometer (Lambda 35, Perkin-Elmer, Whaltham-MA, USA) in transmittance mode and in the wavelength from 200 to 800 nm (Tessaro et al., 2021b). Films samples (10 x 40 mm) were fixed in the cuvette so that to light passed through the films.

6.2.5.11 Fourier-transformed infrared spectroscopy

Fourier-transformed infrared spectroscopy (FTIR) analyzes were performed in a spectrophotometer (Spectrum-One, Perkin-Elmer, Whaltam-MA, USA) equipped with a UATR accessory (Universal Attenuator Total Reflectance), according to Tessaro et al. (2021b). No prior preparation of the films was necessary. FTIR spectra were obtained by performing 20 scans in the spectral range from 4000 to 650 cm^{-1}, with a resolution of 4 cm, and analyzed with the Spectrum-One 5.3 software (Perkin-Elmer, Whaltam-MA, USA).

6.2.5.12 Thermal properties

The thermal properties of the films were determined using a differential scanning calorimeter (DSC TA2010, TA Instruments, New Castle-DE, USA) (Tessaro et al., 2021a). The film samples, placed in hermetically sealed aluminum TA pans, were heated from -50 to 150 °C at 5 °C/min, twice, in an inert atmosphere (45 mL/min N_2). An empty pan was used as a reference. Before both scans, the DSC cell was cooled using liquid nitrogen. The glass transition (Tg) and melting (Tm) temperatures, and the melting enthalpy (ΔHm) were calculated directly from the thermal curves using the Universal Analysis V1.7F software (TA Instruments, New Castle-DE, USA).

6.2.5.13 Mechanical properties

The mechanical properties of the films were determined using D882/12 axial tension tests (ASTM, 2001), in a texturometer (TA.XT2i, Stable Micro Systems, Surrey, England) at room temperature. Film samples (15 x 100 mm) were fixed on grips separated by 50 mm, and the test was carried out with grips separation speed of 1 mm/s. The tensile strength and the elongation at break were obtained directly from the stress versus strain curve, and the elastic modulus was calculated from the slope of the linear part of the curve, using the equipment software (Exponent Line Express, v4.0.13.0).

6.2.5.14 Folin-Ciocalteu reagent reducing compounds and antioxidant activity

Before testing, the films were cut into small fragments and shaken in an orbital shaker at 50 rpm (MA141, Marconi, Piracicaba-SP, Brazil) for 12 h, protected from light, with 50% hydroethanolic solution. Supernatants were used for analyses.

The quantification of Folin-Ciocalteu reducing capacity (FCRC) were carried out using the methodology described by Singleton, Orthofer and Lamuela-Raventós (1999). Antioxidant activities were determined by the ABTS free radical capture method (ABTS$^{\bullet+}$ method) (Re et al., 1999), and Ferric reduction antioxidant power method (FRAP method) (Benzie; Strain, 1996; Pulido; Bravo; Saura-Calixto, 2000). The antioxidant activities by the ABTS$^{\bullet+}$ and FRAP methods were expressed in mg Trolox equivalent (TE)/g of film, and the CRFC were expressed in mg Gallic acid equivalent (GAE)/g of film.

6.2.6 Statistical analysis

All samples were produced in triplicate and analyzes were performed with at least three measurements from each replicate. The results of the films and nanocomposite films characterizations were presented as mean ± standard deviation and were subjected to analysis of variance (ANOVA) and mean comparisons using the Tukey's test (α = 0.05), using the Statistica 7.0 software.

6.3 RESULTS AND DISCUSSIONS

6.3.1 Visual aspect and thickness

After drying, the films (F-C and F-PLE) were transparent and presented a homogeneous and uniform appearance, without visible bubbles (Figure 6.2). The nanocomposite films (N-C and N-PLE) were translucent and presented a less homogeneous appearance, possibly due to some CN agglomerates; however, they remained without bubbles or fractured regions (Figure 6.2).

Regarding thickness, no difference ($p > 0.05$) was observed between all samples (Table 6.1), indicating that the control of the mass of FFSs deposited on the plates (1.25 g dry matter/plate) was efficient. This achievement is important because thickness can influence some physical properties of biopolymer-based films (Tyuftin; Kerry, 2021).

Figure 6.2 – Examples of films (F) and nanocomposite films (N): control (C) and activated with "pitanga" leaf extract (PLE)
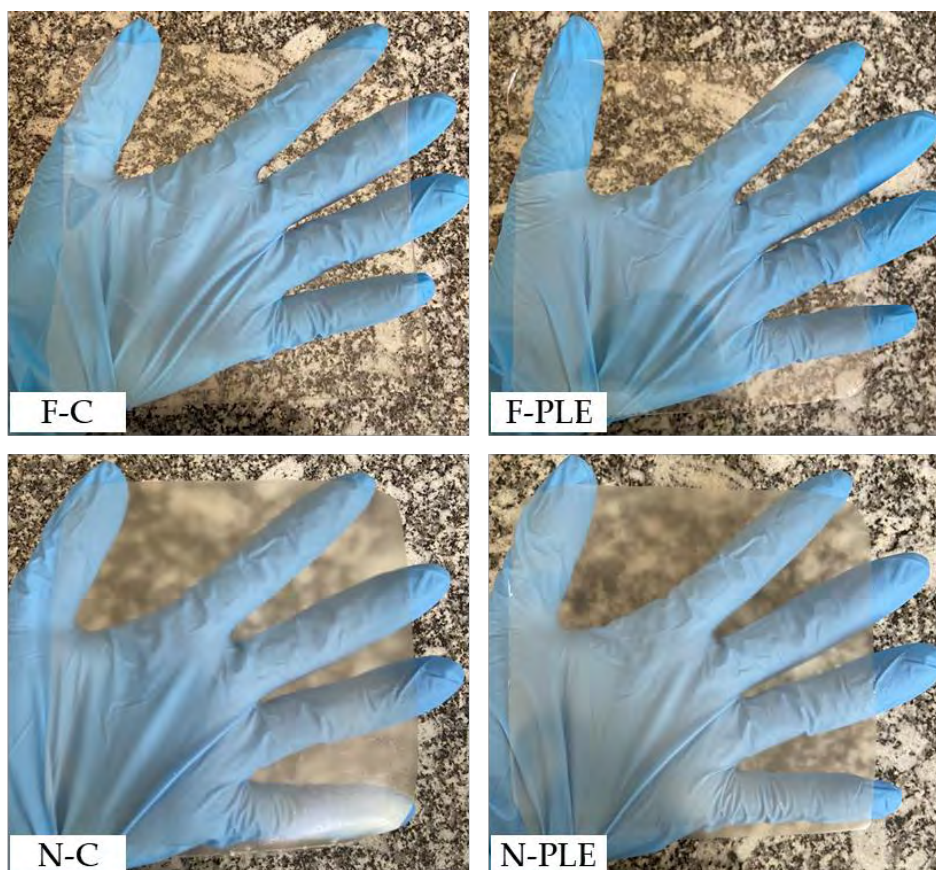
Source: Own authorship.

Table 6.1 - Physicochemical properties of films (F) and nanocomposite films (N), control (C) and activated with "pitanga" leaf extract (PLE)*

Properties	Treatments	C	Active (PLE)
Thickness (mm)	F	0.083 ± 0.002 [aA]	0.077 ± 0.004 [aA]
	N	0.084 ± 0.006 [aA]	0.077 ± 0.005 [aA]
Moisture content (%)	F	13.5 ± 0.3 [bA]	14.4 ± 0.4 [aA]
	N	13.7 ± 0.2 [aA]	12.2 ± 0.7 [bB]
Solubility in water (%)	F	43.4 ± 0.4 [bA]	48.9 ± 0.8 [aA]
	N	42.9 ± 0.7 [aA]	44.1 ± 1.0 [aB]
WVP (x10^{1} mm.g/m².h.kPa)	F	3.2 ± 0.3 [aA]	3.0 ± 0.1[aA]
	N	3.6 ± 0.2 [aA]	3.2 ± 0.1[aA]

*Means ± standard deviation (n = 3). Different lowercase letters on the same line and different uppercase letter in the same column indicate significant differences between means, according to Tukey's test ($p < 0.05$). PLE: "Pitanga" leaf extract; WVP: Water vapor permeability.
Source: Own authorship.

6.3.2 Moisture content

The moisture content can influence some physical properties of biopolymer-based films. Thus, it is important to know the moisture content of films, which is linked with their hygroscopicity (Tyuftin; Kerry, 2021). The effect of adding PLE on moisture content was different for films and nanocomposite films (Table 6.1).

F-PLE showed higher moisture content than F-C, while the opposite effect was observed between N-C and N-PLE ($p < 0.05$). The increase in moisture content in F-PLE can be explained by the interactions that occurred between the PLE's compounds and gelatin, increasing the affinity of the film for water molecules. In a previous study, the same occurred for gelatin-based films with haskap berries extract (Liu et al., 2019). For nanocomposite films, PLE caused a decrease in moisture content, possibly due to the ability of PLE to interact with CN chains. According to Alzate-Arbeláez et al. (2019) extracts rich in polyphenols form stable complexes with CN, due to the various interactions that can occur between them. More specifically, the -OH groups of PLE bind to the -OH groups of CN and gelatin through hydrogen bonds, reducing the hydrophilic groups available to interact with water molecules (Yan et al., 2021). This decrease in moisture content was also observed in gelatin/chitosan nanocomposite films incorporated with anthocyanin-rich hawthorn fruit extract (Yan et al., 2021).

In the case of the effect of CN addition, F-C and N-C did not present different moisture content ($p > 0.05$), while N-PLE presented lower moisture content than the F-PLE film ($p < 0.05$). As previously explained, for the N-PLE film, the simultaneous presence of PLE and CN gave rise to stable complexes within the biopolymeric matrix (Figure 6.1), which interacted with each other and with the gelatin, possibly decreasing water absorption when compared to F-PLE, incorporated only with PLE.

6.3.3 Solubility in water (SW)

The PLE increased ($p < 0.05$) the solubility in water of F-PLE in relation to F-C, but did not change ($p > 0.05$) the SW between N-PLE and N-C (Table 6.1). In the case of N-PLE, the presence of PLE did not affect the solubility in water, possibly because PLE can interact with CN structures (Yan et al., 2021), while in F-PLE, it can increase the hydrophilicity of the film and, consequently, its SW. Luciano et al. (2021), who studied bi-layer gelatin-based films incorporated with PLE, reported that the addition of PLE did not affect the solubility in water of the films.

Regarding the effect of CN, a decrease in the solubility in water of N-PLE was noted in relation to the F-PLE film ($p < 0.05$), but no difference was observed between F-C and N-C ($p > 0.05$), thus as observed for moisture content. Likewise, this behavior has been observed for gelatin/carboxymethylcellulose incorporated with pomegranate peel extract (Vargas-Torrico et al., 2023). Although CN presents greater interfacial bonding, forming networks, which theoretically hinders the diffusion of water through the films (Pelissari et al., 2017), this effect was not observed between the film and nanocomposite film controls.

6.3.4 Water vapor permeability (WVP)

Among all of the treatments studied, there was no difference ($p > 0.05$) in relation to WVP, that is, the effect of adding NC and/or PLE did not change the WVP of the films and nanocomposite films (Table 6.1).

Regarding the effect of PLE, the amount of PLE added was not able to change and cause differences between the WVP of films and nanocomposite films, as observed by Luciano et al. (2021). Because they were gelatin-based, the films and

nanocomposite films had great affinity and solubility in water, justifying the high WVP presented by them Tessaro et al. (2021b), even charged with CN. The WVP values were similar to those determined by other authors working on gelatin-based films with PLE or nisin (3.1 to 4.0 × 10^{-1} g.mm/m^2.h.kPa) (Luciano et al., 2021) and carboxymethyl cellulose and pomegranate peel extract (around 2 × 10^{-1} g.mm/m^2.h.kPa) (Vargas-Torrico et al., 2023). In terms of application, all of these films can be considered very permeable to water vapor (Tessaro et al., 2021a).

6.3.5 Water contact angle (WCA)

WCA results provide information regarding the hydrophobicity of the film surface, and several factors can interfere with this parameter, such as surface roughness and the hydrophobicity of the components of the biopolymeric matrix. If the surface of the film is rougher, the contact surface of the water with the film will consequently be larger, causing its contact angle to increase (Tessaro et al., 2021b).

All of the films and nanocomposite films were considered to have a hydrophobic air-side surface, with θ > 65° (Kaya et al., 2018) (Table 6.2). When analyzing the effect of PLE, it was observed that F-C presented higher WCA than F-PLE ($p < 0.05$), which has also been reported for gelatin/inulin nanocomposite films incorporated with crystalline nanocellulose and *Malva sylvestris* extract (Nikoukheslat et al., 2022). PLE's hydrophilic molecules can increase the hydrophilicity of the film, increasing its affinity for water (Liu et al., 2019). Although the average roughness of the air-side surface of F-PLE was higher than that of F-C (Table 6.2), this was not the main factor that affected the WCA of F-PLE, since both films (F-C and F-PLE), showed very low average roughness. For nanocomposite films, PLE did not affect WCA ($p > 0.05$), nor did it affect the average roughness (Table 6.2). In other words, the addition of PLE did not affect the contact surface of the N-PLE film with water.

The addition of CN decreased the WCA of N-C compared to that of F-C ($p < 0.05$). The same behavior was observed by Pereda et al. (2011) for sodium caseinate-based films and nanocomposite films, which was related to increased film roughness. Comparing F-PLE and N-PLE, no difference was observed in WCA ($p > 0.05$).

Table 6.2 - Air-side surface properties and color parameters of films (F) and nanocomposite films (N), control (C) and activated with "pitanga" leaf extract (PLE)**

Properties	Treatments	C	Active (PLE)
Water contact angle (°)	F	80.9 ± 0.3 [aA]	71.3 ± 0.9 [bA]
	N	72.7 ± 0.3 [aB]	72.1 ± 0.3 [aA]
Average roughness (nm)	F	3.5 ± 0.3 [bB]	5.2 ± 0.7 [aB]
	N	(10.6 ± 0.8) ×10^4 [aA]	(10.2 ± 1.1) ×10^4 [aA]
Gloss (GU)	F	148 ± 3 [aA]	142 ± 8 [aA]
	N	49 ± 7 [aB]	41 ± 1 [aB]
L^*	F	90,2 ± 0.1 [aA]	88.8 ± 0.2 [bA]
	N	88,7 ± 0.2 [aB]	87.4 ± 0.1 [bB]
a^*	F	-1.3 ± 0.0 [aA]	-0.9 ± 0.0 [bA]
	N	-0.6 ± 0.0 [aB]	-0.4 ± 0.0 [bB]
b^*	F	3.5 ± 0.1 [bB]	4.0 ± 0.1 [aB]
	N	6.9 ± 0.2 [aA]	7.3 ± 0.3 [aA]
ΔE^*	F	4.1 ± 0.1 [bB]	5.5 ± 0.2 [aB]
	N	7.2 ± 0.1 [bA]	8.5 ± 0.3 [aA]
Opacity (%)	F	0.8 ± 0.1 [aB]	0.8 ± 0.1 [aB]
	N	2.0 ± 0.3 [aA]	1.9 ± 0.2 [aA]

**Means ± standard deviation (n = 3). Different lowercase letters on the same line and different uppercase letter in the same column indicate significant differences between means, according to Tukey's test ($p < 0.05$). ΔE^*: total difference of color; PLE: "Pitanga" leaf extract.
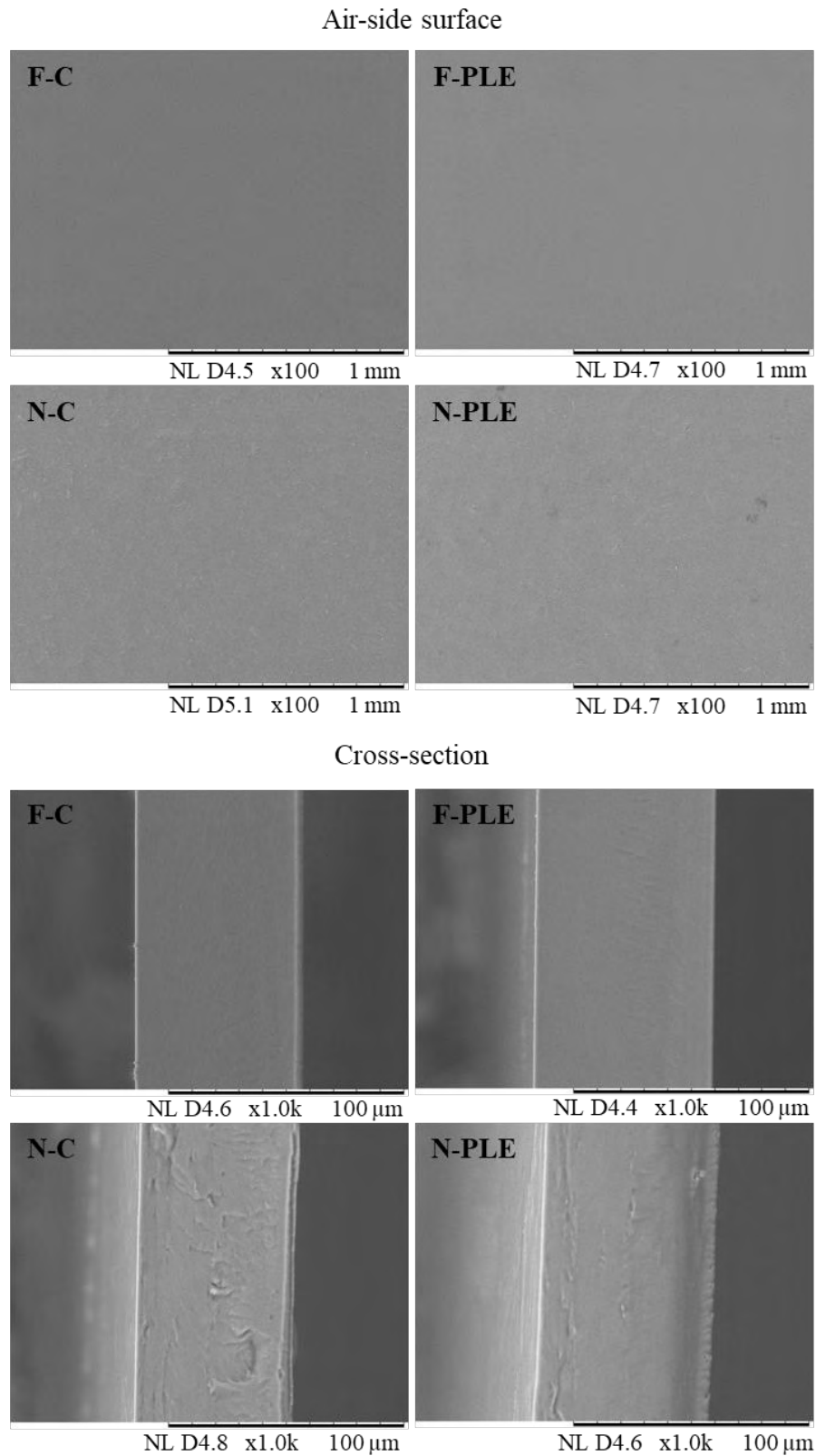
Source: Own authorship.

6.3.6 Scanning electron microscopy (SEM)

SEM was used to analyze the microstructure of the samples. No differences were observed between F-C and F-PLE, both in the air-side surfaces and in the cross sections (Figure 6.3). These films presented smooth, continuous, and homogeneous surfaces, without any phase separation, demonstrating a good incorporation of PLE into the biopolymeric matrix, as observed for bi-layer gelatin films incorporated with PLE and/or nisin (Luciano et al., 2021) and gelatin-based films with haskap berries extract (Liu et al., 2019).

Figure 6.3 – Electronic scanning micrographs of the air-side surfaces and cross-section of films (F) and nanocomposite films (N), control (C) and activated with "pitanga" leaf extract (PLE)

Air-side surface

F-C
NL D4.5 x100 1 mm

F-PLE
NL D4.7 x100 1 mm

N-C
NL D5.1 x100 1 mm

N-PLE
NL D4.7 x100 1 mm

Cross-section

F-C
NL D4.6 x1.0k 100 μm

F-PLE
NL D4.4 x1.0k 100 μm

N-C
NL D4.8 x1.0k 100 μm

N-PLE
NL D4.6 x1.0k 100 μm

Source: Own authorship.

For N-C and N-PLE, a certain heterogeneity and discontinuity was noted on the air-side surfaces and in the cross sections (Figure 6.3) of both, possibly caused by CN agglomerations, as has been previously observed for gelatin/inulin-based nanocomposite films containing CN and *Malva sylvestris* extract (Nikoukheslat et al., 2022). However, no fracture or phase separation was observed, indicating that there was good incorporation of CN into the biopolymeric matrices. Furthermore, in N-PLE, the heterogeneity and possible agglomerations of CN were less evident than in N-C, especially in the cross section, which may indicate that there was interaction between the PLE and the CN that improved the incorporation of the CN in the biopolymeric matrix (Nikoukheslat et al., 2022).

6.3.7 Atomic force microscopy (AFM)

The results obtained by AFM analysis (Figure 6.4) showed that the films presented smoother topographies and small peaks, almost insignificant compared to the large peaks and valleys of the nanocomposite films. These observations corroborated the results presented in the SEM analysis (Figure 6.3). Similar results have previously been obtained for gelatin-based nanocomposite films with CN and PLE encapsulated in double emulsion (Tessaro et al., 2021a).

Given the average roughness (Ra), obtained from the analysis of the topography of the samples, the effect of adding PLE and NC to the films and nanocomposite films was studied. Regarding the effect of PLE, F-PLE showed higher average roughness than F-C ($p < 0.05$) (Table 6.2), possibly because the incorporation of PLE caused slight accumulations, causing rougher regions. Similar observations were presented by Luciano et al. (2021). For N-C and N-PLE, there were no differences in Ra ($p > 0.05$). In this case, PLE did not increase, at least not detectably, the roughest regions already caused by CN.

Regarding the effect of adding CN, both between F-C and N-C, and between F-PLE and N-PLE, the Ra increased in the order of approximately 20,000 times (Table 6.2). CNs possess a nanoscale diameter, although their length can be in the range of submicrometers. The dispersion of these fibers throughout the bulk material may extend to the surface, leading to increased surface roughness. Additionally, structures tend to agglomerate, increasing the Ra of the nanocomposite films. High Ra was also found by Tessaro et al. (2021a) for gelatin-based nanocomposite films.

Figure 6.4 – 3D atomic force micrographs of the air-side surfaces of films (F) and nanocomposite films (N), control (C) and activated with "pitanga" leaf extract (PLE)
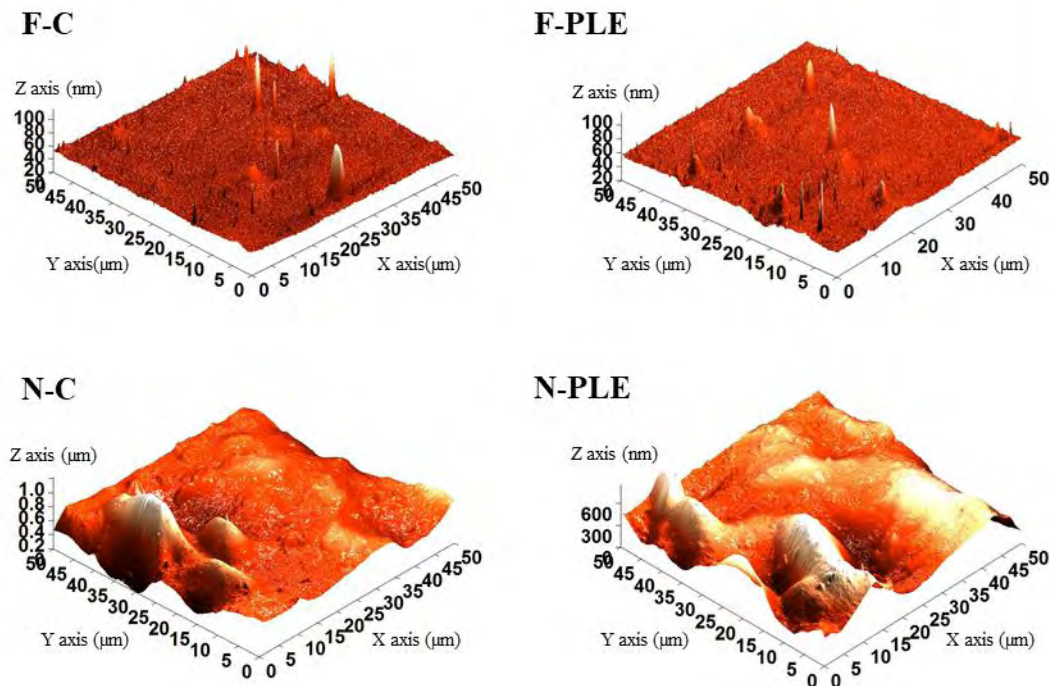
Source: Own authorship.

6.3.8 Gloss

The addition of PLE did not affect ($p > 0.05$) the gloss of F-PLE compared to the gloss of F-C, nor the gloss of N-PLE compared to the gloss of N-C (Table 6.2). The good incorporation of PLE into the biopolymeric matrices had little effect on the air-side surface roughness of the active films and nanocomposite films compared to their respective controls. This is certainly why the gloss was also not affected by the incorporation of PLE. The same behavior was observed by Luciano et al. (2021) in their studies on bi-layer gelatin films with PLE. Tessaro et al. (2021a) observed a decrease in the gloss of films when studying gelatin-based films with CN and with or without the addition of PLE encapsulated in a double emulsion, possibly as an effect of the presence of the double emulsion, and not of the PLE itself.

The addition of CN decreased ($p < 0.05$) the gloss of N-C and N-PLE compared to F-C and F-PLE, respectively (Table 6.2), as the presence of CN can cause nanocomposite films with less polished and shiny air-side surfaces than the respective films, due to non-uniform distribution of nanoparticles or even agglomerations

(Pelissari et al., 2017). In fact, the air-side surface of the nanocomposite films was much rougher than that of the films, as already discussed. The same result was reported by Pelissari et al. (2017) when studying nanocomposite films based on banana starch reinforced with cellulose nanofibers.

The film gloss is a surface property that is directly related to the morphology and roughness of the air-side surface of the films, that is, the degree of surface polishing. A negative linear dependence was observed in this case (Gloss = −16.0 Ra + 212.7, R^2 = 0.966). Similar behavior was observed by Luciano et al. (2021).

6.3.9 Color and opacity

Color is an important property that affects the physical appearance of films and consequently consumer acceptance (Vargas-Torrico et al., 2023). PLE has a greenish-yellow color (L* = 30.4, a* = 12.1, b* = 41.3), which may be associated with light dispersions from the phenolic compounds present in the PLE; therefore, it was expected that the color of the films and nanocomposite films would be affected by the PLE (Tessaro et al., 2021b). In fact, all of the color parameters (L*, a*, b* and ΔE*) showed differences ($p < 0.05$) when studying the effect of adding PLE on F-PLE and N-PLE compared to F-C and N-C, respectively (Table 6.2), except for the b* parameter for nanocomposite films, which showed no difference ($p > 0.05$).

For the L* parameter (brightness value), which varies from zero (white = light) to 100 (black = dark), the addition of PLE decreased its value ($p < 0.05$) in the film and nanocomposite film compared to their respective controls. The low L* value of the PLE may have caused the decrease in this parameter in the F-PLE and N-PLE.

For a*, b*, and ΔE*, the presence of PLE caused an increase in the values of these parameters in F-PLE and N-PLE. As expected, the color parameters of the films and nanocomposite films were influenced by the color parameters of the PLE, which has positive values for the a* and b* parameters, that is, it presents a reddish and yellowish color, respectively. Therefore, F-PLE and N-PLE showed stronger reddish and yellowish colors than their controls (F-C and N-C, respectively). The total color difference of F-PLE and N-PLE (evaluated by the ΔE* parameter) was also greater than that of F-C and N-C, which indicates that the active film and nanocomposite film were more colorful than the controls. Luciano et al. (2021) also reported differences in the color parameters of their films caused by PLE, but their differences presented a less reddish color than those studied in this study. Vargas-Torrico et al. (2023) also

reported changes in all color parameters of gelatin-carboxymethylcellulose films and nanocomposite films upon addition of pomegranate peel extract.

The incorporation of CN also resulted in alterations to the color parameters. For the parameters L* and a*, there was a decrease in them when comparing the nano-composite films with their respective films (Table 6.2), indicating that the nanocomposite films were less clear and less greenish, respectively. For the parameters b* and ΔE*, the opposite occurred, indicating that the nanocomposite films were more yellowish and more colorful, respectively. In short, CN produced darker, less greenish and more yellowish nanocomposite films, probably due to the color of CN from soybean straw, which is slightly yellowish. The same trend in nanocomposite film coloring was observed by Pelissari et al. (2017). Nikoukheslat et al. (2022) also reported changes in the color parameters of gelatin/inulin-based nanocomposite films by incorporation of CN and *Malva sylvestris* extract.

It is worth mentioning that although PLE and/or CN caused changes in the color parameters of films and nanocomposite films, all of the samples studied showed high luminosity (bright, with L* > 85), and values of a*, b*, and ΔE* closer to zero, indicating that the films and nanocomposite films produced were poorly colored.

The opacity was similar ($p > 0.05$) for F-C and F-PLE, and N-C and N-PLE (Table 6.2). Therefore, it can be considered that the amount of PLE used in the production of F-PLE and N-PLE did not generate insoluble regions that made it impossible for light to pass through them (Luciano et al., 2021). Luciano et al. (2021) presented opacity values very close to those obtained in this study for F-C and F-PLE. N-C and N-PLE presented higher opacity than F-C and F-PLE, respectively. In other words, the nanocomposite films were less transparent, due to the solid particles of the CN and the strong interactions between the CN and gelatin, which decreased the passage of light through the nanocomposite films. The same behavior was observed by Pelissari et al. (2017).

6.3.10 UV/Vis light barrier

The UV/Vis light barrier is an important and desirable property for food packaging, as it can prevent and reduce lipid oxidation and nutrient loss induced by light incidence (Liu et al., 2019). Between wavelengths of 200 and 300 nm (UV light),

all samples showed low transmittance (<20%), that is, having high barrier properties to UV light (Figure 6.5a). The F-PLE, N-C, and N-PLE showed better performance in this region (~10% transmittance) than the F-C (~15% transmittance). Therefore, in the UV light region, the barrier properties varied as follows: N-PLE > N-C = F-PLE > F-C.

Figure 6.5 – (a) UV/Vis spectra and (b) FTIR spectra of films (F) and nanocomposite films (N), control (C) and activated with "pitanga" leaf extract (PLE)
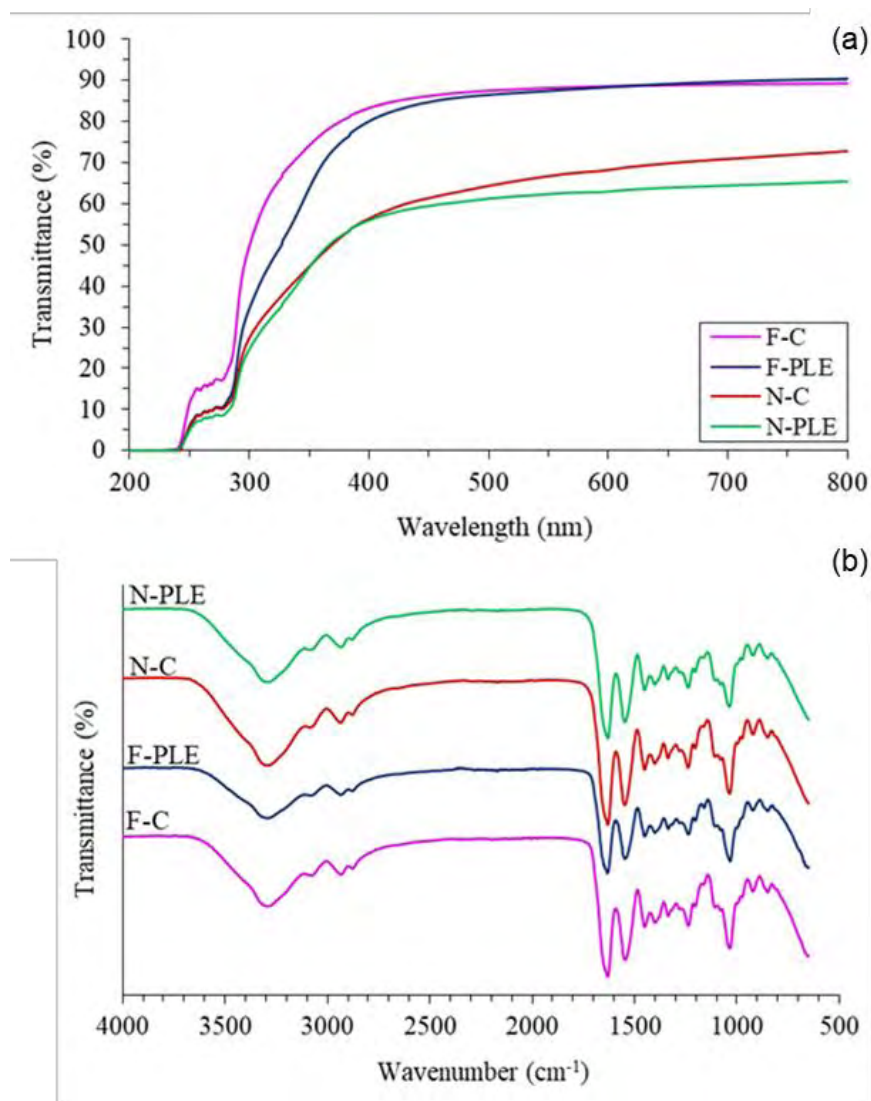
Source: Own authorship.

In the visible light region (above 300 nm), F-C showed higher transmittance than F-PLE up to 450 nm, while N-C and N-PLE showed the lowest transmittance in this same region, with no major differences between them. From 450 nm onwards, the transmittance of F-C and F-PLE was practically the same, with no notable differences, while N-PLE started to present lower transmittance than N-C. In general, the barrier

properties in the visible light region were ordered as follows: N-PLE > N-C > F-PLE > F-C.

PLE is rich in polyphenols, which are capable of absorbing visible light, reducing the transmittance through films and nanocomposite films (Vargas-Torrico et al., 2023). Other studies on gelatin films incorporating substances rich in polyphenols have also shown better barrier properties to UV/Vis light compared to control films (Liu et al., 2019; Luciano et al., 2021; Vargas-Torrico et al., 2023). For nanocomposite films, from 300 nm onwards, the transmittance was explicitly lower, that is, they had better barrier properties to visible light. This happened because NC makes light scatter more easily, reducing transmittance in nanocomposite films (Pereda et al., 2011). Similar results have been reported for potato starch-based nanocomposite films with bacterial nanocellulose and gallic acid (Almeida et al., 2023).

The combination of the good visible light barrier properties of PLE and CN, as mentioned above, caused N-PLE to have lower transmittance and better efficiency. Furthermore, another important factor was the presence of amino acid residues containing aromatic rings in gelatin, which grants it excellent UV barrier properties (Tessaro et al., 2021b).

6.3.11 Fourier-transform infrared spectroscopy (FTIR)

The films and nanocomposite films showed characteristic bands of gelatin-based materials in the FTIR spectrum, with no difference observable due to the presence of PLE and/or CN (Figure 6.5b). The lack of differentiation between the samples may have been the result of similar chemical bonds that formed between the components, as well as in the gelatin–CN–PLE interaction, resulting in overlapping bands.

FTIR spectra showed bands at approximately 3287–3289 cm^{-1} (overlap of O-H and N-H stretching coupled with hydrogen bonding of amide A groups), probably due to hydrogen interactions between gelatin and glycerol (Figure 6.1), 2936–2935 cm^{-1} (=C–H and –NH_3^+ asymmetric stretching vibration, from amide B groups), 1636–1630 cm^{-1} (C-O stretching and hydrogen bonding coupled with COO, from amide-I groups) (Vargas-Torrico et al., 2023), due to ionic interactions between acyl groups of some amino acids of gelatin and functional groups of phenolic compounds of PLE (Figure

6.1); 1548 cm^{-1} (bending vibrations and N–H and C–N stretching, respectively, of the amide-II groups), 1451–1452 cm^{-1} (vibration of the -OH groups of the gelatin structure and/or CN and/or glycerol), and 1236 cm^{-1} (in-plane vibrations of the C–N and N–H groups, from amide-III groups, or CH_2 vibrations from glycerol) (Vargas-Torrico et al., 2023).

6.3.12 Thermal properties

The Tg, Tm, and ΔHm of the biopolymer matrix were not affected (p > 0.05) by the addition of PLE nor CN (Table 6.3), that is, the added amount of these compounds was not sufficient to cause changes in thermal properties. Therefore, the thermograms (Figure 6.6) displayed by the films and nanocomposite films were similar.

Table 6.3 - Thermal properties of films (F) and nanocomposite films (N), control (C) and activated with "pitanga" leaf extract (PLE)*

Scan	Properties	Treatments	C	Active (PLE)
1st	T_{g1} (°C)	F	-75.7 ± 3.3 [aB]	-70.9 ± 3.4 [aA]
		N	-68.1 ± 1.2 [aA]	-67.4 ± 1.6 [aA]
	T_{g2} (°C)	F	44.4 ± 0.2 [aA]	44.2 ± 1.4 [aA]
		N	48.0 ± 3.1 [aA]	44.1 ± 3.2 [aA]
	T_m (°C)	F	69.6 ± 2.1 [aA]	69.3 ± 1.0 [aA]
		N	70.6 ± 0.5 [aA]	69.4 ± 1.6 [aA]
	ΔH (J/g)	F	18.3 ± 0.4 [aA]	16.7 ± 1.2 [aA]
		N	16.4 ± 1.5 [aA]	17.3 ± 1.1 [aA]
2st	T_{g1} (°C)	F	-73.3 ± 3.7 [aA]	-74.3 ± 4.0 [aA]
		N	-72.4 ± 1.3 [aA]	-73.8 ± 3.3 [aA]
	T_{g2} (°C)	F	36.3 ± 1.9 [aA]	34.8 ± 0.9 [aA]
		N	35.5 ± 3.0 [aA]	34.4 ± 3.3 [aA]

*Means ± standard deviation (n = 3). Different lowercase letters on the same line and different uppercase letter in the same column indicate significant differences between means, according to Tukey's test (*p* < 0.05). *T_g*: glass transitions temperatures; *T_m*: melting temperatures of gelatin microcrystals; *ΔH*: melting enthalpy of gelatin microcrystals.

Source: Own authorship.

Figure 6.6 – DSC thermal curves (Exo up) of films (F) and nanocomposite films (N) control (C) and activated with "pitanga" leaf extract (PLE)
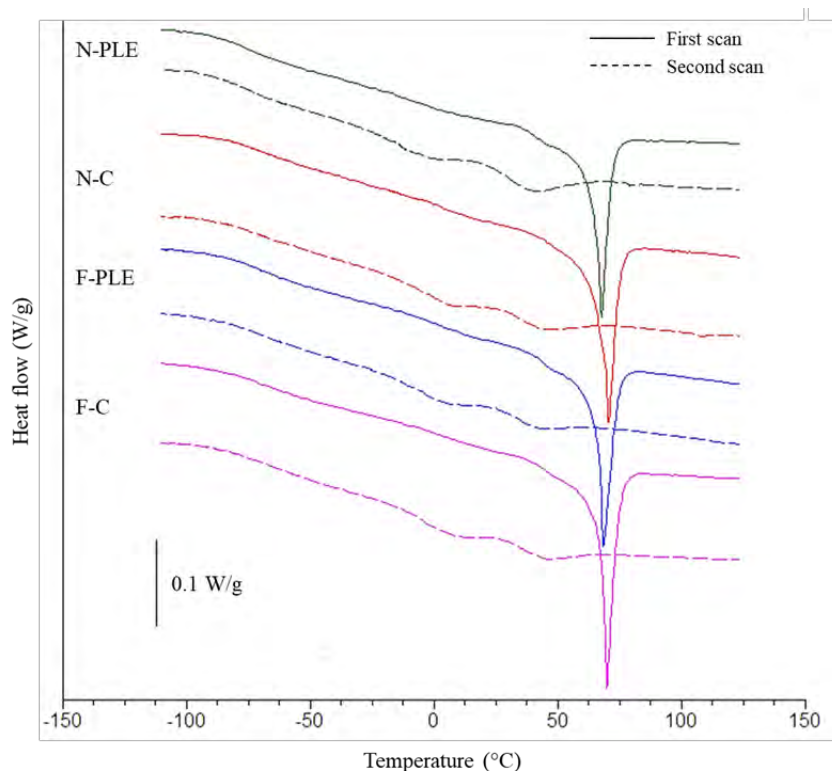
Source: Own authorship.

For all of the samples studied, the thermograms of the first scan showed characteristics typical of partially crystalline materials. In the first scan, two T_gs were observed, T_{g1} (around −70 °C) and T_{g2} (around 45 °C), associated with the fractions rich in glycerol and gelatin, respectively. An endothermic peak was also observed in the first scan ($T_m \approx$ 69.5 °C), related to the melting of gelatin microcrystals (Al-Maqtari et al., 2022) whose ΔH_m was ~17 J/g.

In the second scan, the thermograms obtained were characteristic of amorphous materials (Luciano et al., 2021), showing only T_{g1} (~73.5 °C) and T_{g2} (~35 °C). In the case of T_{g2}, the value observed in the second scan was lower than the value obtained in the first scan (~45 °C), as the absence of gelatin microcrystals, which melted in the first scan, facilitated biopolymeric mobility and, consequently, decreased the T_{g2}. The T_{g1} varied little be-tween the two scans, as glycerol was found to be amorphous in both cases.

The values of thermal properties observed were similar to those of other authors who have studied gelatin-based films and nanocomposite films with the addition of plant extracts and/or CN (Luciano et al., 2021; Nikoukheslat et al., 2022).

6.3.13 Mechanical properties

The insufficient performance of the mechanical properties of biopolymer-based films is one of the limitations that hinder their wide application in food packaging (Almeida et al., 2023). The incorporation of additives into biopolymer film matrices, such as reinforcing fillers, mainly seeks to improve the performance of mechanical properties and the applicability of these materials.

Regarding the effect of PLE, F-PLE and N-PLE presented higher tensile strength and elastic modulus ($p < 0.05$) than F-C and N-C, respectively (Table 6.4). The presence of PLE did not change ($p > 0.05$) the elongation at break of the films and nanocomposite films (Table 6.4). PLE's polyphenols can interact with gelatin by (i) hydrogen bonding (-OH of the polyphenol interacts with -COOH and -NH$_2$ of gelatin), (ii) hydrophobic interactions (non-polar aromatic ring of PLE interacts with hydrophobic amino acid residues of gelatin), and (iii) positively charged groups of the protein interacting with negatively charged hydroxyl groups of the PLE, forming a kind of crosslink (Hosseini; Gómez-Guillén, 2018), as can be observed in Figure 6.1, which increases the resistance and stiffness of the films (tensile strength and elastic modulus, respectively). Liu et al. (2019) and Vargas-Torrico et al. (2023) observed the same behavior in gelatin-based films with haskap berries extract, and gelatin/carboxymethylcellulose-based nanocomposite films with pomegranate peel extract, respectively.

Table 6.4 - Mechanical properties of films (F) and nanocomposite films (N), control (C) and activated with "pitanga" leaf extract (PLE)*

Properties	Treatments	C	Active (PLE)
Tensile strength (MPa)	F	30.2 ± 1.9 [bB]	40.6 ± 5.3 [aB]
	N	53.6 ± 2.6 [bA]	59.5 ± 1.4 [aA]
Elongation at break (%)	F	23.0 ± 1.3 [aA]	26.7 ± 3.4 [aA]
	N	12.7 ± 2.9 [aB]	12.0 ± 1.2 [aB]
Elastic modulus (MPa)	F	9.3 ± 0.9 [bA]	11.3 ± 0.4 [aB]
	N	10.9 ± 0.8 [bA]	15.1 ± 0.4 [aA]

*Means ± standard deviation (n = 15). Different lowercase letters on the same line and different uppercase letter in the same column indicate significant differences between means, according to Tukey's test ($p < 0.05$).

Source: Own authorship.

As for the effect of CN, the films showed lower ($p < 0.05$) tensile strength and elongation at break than nanocomposite films (Table 6.4). N-PLE had a higher elastic modulus than F-PLE ($p < 0.05$), while F-C and N-C had the same elastic modulus ($p > 0.05$). The increase in the resistance of the nanocomposite films, and the decrease in flexibility, was possibly a consequence of the interactions that the CN made with the biopolymer matrix, forming an interconnected and more rigid network with reduced elongation of the biopolymer chains (Tibolla et al., 2019). In the N-PLE case, the interactions between PLE and CN, simultaneously present in this nanocomposite film, may have resulted in the formation of a more stable matrix, increasing the rigidity of the film. Similar behaviors have been observed by Pelissari et al. (2017).

Pereda et al. (2011) also observed higher tensile strength and EM and lower elongation at break for sodium caseinate-based nanocomposite films with nanocellulose fibers. Likewise, in another study, potato starch-based nanocomposite films showed increased tensile strength and elastic modulus compared to films without bacterial nanocellulose (Almeida et al., 2023). This increase was more significant in the presence of gallic acid, and Almeida et al. (2013) explained that hydrogen bonds possibly occur between the -OH groups of gallic acid, bacterial nanocellulose, and potato starch, forming a more stable and compact matrix.

Finally, the fact that N-PLE presented the highest tensile strength and elastic modulus, and lowest elongation at break, may also have been related to its moisture content, which was lower than in the other treatments. Reducing the moisture content in films and nanocomposite films can increase tensile strength and elastic modulus, and decrease elongation at break, as water has a plasticizing effect on hydrophilic components, such as gelatin (Liu et al., 2024).

6.3.14 Folin-Ciocalteu reducing capacity (FCRC) and antioxidant activity (AA)

The oxidative degradation of some foods, such as foods rich in lipids, is an important issue in the food industry, as undesirable products originating from the oxidation reaction can negatively alter the chemical and sensory characteristics of foods. The incorporation of antioxidant compounds into active food packaging is a very attractive alternative compared to adding them directly to food, due to the sensorial changes that can occur (Almeida et al., 2023).

The films and nanocomposite films with PLE showed higher FCRC and AA ($p <$ 0.05) than the respective controls (Table 6.5), as expected. The AA of the active film and nanocomposite film was due to the different classes of polyphenols present in PLE (Fidelis et al., 2022), which even at low concentrations, have an advantageous biological activity (Ramalho et al., 2019).

Table 6.5 - Folin-Ciocalteu reducing capacity (FCRC) and antioxidant activity of films (F) and nanocomposite films (N), control (C) and activated with "pitanga" leaf extract (PLE)*

Properties	Treatments	C	Active (PLE)
FCRC (mg GAE/g sample)	F	0.0 ± 0.0 [bA]	0.7 ± 0.0 [aA]
	N	0.0 ± 0.0 [bA]	0.7 ± 0.0 [aA]
ABTS[•+] (mg TE/g sample)	F	0.0 ± 0.0 [bA]	3.2 ± 0.2 [aA]
	N	0.0 ± 0.0 [bA]	2.7 ± 0.2 [aB]
FRAP (mg TE/g sample)	F	3.6 ± 0.3 [bA]	10.6 ± 0.6 [aA]
	N	3.2 ± 0.4 [bA]	9.3 ± 0.4 [aB]

*Means ± standard deviation (n = 3). Different lowercase letters on the same line and different uppercase letter in the same column indicate significant differences between means, according to Tukey's test ($p < 0.05$). GAE: gallic acid equivalent. TE: Trolox equivalent.

The presence of CN did not interfere with the FCRC of the nanocomposite films compared to the films ($p > 0.05$), but decreased the AA in N-PLE compared to F-PLE ($p < 0.05$). Some polyphenols can be adsorbed on CN surfaces, reducing the availability of these compounds, and hindering the extraction, which would explain the lower AA in N-PLE (Tessaro et al., 2021a). The greater AA provided by the FRAP method can be justified by the difference in the mechanism of action. The ABTS[•+] method is based on the reduction of ABTS[•+] by receiving hydrogen atoms or electrons from antioxidant compounds, and can be used for both hydrophilic and lipophilic substances (Gupta, 2015). On the other hand, the FRAP method is based on the reduction of ferric ions (Fe^{3+}) to ferrous ions (Fe^{2+}), which occurs in the presence of antioxidant compounds and, therefore, is an electron transfer method and can also be used to determine the AA of lipophilic and hydrophilic substances (Gulcin, 2020). However, it presents some limitations, such as the fact that any compound with a redox potential lower than that of the Fe^{3+}/Fe^{2+} pair can, in theory, reduce Fe^{3+} to Fe^{2+}, thus

generating overestimated results (Gulcin, 2020). In the case of gelatin-based films, the higher AA in the FRAP method may be due to the activity of some functional groups of amino acids in bovine gelatin, such as proline and glycine, which can act as electron donors, providing an antioxidant effect (Gómez-Estaca et al., 2009). Another factor that may influence the highest AA given by the FRAP method is the acidic pH of the assay, as phenolic compounds may eventually be more active in this media (Gupta, 2015).

Gelatin-based films and nanocomposite films activated with plant extracts have also shown increased AA due to the presence of the extract rich in polyphenols (Luciano et al., 2021; Liu et al., 2024; Vargas-Torrico et al., 2023).

6.4 CONCLUSIONS

The development of gelatin-based films and nanocomposite films incorporating polyphenol-rich extracts (PLE) and cellulose nanocrystals (CN) from soybean straw has demonstrated promising advancements in the field of active food packaging. The chemical interactions between gelatin, PLE polyphenols, and CN resulted in enhanced mechanical properties, UV/Vis light barrier capabilities, antioxidant activity, and surface properties in the films. Furthermore, the active nanocomposite films exhibited even greater improvements, including lower moisture content and solubility in water, compared to the active films. Despite these enhancements, both materials maintained desirable aesthetic qualities, being light, shiny, and translucent. These findings highlight the potential of utilizing sustainable components derived from natural and renewable sources in the production of active food packaging, offering both functional and environmental benefits for the food industry.

References

AL-MAQTARI, A. Q. et al. Fabrication and characterization of chitosan/gelatin films loaded with microcapsules of *Pulicaria Jaubertii* extract. **Food Hydrocolloids**, v. 129, p. 107624, 2022.

ALMEIDA, T. et al. Biobased ternary films of thermoplastic starch, bacterial nanocellulose and gallic acid for active food packaging. **Food Hydrocolloids**, v. 144, p. 108934, 2023.

ALZATE-ARBELÁEZ, A. F. et al. Immobilization of Andean berry (*Vaccinium meridionale*) polyphenols on nanocellulose isolated from banana residues: A natural food additive with antioxidant properties. **Food Chemistry**, v. 294, p. 503–517, 2019.

ASTM—American Society for Testing and Materials E96-E80. Standard test methods for water vapor transmission of materials. In **Annual Book of ASTM Standards**; ASTM: West Conshohocken, PA, USA, 1989.

ASTM—American Society for Testing and Materials D523. Standard test method for specular gloss. In **Annual Book of ASTM Standards**; ASTM: West Conshohocken, PA, USA, 1999.

ASTM—American Society for Testing and Materials D882/12. Standard test method for tensile properties of thin sheeting. In **Annual Book of ASTM Standards**; ASTM: West Conshohocken, PA, USA, 2001.

BENZIE, I. F. F.; STRAINS, J. J. The Ferric Reducing Ability of Plasma (FRAP) as a Measure of "Antioxidant Power": The FRAP Assay. **Analytical Biochemistry**, v. 239, n. 1, p. 70–76, 1996.

FIDELIS, E.M. et al. Pitanga (*Eugenia uniflora* L.) as a source of bioactive compounds for health benefits: A review. **Arabian Journal of Chemistry**, v. 15, n. 4 p. 103691, 2022.

FIGUEROA-ENRIQUEZ, C. E. et al. Nanoparticles of Betalain-gelatin with antioxidant properties by coaxial electrospraying: Preparation and characterization. **ACS Omega**, v. 8, p. 41156-41168, 2023.

GARMUS, T. T. et al. Extraction of phenolic compounds from Pitanga (*Eugenia Uniflora* L.) leaves by sequential extraction in fixed bed extractor using supercritical CO_2, ethanol and water as solvents. **Journal of Supercritical Fluids**, v. 86, p. 4-14, 2014.

GÓMEZ-ESTACA, J., et al. Antioxidant properties of tuna-skin and bovine-hide gelatin films induced by the addition of oregano and rosemary extracts. **Food Chemistry**, v.112, n. 1, p. 18–25, 2009.

GONTARD, N.; GUILBERT, S.; CUQ, J.-L. Edible wheat gluten films: Influence of the main process variables on film properties using response surface methodology. **Journal of Food Science**, v. 57, n. 1, p. 190–195, 1992.

GULCIN, I. Antioxidants and antioxidant methods: An updated overview. **Archives of Toxicology**, v. 94, p. 651-715, 2020.

GUPTA, D. Methods for determination of antioxidant capacity: A Review. International **Journal of Pharmaceutical Sciences and Research**, v. 6, p. 546-566, 2015.

HOSSEINI, S. F.; GÓMEZ-GUILLÉN, M. C. A state-of-the-art review on the elaboration of fish gelatin as bioactive packaging: Special emphasis on nanotechnology-based approaches. **Trends in Food Science and Technology**, v. 79, p. 125–135, 2018.

KAYA, M. et al. Production and characterization of chitosan based edible films from *Berberis Crataegina's* fruit extract and seed oil. Innovative **Food Science & Emerging Technologies**, v. 45, p. 287-297, 2018.

LIU, J. et al. Preparation and characterization of active and intelligent films based on fish gelatin and haskap berries (*Lonicera caerulea* L.) extract. **Food Packaging and Shelf Life**, v. 22, p. 100417, 2019.

LIU, S. et al. Enhanced barrier and antioxidant properties of gelatin films by structural-colored bioactive materials for food packaging. **Food Hydrocolloids**, v. 150, p.109744, 2024.

LUCIANO, C. G. Bi-layer gelatin film: activating film by incorporation of "Pitanga" leaf hydroethanolic extract and/or nisin in the second layer**. Food and Bioprocess Technology**, v. 14, n. 1, p. 106–119, 2021.

LUCIANO, C. G. et al. Application of bi-layers active gelatin films for sliced dried-cured Coppa conservation. **Meat Science**, v. 189, p. 108821, 2022.

MARTELLI-TOSI, M. et al. Soybean straw nanocellulose produced by enzymatic or acid treatment as a reinforcing filler in soy protein isolate films. **Carbohydrate Polymers**, v. 198, p. 61-68, 2018.

NIKOUKHESLAT, H. D. et al. Characterization of physicochemical and antibacterial properties of gelatin and inulin nanobiocomposite films containing crystalline nanocellulose and *Malva sylvestris* extract. **Journal of Polymers and the Environment**, v. 30, n. 7, p. 3078–3090, 2022.

PELISSARI, F. M. et al. Nanocomposites based on banana starch reinforced with cellulose nanofibers isolated from banana peels. **Journal of Colloid and Interface Science**, v. 505, p. 54–167, 2017.

PEREDA, M. et al. Structure and properties of nanocomposite films based on sodium caseinate and nanocellulose fibers. **Journal of Food Engineering**, v. 103, n. 1, p. 76–83, 2011.

PULIDO, R.; BRAVO, L.; SAURA-CALIXTO, F. Antioxidant activity of dietary polyphenols as determined by a modified ferric reducing/antioxidant power assay. **Journal of Agricultural and Food Chemistry**, v. 48, n. 8, p. 3396–3402, 2000.

QUAN, TT.H. et al. Protein-polyphenol conjugates: Antioxidant property, functionalities and their applications. **Trends in Food Science & Techonology**, v. 91, p. 507-517, 2019.

RAMALHO, R. R. F. et al. Variability of polyphenols and volatiles during fruit development of three Pitanga (*Eugenia Uniflora* L.) biotypes. **Food Research International**, v. 119, p. 850-858, 2019.

RE, R., et al. Antioxidant activity applying an improved ABTS radical cation decolorization assay. **Free Radical Biology and Medicine**, v. 26, n. 9–10, p. 1231–1237, 1999.

RODRÍGUEZ-FÉLIX, F. et al. Physicochemical, structural, mechanical and antioxidant properties of zein films incorporated with no-ultrafiltered and ultrafiltered Betalains extract from the Beetroot (*Beta Vulgaris*) bagasse with potential application as active food packaging. **Journal of Food Engineering**, v. 334, p. 111153, 2022.

SINGLETON, V. L.; ORTHOFER, R.; LAMUELA-RAVENTÓS, R. M. Analysis of total phenols and other oxidation substrates and antioxidants by means of Folin-Ciocalteu reagent. **Methods in Enzymology**, v. 299, p. 152–178, 1999.

TESSARO et al. Gelatin and/or chitosan-based films activated with "Pitanga" (*Eugenia uniflora* L.) leaf hydroethanolic extract encapsulated in double emulsion. **Food Hydrocolloids**, v. 113, p. 106523, 2021b.

TESSARO, L. et al. Gelatin/chitosan based films loaded with nanocellulose from soybean straw and activated with "Pitanga" (*Eugenia uniflora* L.) leaf hydroethanolic extract in W/O/W emulsion. **International Journal of Biological Macromolecules**, v. 186, p. 328–340, 2021a.

TIBOLLA, H. et al. Banana starch nanocomposite with cellulose nanofibers isolated from banana peel by enzymatic treatment: *In vitro* cytotoxicity assessment. **Carbohydrate Polymers**, v. 207, p. 169–179, 2019.

TYUFTIN, A. A.; KERRY, J. P. Gelatin films: Study review of barrier properties and implications for future studies employing biopolymer films. **Food Packaging and Shelf Life**, v. 29, p. 100688, 2021.

VARGAS-TORRICO, M. F. et al. Preparation and characterization of gelatin-carboxymethylcellulose active film incorporated with pomegranate (*Punica granatum* L.) peel extract for the preservation of raspberry fruit. **Food Hydrocolloids**, v. 150, p. 109677, 2023.

YAN, J. et al. Development of pH-sensitive films based on gelatin/chitosan/nanocellulose and anthocyanins from hawthorn (*Crataegus scabrifolia*) fruit. **Journal of Food Measurement and Characterization**, v. 15, n. 5, p. 3901–3911, 2021.

7 CAPÍTULO 4: Gas permeability of gelatin nanocomposite films incorporated with "pitanga" leaf extract encapsulated into double emulsion

Larissa Tessaro [a], Paula Benoso [a, b], Valentina Siracusa [c], Rodrigo V. Lourenço [a], Marco Dalla Rosa [b, d], Paulo J.A. Sobral [a, e]

[a] Department of Food Engineering, Faculty of Animal Science and Food Engineering, University of São Paulo, Av Duque de Caxias Norte, 225, 13635-900 Pirassununga, SP, Brazil

[b] Department of Agricultural and Food Science, University of Bologna, Via Cesare Pavese, 50, 47521 Cesena FC, Italy

[c] Department of Chemical Science (DSC), University of Catania, Viale A. Doria 6, 95125 Catania (CT), Italy

[d] Interdepartmental Centre for Agri-Food Industrial Research, Alma Mater Studiorum University of Bologna, Campus of Food Science, Cesena, Italy

[e] Food Research Center (FoRC), University of São Paulo, Rua do Lago, 250, Semi-industrial Building, Block C, 05508-080 São Paulo, SP, Brazil

Abstract

The influence of relative humidity on O_2 and CO_2 permeability of gelatin-based films and nanocomposite films incorporated with crystalline nanocellulose (CN), non-encapsulated "Pitanga" leaf extract (PLE) or encapsulated in a water-in-oil-in-water double emulsion (DE) was studied. Cross-section morphology by scanning electron microscopy, crystallinity, moisture content, thickness, and O_2 and CO_2 transmission rate (GTR) were determined. The addition of CN, PLE and/or DE caused modification on the morphology and crystallinity of the films and nanocomposite films, especially those with DE, which presented pores formed by oil droplets, and lower crystallinity. Moisture content and thickness increased with increasing relative humidity, with only the latter apparently affecting the GTR. In general, the GTR in films and nanocomposite films increased with increasing relative humidity, due to the swelling effects and plasticizing effect of water. Regarding the treatment, some effects were observed, however, nanocomposite films with non-encapsulated PLE or DE showed good oxygen barrier properties at high relative humidity. The perm-selectivity ratio (CO_2/O_2) was greater than 1 in the treatments studied, except for dehydrated materials or with the addition of DE. The outcome of this study was that the addition of CN with PLE or DE improved the gas barrier properties of gelatin-based films, especially in high relative humidity conditions.

Keywords: gas transmission rate; crystallinity; perm-selectivity; nanocellulose; plant extract; biopolymer films.

7.1 INTRODUCTION

Gelatin is a well know protein obtained by partial hydrolysis of collagen from the skin, bones and connective tissues of animals and produced worldwide (Shamsallah; Rashid, 2024). In recent decades, gelatin has been widely studied for the development of biopolymeric films for food packaging applications due to its excellent film-forming capacity, biodegradability, biocompatibility, safety and because it comes from renewable and natural sources (Li et al., 2024; Sobral et al., 2001). Gelatin films are edible, thin, flexible and semi-crystalline materials with good physical properties but very sensitive to water (Sobral; Habitante, 2000; Sobral et al., 2001).

Gelatin has a structure formed by polypeptide chains α (single chain), β (two α-chains joined by covalent bonds) and γ (three α-chains joined by covalent bonds) (Hanani, et al., 2014). Additionally, it has a typical Ala-Gly-Pro-Arg-Gy-Glu-4Hyp-Gly-Pro amino acid composition, and elemental composition of 50.5% carbon, 25.2% oxygen, 17% nitrogen and 6% hydrogen (Hanani; Roos; Kerry, 2014). The gelatin structure gives its films great versatility, from the ability to incorporate different types of active components and fillers, to the ability to form blends with other biopolymers, such as chitosan (Acharya et al., 2024; Al-Maqtari et al., 2022). The addition of other components to gelatin films for use as food packaging is intended to improve some of their properties, such as mechanical and/or barrier properties (Flaker et al., 2015).

The function of a biopolymeric food packaging is to protect the packaged food in a safe and sustainable way, functioning as a barrier to gases and humidity, microorganisms, aromatic compounds and grease (Ilyas et al., 2022). Specifically in the case of gas barriers, gas permeability is extremely important, as it controls the exchange of oxygen (O_2) and carbon dioxide (CO_2) between the inside and outside of the packaging, which directly affects the quality of the packaged food (Xue et al., 2023). For example, controlling O_2 permeability is crucial to extending the shelf life of lipid-rich foods and foods susceptible to microbial growth, among others, as O_2 induces oxidation reactions and provides a favorable environment for the growth of aerobic microorganisms (Trinh; Chang; Mekonnen, 2023). On the other hand, it must be sufficient to ensure the respiration of fruits and vegetables and inhibit the growth of anaerobic microorganisms (Xue et al., 2023).

Despite their great versatility, gelatin-based films present low performance in terms of mechanical properties, high sensitivity to water, and good gas barrier

properties only in conditions of low relative humidity (Li et al., 2024), which limits its application in certain food categories. One of the approaches explored to overcome these disadvantages is to incorporate reinforcing fillers (such as natural fibers or nanoparticulates, as nanocelluloses) in the biopolymeric matrix, forming composite or nanocomposite films (Flaker et al., 2015, Ilyas et al., 2022). Nanocelluloses are nanosized natural fibers extracted from renewable lignocellulosic materials, and can satisfactorily act as reinforcing fillers due to their physical properties (Li et al., 2024; Martelli-Tosi et al., 2018; Tessaro et al., 2021b).

When nanocellulose is extracted by acid hydrolysis, it can be obtained in the form of crystalline nanocellulose (CN), with a rigid structure due to high crystallinity (>65%), diameters ranging from 2 to 100 nm, and a length of 500 nm to 2 μm (Ilyas et al., 2022; Martelli-Tosi et al., 2018). As fillers, they can act as a physical barrier to gas, as they are similar sizes to the pores created in the biopolymeric network and, therefore, create a tortuous path (Fukusumi et al., 2011). CN can also act by improving the mechanical and water sensitivity of gelatin-based packaging (Ilyas et al., 2022; Li et al., 2024; Tessaro et al., 2021b).

On the other hand, the incorporation of active compounds into gelatin films for use as food packaging aims to enhance the functionality of these materials, creating the so-called active films. For example, the incorporation of plant extracts, rich in polyphenols, into gelatin-based films can confer antioxidant and antimicrobial activity to these materials (Luciano et al., 2022).

"Pitanga" leaf extract (PLE) is extracted from the leaves of the Pitanga tree (*Eugenia uniflora* L.), a native Brazilian fruit tree found in tropical regions of the world, and which has been satisfactorily used to produce active films based on gelatin and other biopolymers with excellent bioactivities (Chakravartula et al., 2020; Luciano et al., 2021, 2022). The bioactivity of PLE is related to the high polyphenol content in its composition (Lorenzo et al., 2018; Vargas et al., 2016).

PLE can be incorporated into the biopolymeric matrix in free form, which means, as it is (Chakravartula et al., 2020; Luciano et al., 2021), or encapsulated into double emulsions (Tessaro et al., 2021a,b). Encapsulation can protect the biological properties of active compounds, but encapsulation systems can also improve active packaging properties, such as barrier and mechanical properties (Al-Maqtari et al., 2022; Tessaro et al., 2021a). These improvements are cost-effective and can occur due to the interactions between the components of the encapsulated system with the

biopolymeric matrix. Moreover, it can contribute to reduce the hydrophilicity characteristic of films due, for example, to the oil emulsion formulation (Tessaro et al., 2021b; Trinh; Chang; Mekonnen, 2023).

In this study, gelatin-based active films and nanocomposite films were produced with incorporation of CN extracted from soybean straw by acid hydrolysis and by addition of non-encapsulated PLE or PLE encapsulated into water-in-oil-in-water double emulsions (DE). We hypothesize that chemical interactions occurring between gelatin and CN, PLE and/or DE (hydrogen and ionic bonds, for example) can produce materials that have a lower transmission rate to O_2 and CO_2 under different relative humidity conditions. The aim of this study was, therefore, to investigate the gas transmission rate in these films and nanocomposite films, conditioned at different relative humidities.

7.2 MATERIAL AND METHODS

7.2.1 Material

Type-B bovine gelatin (molecular weight: ~50 kDa; 250 bloom), sodium caseinate, and Grinsted PGPR® (Polyglycerol Polyricinoleate) were donated by Gelco (Pedreira-SP, Brazil), Alibra Ingredientes SA (Campinas-SP, Brazil), and DuPont (São Paulo-SP, Brazil), respectively. Food grade soybean oil, sodium hypochlorite and Tween 80 were purchased from Cargill (Primavera do Leste-MT, Brazil), Candura (Piracicaba-SP, Brazil) and Sigma-Aldrich (St Louis-MO, USA), respectively. Acetone P.A., ethanol P.A., sulfuric acid (H_2SO_4) P.A., sodium hydroxide (NaOH) P.A., magnesium sulfate heptahydrate ($Mg_2SO_4.7H_2O$), sodium carbonate (Na_2CO_3), hydrogen peroxide (H_2O_2, >50%) and glycerol (≥99.5%) were purchased from Labsynth® (São Paulo-SP, Brazil). Soybean straw was supplied by the Embrapa Soja, Londrina-PR, Brazil (23°17′ 34″ S, 51°10′24″ W).

7.2.2 Production of "pitanga" leaf extract

"Pitanga" leaves were collected at the Faculty of Animal Science and Food Engineering campus at Pirassununga-SP, Brazil (21°59′46″ S, 47°25′36″ W). "Pitanga"

leaf extract (PLE) was produced according to Tessaro et al. (2021a), by ultrasound assisted and a hot solvent extraction (60% v/v hydroethanolic solvent at 80 °C). The extract obtained was freeze-dried (Freeze-dryer, FD 1.0-60E, Heto-Holten A/S, Allerod, Dinamarca) to produce the PLE. The PLE was stored in the dark at -18 °C.

7.2.3 Production of double emulsion

The DEs were prepared according to Tessaro et al. (2021a), in two steps. In the first step, a single emulsion (SE) was produced using the PLE resuspended in distilled water (1 g PLE freeze-dried/10 mL distilled water) as inner aqueous phase (20 g/100 g SE) and soybean oil with PGPR (3 g/100 g oil) as oil phase (80 g/100 g SE). In the second step, DE was produced using the SE as inner lipid phase (40 g/100 g DE) and distilled water with Tween 80 (3 g/100 g distilled water) and sodium caseinate (0.5 g/100 g distilled water) as dispersant aqueous phase (60 g/100 g DE). The SE and DE were stored in the dark at 4 °C.

The properties of these emulsions (droplet size, droplet size distribution, physical stability, morphology and biological activities, among others) have been studied and these data can be seen in Tessaro, Martelli-Tosi and Sobral (2021) and Tessaro et al. (2022).

7.2.4 Production of crystalline nanocellulose

The CN was extract from soybean straw using alkaline pre-treatment, bleaching, acid hydrolysis and mechanical treatment, according to Martelli-Tosi et al. (2018). The CN suspension was freeze-dried, and the CN was storage at room temperature. This nanomaterial has been characterized previously (Tessaro et al., 2021b).

7.2.5 Production of gelatin-based films and nanocomposite films

For both films and nanocomposite films, the film-forming solution (FFS) was prepared by the hydration of gelatin (4 g/100 g FFS) in distilled water for 30 min, and subsequent solubilization at 55 °C for 10 min (Thermostatic bath, MA-184/20, Marconi, Piracicaba-SP, Brazil) and addition of the glycerol (25 g/100 g gelatin) (Tessaro et al., 2021a,b). In the case of nanocomposite films, the gelatin hydration was carried out in

distilled water with CN (4.5 g/100 g gelatin). The DE was added dropwise under a magnetic stirrer integrated with temperature digital control at 500 rpm to FFSs at the concentration of 0.25 g PLE/100 g gelatin (Tessaro et al., 2021a,b). Negative and positive-control films and nanocomposite films were also made, without the addition of DE or by adding non-encapsulated PLE instead of DE, at the same concentration (0.25 g PLE/100 g gelatin), respectively. The FFSs were transferred to acrylic plates and dried at 30 °C for 24 h (Forced-air circulation drying oven, MA035, Marconi, Piracicaba-SP, Brazil). Then, six treatments were produced: gelatin-based films without DE (F-C), with DE (F-DE) or PLE (F-PLE) and gelatin-based nanocomposite films without DE (N-C), with DE (N-DE) or PLE (N-PLE).

Before analyses, films and nanocomposite films were conditioned for 7 days in desiccators at different relative humidities (RH, 0%, 34%, 59% and 76%) at 25 °C. For X-ray diffraction analysis and scanning electron microscopy characterizations, films and nanocomposite films were previously conditioned for 15 days in desiccators over silica gel. The main physical and functional properties of these gelatin-based films and nanocomposite films (water vapor permeability, solubility in water, UV/Vis light barrier properties, color and opacity, microstructure, thermal properties, mechanical properties and antioxidant activity, among others) were previously characterized and the data can be seen in Tessaro et al. (2021a) and Tessaro et al. (2021b), respectively.

7.2.6 Films and nanocomposite characterizations

7.2.6.1 Scanning electron microscopy

Cryo-fractured cross-section of the films and nanocomposite films were analyzed by scanning electron microscopy (SEM, TM3000, Hitachi Ltd, Tokyo, Japan) in a random position at an accelerating voltage of 15 kV (Valencia et al., 2016). Sample films and nanocomposite films were cryo-fractured after quench freezing using liquid nitrogen.

7.2.6.2 X-ray diffraction (XRD)

The X-ray spectrum of films and nanocomposite films was obtained using an X-ray diffractometer (Miniflex 600, Rigaku Corporation, Tokyo, Japan) operated at 25 °C, 40 kV and 15 mA (CuKβ radiation, λ = 0,15405 nm), for a range of angles of 2θ = 2 to 70° with 2°/min of speed scan (Iaccheri et al., 2023). Relative crystallinity was calculated as the ratio between the upper area of the diffraction peak and the total diffraction area.

7.2.6.3 Moisture content

The moisture content of films and nanocomposite films conditioned at different relative humidity (RH) was determined gravimetrically, according to Gontard, Guilbert and Cuq (1992). Films and nanocomposite films samples were dried using a forced-air circulation drying oven at 105 °C for 24 h, and the moisture content was expressed as g water/100 g of wet film or nanocomposite.

7.2.6.4 Thickness

The thickness of films and nanocomposite films was determined according to Siracusa et al. (2020), with some modifications, using a Sample Thickness Tester DM-G with a digital dial indicator (MarCartor 1086 type, Mahr GmbH, Esslingen, Germany) with associated DM-G software. The reading was made twice per second, with a resolution of 0.001 mm. The minimum, maximum, and average of each reading was recorded in triplicates, in 15 different positions of each film, at room temperature and reported as mean thickness value, expressed in micrometer (µm).

7.2.6.5 CO_2 and O_2 transmission rate

The gas transmission rate measurement of films and nanocomposite films was performed using a manometric method with a Permeance Testing Device, type GDP-C (Brugger Feinmechanik, GmbH, München, Germany), according to ASTM 1434-82 (Standard test Method for Determining Gas Permeability Characteristics of Plastic Film

and Sheeting), DIN 53 536 in compliance with ISO/DIS 15 105-1 and according to *Gas Permeability Testing Manual* (Registergericht München HRB 77020, Brugger Feinmechanik GmbH).

As previously described by Siracusa et al. (2012), the equipment consists of two chambers between which the sample (12 x 12 cm) is placed. The chamber on the top of the film is filled with the gas used in the test (CO_2 or O_2), at a pressure of 1 atm. A pressure transducer, set in the chamber below the film, records the increasing of gas pressure (P) as a function of the time (t). From pressure/time data the software automatically calculates permeation rate, which can be converted in permeability knowing the film thickness. The Gas Transmission Rate values (GTR) of the films and nanocomposite films were determined considering the increase in pressure in relation to the time and the volume of the device (Siracusa; Ingrao, 2017).

The operation conditions were temperature of 20 °C; gas stream of 100 cm^3/min; sample area of 78.4 cm^2, and different RH. Permeability measurements were performed in triplicate, at least.

7.2.7 Statistical analysis

The analyses were performed with at least three measurements (triplicate) and presented as mean ± standard deviation (SD). Statistical analysis was carried out using Statistica data analysis software system (version 7, StatSoft. Inc. GmbH, Hamburg, Germany). Results were analyzed using one-way and two-way analysis of variance (ANOVA) and Tukey's test comparison ($\alpha = 0.05$) for determining significant differences between the means.

7.3 RESULTS AND DISCUSSION

7.3.1 Scanning electron microscopy

The SEM images showed that the internal structures of the films and nanocomposite films were affected by the addition of PLE, CN and DE (Table 7.1). F-C and F-PLE presented more homogeneous, smooth and compact internal structures compared to the other treatments. This indicated that PLE was satisfactorily

incorporated into F-PLE, as observed for gelatin films with PLE at higher concentrations (Luciano et al., 2021).

Figure 7.1 - Scanning electron microscopy images of the cross-section of gelatin films (F) and nanocomposite films (N) control (C), with "Pitanga" leaf extract (PLE), or with double emulsion (DE). The scale bar is 100 µm
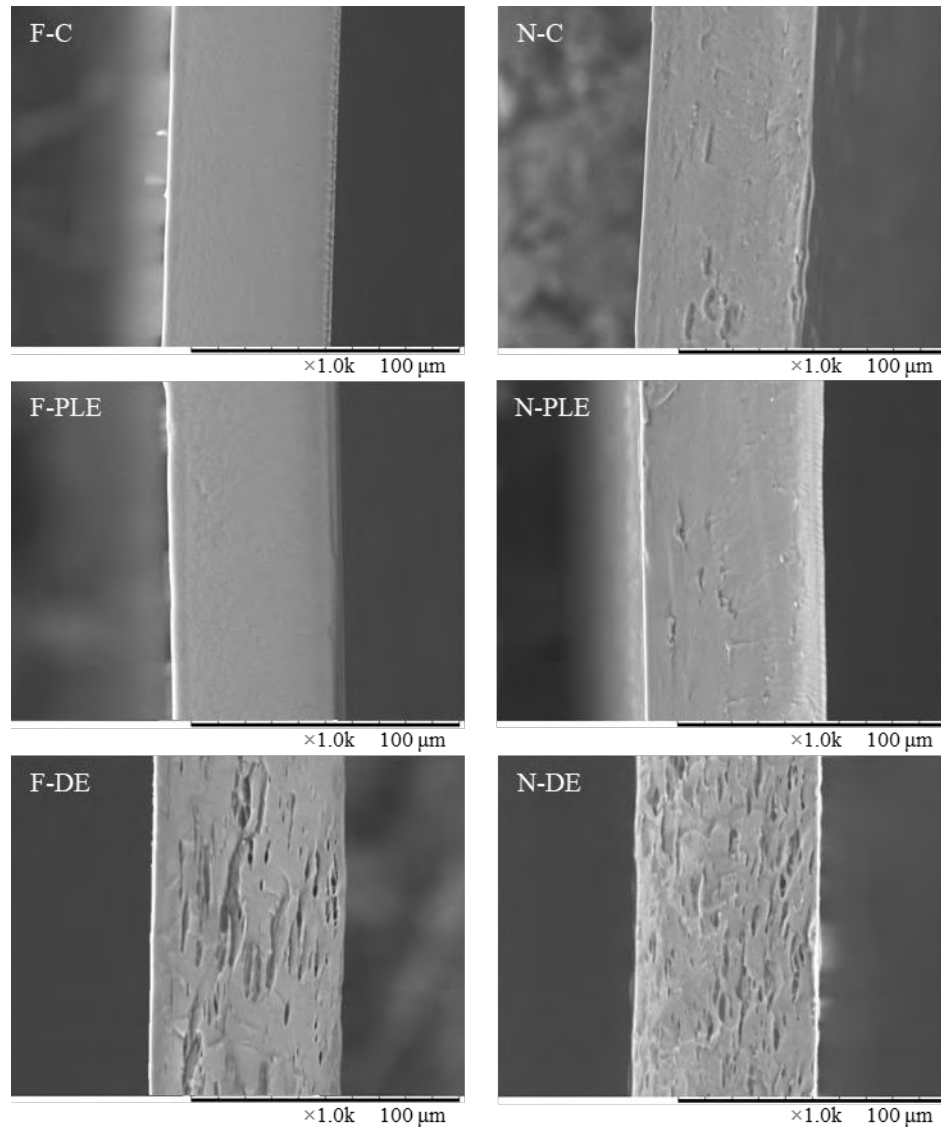
Source: Own authorship.

In nanocomposite films without DE (N-C and N-PLE), it was possible to observe white spots and some pores possibly generated by agglomeration of CN particles. In the case of N-PLE, the pores were less visible, which indicates that in the presence of PLE, the CN is better incorporated into the nanocomposite matrix. This may occur due to the complex formed between gelatin and PLE polyphenols, which can help to

disperse CN more evenly, reducing agglomerations and increasing homogeneity, as CN can interact with both gelatin and PLE (Acharya et al., 2024). Vargas-Torrico et al. (2023) also observed that pomegranate peel extract agglomerated into films based on gelatin and carboxymethyl cellulose, forming layers, possibly due to the effect of the concentration and composition of the extract.

The addition of DE, into both F-DE and N-DE, caused the formation of pores in the internal structure of these treatments, probably due to the presence of DE oil droplets. Despite the changes observed in the internal structure of the different treatments, all incorporated components were well dispersed in the matrix, without causing fractures nor discontinuity (Ranjbaryan; Pourfathi; Almasi, 2014; Tessaro et al., 2021a,b). The gelatin matrix surrounded the DE and stabilized the interfaces of different phases, resulting in an internal structure of the film and nanocomposite with homogeneously distributed oil droplets. The emulsifiers present in the external aqueous phase of DE (sodium caseinate and Tween 80) may also have contributed to the uniform dispersion of DE in the film and nanocomposite (Ranjbaryan; Pourfathi; Almasi, 2014). Acharya et al. (2024) also observed similar morphology on gelatin/bacterial nanocelluloses films with oil-in-water (O/W) nanoemulsions.

7.3.2 X-ray diffraction

Characteristic patterns of gelatin-based materials were observed in the X-ray diffractograms of films and nanocomposite films (Table 7.2). The peaks observed at $2\theta = 7.3-9.7°$, and $20-22.8°$ were characteristic of the α-helix (crystalline) and β-sheet (amorphous) structures of gelatin, respectively (Acharya et al., 2024; Luciano et al., 2021). These peaks confirm the semi-crystalline structure of gelatin (Ranjbaryan; Pourfathi; Almasi, 2014). The peaks at $2\theta = 14.5$ and $17.3°$, present in F-PLE, N-C and N-PLE (Table 7.2), may be the result of some crystal formed by PLE and/or crystalline structure of CN (Luciano et al., 2021).

In the N-DE, no peak relating to the α-helix structures was observed, while in the F-DE only the peak at $2\theta = 7.3°$ was observed in low intensity. The formation of a protein complex between gelatin and sodium caseinate present in the external aqueous phase of DE, through hydrogen and ionic interactions, can reduce the formation of gelatin microcrystalline structures (Ranjbaryan; Pourfathi; Almasi, 2014). This may explain the disappearance of the characteristic peaks of the gelatin

crystalline phase in the DE film and nanocomposite, and the fact that these treatments present the lowest crystallinity (Table 7.2), as observed for sodium caseinate films incorporated with nanoemulsified cinnamon essential oil (Ranjbaryan; Pourfathi; Almasi, 2014) and gelatin films reinforced with tannin-nanocellulose microgel (Li et al., 2024).

Figure 7.2 - X-ray diffractograms of gelatin films (F) and nanocomposite films (N) control (C), with "Pitanga" leaf extract (PLE), or with double emulsion (DE). The values of crystallinity were presented over each spectrum
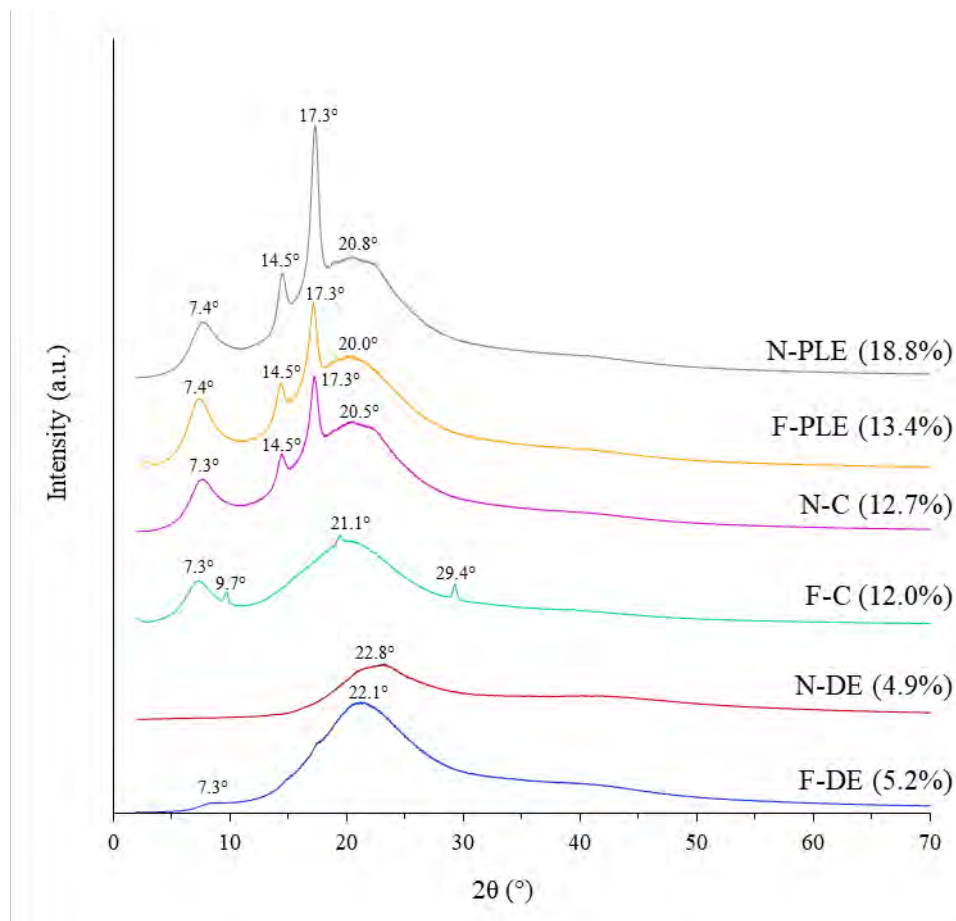
Source: Own authorship.

The crystallinity of films and nanocomposite films ranged from 4.9 to 18.8%, in ascending order: N-DE < F-DE < F-C < N-C < F-PLE < N-PLE (Table 7.2). N-PLE presented the highest crystallinity index possibly due to the crystalline structures that NCs have and some crystals formed by PLE (Luciano et al., 2021; Ranjbaryan; Pourfathi; Almasi, 2014), followed by F-PLE.

7.3.3 Moisture content

For the RH effect, the moisture content of all films and nanocomposite films increased ($p < 0.05$) with increasing RH (Table 7.1), as could be expected, due to the hygroscopic character of gelatin and glycerol (Sobral et al., 2001). The same behavior was observed for cassava starch films containing glycerol or sorbitol, as plasticizers (Lagos et al., 2015) and gelatin/chitosan films containing glycerol, as plasticizers (Benbettaïeb et al., 2014).

Table 7.1 - Moisture content and thickness of gelatin films (F) and nanocomposite films (N) control (C), with "Pitanga" leaf extract (PLE), or with double emulsion (DE) at different relative humidity*

Properties	Treatment	Relative humidity (%)			
		0	34	59	76
Moisture content (%)	F-C	-	9.9 ± 0.7^{cA}	13.6 ± 0.2^{bB}	21.6 ± 1.1^{aAB}
	F-PLE	-	10.8 ± 0.4^{cA}	14.5 ± 0.2^{bA}	22.2 ± 0.4^{aA}
	F-DE	-	8.5 ± 0.4^{cB}	13.0 ± 0.1^{bBC}	19.6 ± 0.1^{aBC}
	N-C	-	8.7 ± 0.3^{cB}	13.3 ± 0.4^{bCD}	19.7 ± 0.4^{aBC}
	N-PLE	-	8.2 ± 0.1^{cB}	12.2 ± 0.4^{bCD}	19.4 ± 1.3^{aC}
	N-DE	-	8.2 ± 0.3^{cB}	12.0 ± 0.4^{bD}	20.0 ± 0.2^{aBC}
Thickness (µm)	F-C	69 ± 3^{dA}	83 ± 6^{cA}	100 ± 6^{bA}	119 ± 10^{aA}
	F-PLE	71 ± 3^{dA}	85 ± 4^{cA}	95 ± 4^{bA}	120 ± 5^{aA}
	F-DE	73 ± 5^{dA}	88 ± 7^{cA}	102 ± 10^{bA}	125 ± 12^{aA}
	N-C	70 ± 2^{dA}	86 ± 5^{cA}	98 ± 9^{bA}	129 ± 12^{aA}
	N-PLE	67 ± 3^{dA}	87 ± 3^{cA}	101 ± 7^{bA}	122 ± 6^{aA}
	N-DE	70 ± 4^{dA}	87 ± 2^{cA}	103 ± 5^{bA}	120 ± 8^{aA}

*Means ± standard deviation (n = 3). Different lowercase letters on the same line and different uppercase letters in the same column indicate significant differences between samples according to Tukey's test ($p < 0.05$).

Source: Own authorship.

Regarding the effect of the treatment, the moisture content of the films and nanocomposite films was affected by the presence of CN, PLE and/or DE, at the same RH (Table 7.1). Overall, F-PLE had the highest moisture content ($p < 0.05$) considering

all RHs, while N-PLE had the lowest ($p < 0.05$). The presence of CN and DE in the films and nanocomposite films also generally reduced the moisture content, except at RH of 76%, where all treatments showed no difference ($p > 0.05$) in moisture content, except F-PLE, whose moisture content was the highest ($p < 0.05$).

The presence of PLE in F-PLE may have caused the higher moisture content in this film due to the hydrophilic groups of the PLE polyphenols. The greater number of hydrophilic groups in F-PLE, as well as interactions between gelatin and PLE, may increase sensitivity to water, as observed for gelatin films with haskap berries extract (Liu et al., 2019). In the case of N-PLE, the observed effect was the opposite, since PLE polyphenols can interact with both CN and gelatin, forming a complex between PLE-CN-gelatin, which can reduce the free hydrophilic groups in this nanocomposite and, consequently, the moisture content (Vargas-Torrico et al., 2023). The same trend was observed for gelatin and carboxymethylcellulose nanocomposite films incorporated with pomegranate peel extract (Vargas-Torrico et al., 2023).

Any decrease in moisture content due to treatments incorporated with CN and/or DE may be a consequence of the rigid structure of CN and the interactions of hydrogen with the hydrophilic groups of gelatin and the presence of oil in DE, which increases the hydrophobic character of the films and nanocomposite films (Tessaro et al., 2021a,b). At RH of 76%, these influences were not evident, possibly because the higher moisture content can modify the interactions between the matrix components of the films and nanocomposite films.

7.3.4 Thickness

The mass of the film-forming solution deposited in the Petri dishes was controlled (1.25 g dry matter/Petri dish) and possibly for this reason no difference ($p > 0.05$) in thickness was observed between all treatments, at the same RH (Table 7.1). Regarding the effect of RH, as expected, the increase in RH caused an increase in the thickness of the films and nanocomposite films ($p < 0.05$).

It is interesting to observe that water absorption caused swelling in both materials (Xue et al., 2023), with a linear increasing of thickness (x) as a function of the moisture content (MC): $x = 2.3MC + 68.2$ ($R^2 = 0.915$) for films, and $x = 2.8MC + 67.0$ ($R^2 = 0.970$) for nanocomposite films. Curiously, the presence of NC in gelatin matrix slightly increased the swelling capacity of this material (2.8 µm/% of moisture)

compared to films without NC (2.3 μm/% of moisture). Murray and Dutcher (2006) also observed that chitosan films presented an increase in thickness as the conditioning RH increased, and the authors also attributed this behavior to the swelling phenomenon of the films due to water absorption.

7.3.5 CO_2 and O_2 transmission rate

The gas permeation in biopolymeric films basically occurs in three stages: i) the gas molecules adsorb on the biopolymeric surface (Henry's law), ii) the dissolution/diffusion of gas molecules occurs through the biopolymer matrix, from the most concentrated area to the least concentrated (Fick's law), and iii) finally, the desorption of gas molecules from the opposite surface of the biopolymer films occurs (Henry's law) (Trinh; Chang; Mekonnen, 2023).

The gas permeability of a biopolymer matrix therefore basically depends on the "solubility" of the gas in the films, which is affected by the chemical affinity between the gas molecules and film components influenced by polarity, molecular weight and size, and by those conditions that affect the gas diffusivity, such as film crystallinity, porosity, thickness, homogeneity, among others (Siracusa et al., 2018; Trinh; Chang; Mekonnen, 2023). Evidently, external conditions, such as pressure difference, temperature and RH can also influence gas permeability. Generally, biopolymers-based films have good gas barrier properties at low RH (Kurek et al., 2014), but still perform worse than synthetic plastics.

The gas transmission rate (GTR) of O_2 (O_2TR) and CO_2 (CO_2TR) through films and nanocomposite films conditioned at different RH was determined and allowed to observe that films and nanocomposite films presented different GTR behaviors and trends as a function of RH and treatment (Table 7.3). This behavior occurred because, as observed in the SEM images and X-ray patterns, the structure of films and nanocomposite films was affected by the film composition (with PLE or DE, with or without CN). Therefore, different treatments were expected to show different gas permeability behaviors of the films. However, some trends can be observed.

Figure 7.3 - a) Oxygen transmission rate (O_2TR), b) Carbon dioxide transmission rate (CO_2TR), and c) Perm-selectivity ratio (CO_2TR/O_2TR) for gelatin films (F) and nanocomposite films (N) control (C), with "Pitanga" leaf extract (PLE), or with double emulsion (DE)
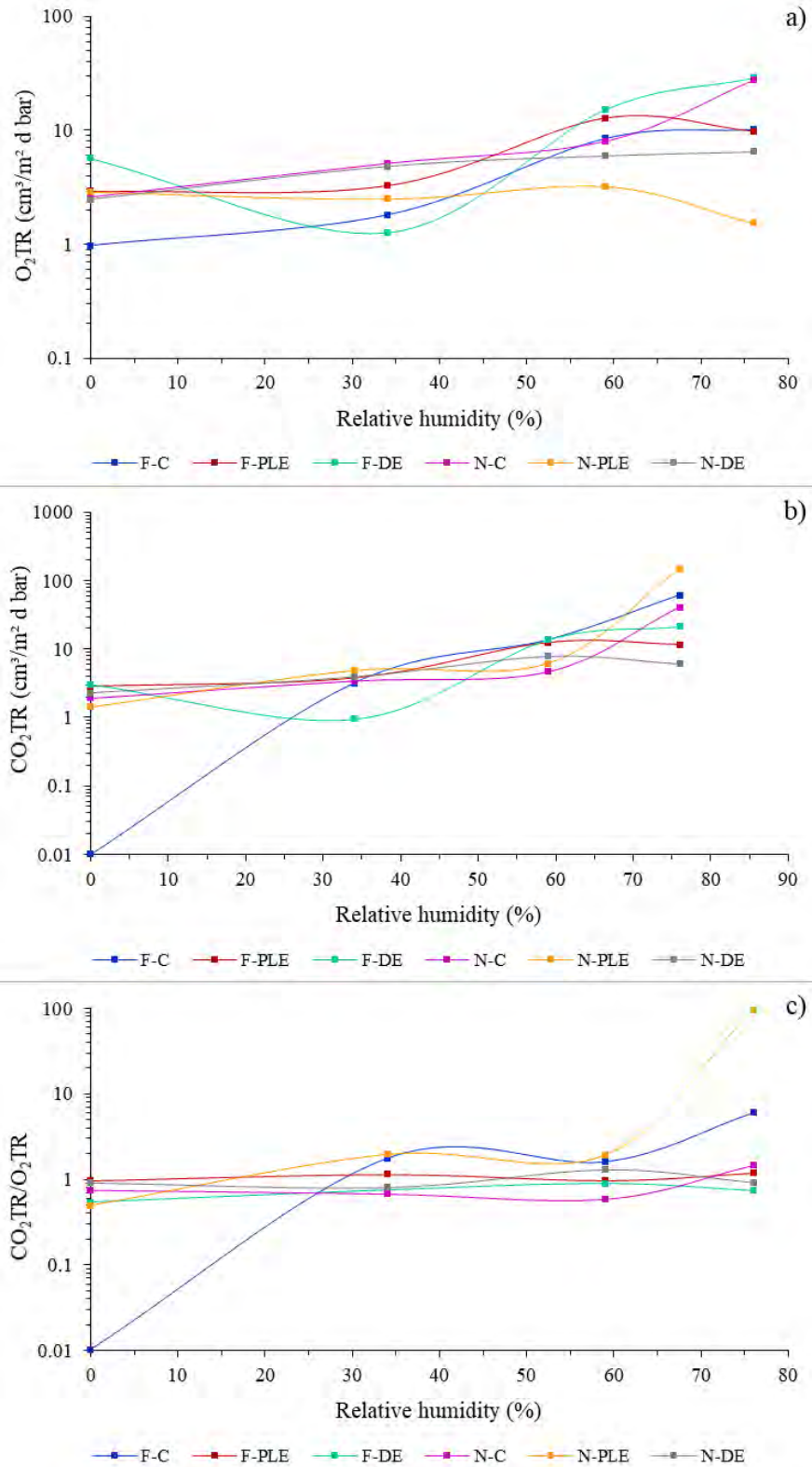
Source: Own authorship.

Regarding the effect of RH, the O_2TR and CO_2TR increased, in general, with increasing RH, except for F-DE, where both GTR decreased at RH of 34% and then increased in other RH levels. For N-PLE, the O_2TR decreased at RH of 76%, and for N-DE, the CO_2TR decreased at RH of 76%. As previously noted, increasing RH leads to an increase in the moisture content of films and nanocomposite films causing a plasticizing effect (Sobral et al., 2001).

Plasticization of films and nanocomposite films results in an increase in macromolecular free volume or, in another words, an increase in macromolecular mobility, facilitating gases permeation into the biopolymer matrix (Xue et al., 2023, Trinh; Chang; Mekonnen, 2023). Although GTR is influenced by film thickness, it is expected to be independent from it for thicker samples (> 10 μm) (Wang et al., 2018). Kurek et al. (2014) also observed that carvacrol-activated chitosan films and coatings presented increased O_2TR and CO_2TR with increased RH. The same behavior was observed for films based on whey protein isolate (Schmid et al., 2015).

The effect of films and nanocomposite films composition was also observed. Under dry conditions (RH = 0%), F-C, which does not contain PLE, DE or CN, presented the lowest values of O_2TR and CO_2TR, and it was practically impermeable to CO_2 (CO_2TR ~ 0.01 cm³/m².d.bar). Also, for the other treatments, O_2TR was higher than CO_2TR, varying from 2.5 to 5.7 (cm³/m².d.bar) and from 1.4 to 3.1 (cm³/m².d.bar), respectively, with F-DE presenting the highest values for both gases. This may have occurred because the oil present in DE can create microchannels or porosity in the structure of the films, facilitating gas permeation under these conditions. The effect of DE was less pronounced in N-DE, possibly due to the effect of chemical interactions occurred between gelatin-DE-CN, forming a more cohesive matrix that was difficult to penetrate. The fact that CO_2TR was lower than O_2TR in all treatments at RH = 0% can be explained by the fact that the size of the CO_2 molecule is larger than that of O_2 (3.4 Å and 3.1 Å, respectively) (Gigli et al., 2014, Siracusa et al., 2012), which makes passage through the dehydrated biopolymeric matrix difficult (Table 7.1). The same behavior was observed for chitosan coated polyethylene films, by Kurek et al. (2014).

At the other RHs, the effects observed were varied, because the presence of water into biopolymer matrix. F-C, F-PLE and N-PLE presented higher CO_2TR than O_2TR at RH of 34, 59 and 76%, possibly related to the fact that CO_2 has a higher solubility in water than O_2, thus increasing the permeation of this gas in the hydrated material (Galus; Kadzinska, 2019). This greater solubility of CO_2 in water can be also

explained by the fact that it is capable of reacting with water to form carbonic acid. Furthermore, CO_2 can interact with the free amino groups of gelatin, increasing its sorption and permeation, unlike O_2 (Biscarat et al., 2015). Kurek et al. (2014) observed that, in hydrated chitosan-based films and coatings, the CO_2TR was higher than the O_2TR, and attributed this behavior to the greater solubility of CO_2 in water.

Under these same conditions, O_2TR was greater than CO_2TR in F-DE, N-C and N-DE. For F-DE and N-DE, this behavior can be explained by the presence of DE oil, which can increase the non-polar character of these materials, which causes non-polar molecules such as O_2 and CO_2 to have greater affinity. In these cases, the O_2 molecule, being smaller, was probably able to migrate more easily through the biopolymeric matrix (Galus; Kadzinska, 2019). The presence of oil can also affect all chemical interactions and rearrangements in biopolymer matrices, influencing the affinity of CO_2 for the amino groups of gelatin and for water. In particular, F-DE presented the lowest values of O_2TR and CO_2TR at RH = 34%, possibly because in this condition, the chemical interactions (such as hydrogen interaction) between gelatin and sodium caseinate present in the external aqueous phase of DE, in the presence of water, have been maximized, forming a more compact structure. In the remaining RH (59 and 76%), O_2TR and CO_2TR were, in general, among the highest in F-DE, given that increasing the amount of water present in the film can rehydrate the gelatin, causing destabilization and separation of the DE oil. This separation can compromise the film structure and form pores, which can create preferential path for gas permeation.

N-PLE presented the lowest O_2TR values ($p < 0.05$) at RH = 59 and 76%. This could be a consequence of its greater crystallinity (Table 7.2), since the permeation of gases and vapors occurs in the amorphous portion (Iaccheri et al., 2023). Overall, crystallinity plays a fundamental role as gases cannot diffuse and permeate through the crystalline phase due to the restricted mobility of the biopolymer chain (Xue t al., 2023). Biopolymer matrix crystals are impenetrable to gas molecules and consequently biopolymers with the highest crystallinity were generally the best barrier materials. N-C, on the other hand, presented a lower crystallinity index than N-PLE, therefore, higher O_2TR and CO_2TR values. Although N-DE had a lower crystallinity index, its O_2TR was the lowest at RH = 76%, possibly due to the effect of the gelatin-DE-CN interaction.

To predict the behavior of films and nanocomposite films under certain RH conditions, it was interesting to mathematically model the obtained data (Table 7.2).

Good correlations ($R^2 > 0.6$) were observed when the linear equation was fitted to O_2TR and CO_2TR data, excepted for N-PLE, N-C and N-PLE, respectively (Table 7.2). On the other hand, when the second-order polynomic equation was fitted for the TR data of both gases, a good correlation was observed in general, excepted that of O_2TR for N-PLE (Table 7.2). Kurek et al. (2014) also observed a non-linear behavior working on chitosan-based films and coatings as a consequence of increasing RH.

Table 7.2 - Parameters of the linear (y = ax + b) and quadratic (y = ax² + bx + c) equations calculated by linear and non-linear regression with the dates of GTR (y) and RH (x) of the gelatin films (F) and nanocomposite films (N) control (C), with "Pitanga" leaf extract (PLE), or with double emulsion (DE) at different relative humidity. R^2 is the regression coefficient

GTR (cm³/m² d bar)	Treatment	Linear equation			Quadratic equation			
		a	b	R²	a	b	c	R²
O_2	F-C	0.13	-0.19	0.87	1.7×10^{-3}	6.8×10^{-3}	0.72	0.94
	F-PLE	0.12	2.08	0.67	0.4×10^{-3}	9.1×10^{-2}	2.30	0.67
	F-DE	0.30	0.12	0.65	9.9×10^{-3}	-0.44	5.49	0.99
	N-C	0.28	-0.96	0.66	7.9×10^{-3}	-0.31	3.34	0.91
	N-PLE	-0.01	3.00	0.26	-0.4×10^{-3}	2.2×10^{-2}	2.76	0.45
	N-DE	0.05	2.68	0.98	-0.4×10^{-3}	8.2×10^{-2}	2.47	1.00
CO_2	F-C	69.64	-9.81	0.65	210.61	-87.19	1.62	0.93
	F-PLE	13.76	1.84	0.80	9.64	6.58	2.36	0.82
	F-DE	24.64	-0.71	0.74	63.00	-22.28	2.71	0.97
	N-C	40.69	-4.59	0.52	148.18	-69.66	3.46	0.86
	N-PLE	153.06	-24.46	0.49	591.35	-287.29	7.65	0.84
	N-DE	6.28	2.35	0.74	-6.01	10.75	2.02	0.77

Source: Own authorship.

The gas permeability ratio (CO_2TR/O_2TR, also called perm-selectivity ratio) is an important parameter for food packaging, as it informs about the proportion of gases inside the packaging (Barbato et al., 2023) and about what type of food it is suitable for. CO_2TR/O_2TR perm-selectivity ratio is already known for several polymers

(Siracusa et al., 2012). According to Schmid et al. (2015), for non-condensable gases, the gas perm-selectivity ratio is relatively constant and is not related to the polymer chemical structure. This means that although molecular size of permeating species could affect the transmission rate, in the case of O_2 and CO_2 there is no relationship between gas molecular size and permeability behavior (Gigli et al., 2014). Generally, in biopolymeric films, CO_2 is much more permeable than O_2, as it has a higher solubility in water and a higher affinity for gelatin, for example, as previously mentioned (Biscarat et a., 2015). Therefore, the CO_2TR/O_2TR value in gelatin films are generally numbers greater than 1. For gelatin/polyethylene glycol blends it varies from 4 to 8 (Biscarat et al., 2015).

In this study, O_2TR was higher than CO_2TR for all treatments at RH = 0%, and the CO_2TR/O_2TR ranged from 0.01 to 0.97 (Table 7.3c). At the other RHs, F-DE and N-DE presented higher O_2TR than CO_2TR, with CO_2TR/O_2TR smaller than 1, except for N-DE in RH = 59% (CO_2TR/O_2TR = 1.31). In the other treatments, the CO_2TR/O_2TR was greater than 1, with values varying between 1.15 and 1.96, with the exception of F-C at RH = 76%, where the value was 6.05. This result indicates that, in films and nanocomposite films with some incorporated component (CN, PLE and/or DE), the CO_2 permeability was reduced and the CO_2TR/O_2TR ratio remained practically constant, possibly because the hydrogen interactions occurring between gelatin and these components reduced the free amino groups in gelatin, for which the CO_2 molecule has affinity.

To conclude, all studied films and nanocomposite films can be considered as medium barrier to O_2 (400-4000 cm³.µm/m².d.bar, Wang et al., 2018), with the best performances being observed at RH = 0% and 34%. Especially N-PLE and N-DE presented good O_2 barrier properties at higher RH (59 and 76%).

7.4 CONCLUSIONS

The O_2 and CO_2 permeability of gelatin-based films and nanocomposite films activated with non-encapsulated PLE and encapsulated in double emulsion was influenced, mainly, by the rearrangement of chemical interactions occurring in the biopolymeric matrix as a consequence of their moisture content. The increase in relative humidity has increased the moisture content of these materials, thus contributing to the occurrence of phenomena such as swelling, the increase in free

volume in the biopolymer matrix due to the water plasticizing effect and, consequently, the increase in gas permeability. At higher relative humidity, the nanocomposite films generally presented the best gas barrier properties, especially the nanocomposite with double emulsion, for both gases, and the non-encapsulated PLE nanocomposite, with lower O_2 permeability. Accordingly, the addition of crystalline nanocellulose and non-encapsulated or doubly emulsified PLE into gelatin-based films improved the gas barrier properties, especially under high relative humidity conditions.

References

ACHARYA, D.R. et al. Nanoemulsion-integrated gelatin/bacterial cellulose nanofribril-based multifunctional film: Fabrication, characterization, and application. **International Journal of Biological Macromolecules**, v. 257, p. 128341, 2024.

AL-MAQTARI, Q.A. et al. Fabrication and characterization of chitosan/gelatin films loaded with microcapsules of *Pulicaria jaubertii* extract. **Food Hydrocolloids**, v. 129, p. 107624, 2022.

BARBATO, A. et al. High-barrier, biodegradable films with polyvinyl alcohol/polylactic acid + wax double coatings: Influence of relative humidity on transport properties and suitability for modified atmosphere packaging applications. **Polymers**, v. 15, p. 4002, 2023.

BENBETTAÏEB, N. et al. Barrier, structural and mechanical properties of bovine gelatin–chitosan blend films related to biopolymer interactions. **Journal of the Science of Food and Agriculture**, v. 94, n. 12, p. 2409-2419, 2014.

BISCARAT, J. et al. Development of a new family of food packaging bioplastics from cross-linked gelatin bases films. **The Canadian Journal of Chemical Engineering,** v. 93, n. 2, p. 176-182, 2015.

CHAKRAVARTULA, S.S.N. et al. Influence of pitanga (*Eugenia uniflora* L.) leaf extract and/or natamycin on properties of cassava starch/chitosan active films. **Food Packaging and Shelf Life**, v. 24, p. 100498, 2020.

FLAKER, C.H.C. et al. Gelatin-based nanocomposite films: a study on montmorillonite dispersion methods and concentration. **Journal of Food Engineering**, v. 167, p. 65-70, 2015.

FUKUZUMI, H. et al. Transparent and high gas barrier films of celulose nanofibers prepared by TEMPO-Mediated oxidation. **Biomacromolecules**, v. 10, n. 1, 162-165, 2009.

GALUS, S.; KADZINSKA, J. Gas barrier and wetting properties of whey protein isolated-based emulsion films. Polymer Engineering & Science, v. 59, p. E375-E383, 2019.

GIGLI, M. et al. Biodegradable aliphatic copolyesters containing PEG-like sequences for sustainable food packaging applications. **Polymer degradation and stability**, v. 105, p. 96-106, 2014.

GONTARD, N.; GUILBERT, S.; CUQ, J.-L. Edible Wheat Gluten Films: Influence of the Main Process Variables on Film Properties using Response Surface Methodology. **Journal of Food Science**, v. 57, n. 1, 190–195, 1992.

HANANI, Z. N.; ROOS, Y. H.; KERRY, J. P. Use and application of gelatin as potential biodegradable packaging materials for food products. **International journal of biological macromolecules**, v. 71, p. 94-102, 2014.

IACCHERI, E. et al. Studying physical state of films based on casava starch and/or chitosan by dielectric and thermal properties and effects of pitanga leaf hydroethanolic extract. **Journal of Food Engineering**, v. 339, p. 111280, 2023.

ILYAS, Q.A. et al. Oxygen permeability properties of nanocellulose reinforced biopolymer nanocomposites. **Materials Today: Proceedings**, v. 52, p. 2414-2419, 2022.

KUREK, M. et al. Effect of relative humidity on carvacrol release and permeation properties of chitosan based films and coatings. **Food Chemistry**, v. 144, p. 9-17, 2014.

LAGOS, J.B. et al. Mechanical properties of cassava starch films as affected by different plasticizers and different relative humidity conditions. **International Journal of Food Studies**, v. 4, p. 116-125, 2015.

LI, M. et al. Gelatin films reinforced by tannin-nanocellulose microgel with improved mechanical and barrier properties for sustainable active food packaging. **Food Hydrocolloids,** v. 149, p. 109642, 2024.

LIU, J. et al. Preparation and characterization of active and intelligent films based on fish gelatin and haskap berries (*Lonicera caerulea* L.) extract. **Food Packaging and Shelf Life**, v. 22, p. 100417, 2019.

LORENZO, J. M. et al. Influence of pitanga leaf extracts on lipid and protein oxidation of pork burger during shelf-life. **Food Research International**, v. 114, p. 47–54, 2018.

LUCIANO, C. G. et al. Bi-layer Gelatin Film: Activating Film by Incorporation of "Pitanga" Leaf Hydroethanolic Extract and/or Nisin in the Second Layer. **Food and Bioprocess Technology**, v. 14, n. 1, p. 106–119, 2021.

LUCIANO, C. G. et al. Application of bi-layers active gelatin films for sliced dried-cured Coppa conservation. **Meat Science**, v. 189, p. 108821, 2022.

MARTELLI-TOSI, M. et al. Soybean straw nanocellulose produced by enzymatic or acid treatment as a reinforcing filler in soy protein isolate films. **Carbohydrate Polymers**, v. 198, p. 61-68, 2018.

MURRAY, C.A.; DUTCHER, J.R. Effect of changes in relative humidity and temperature on ultrathin chitosan films. **Biomacromolecules**, v. 7, p. 3460-3465, 2006.

RANJBARYAN, S.; POURFATHI; B.; ALMASI, H. Reinforcing and release controlling effect of cellulose nanofiber in sodium caseinate films activated by nanoemulsified essential oil. **Food Packaging and Shelf Life,** v. 21, p. 100341, 2019.

SCHMID, M. et al. Permeation of water vapour, nitrogen, oxygen and carbon dioxide through whey protein isolate based films and coatings - Permselectivity and activation energy. **Food Packaging and Shelf Life**, v. 6, p. 21-29, 2015.

SHAMSALLAH, A. A.; RASHID, S. O. Development in gelatin-matrix composite films: The incorporation of vitamin C adducts enhances the optical behaviors of gelatin films. **Arabian Journal of Chemistry**, v. 17, n. 2, p. 105541, 2024.

SIRACUSA, V. et al. Poly (lactic acid)-modified films for food packaging application: Physical, mechanical, and barrier behavior. **Journal of Applied Polymer Science**, v. 125, n. S2, p. E390-E401, 2012.

SIRACUSA, V. et al. Barrier properties of poly (propylene cyclohexanedicarboxylate) random eco-friendly copolyesters. **Polymers**, v. 10, n. 5, p. 502, 2018.

SIRACUSA, V. et al. Gas transport phenomena and polymer dynamics in PHB/PLA blend films as potential packaging materials. **Polymers**, v. 12, n. 3, p. 647, 2020.

SOBRAL, P. J. A. ; HABITANTE, A. M. Q. B. Phase transitions of pigskin gelatin. **Food Hydrocolloids**, v. 15, n. 4–6, p. 377–382, 2001.

SOBRAL, P. J. A. et al. Mechanical, water vapor barrier and thermal properties of gelatin based edible films. **Food Hydrocolloids**, v. 15, n. 4–6, p. 423–432, 2001.

TESSARO, L. et al. Gelatin/chitosan based films loaded with nanocellulose from soybean straw and activated with "Pitanga" (*Eugenia uniflora* L.) leaf hydroethanolic extract in W/O/W emulsion. **International Journal of Biological Macromolecules**, v. 186, p. 328–340, 2021b.

TESSARO, L. et al. Gelatin and/or chitosan-based films activated with "Pitanga" (*Eugenia uniflora* L.) leaf hydroethanolic extract encapsulated in double emulsion. **Food Hydrocolloids**, v. 113, p. 106523, 2021a.

TRINH, B.M.; CHANG, B.P.; MEKONNEN, T.H. The barrier properties of sustainable multiphase and multicomponent packaging materials: A review. **Progress in Materials Science**, v. 133, p. 101071, 2023.

VALENCIA, G. A. et al. Physical and morphological properties of nanocomposite films based on gelatin and Laponite. **Applied Clay Science**, v. 124–125, p. 260–266, 2016.

VARGAS, F. C. et al. Rosemary and pitanga aqueous leaf extracts on beef patties stability under cold storage. **Brazilian Archives of Biology and Technology**, v. 59, p. e16160139, 2016.

VARGAS-TORRICO, M. F. et al. Preparation and characterization of gelatin-carboxymethylcellulose active film incorporated with pomegranate (Punica granatum L.) peel extract for the preservation of raspberry fruit. **Food Hydrocolloids,** v. 150, p. 109677, 2023.

WANG, J. et al. Moisture and oxygen barrier properties of cellulose nanomaterial-based films. **ACS Sustainable Chemistry & Engineering**, v. 6, n. 1, p. 49-70, 2018.

WANG, Y. et al. Physicochemical properties of gelatin films containing tea polyphenol-loaded chitosan nanoparticles generated by electrospray. **Material & Design**, v. 185, p. 108277, 2020.

XUE, W. et al. Permeability of biodegradable film comprising biopolymers derived from marine origin for food packaging application: A review. **Trends in Food Science & Technology**, v. 136, p. 2945-307, 2023.

8 CAPÍTULO 5: Gelatin-based nanocomposite films activated by double emulsion loaded with "pitanga" leaf extract: Bioaccessibility and cytotoxicity of emulsions and films after *in vitro* digestion

Larissa Tessaro [a, b], Raquel F. S. Gonçalves [b], Joana T. Martins [b, c], Ana C. Pinheiro [b, c], António A. Vicente [b,c], Paulo J. A. Sobral [a, d]

[a] *Department of Food Engineering, Faculty of Animal Science and Food Engineering, University of São Paulo, Av Duque de Caxias Norte, 225, 13635-900 Pirassununga, SP, Brazil.*

[b] *Centre of Biological Engineering, University of Minho, Campus de Gualtar, 4710-057 Braga, Portugal.*

[c] *LABBELS – Associate Laboratory on Biotechnology and Bioengineering, and Electromechanical Systems, University of Minho, Campus de Gualtar, 4710-057 Braga, Portugal.*

[d] *Food Research Center (FoRC), University of São Paulo, Rua do Lago, 250, Semi-industrial building, block C, 05508-080 São Paulo, SP, Brazil.*

Abstract

The main aim of this study was to carry out an *in vitro* digestion of gelatin-based films and nanocomposite films activated with "Pitanga" (*Eugenia uniflora* L.) leaf extract (PLE) encapsulated in a W/O/W double emulsion. Also, the effects of encapsulation and addition of crystalline nanocellulose on PLE bioaccessibility, and on Caco-2 cells viability, after *in vitro* digestion, were evaluated. The free PLE, W/O (SE) emulsions and W/O/W (DE) emulsions were also submitted to *in vitro* digestion. The encapsulation of PLE within DE considerably increased the stability and bioaccessibility of PLE after *in vitro* digestion, which was also higher compared to SE. The PLE encapsulation within DE was positive compared to encapsulation only in SE, as DE also showed higher digestibility and lower cytotoxicity than SE. The active films and nanocomposite films showed lower PLE bioaccessibility when compared to SE and DE, but they were not cytotoxic to Caco-2 at all PLE concentrations studied. The PLE stability and bioaccessibility were higher using N-DE (nanocomposite film activated with DE). The effect of previously encapsulating PLE in DE, and the addition of crystalline nanocellulose in the film matrix, contributed to the protection of PLE's biological activity. Gelatin-based films and active nanocomposite films may have additional properties and applications in the food industry, as they have been shown to be active after *in vitro* digestion. Furthermore, DE was an effective encapsulation system for aqueous active compounds and can be potentially applied to several other areas of the food industry.

8.1 INTRODUCTION

Active packaging, such as active films, can extend the shelf life and improve the quality and safety of packaged food. These materials can be produced based on biopolymers, and have properties such as biocompatibility, non-toxicity, biodegradability and ability to carry different active compounds (López de Lacey et al., 2012; Tessaro et al., 2021a).

"Pitanga" (*Eugenia uniflora* L.) leaf extract (PLE) is rich in active compounds and can be used to produce active material with antioxidant and antimicrobial properties (Luciano et al., 2022; Chakravartula et al., 2020). The "Pitanga" is a fruit tree native from Brazil, but it is already cultivated in several regions of the world with a tropical climate (Luciano et al., 2022). "Pitanga" leaves are interesting because they have a high content of phenolic compounds, which is related to the excellent antioxidant, antimicrobial and anti-inflammatory activities of PLE (Cunha et al., 2016; Lorenzo et al., 2018).

Despite the potential applications of PLE, it can undergo oxidative degradation when exposed to environmental or gastrointestinal conditions (Rakshit; Srivastav, 2022). One way to increase the PLE value before application in active films or nanocomposite films is to promote its encapsulation (Tessaro et al., 2021a). Gelatin-based active films produced with PLE encapsulated in a water-in-oil-in-water (W/O/W) double emulsion showed excellent physical properties (Tessaro et al., 2021a). The same results were observed for this material when incorporating crystalline nanocelluloses as a reinforcing filler, the active nanocomposite films (Tessaro et al., 2021b).

W/O/W emulsions can be defined as "emulsions of emulsions" (Dickinson, 2011), which present W/O and O/W interfaces. These structures may be interesting for food applications because, i) the lipid phase of the W/O interface functions as a physical barrier, which protects hydrophilic phenolic compounds present in the inner W phase, and ii) the (W/O)/W interface increases the dispersibility of the W/O emulsion in water-based foods (He et al., 2023). Besides protecting hydrophilic phenolic compounds, W/O/W emulsions can also promote their controlled release and increase their bioaccessibility in the intestine (Rakshit; Srivastav, 2022).

In addition to the essential function of extending the shelf life of food and increase its value, active nanocomposite films containing PLE encapsulated on W/O/W

emulsions can possibly provide benefits to human health if consumed with the food product. Therefore, it is very important to study their behavior and bioaccessibility during digestion (Giménez et al., 2013; López de Lacey et al., 2012).

In this study, only GRAS materials from natural and renewable sources were used to produce active nanocomposite films namely, "Pitanga" leaves (used in the Brazilian folk medicine) (Araújo et al., 2021) and nanocellulose (naturally present in the soybean straw) (Tessaro et al., 2021b). Thus, it was hypothesized that the materials used are not cytotoxic after *in vitro* digestion, which will be started to be investigated by adequate experimental settings in another study. Therefore, our work focuses on i) the evaluation of the effects of PLE encapsulation in the internal aqueous phase of a W/O/W emulsion and the addition of crystalline nanocellulose on the bioaccessibility and stability of PLE, and ii) the assessment of gelatin-based active films and nanocomposite films' cytotoxicity after *in vitro* digestion. As controls, free PLE, and W/O and W/O/W emulsions were also submitted to an *in vitro* digestion. No data was found in the literature regarding these issues, which demonstrated the originality of the present research. Emulsions were analyzed regarding droplet size, polydispersity index (PDI), ζ-potential, morphology, free fatty acids release, bioaccessibility and stability of PLE, and cytotoxicity, before and after *in vitro* digestion.

8.2 MATERIAL AND METHODS

8.2.1 Material

"Pitanga" leaves were collected at the Faculty of Animal Science and Food Engineering, in the city of Pirassununga-SP, Brazil (21°59′46″ S, 47◦25′36″ W). Soybean straw was donated by the Embrapa Soja, Londrina-PR, Brazil (23°17′ 34″ S, 51°10′24″ W). Grinsted PGPR® (Polyglycerol Polyricinoleate) was donated by DuPont (São Paulo-SP, Brazil) and sodium caseinate by Alibra Ingredientes SA (Campinas-SP, Brazil). Type B bovine gelatin (molecular weight: ~45 kDa; 250 bloom) was donated by Gelco (Pedreira-SP, Brazil).

Food grade soybean oil was purchased from Cargill (Primavera do Leste-MT, Brazil). Acetone P.A. (100%), ethanol P.A. (≥95%), H_2SO_4 P.A. (98%), NaOH (P.A.), H_2O_2, $Mg_2SO_4.7H_2O$, and Na_2CO_3 were purchased from Labsynth® (São Paulo-SP, Brazil). Bile extract porcine, dimethyl sulfoxide (DMSO), glycerol (≥99.5%), Nile red,

pancreatin from porcine pancreas (8x USP), Pefabloc® sodium caseinate, pepsin from porcine gastric mucosa (≥ 2500 U/mg), salts used to prepare electrolyte solutions, Folin-Ciocalteu reagent, gallic acid, Tween® 80, and penicillin/streptomycin (P/S) were purchased from Sigma-Aldrich (St Louis-MO, USA). Hexane P.A. was obtained from Fisher Scientific (Branchburg-NJ, USA).

Dulbecco's modified Eagle's medium (DMEM), phosphate buffered saline (PBS), and non-essential amino acids (NEAA) were purchased from Lonza (Basel, Switzerland). Fetal bovine serum (FBS) was purchased from Merck KGaA (Darmstadt, Germany), and 3-(4,5-Dimethyl-2-thiazolyl)-2,5-diphenyl-2H-tetrazolium Bromide (MTT) was obtained from Sigma-Aldrich (St Louis-MO, USA). Caco-2 cell line was obtained from Deutsche Sammlung von Microorganismen und Zellkulturen (Braunschweig, Germany).

8.2.2 Production of "Pitanga" leaf extract

PLE was produced according to Lorenzo et al. (2018) and Tessaro et al. (2021a). "Pitanga" leaves were sanitized (sodium hypochlorite 0.01% m/v), dried (42 °C/72 h), ground (using a commercial blender), and sieved (48 mesh). One g of powder was dispersed in 10 mL of 60% (v/v) hydroethanolic solution, treated with an ultrasonic bath (at room temperature for 40 min), heated (80 °C for 30 min), and filtered through filter paper (Whatmann n°1). The extract obtained was rotoevaporated (42 °C for 4 h), and freeze-dried using a Freeze-dryer (FD 1.0-60E, Heto-Holten A/S, Allerod, Denmark) and stored in the dark at -18 °C until further use.

8.2.3 Production of W/O and W/O/W emulsions

The W/O (SE) and W/O/W (DE) emulsions were prepared according to Tessaro et al. (2021c, 2022), in two emulsification steps. Briefly, SE was produced using 1 g PLE freeze-dried resuspended on 10 mL distilled water as the inner W phase (20% w/w) and soybean oil with 3 g PGPR on 100 g oil as the O phase (80% w/w). These phases were homogenized using a rotor-stator homogenizer (IKA ULTRA-TURRAX® T18 basic, Labotechnik, Staufen, Germany) at 15,000 rpm for 5 min, and with a probe-type sonicator (Vibra-cell VCX 500, Sonics, Newtown-CT, USA) for 90 s (27% amplitude; work time: 2 s; rest time: 1 s) (Tessaro; Martelli-Tosi; Sobral, 2021). DE was

produced using the SE as inner phase (40% w/w) and distilled water with 3 g Tween 80 /100 g distilled water and 0.5 g sodium caseinate/100 g distilled water, as dispersant O phase (60% w/w). These phases were homogenized using a hotplate stirrer (IKA® C-MAG HS 7, Werke GmbH & Co. KG, Mindelheim, Germany) at 1,000 rpm for 10 min, and a probe-type sonicator for 120 s (19% amplitude; work time: 2 s; rest time: 1 s) (Tessaro et al., 2022). The SE and DE were stored in the dark at 4 °C. The main properties of these emulsions have been studied and these results were published previously (Tessaro et al., 2022; Tessaro; Martelli-Tosi; Sobral, 2021).

8.2.4 Production of crystalline nanocelluloses

The crystalline nanocellulose was extract from soybean straw, using an alkaline pre-treatment, bleaching, acid hydrolysis and mechanical treatment, according to Martelli-Tosi et al. (2017). Soybean straw was sanitized with distilled water, dried (50 °C/ for 2 h), ground (knife mill), and sieved (100 mesh). Powdered soybean straw was dispersed in a 17.5% (w/v) NaOH solution and stirred at room temperature for 15 h. The fibers obtained were filtered, washed with distilled water until they reached with pH 7.0, and stirred with a bleaching solution (4% H_2O_2, 2% NaOH, and 0.3% $MgSO_4.7H_2O$, w/v) under stirring (90 °C for 3 h). The bleached fibers were washed with distilled water (until pH 7.0), and with ethanol and acetone, and dried (50 °C for 72 h).

The bleached fibers were dispersed in a 64% (w/v) H_2SO_4 solution at 70 °C/40 min, being that hydrolysis reaction was stopped by the addition of cold distilled water. The excess acid was separated by decantation of the crystalline nanocellulose, which were dialyzed until neutral pH. After that, crystalline nanocellulose suspension was treated with a rotor-stator homogenizer at 14,000 rpm/5 min followed by 3 min of probe-type sonication. The crystalline nanocellulose suspension was freeze-dried, and stored at room temperature. This nanomaterial has been characterized previously (Tessaro et al., 2021b).

8.2.5 Production of gelatin-based active films and nanocomposite films

The gelatin-based films and nanocomposite films were produced according to Tessaro et al. (2021a,b). For both films, the film-forming solution (FFS) was prepared

by the hydration of 4 g type B bovine gelatin/100 g FFS in distilled water for 30 min, followed by solubilization at 55 °C/10 min, and addition of 25 g glycerol/100 g gelatin.

In the case of active nanocomposite films, the gelatin hydration was carried out in distilled water with 4.5 g crystalline nanocellulose/100 g gelatin. The DE was added dropwise to the FFSs at the concentration of 0.25 g PLE/100 g gelatin under agitation at 500 rpm. Positive-control films and nanocomposite films were also produced, adding free PLE instead of DE, at the same concentration (0.25 g PLE/100 g gelatin). The FFSs were transferred to acrylic plates and dried (30 °C/24 h).

Four different film samples were produced: gelatin-based active films with DE (F-DE) or PLE (F-PLE) and gelatin-based active nanocomposite films with DE (N-DE) or PLE (N-PLE). Before analyses, films were conditioned for 7 days in desiccators with NaBr saturated solution (relative humidity = 58%) at 25 °C. The main physical and functional properties of gelatin-based active films and nanocomposite films were characterized and these data can be found in Tessaro et al. (2021a) and Tessaro et al. (2021b), respectively.

8.2.6 *In vitro* digestion

In vitro digestion was performed for the PLE, SE, DE, active films (F-PLE and F-DE) and nanocomposite films (N-PLE and N-DE) using a static model, according to the protocol validated by international consensus INFOGEST group (Brodkorb et al., 2019). This method simulates gastrointestinal digestion in the oral, stomach and intestinal phases. In the oral phase, 4 mL of simulated salivary fluid (SSF), composed of KCl (15.1 mM), KH_2PO_4 (3.7 mM), $NaHCO_3$ (13.6 mM), $MgCl_2(H_2O)_6$ (0.15 mM), $(NH_4)_2CO_3$ (0.06 mM) and HCl (1.1 mM), 25 µL of $CaCl_2.(H_2O)_2$ (0.3 M) and 975 µl of Milli-Q water, were added to 5 g of sample. The use of amylase was waived, as there was no starch in any of the samples. The samples were then incubated at 37 °C for 2 min using an incubated tube rotator (Roto-THERM Mini Plus, Benchmark, Edison-NJ, USA) at 50 rpm. In the gastric phase, 8 mL of simulated gastric fluid (SGF) composed of KCl (6.9 mM), KH_2PO_4 (0.9 mM), $NaHCO_3$ (25 mM), NaCl (47.2 mM), $MgCl_2(H_2O)_6$ (0.12 mM), $(NH_4)_2CO_3$ (0.5 mM) and HCl (15.6 mM), 5 µL of $CaCl_2.(H_2O)_2$ (0.3 M) and 1 mL of pepsin solution (2,000 U/mL in the final volume) were added. Then, the pH was adjusted to 3.0 with HCl (1 M), and Milli-Q water was added to adjust the final volume to 20 mL. Samples were incubated at 37 °C for 2 h at 50 rpm. In the intestinal

phase, 8.5 mL of simulated intestinal fluid (SIF) composed of KCl (6.8 mM), KH_2PO_4 (0.8 mM), $NaHCO_3$ (85 mM), NaCl (38.4 mM), $MgCl_2(H_2O)_6$ (0.33 mM) and HCl (8.4 mM), 40 µL of $CaCl_2.(H_2O)_2$ (0.3 M), 2.5 mL of bile salts (10 mM in the final volume) and 5 mL of pepsin solution (100 U/mL trypsin activity on pancreatin in the final volume) in were added. The pH was adjusted to 7.0 with HCl (1 M) or NaOH (2 M), and Milli-Q water was added to bring the final volume to 40 mL. Samples were incubated at 37 °C for 2 h at 50 rpm.

For the analysis of droplet size and ζ-potential, and fluorescence microscopy, at the end of each phase of *in vitro* digestion, 500 µL of samples were collected and stored on ice bath until analyzed. In samples from intestinal phase, Pefabloc® 5 mM (10 µL/mL sample) was further added to inhibit pancreatin activity. For stability and bioaccessibility analyzes and viability cell assay, samples were collected only at the end of intestinal phase.

8.2.7 Droplet size and ζ-potential

The droplet size (indicated by z-average) and PDI of the SE and DE, and the ζ-potential of the DE, were determined for the initial samples and after each *in vitro* digestion phase, using a dynamic light scattering apparatus (Zetasizer Nano SZ, Malvern Instruments, Worcestershire, UK). The emulsions were diluted (SE: 1:200; DE: 1:800) in buffer solutions of the same pH of each *in vitro* digestion phase (Gonçalves et al., 2021).

8.2.8 Fluorescence microscopy

The morphology of the SE and DE was analysed before and after each phase of the *in vitro* digestion using a fluorescence microscopy (BX51, Olympus®, Tokyo, Japan) with a 100x oil immersion objective lens. Nile red dye (0.25 mg/mL DMSO) was used to stain the lipid phase of the samples at 1:10 ratio (dye:sample, v/v) (Gonçalves et al., 2021).

8.2.9 Free fatty acids release

Free fatty acid (FFA) release was used to evaluate the digestibility of SE and DE (Gonçalves et al., 2021). *In vitro* digestion of SE and DE was carried out up to the gastric phase, according to the methodology described in section *9.2.6*. At the end of the gastric phase, the samples were transferred to a heated jacketed reactor at 37 °C, and the pH was adjusted to 7.0 with HCl or NaOH 0.1 M. Then, pancreatin solution was added and the pH was monitored and maintained at 7.0 throughout the intestinal phase (2 h), using an auto-titration unit (902 Titrando, Metrohm, Herisau, Switzerland) with NaOH 0.05 M. The same procedure was performed on the blank samples, without adding pancreatin solution. The percentage of FFA release (%) was calculated using the eq. (9.1), where $V_{NaOH\ sample}$ and $V_{NaOH\ blank}$ are the volume of NaOH spent in the titration of the samples and the blank (L), respectively, m_{NaOH} is the molarity of the NaOH titrant solution (0.05 M), M_{lipid} is the molecular weight of the lipid in the samples (soybean oil: 880 g/mol), and w_{lipid} is the initial mass of lipid (g).

$$FFA = \left(\frac{(V_{NaOH\ sample} - V_{NaOH\ blanck}) \times m_{NaOH} \times M_{lipid}}{w_{lipid} \times 2} \right) \times 100 \tag{8.1}$$

8.2.10 Bioaccessibility and stability of PLE

Stability and bioaccessibility of PLE were determined by Folin-Ciocalteu reducing capacity (FCRC) method, according to Singleton, Orthofer and Lamuela-Ravéntos (1999), with slight modifications, using 96-multiwall plates. The FCRC quantification was measured in PLE, emulsions, films and nanocomposite films initial (i.e. non-digested) and digested samples. For PLE stability, the unmodified PLE present in the digesta phase (final phase of intestinal digestion) was quantified. As for the PLE bioaccessibility, it was considered that the fraction of PLE inside the micellar phase was the bioaccessible fraction, and therefore PLE was quantified in this fraction. The digesta phase was centrifuged to separate the micellar phase, using a refrigerated centrifuge (Heraeus Multifuge X3R, Thermo Scientific, Osterode am Harz, Germany) at 18,000 g and 4 °C for 30 min, and the supernatant was assumed to be the micellar phase. Then, 40 µL of both digest and micellar phases were mixed with 2 mL of 60% hydroethanolic solution and 1 mL of 100% hexane for 30 s on a vortex (ZX3 Advanced

Vortex Mixer, VELP® Scientific Srl, Usmate, Italy), and centrifuged at 6,000 rpm for 10 min (EBA 20 centrifuge, Hettich®, Tuttlingen, Germany) at room temperature.

The extraction procedure was again performed in the top phase (hydrophobic phase). Regarding FCRC quantification, the bottom phases obtained in both extractions were mixed, and 20 µL of each one was added to 100 µL of 10% (v/v) Folin-Ciocalteu reagent. After 5 min of reaction, 75 µl of 7.5% (w/v) Na_2CO_3 was added, and the reaction was carried out in the dark for 2 h. Then, the absorbance was measured at 760 nm using a microplate reader (Synergy™ HT multi-detection microplate reader, Bio-Tek Instruments Inc., Winooski-VT, USA). To quantify FCRC, a standard curve of gallic acid (10 – 200 µg/mL) was used, and the results were expressed in mg of gallic acid equivalent (GAE)/g PLE.

Stability (S, %), bioaccessibility (B, %) and effective bioaccessibility (EB, %) were calculated according to Liu et al. (2018) (eqs. 8.2 – 8.4, respectively), where $C_{initial}$, $C_{digesta}$ and $C_{micellar}$, are PLE total concentrations in the initial, digesta and micellar samples, respectively.

$$S = \left(\frac{C_{digesta}}{C_{initial}}\right) \times 100 \tag{8.2}$$

$$B = \left(\frac{C_{micellar}}{C_{digesta}}\right) \times 100 \tag{8.3}$$

$$EB = \left(\frac{C_{micellar}}{C_{initial}}\right) \times 100 \tag{8.4}$$

8.2.11 Viability cell assay

The cell viability assay was carried out using the methodologies described by Silva et al. (2019) and Gonçalves et al. (2021). A Caco-2 cell line (cells between passages 40 and 45) was cultured in DMEM with 10% of the supplement containing FBS, 1% of NEAA solution and 1% of P/S. Caco-2 cells were seeded in 96-well culture plates at 2×10^4 cells/well. To carry out the assay, the non-digested samples (i.e., free PLE, SE, DE, film-forming solutions of active films and nanocomposite films) were dissolved in Milli-Q water and soybean oil (for SE). Then, these non-digested samples and digested samples of PLE, SE, DE emulsions, film-forming solutions of active films

and nanocomposite films were filtered (Amicon® Ultra-4 centrifugal filter, 10 kDa, Merck KGaA, Darmstadt, Germany) and centrifuged (Mikro 220R, Hettich, Germany) at 4,000 g for 40 min. The tested samples were then diluted in DMEM culture medium with 0.5% FBS. Samples (200 µL) were added to cells and the culture plates were incubated in a 5% CO_2 humidified atmosphere incubator at 37 °C, for 24 h. After the incubation period, Caco-2 cells were washed with FBS and mixed with 100 µL of MTT (0.5 mg/mL). The reaction occurred for 3 h at 37 °C in a 5% CO_2 humidified atmosphere incubator. After incubation, 200 µL DMSO was added to solubilize the formazan crystals. Cell viability was determined in a spectrophotometer (EPOCH, 219 BioTek, USA) at 570 nm (reference wavelength 630 nm). at 490 nm. The amount of "formazan" dye formed was directly proportional to the number of survive cells in culture. Cell viability (%) was calculated by the absorbance obtained from the wells containing treated cells in relation to the absorbance of untreated cells in DMEM medium Four replicates of each sample were analyzed.

8.2.12 Statistical analysis

At least three measurements (triplicate) were performed for each analyses and results were presented as mean ± standard deviation (SD). Statistical analysis was carried out using Statistica data analysis software system (version 7, StatSoft. Inc. GmbH, Hamburg, Germany). Results were analysed using one-way analysis of variance (ANOVA) and Tukey's test comparison ($p < 0.05$) for determining significant differences between the means.

8.3 RESULTS AND DISCUSSION

8.3.1 Droplet size, ζ-potential and morphology

The droplet size of SE and DE changed over the different phases of *in vitro* digestion, and the observed changes were different for each type of emulsion (Table 8.1). Regarding SE, the z-average size was the same before *in vitro* digestion (initial) and after *in vitro* digestion in the oral and gastric phases ($p > 0.05$), with nanometric sizes up to 200 µm. This behavior may occur as consequence of the high physical stability of this system, as previously discussed (Tessaro; Martelli-Tosi, Sobral, 2021).

Although not statistically different, slight changes occurred on SE size in the gastric phase, which are also visible in Figure 8.1, with z-average sizes varying between 0.109 and 0.206 μm (Table 8.1). At the end of the intestinal digestion phase, the z-average size increased ($p < 0.05$) to micrometric size. Regarding DE, the z-average size increased in the gastric phase ($p < 0.05$) when compared to initial and oral phase, which presented equal values ($p < 0.05$), and decreased in the intestinal phase ($p < 0.05$) when compared to other phases. For all phases, the z-average size was above 200 μm.

According to Chaudhary, Sabikhi and Hussain (2020), salivary fluid from the oral phase does not contain significant amount of surface-active molecules that can cause the desorption or digestion of the emulsifiers or other components responsible for the stability of an emulsion. This may explain why SE, and DE, did not undergo significant changes after *in vitro* digestion in the oral phase. Furthermore, the specific superficial area of the oil in SE is low, as it is the dispersing phase of the emulsion, which can reduce the action of the digestive enzymes present in the gastric fluid (He et al., 2023). He et al. (2023) and Zhang et al. (2022) observed the same behavior for W/O emulsions. Iqbal et al. (2022) reported that *in vitro* digestion of W/O emulsions (produced with soybean oil and PGPR in the lipid phase) caused a considerable increase in the average droplet size on the gastric phase, possibly due to W/O emulsions dilution in the gastric juice, enzymatic action and low pH, which may have altered the morphology of these systems.

Regarding the considerable increase in the z-average size of SE from 0.206 to 2.336 μm observed in the intestinal phase digestion, it can be explained by a phase inversion, which is visible in Figure 8.1, possibly caused by the number of digestive fluids (aqueous) added during *in vitro* digestion and by the action of lipase, present in the intestinal fluid. Also, the action of the phospholipids and bile salts at the SE surface could cause desorption of the emulsifier layer and consequently, aggregation (Pinheiro et al., 2013). In fact, it is known that phase inversion can be induced by several parameters such as the increase in salt concentration and water input (i.e., alteration of the oil/water volume ratio) (Mushtaq et al., 2023), which occurred throughout digestion and are more accentuated the intestinal phase. He et al. (2023) also observed an increase in the droplet size of the W/O emulsion (capsaicin/corn oil with PGPR and beeswax) in the intestinal phase.

Figure 8.1 – Fluorescence microscopy images of W/O (SE) and W/O/W (DE) emulsions before and after each *in vitro* digestion phase. The scale bar is 10 μm
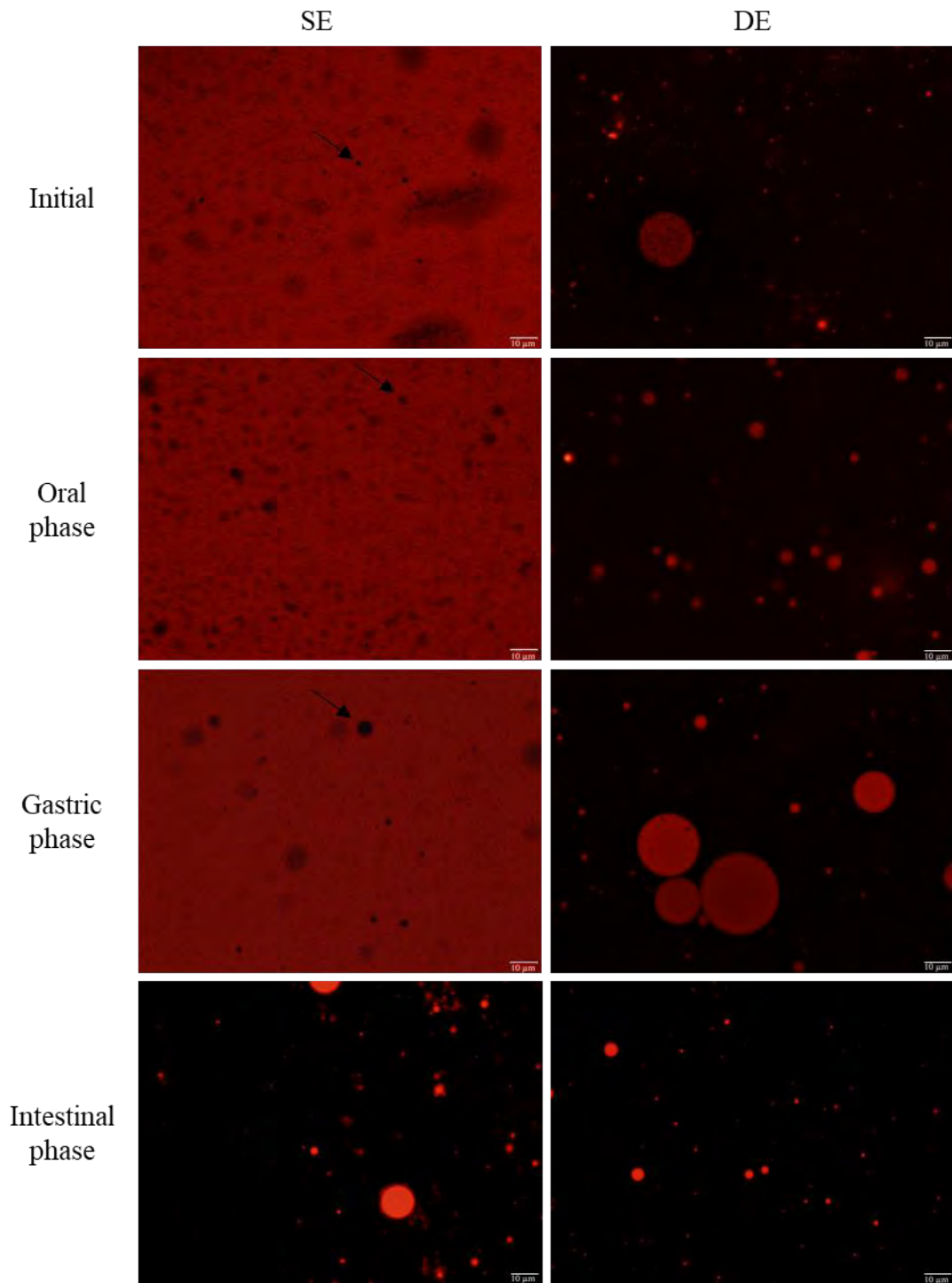
Source: Own authorship.

Table 8.1 – Droplet size, polydispersity index (PDI), and ζ-potential of W/O (SE) and W/O/W (DE) emulsions after each *in vitro* digestion phases*

In vitro digestion phases	z-average size (µm)		PDI		ζ-potential (mV)
	SE	DE	SE	DE	DE
Initial	0.109 ± 0.013[b]	1.326 ± 0.096[b]	0.237 ± 0.037[c]	0.764 ± 0.052[b]	-41.7 ± 1.7[b]
Oral phase	0.167 ± 0.022[b]	1.016 ± 0.099[b]	0.183 ± 0.024[c]	0.799 ± 0.079[b]	-50.9 ± 2.2[a]
Gastric phase	0.206 ± 0.044[b]	2.034 ± 0.291[a]	0.399 ± 0.007[b]	0.959 ± 0.038[a]	-6.4 ± 0.5[c]
Intestinal phase	2.336 ± 0.516[a]	0.631 ± 0.038[c]	1.000 ± 0.000[a]	0.658 ± 0.086[b]	-45.1 ± 3.4[a,b]

*Means ± standard deviation (n = 3). Different letters in the same column indicate significant differences between *in vitro* digestion phases according to Tukey's test ($p < 0.05$).
Source: Own authorship.

As for DE, the increase in z-average size at the end of the gastric phase may be related to the droplets' coalescence (Figure 8.1). The DE droplets coalescence can possibly occur due to two main factors (Han et al., 2022). Firstly, changes in ionic strength and pH can cause droplet coalescence, as they accelerate aggregation due to a decrease in electrostatic repulsion between droplets (Chaudhary; Sabikhi; Hussain, 2020; Han et al., 2022; Rakshit; Srivastav, 2022). Secondly, the pepsin action can also cause coalescence, as it induces the hydrolysis of proteins adsorbed at the interface of the oil droplets (as the case of sodium caseinate present in DE), decreasing the stability of the droplet (Han et al., 2022; Huang & Zhou, 2019). These changes in the interfacial surface of the droplets are reflected on ζ-potential value (Table 8.1). In fact, as the ζ-potential value of DE in the gastric phase was lower ($p < 0.05$) than the values observed in the other phases, the repulsion between the oil droplets may have decreased on this phase, leading to coalescence and consequently, z-average size increase. Other authors observed the same behavior for different W/O/W emulsions (Chaudhary; Sabikhi; Hussain, 2020; Han et al., 2022; Huang; Zhou, 2019; Rakshit; Srivastav, 2022).

In the intestinal phase, the DE average droplet size decreased possibly due to the effect of coalesced oil droplets digestion, as a result of lipase action. According to Rakshit and Srivastav (2022), the reduction of W/O/W droplet size at the end of the intestinal phase may also indicate a release of the encapsulated active compound into the external aqueous phase. In this case, the ζ-potential negative value decrease ($p < 0.05$). Han et al. (2023), who observed the same behavior, reported that the decrease of ζ-potential value in the intestinal phase was possibly due to the presence of several

species with negative charge resulting from digestion (i.e., non-digested protein aggregates, lipid droplets, micelles or vesicles) on the surface of the digested material, such as peptides and free fatty acids.

The PDI values of SE and DE also changed during *in vitro* digestion, which was consistent with the z-average size (Table 8.1). The lowest PDI values ($p < 0.05$) of SE were observed for initial and oral phases (around 0.200). However, PDI value increased ($p < 0.05$) in the gastric phase and in the intestinal phase, the PDI reached the highest value ($p < 0.05$), which indicates wide droplet size distribution. These results were corroborated by monomodal and narrow droplet nano-sized distribution (Figure 8.2) on initial and oral phase samples. On the other hand, a monomodal and wide droplet micro-sized distribution on gastric phase was observed. The droplet size distribution was bimodal and wide on the intestinal phase, with nano- and micro-sized droplet populations. As previously discussed, the fluorescence micrography images (Figure 8.1) showed that the PLE droplets (black color) were more homogeneously dispersed in the oil (red color) up to the gastric phase, and a phase inversion possible occurred in the intestinal phase, i.e., oil droplets (red color) dispersed in an aqueous phase (black color). These results also indicated that the SE remained quite stable and was poorly digested at least until the end of the gastric phase.

DE presented a different behavior from SE. In general, PDI values of DE were higher than for SE. The highest PDI value of DE was detected on the gastric phase ($p < 0.05$). These results were supported by nano- and micro-sized droplet distribution, which was trimodal in the gastric phase, and bimodal in the other phases (Figure 8.2). For intestinal phase, both nanometric and submicrometric populations showed narrow peaks. These droplet size distributions were visible in the fluorescence microscopy' images (Figure 8.1). Until the gastric phase, it was possible to observe small PLE droplets (black color) dispersed in larger oil droplets (red color) which, in turn, were dispersed in a dispersing aqueous phase (black color). In the gastric phase, it was possible to notice large oil drops. In the intestinal phase, only small droplets (red color) were observed, which could be non-digested oil droplets or vesicles. This instability phenomenon could have been provoked by aggregation, coalescence or flocculation mechanisms induced by the action of digestive enzymes, as well as changes in pH and ionic strength.

Figure 8.2 – Droplet size distribution of W/O (SE) and W/O/W (DE) emulsions before and after each *in vitro* digestion phase
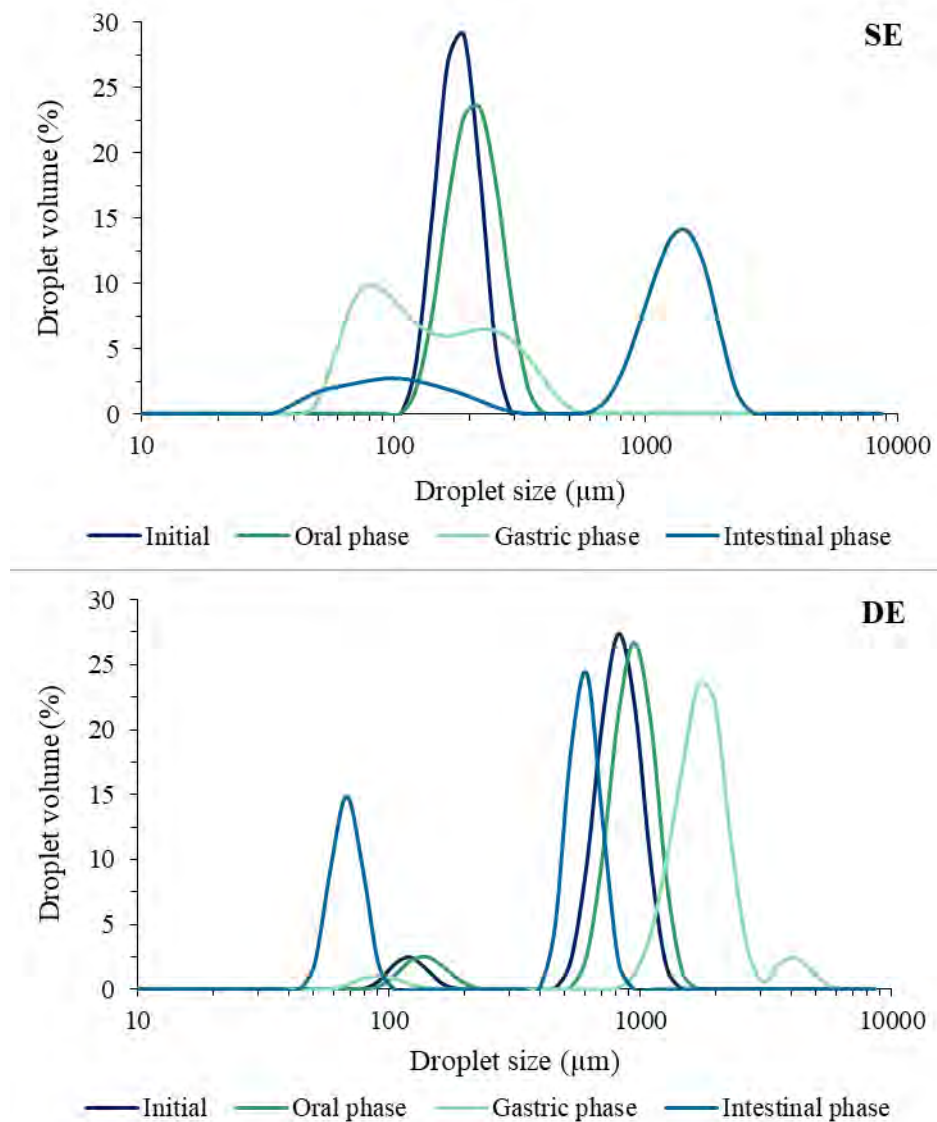
Source: Own authorship.

8.3.2 Free fatty acids release

The FFA assessment allows evaluating the impact of each type of emulsion on the rate and degree of lipid digestion (Han et al., 2022). The FFA results for the SE and DE emulsions corroborated the results presented for the droplet size, regarding the digestibility of each emulsion. The FFA concentration was lower for SE (44.9 ± 4.6%) ($p < 0.05$) than for DE (88.1 ± 2.8%), indicating a higher digestibility of DE than SE. This difference is possibly related to the type/structure of the emulsions.

According to Iqbal et al. (2022), the molecules that act at the W-O interface of the W/O emulsion can strongly stabilize these systems, inhibiting the enzymatic action of lipase and, consequently, reducing lipid digestion. In this case, the PLE's polyphenols may have helped stabilize SE, decreasing lipolysis (Zhang et al., 2022). Furthermore, in the case of SE, the oil is the dispersed phase, that is, the specific superficial area of lipase and bile with the oil is smaller than the emulsions such as O/W and DE itself, which may decrease lipolysis in the intestinal phase (Wu et al., 2022). There are fewer sites for the lipase to act, due to the relatively smaller specific superficial area (He et al., 2023). Compared to SE, Huang et al. (2022) reported similar FFA for a W/O emulsion produced with vitamin C and gelatin in the internal aqueous phase, and Camellia seed oil and PGPR in the lipid phase (39.11%). Wu et al. (2022) reported FFA close to 100% for a W/O emulsion produced with capsaicin in the internal aqueous phase and corn oil, beeswax and PGPR in the lipid phase.

In the case of DE, the soybean oil was practically all digested. As the oil was present in the form of droplets dispersed in an aqueous phase, a higher specific superficial area can favor bile and lipase adsorption, and consequently, lipolysis (Gonçalves et al., 2021) which increased FAA release. Also, the high FFA release from this type of emulsion may be related to the relatively low droplets' stability, favoring emulsion breakdown and lipolysis (Han et al., 2022). Han et al. (2022) reported a similar FFA release (≥ 88%) for W/O/W emulsions encapsulating quercetin and insulin in the internal aqueous phase, and soybean oil and PGPR as the lipid phase, and different emulsifiers in the dispersing aqueous phase.

8.3.3 Bioaccessibility and stability of "Pitanga" leaf extract

To determine the bioaccessibility and stability of PLE in emulsions, active films and nanocomposite films, FCRC concentration were quantified in all samples (Table 8.2).

PLE presented the highest concentration of FCRC ($p < 0.05$), as expected. However, the emulsions, active films and nanocomposite films showed very satisfactory FCRC concentrations, which were reduced between 13 and 28% in relation to the PLE. Only F-PLE presented a FCRC concentration below that of the other samples ($p < 0.05$), with a reduction of 64% in relation to PLE. The lower amount of FCRC in the samples concerning PLE was probably a result of losses that occurred

during processing such as heating, aeration and drying. This difference may also occur due to the extraction of phenolic compounds from PLE in ready-made samples, as PLE can interact with the components of emulsions and films, which can reduce extraction efficiency.

Table 8.2 - Folin-Ciocalteu reducing capacity (FCRC) and sample/ "Pitanga" leaf extract (PLE) ratio of free PLE, W/O (SE) and W/O/W (DE) emulsions, and active films (F-PLE and F-DE) and nanocomposite films (N-PLE and N-DE) before *in vitro* digestion*

Initial sample	FCRC (mg GAE/g sample)	FCRC (mg GAE/g PLE)	Sample/PLE ratio
Free PLE	415.52 ± 24.43[a]	415.52 ± 24.43[a]	1.00
SE	44.05 ± 2.28[b]	300.84 ± 15.35[b]	0.72
DE	24.23 ± 0.67[c]	331.99 ± 9.13[b]	0.80
F-PLE	0.38 ± 0.05[e]	150.73 ± 18.77[c]	0.36
F-DE	0.87 ± 0.09[d]	346.67 ± 26.03[b]	0.87
N-PLE	0.88 ± 0.02[d]	322.62 ± 54.85[b]	0.78
N-DE	0.85 ± 0.09[d]	311.73 ± 61.99[b]	0.75

*Means ± standard deviation (n = 3). Different letters in the same column indicate significant differences between samples according to Tukey's test ($p < 0.05$).
Source: Own authorship.

At the end of *in vitro* digestion, PLE showed different stability, bioaccessibility and effective bioaccessibility in each digested sample (Figure 8.3). The stability and bioaccessibility of free PLE was relatively high when compared to other free active compounds (53.45 ± 1.79 and 65.90 ± 6.28%, respectively). For example, a bioaccessibility of 14.62% was observed for proanthocyanidins extracted from grape seeds (Zhuang et al., 2023), 12.34% for hydrolysable tannin extracted from pomegranate peel (Rakshit; Srivastav, 2022), and 18.50% for capsaicin (He et al., 2023). According to Sęczyk et al. (2023), the high chemical stability and bioaccessibility of plant extracts rich in active compounds after digestion is possibly related to the favorable composition of the extract due to the high number of active compounds and/or their low affinity with the digestion components (Sęczyk et al., 2023). The PLE, which presented high FCRC concentration, shows more than 160 identified phenolic compounds from different classes (Lorenzo et al., 2018), and this may have contributed to its high stability and bioaccessibility after *in vitro* digestion.

Figure 8.3 – Stability, bioaccessibility and effective bioaccessibility of "Pitanga" leaf extract (PLE) after *in vitro* digestion of free PLE, W/O (SE) and W/O/W (DE) emulsions, films (F-PLE and F-DE) and nanocomposite films (N-PLE and N-DE). Error bars represent the standard deviation of n = 6 replicates. Different letters indicate significant differences between the samples in each parameter according to Tukey's test (*p* < 0.05)
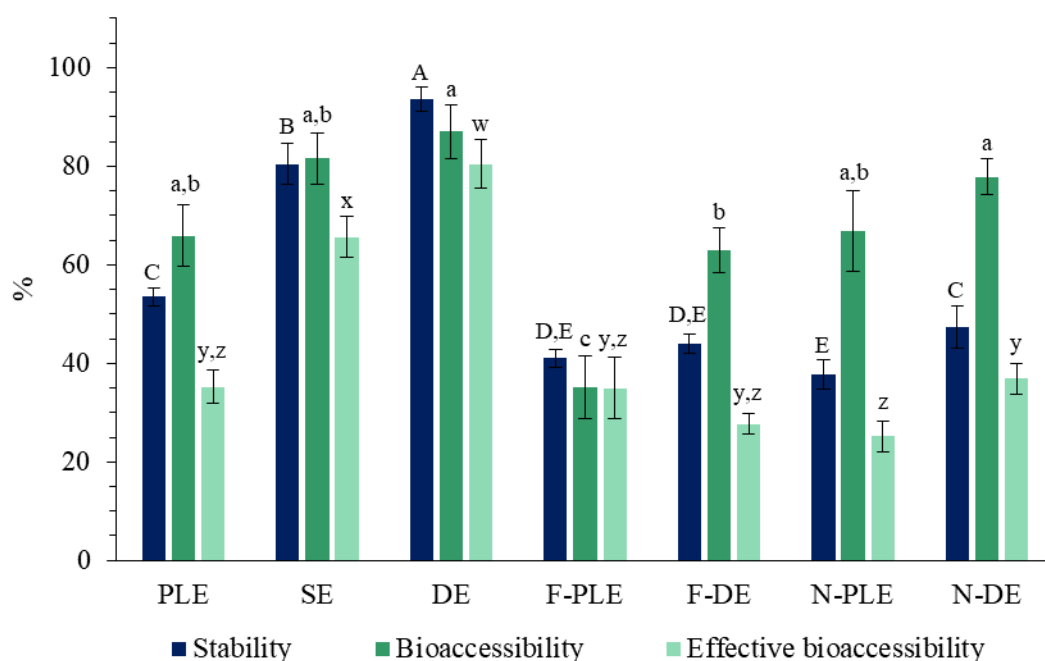
Source: Own authorship.

It was observed that PLE encapsulation in SE and DE increased (*p* < 0.05) its stability. This indicates that the lipid phase of the emulsions promotes the protection of the biological activity of the PLE. The stability of PLE in SE (80.44 ± 4.16%) was lower than in DE (93.52 ± 2.41%) (*p* < 0.05). DE showed high digestibility (i.e., high triacylglycerols hydrolysis into FFA and monoacylglycerols by lipase), resulting on a high PLE release from the lipid phase (He et al., 2023). Despite this, there was no destabilization of PLE released from DE exposed to gastrointestinal conditions.

The stability of PLE in active films and nanocomposite films was lower (*p* < 0.05) than in SE and DE, and free PLE, being around 40%, except for N-DE, which showed the same stability as free PLE (*p* > 0.05). The lower stability of PLE in active films and nanocomposite films may be the result of interactions that occur between PLE' polyphenols and gelatin. Proteins are quite unstable to pH variations and are easily hydrolyzed by digestive enzymes (López de Lacey et al., 2012). When the protein

transports active compounds, or forms complexes with them, as is the case of protein-polyphenol complexes, protein hydrolysis can lead to the degradation of part of the active compounds during the gastric phase of digestion (Giménez et al., 2013). Covalent bonds formed between polyphenols and proteins could improve the stability of the systems during the digestive process in addition to improving thermal stability (Li et al., 2021). Further research is necessary to study how the stability of polyphenols-proteins complex can be affected by the pH (Chen et al., 2024).

PLE bioaccessibility was similar to free PLE, SE, DE and active nanocomposite films (N-PLE and N-DE) ($p > 0.05$), with values that varied between 65.90 and 87.02% (Figure 8.3). F-DE presented a bioaccessibility value of 62.99 ± 4.51%, not significantly difference ($p > 0.05$) from PLE, SE and N-PLE ($p < 0.05$), while F-PLE presented the lowest bioaccessibility ($p < 0.05$) value among all samples tested (35.18 ± 6.29%). The lower bioaccessibility of PLE in F-PLE can be due also to the interactions that occurred between gelatin and PLE's polyphenols. According to Giménez et al. (2013), polyphenols have great affinity with proteins and together they can form very stable complexes. The formation of these possible complexes may prevent the release and quantification of polyphenols linked to the gelatin chain at the end of *in vitro* digestion, thus reducing the bioaccessibility of PLE. López de Lacey et al. (2012) observed that agar-based films incorporated with green tea showed lower bioaccessibility of polyphenols after *in vitro* digestion when gelatin was present in the film matrices. Gelatin can sequester the polyphenols released during *in vitro* digestion or prevent their release. Furthermore, gelatin-polyphenol interactions can decrease the reducing capacity of polyphenols in FCRC-type assays, which involve redox reactions (López de Lacey et al., 2012). In the case of F-DE and N-DE, encapsulation of PLE can reduce gelatin-polyphenol interactions, thus increasing bioaccessibility compared to F-PLE. For N-PLE, this result was possibly due to the effect of crystalline nanocellulose, as polyphenols can adsorb on the crystalline nanocellulose surfaces, form hydrogen bonds with -OH groups of crystalline nanocellulose, and be protected (Tessaro et al., 2021b).

He et al. (2023) found similar results on the bioaccessibility of capsaicin encapsulated in W/O (78%) and W/O/W (85%) emulsions, produced with corn oil, beeswax and PGPR, as lipid phase, and aqueous solution of starch and carrageenan, as aqueous dispersing phase. Rakshit and Srivastav (2022) reported that the

bioaccessibility of hydrolyzed tannins encapsulated in W/O/W emulsions was up to 64%, values lower than the bioaccessibility determined for SE and DE.

Finally, the effective bioaccessibility of PLE was higher in DE, followed by SE, being 80.5 ± 5.0%, and 65.5 ± 4.2%, respectively ($p < 0.05$). F-PLE and N-DE showed the same effective bioaccessibility as the free PLE ($p > 0.05$) (around 35%), while F-DE and N-PLE showed the lowest ($p < 0.05$) effective bioaccessibility (~27%). The effective bioaccessibility is an estimative value and it must be analyzed with care, once there are other factors that influence the bioaccessibility that were not considered, such as metabolism and absorption (Zou et al., 2016). Data regarding stability, bioaccessibility and effective bioaccessibility of active compounds incorporated into films are scarce. However, Helal et al. (2015) determined that the bioaccessibility of different polyphenols content in edible casein/caseinate coatings ranged from 79% to 100%, where gallic acid was the most degraded polyphenol after *in vitro* digestion.

8.3.4 Cell viability assay

For the cytotoxicity study, the effect of free PLE, SE, DE, F-DE and N-DE, digested and non-digested, were evaluated on cell viability. In the case of free PLE, SE and DE non-digested, the PLE concentration range studied was 10 to 200 µg/mL (Figure 8.4A), based on the study by Cunha et al. (2016). For non-digested F-DE and N-DE, which have 100 µg/mL of PLE in their formulations, the PLE concentration range studied was 10 to 50 µg/mL (Figure 8.4B).

All non-digested samples were not cytotoxic (cell viability above 93%) (Figure 8.4A,B). Except for free PLE, all the other samples showed some benefit for cell growth in at least two PLE concentrations as the cell viability was higher than 100%. Gonçalves et al. (2021) also observed non-cytotoxic effect on Caco-2 cells of non-digested O/W emulsions encapsulating curcumin.

For the digested samples, free PLE, F-DE and N-DE did not show cytotoxicity for cells at all concentrations studied (Figure 8.4C). In fact, digested F-DE and N-DE were beneficial for cell growth, i.e., cell viability above 100% at PLE concentrations of 0.10 and 0.17 µg/mL, and at a PLE concentration of 0.25 µg/mL only for N-DE. These results indicate that none of the components present in the active film matrices (gelatin, glycerol, DE and crystalline nanocellulose) caused significant damage to Caco-2 cells, at the concentrations studied. Giménez et al. (2013) reported a cytotoxic effect of

gelatin-based films incorporated with green tea for mouse fibroblast cells after *in vitro* digestion, which was related to the concentration of green tea.

However, DE did not present cytotoxicity and was beneficial for cell growth in PLE concentrations of 0.10 and 0.17 µg/mL. However, the highest PLE concentration (0.25 µg/mL), it was quite cytotoxic (5.0 ± 0.5%) most likely due to the PLE concentration and DE size. SE showed high cytotoxicity in all PLE concentrations studied, whose cell viability varied from 1.2 to 2.2%. In order to evaluate the origin of this cytotoxicity, digestive fluids and all SE and DE components (PGPR, Tween 80, sodium caseinate and soybean oil) were digested separately in the concentrations necessary to reach PLE concentrations of 0.10, 0.17 and 0.25 µg/mL, and their effects on cell viability were evaluated (Figure 8.4D).

In general, digestive fluids and all components studied were not cytotoxicity, except the soybean oil, which was cytotoxic at all PLE concentrations studied. At the highest PLE concentration studied (0.25 µg/mL), cell viability varied between 89 and 96% in contact with non-cytotoxic components ($p > 0.05$), while it was 4.6% when in contact with soybean oil. At the lowest PLE concentration studied (0.10 µg/mL), cell viability varied between 96.9% and 102.5% when in contact with non-cytotoxic components ($p > 0.05$), while cell viability was 17.0% in contact with soybean oil. According to Gonçalves et al. (2021), digestive fluids and emulsifiers such as Tween 80 also did not show a cytotoxic effect on Caco-2 cells, but the product of lipid digestion, such as some monoglycerides, can be cytotoxic to cells. It has been previously reported that monoglycerides induced dose-dependent apoptosis in other mammalian cells (i.e., murine thymocytes), due to various processes such as reactive oxygen species' production and mitochondrial transmembrane potential reduction (Philippoussis et al., 2002). In our study, lipid digestion products which likely contained free fatty acids and monoglycerides, plus the presence of emulsifiers, contributed to damage of cell integrity (Gasa-Falcon et al., 2021). Moreover, the cytotoxicity effects of digestion products on Caco-2 cells could be dependent on: i) emulsions basic characteristics (as shape, size, surface charge and chemical composition); ii) the initial seeding cell density used on 96-well culture plate and iii) the digestion products concentration, as previously stated by other authors (Bu et al., 2016). Thus, the higher % of PLE in the DE than in the other studied systems indicated that the more toxic nature of the former system was most likely due to the concentration of PLE and size and charge distribution properties of the surfactants.

Figure 8.4 – Cell viability of Caco-2 cells when in contact with non-digested free "Pitanga" leaf extract (PLE), W/O (SE) and W/O/W (DE) emulsions (A), film (F-DE) and nanocomposite film (N-DE) (B), and digested free PLE, SE, DE, F-DE and N-DE (C), and digested fluids, PGPR, Tween 80, sodium caseinate (SC), and soybean oil (D). Error bars represent the standard deviation of n = 3 replicates. Different letters indicate significant differences between PLE concentrations for each sample according to Tukey's test ($p < 0.05$)
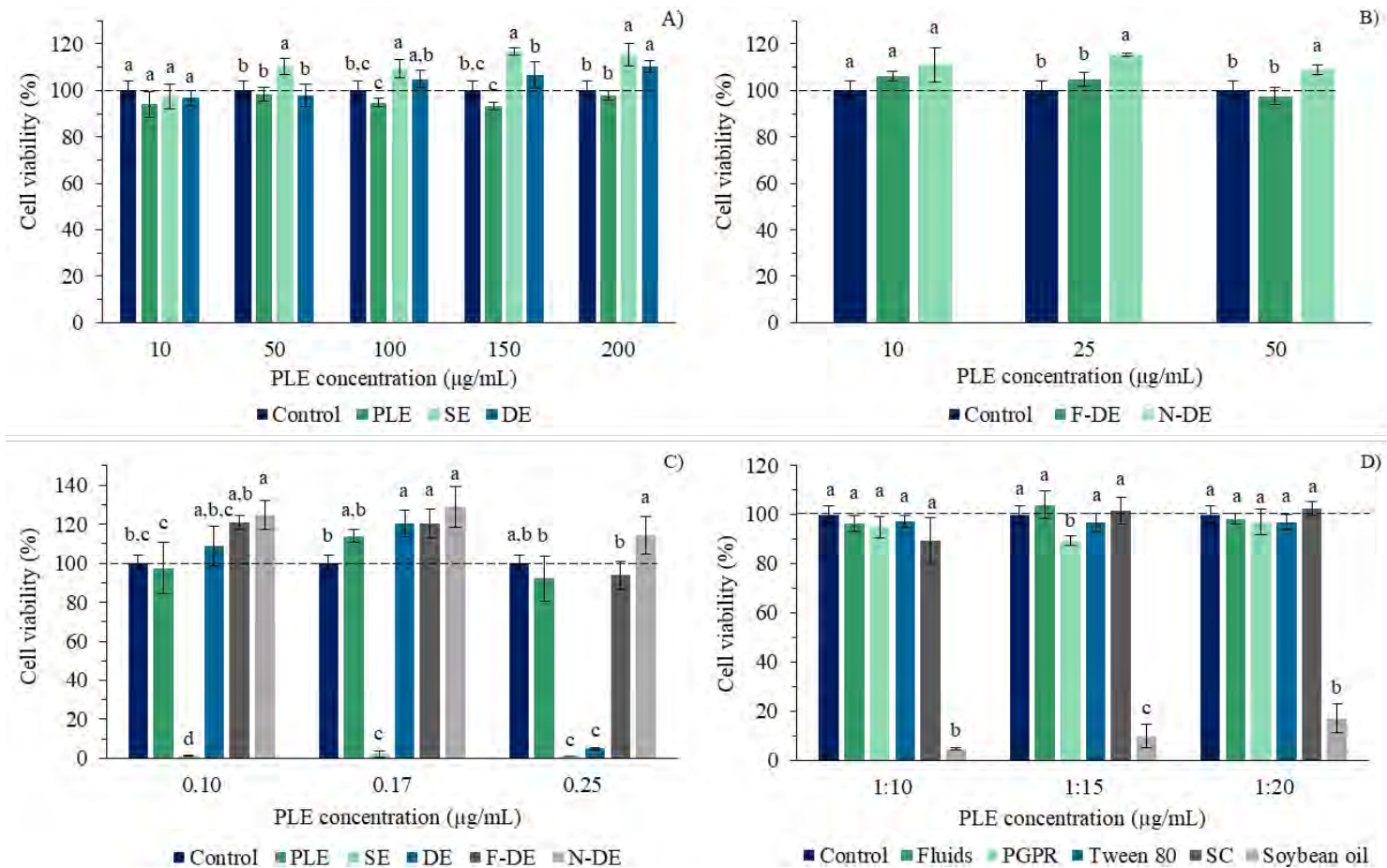
Source: Own authorship.

8.4 CONCLUSIONS

The results obtained in this study demonstrated that the bioaccessibility of PLE in active films and nanocomposite films was influenced by the encapsulation of PLE in DE and by the presence of crystalline nanocellulose. The active nanocomposite films (N-DE and N-PLE) showed greater bioaccessibility of PLE than active films (F-DE and F-PLE) after *in vitro* digestion. N-DE also showed greater PLE stability than other films and nanocomposite films. This may be a result of PLE encapsulation in DE and the presence of crystalline nanocellulose, which possibly protected PLE's polyphenols under gastrointestinal conditions, since F-PLE presented the lowest PLE bioaccessibility.

Both F-DE and N-DE were not cytotoxic to cells at any of the PLE concentrations studied. Cells treated with N-DE showed the highest cell viability at the highest PLE concentration, before and after *in vitro* digestion. As a control for the entire process, this study also demonstrated that the encapsulation of PLE in DE considerably increased the stability and bioaccessibility of PLE after *in vitro* digestion, which was also higher than SE.

PLE encapsulation in DE had a positive effect compared to encapsulation only in SE, as DE also showed higher digestibility and lower cytotoxicity than SE. The high cytotoxicity and low digestibility of SE may be associated with the high soybean oil concentration in this system. Nevertheless, for a full understanding of nano-scaled effect drivers in physiological systems and thus for the admittance in commercial food products further research is needed.

Therefore, gelatin-based active films and nanocomposite films activated with PLE encapsulated in DE may have additional properties and applications in the food industry, as they were shown to be digested and active after *in vitro* digestion. As an additional outcome, DE proved to be an effective encapsulation system for aqueous active compounds, and can be applied in active films, as well, as delivering systems.

References

ARAUJO, N. M. P. et al. Plants from the genus Eugenia as promising therapeutic agents for the management of diabetes mellitus: A review. **Food Research International**, v. 142, p. 110182, 2021.

BRODKORB, A. et al. INFOGEST static *in vitro* simulation of gastrointestinal food digestion. **Nature Protocols**, v. 14, p. 991-1014, 2019.

BU, P. et al. Cytotoxicity assessment of lipid-based self-emulsifying drug delivery system with Caco-2 cell model: Cremophor EL as the surfactant. **European Journal of Pharmaceutical Sciences**, v. 91, p. 162-171, 2016.

CHAKRAVARTULA, S. N. S. et al. Influence of pitanga (*Eugenia uniflora* L.) leaf extract and/or natamycin on properties of cassava starch/chitosan active films. **Food Packaging and Shelf Life**, v. 24, p. 100498, 2020.

CHAUDHARY, N.; SABIKHI, L.; HUSSAIN, S. A. Emblicanin rich *Emblica officinalis* extract encapsulated double emulsion: controlled release of bioactive during phagocytosis and *in vitro* digestion. **Journal of Food Science and Technology**, v. 57, n. 4, p. 1371-1381, 2020.

CHEN, D. et al. Effect of polyphenols on the rheology, microstructure and *in vitro* digestion of pea protein gels at various pH. **Food Hydrocolloids**, v. 151, p. 109827, 2024.

CUNHA, F. A. B. et al. Cytotoxic and antioxidative potentials of ethanolic extract of *Eugenia uniflora* L. (Myrtaceae) leaves on human blood cells. **Biomedicine & Pharmacotherapy**, v. 84, p. 614-621, 2016.

DICKINSON, E. Double Emulsions Stabilized by Food Biopolymers. **Food Biophysics**, v. 6, n. 1, p. 1–11, 2011.

GASA-FALCON, A. et al. Delivery of β-carotene to the *in vitro* intestinal barrier using nanoemulsions with lecithin or sodium caseinate as emulsifiers. **LWT,** v. 165, p. 110059, 2021.

GIMÉNEZ, B. et al. Antioxidant properties of green tea extract incorped to fish gelatin films after simulated gastrointestinal enzymatic digestion. **LWT**, v. 53, p. 445-451, 2013.

GONÇALVES, R. F. S. et al. Lipid-based nanostructures as a strategy to enhance curcumin bioaccessibility: Behavior under digestion and cytotoxicity assessment. **Food Research International**, v. 143, p. 110278, 2021.

HAN, L. et al. Co-delivery of insulin and quercetin in W/O/W double emulsions stabilized by different hydrophilic emulsifiers. **Food Chemistry**, v. 369, p. 130918, 2022.

HE, J. et al. Capsaicin encapsulated in W/O/W double emulsions fabricated via ethanol-induced pectin gelling: Improvement of bioaccessibility and reduction of irritation. **International Journal of Biological Macromolecules**, v. 235, p. 123899, 2023.

HELAL, A. et al. Antioxidant activity and bioaccessibility of phenols-enriched edible casein/caseinate coatings during *in vitro* digestion. **Journal of Dairy Research**, v. 82, p. 56-63, 2015.

HUANG, Y.; ZHOU, W. Microencapsulation of anthocyanins through two-step emulsification and release characteristics during *in vitro* digestion. **Food Chemistry**, v. 278, p. 357–363, 2019.

IQBAL, S. et al. Modulation of viscosity, microstructure and lipolysis of W/O emulsions by cellulose ethers during *in vitro* digestion in the dynamic and semi-dynamic gastrointestinal models. **Food Hydrocolloids**, v. 128, p. 107584, 2022.

LI, M. et al. Recent progress on protein-polyphenol complexes: Effect on stability and nutrients delivery of oil-in-water emulsion system. **Frontiers in Nutrition**, v. 8, p. 765589, 2021.

LIU, W. et al. Encapsulation of β-carotene-loaded oil droplets in caseinate/alginate microparticles: Enhancement of carotenoid stability and bioaccessibility. **Journal of Functional Foods**, v. 40, p. 527-535, 2018.

LÓPEZ DE LACEY, A. M. et al. Bioaccessibility of green tee polyphenols incorporated into an edible agar film during simulated human digestion. **Food Research International**, v. 48, p. 462-469, 2012.

LORENZO, J. M. et al. Influence of pitanga leaf extracts on lipid and protein oxidation of pork burger during shelf-life. **Food Research International**, v. 114, p. 47-54, 2018.

LUCIANO, C. G. et al. Application of bi-layers active gelatin films for sliced dried-cured Coppa conservation. **Meat Science**, v. 189, p. 108821, 2022.

MARTELLI-TOSI, M. et al. Chemical treatment and characterization of soybean straw and soybean protein isolate/straw composite films. **Carbohydrate Polymers**, v. 157, p. 512-520, 2017.

MUSHTAQ, A. et al. Recent insights into nanoemulsions: Their preparation, properties and applications. **Food Chemistry: X**, v. 18, p. 100684, 2023.

PHILIPPOUSSIS, F. et al. Cellular specificity related to monoglyceride-induced cell death. **Immunology Letters**, v. 83, n. 3, p. 221-230, 2002.

PINHEIRO, A. C. et al. Unravelling the behaviour of curcumin nanoemulsions during *in vitro* digestion: effect of the surface charge. **Soft Matter**, v. 9, n. 11, p. 3147-3154, 2013.

RAKSHIT, M.; SRIVASTAV, P. P. Encapsulation of hydrolysable tannin from pomegranate peel in W/O/W double emulsion: *In-vitro* digestion, release kinetics, storage and physical stabilities. **Food Hydrocolloids for Health**, v. 2, p. 100067, 2022.

SĘCZYK, Ł. et al. Phytochemical profile, *in vitro* bioaccessibility, and anticancer potential of golden root (*Rhodiola rosea* L.) extracts. **Food Chemistry**, v. 404, p. 134779, 2023.

SILVA, H. D. et al. Evaluating the effect of chitosan layer on bioaccessibility and cellular uptake of curcumin nanoemulsions. **Journal of Food Engineering**, v. 243, p. 89–100, 2019.

SINGLETON, V. L.; ORTHOFER, R.; LAMUELA-RAVENTÓS, R. M. Analysis of total phenols and other oxidation substrates and antioxidants by means of folin-ciocalteu reagent. **Methods in Enzymology**, v. 299, p. 152–178, 1999.

TESSARO, L. et al. Gelatin and/or chitosan-based films activated with "Pitanga" (*Eugenia uniflora* L.) leaf hydroethanolic extract encapsulated in double emulsion. **Food Hydrocolloids**, v. 113, p. 106523, 2021a.

TESSARO, L. et al. Gelatin/chitosan-based films loaded with nanocellulose from soybean straw and activated with "Pitanga" (*Eugenia uniflora* L.) leaf hydroethanolic extract in W/O/W emulsion. **International Journal of Biological Macromolecules**, v. 186, p. 328–340, 2021b.

TESSARO, L.; MARTELLI-TOSI, M.; SOBRAI, P. J. A. Development of W/O emulsion for encapsulation of "Pitanga" (*Eugenia uniflora* L.) leaf hydroethanolic extract: droplet size, physical stability and rheology. **Food Science and Technology**, v. 42, 2021.

TESSARO, L. et al. Stable and bioactive W/O/W emulsion loaded with "Pitanga" (*Eugenia uniflora* L.) leaf hydroethanolic extract. **Journal of Dispersion Science and Technology**, v. 43, p. 1890-1900, 2022.

WU, X. et al. Encapsulation of hydrophobic capsaicin within the aqueous phase of water-in-oil high internal phase emulsions: Controlled release, reduced irritation, and enhanced bioaccessibility. **Food Hydrocolloids**, v. 123, p. 107184, 2022.

ZHANG, Y. et al. Probiotic encapsulation in water-in-oil high internal phase emulsions: Enhancement of viability under food and gastrointestinal conditions. **LWT**, v. 163, p. 113499, 2022.

ZHUANG, H. et al. Fabrication of grape seed proanthocyanidin-loaded W/O/W emulsion gel stabilized by polyglycerol polyricinoleate and whey protein isolate with konjac glucomannan: Structure, stability, and *in vitro* digestion. **Food Chemistry**, v. 30, p. 135975, 2023.

ZOU, L. et al. Influence of lipid phase composition of excipient emulsions on curcumin solubility, stability, and bioaccessibility. **Food Biophysics**, v. 11, n. 3, p. 213–225, 2016.

9 CONCLUSÃO GERAL

O extrato hidroetanólico de folha de pitangueira (PLE) é rico em compostos fenólicos que lhe confere atividade antioxidante e antimicrobiana, e que pode ser utilizado para ativar filmes e filmes nanocompósitos a base de gelatina e/ou quitosana, na sua forma não encapsulada ou encapsulada em emulsão A/O/A. Todos os filmes produzidos apresentaram características de materiais finos e flexíveis, foram transparentes ou translúcidos, e de coloração clara.

Os filmes nanocompósitos a base de gelatina e/ou quitosana ativados com a emulsão A/O/A e incorporados com CN apresentaram excelentes propriedades mecânicas e de barreira à luz UV/Vis, diminuição da sensibilidade à água, e boa atividade antioxidante. Como o filme nanocompósito a base de gelatina apresentou maior atividade antioxidante, e deve apresentar um custo de produção relativamente mais baixo, a gelatina foi o biopolímero escolhido para o aprofundamento dos estudos sobre este material. Essas melhorias também foram observadas para os filmes e filmes nanococompósito a base de gelatina ativados com PLE não encapsulado, principalmente para os filmes nanocompósitos, visto que estes materiais apresentaram, também, menor sensibilidade à água.

A permeabilidade ao O_2 e CO_2 de todos os filmes e filmes nanocompósitos aumentou, principalmente, como efeito do aumento da umidade relativa, que pode afetar a mobilidade macromolecular devido ao aumento da umidade, ou seja, efeito plastificante da água. Em elevadas umidades relativas, os filmes nanocompósitos apresentaram as melhores propriedades de barreira a gases, especialmente aqueles ativados com o PLE encapsulado na emulsão A/O/A e não encapsulado. Além disso, os filmes nanocompósitos apresentaram maiores bioacessibilidades do PLE após a digestão *in vitro*, especialmente aquele ativado com a emulsão A/O/A encapsulando o PLE. Todos os filmes e nanocompósitos não foram citotóxicos para células Caco-2.

Adicionalmente, a encapsulação do PLE na emulsão A/O/A apresentou um efeito positivo em comparação à encapsulação somente na emulsão A/O, pois a emulsão A/O/A apresentou melhor digestibilidade, bioacessibilidade do PLE e menor citotoxicidade, possivelmente relacionada ao menor teor de fase lipídica na sua composição.

No geral, este estudo demostrou que filmes e filmes nanocompósitos produzidos com componentes GRAS podem, eventualmente, ser comestíveis e

seguros para a saúde humana. Estes materiais podem ser valorizados e aprimorados pela adição de CN e PLE encapsulado em emulsão A/O/A, e atuar como liberadores do PLE em condições gastrointestinais e como materiais de barreira a gases em diferentes umidades relativas.

Alguns resultados obtidos nesta tese permitem sugerir que esses filmes e filmes nanocompósitos podem ser aplicados com segurança como embalagens ativas de alimentos, como, por exemplo, embalagens comestíveis de alimentos e embalagens de alimentos ricos em lipídeos.

Sugestões para trabalhos futuros

Para trabalhos futuros, sugerem-se:

I) Estudar a estabilidade do PLE, emulsões A/O e A/O/A, e dos filmes e filmes nanocompósitos ao longo do tempo, em condições controladas de umidade relativa e temperatura.

II) Estudar e modelar a liberação dos compostos ativos do PLE das emulsões A/O/A e dos filmes e filmes nanocompósitos em diferentes meios simulantes de alimentos.

III) Aplicar os filmes e filmes nanocompósitos como embalagens de alimentos ricos em lipídeos, já que a barreira à luz UV/Vis foi uma das propriedades que mais foi beneficiada nos filmes e filmes nanocompósitos incorporados com emulsão A/O/A encapsulando o PLE.

IV) Estudar a aplicação desses filmes e filmes nanocompósitos como embalagem de outros tipos de alimentos, considerando-se os estudos de permeabilidade aos gases e digestão *in vitro*.

Attachment A

Paper published in International Journal of Biological Macromolecules.

Attachment B

Paper published in Foods.

Improving the Properties of Gelatin-Based Films by Incorporation of "Pitanga" Leaf Extract and Crystalline Nanocellulose

by **Larissa Tessaro** [1,*] ✉ ⓘ, **Ana Gabrielle R. Pereira** [1] ✉, **Milena Martelli-Tosi** [1] ✉ ⓘ and **Paulo José do Amaral Sobral** [1,2] ✉ ⓘ

[1] Department of Food Engineering, Faculty of Animal Science and Food Engineering, University of São Paulo, Av Duque de Caxias Norte, 225, Pirassununga 13635-900, SP, Brazil

[2] Food Research Center (FoRC), University of São Paulo, Rua do Lago, 250, Semi-Industrial Building Block, São Paulo 05508-080, SP, Brazil

[*] Author to whom correspondence should be addressed.

Attachment C

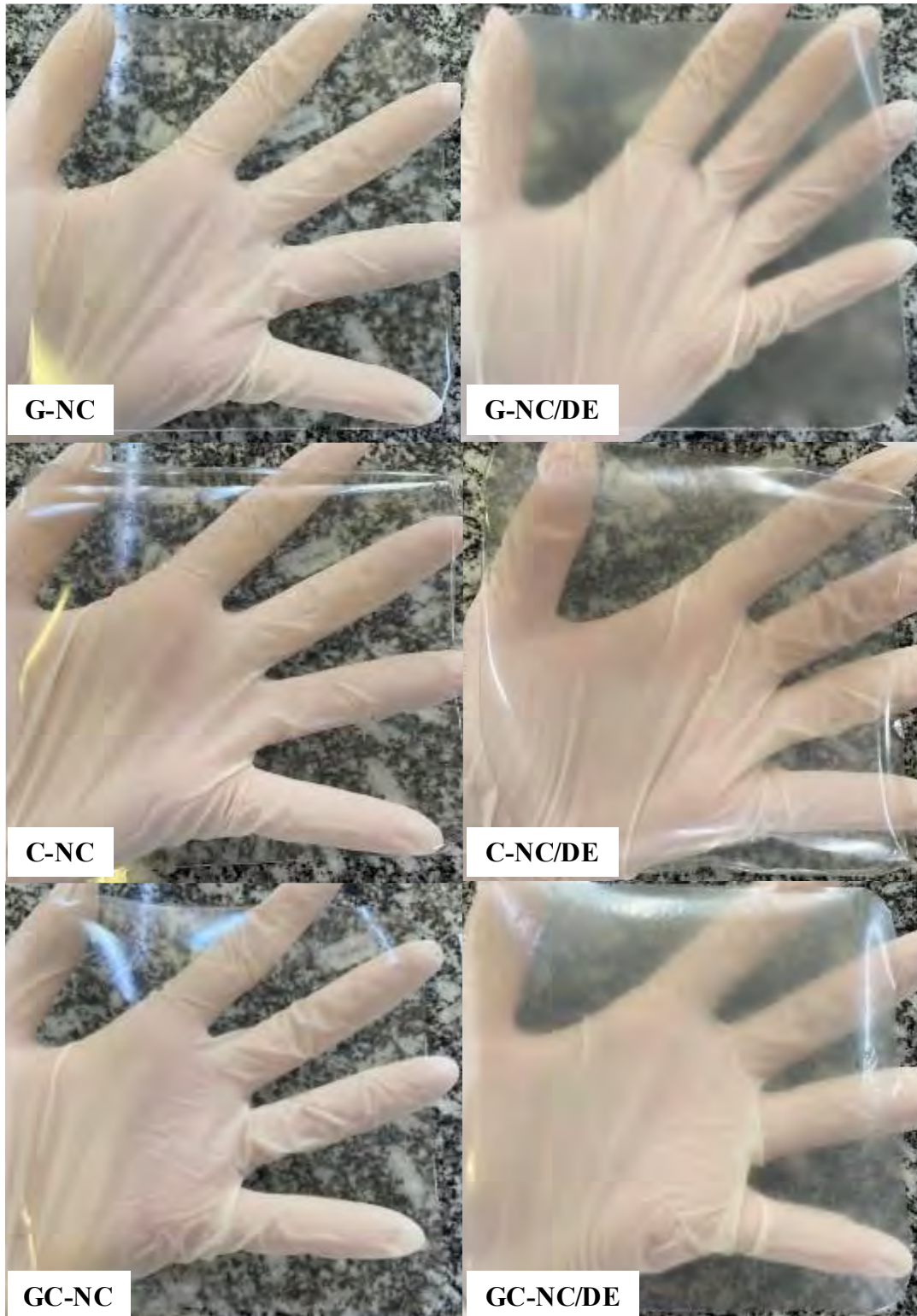Paper published in Food Hydrocolloids.

Appendix A

Figure A1 – Atomic force microscopy cross-section results of the NC: sample height variation.
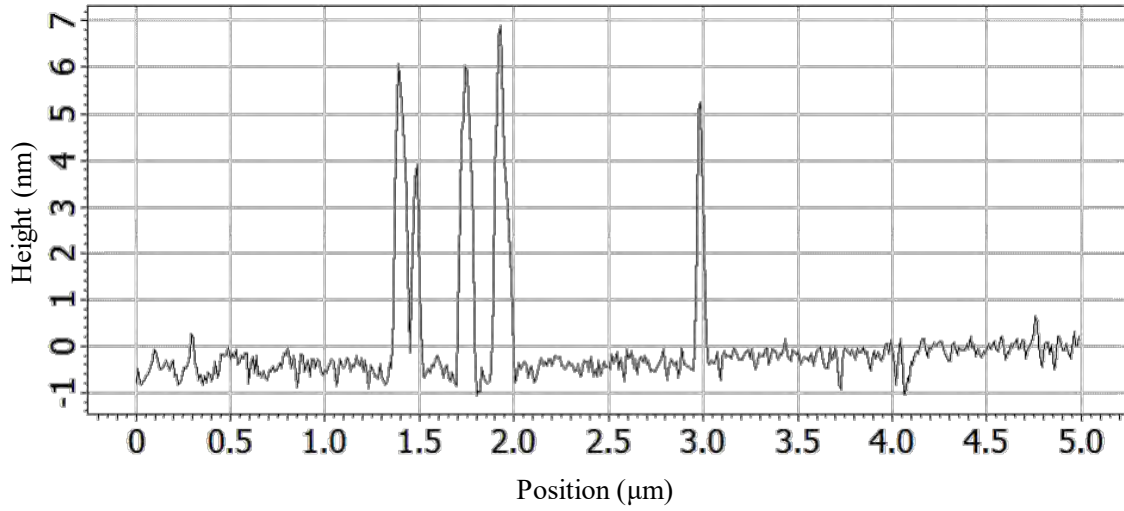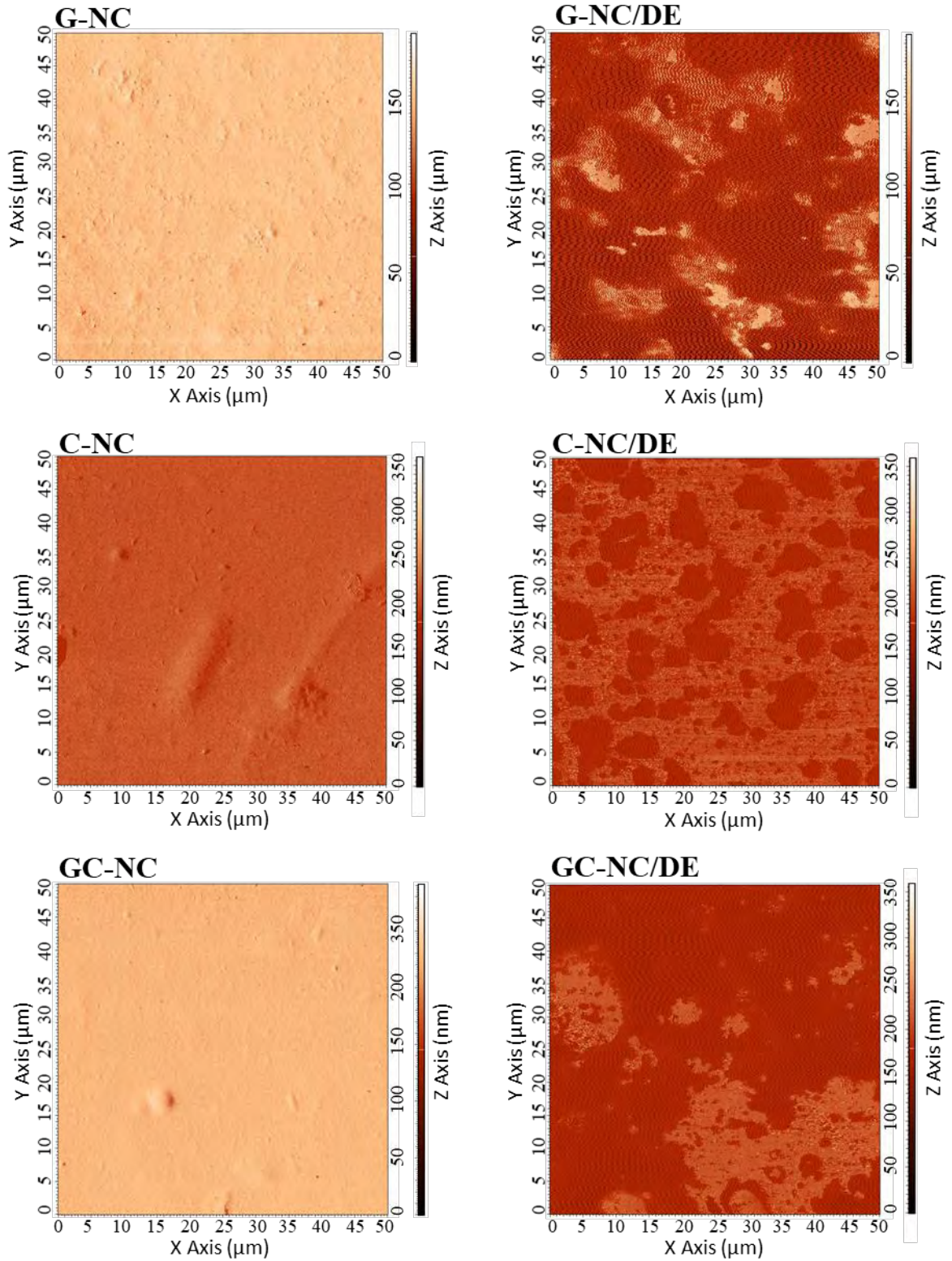

Source: Own authorship.

Figure A2 –Photograph of gelatin (G), chitosan (C) and gelatin/chitosan (GC) films with soybean straw crystalline nanocelluloses without (NC) or with NC and double emulsion (NC/DE)

Source: Own authorship.

Figure A3 - 2D atomic force micrographs of gelatin (G), chitosan (C) and gelatin/chitosan (GC) films with soybean straw crystalline nanocelluloses (NC) or films with NC and double emulsion (NC/DE)
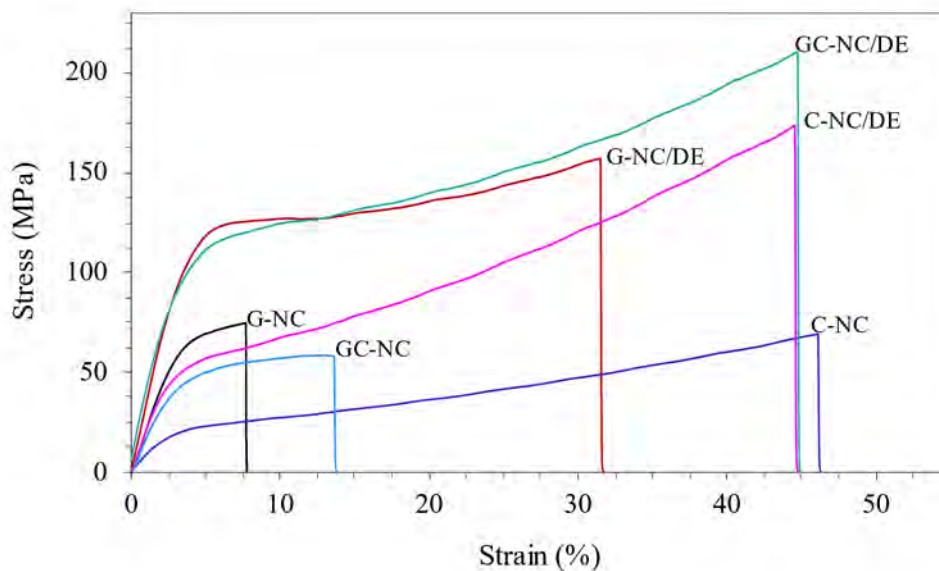

Source: Own authorship.

Table A1 - Range of measured roughness values of gelatin (G), chitosan (C) and gelatin/chitosan (GC) films with soybean straw crystalline nanocelluloses without (NC) or with NC and double emulsion (NC/DE)

Film	Roughness (nm)			
	1	2	3	4
G-NC	16	42	45	16
C-NC	24	49	16	46
GC-NC	31	17	43	32
G-NC/DE	1820	172	164	186
C-NC/DE	95	1120	151	193
GC-NC/DE	201	1490	2970	2180

Source: Own authorship.

Figure A4 – Examples of stress x strain curves of tensile tests of gelatin (G), chitosan (C) and gelatin/chitosan (GC) films with soybean straw crystalline nanocelluloses (NC) or films with NC and double emulsion (NC/DE)

Source: Own authorship.